UNIVERSITÀ DEGLI STUDI DI PALERMO
Dipartimento di Ingegneria
Corso di Dottorato in Ingegneria Civile, Ambientale, Aerospaziale e dei Materiali

Ciclo XXXII

Coordinatore Prof. Antonina Pirrotta

Multiscale Biomechanics Characterization of Ligaments and Tendons of the Human Knee

Dottorando
Ing. Emanuela Bologna

Tutor
Prof. Massimiliano Zingales

ANNO ACCADEMICO 2019 - 2020

Multiscale Biomechanics Characterization of Ligaments and Tendons of the Human Knee

Ing. Emanuela Bologna

September 22, 2020

Acknowledgment

This thesis work was the result of a three-year process during which the initial topic, which started from a few experimental results, gradually expanded and became more and more exciting.

I would like to thank Professor Zingales thanks to whom the topic has become increasingly interesting with its continuous stimuli and curiosities proposed.

I would also like to thank all people at Rizzoli Orthopedic Institute that i had the like to work with as Prof. Zaffagnini, Prof. Lopomo and Ing. Marchiori.

Thanks to Prof. Anne Robertson that supported during my visiting period in Pittsburgh.

Thanks to Prof. Di Paola for the example shown to all young people who approach the world of research.

I thank the coordinator of the PhD for the interesting initiatives proposed during this three years.

I would like to thank you for the opportunity I was given with funds MIUR grant PON FSE-FESR ricerca e innovazione 2014-2020 DOT1320558, with coordinator Prof. Massimiliano Zingales.

Finally, I thank my family for the patience and support they have shown me over the past three years.

Contents

Chapter 1

Introduction

1.1 Problem description

The knee is one of the most frequently injured joints in the human body. Epidemiology studies estimate that 1.6-1.9 million patients, most between 15 and 44 years of age, see a physician for a knee sprain each year. Among those who sustain an acute traumatic hemarthrosis to the knee, the anterior cruciate ligament (ACL) is partially or completely torn in more than 70% of the time. According to a report of the National Center for Health Statistics, 250,000 patients in 1984 were diagnosed as having significant disruption to their ACL. In fact, ACL is probably the most commonly and totally disrupted knee ligament. If left untreated, ACL ruptures lead to increased anterior and rotatory instabilities and meniscal tears and, in one-third of patients, joint space narrowing and unequivocal evidence of osteoarthrosis on x-ray film.

In the mid 1970s, there was much confusion about the role of the ACL in restraining anterior tibial displacement or "drawer." Many studies were performed by selectively cutting ligaments to determine their restraining action. A recent survey of orthopaedic surgeons indicates that autograft replacements are the most frequently used treatment option in cases of ACL ruptures . The success of these procedures is affected by many factors, some mechanical in origin. The studies of the past 10 years have been aimed at assessing the importance of a number of these mechanical factors. Early studies sought to determine the importance of the ACL in restraining anterior tibial displacement. Typically, an anterior force was applied to the tibia of the intact knee, a ligament was cut, the force was reapplied, and the increase in tibial translation was measured. One problem with this approach was that the increased translation depended on the order of ligament cutting; if the cutting order changed, the measured translation changed.

Today, after numerous theories proposed by orthopedic surgeons it is proposed that ACL is one of the major ligaments within the human knee and plays a critical part in stabilizing the joint. Just due to this prominent role, ACL is highly susceptible to injuries, above all during pivoting sport activities, which can alter the overall knee biomechanics and, if not or poorly treated, often lead to catastrophic osteoarthritis. For these reasons, ACL reconstruction results to be one of the most commonly performed procedures in orthopaedics and its incidence is increasing. While, on one side, literature suggests that the short- to mid-term functional performance of this procedure is promising, on the other side it does not still prevent premature knee osteoarthritis. Common paradigm at the basis of ACL surgery implies to replace the injured ligament by using a graft that should ideally mimic the functional behaviour of the native structure. The most commonly used solutions are primarily autologous grafts, including patellar tendon and hamstring tendon graft , biological allografts , xenografts or bioengineered synthetic grafts. Although trying to identify always the optimal solution in terms of clinical and functional outcomes, the choice of any graft may substantially alter the biomechanics of the knee, permitting a return to only moderate physical activities. Besides concerns related to surgery, inappropriate graft properties still remain main issues in reaching a long-term success. Specifically to ACL reconstruction, structural and mechanical differences between native tissue and grafts might be expected, since the physiological functions of ligament and, for example, tendons, are different by nature, thus potentially altering the overall knee biomechanics. The graft, once in situ, should be integrated at bone level and undergo a "ligamentization process" during the healing and rehabilitation process. Nevertheless, the chosen graft may fail in successfully restoring native ACL tissue mechanics, and therefore overall joint biomechanics, due to sub-optimal initial properties. For these reasons a deeper understanding of mechanical characteristics of both native ACL and grafts could guide the surgeon in the definition of the optimal grafts and reconstruction, definitely developing and validating novel and better solutions in terms of long term clinical and functional outcomes. Unfortunately, concerning ACL reconstruction, the characterization on human specimens is still incomplete, overall for what concerns their viscous (i.e. time-dependent) behaviour. This aspect is fundamental to correctly identify the viscoelastic behaviour of tendons and ligaments, as these data will directly contribute towards optimizing bioengineering repairs. Indeed, Creep and stress-relaxation are particularly important viscous phenomena in dense collagen fibrous tissues such as ligaments and tendons. In fact, during normal daily activity, loading of the ACL causes gradual creep and relaxation events. However, because excessive ligament creep and relaxation could re-

sult in increased laxity of the joint after injury or reconstructive surgery, their accurate description is indeed of considerable significance. In partial support, several studies described relaxation and creep as different microstructural phenomena and tested the hypothesis of their stress or strain level dependency, but on animal soft tissues.

The main goal of this work was therefore to identify the different hereditariness behaviour of native ACL and most used grafts in surgical reconstruction, by implementing a complete testing protocol able to both investigate preimplant mechanical characteristics and to provide useful data for hereditariness material modelling. In this thesis we proposed an experimental set up for human tendons and ligaments capable of producing useful data to be reworked for a more complete mechanical characterization of these fibrous tissues. A non-linear hereditary behavior was found , and a three-parameter non-linear mathematical model was proposed that could provide information on creep and relaxation starting from the experimental data of the creep test only or of the relaxation test only. The rheological model corresponding to this model was obtained. Furthermore, as well as its mechanical equivalence other investigation have been carried out to highlight material non-linearity. We assumed that the non-linearity arise at fiber level of the hierarchical packaging of the ligaments. In this regard a structural micromechanics model has been introduced that returns the one-dimensional non-linear behavior of these fibrous tissues. Finally, an analysis was made on the influence of the random fluctuation of the model parameters, an the constitutive equation of ligaments and tendons have been reported.

1.2 Survey of the scientific literature

Since the first studies at the mid of the eighteenth century (Wertheim,1847) it has been shown that the stress increases much faster with increasing strain than Hooke's law predicts. Moreover it also known that tissues in the physiological state are usually not unstressed. If an artery is cut, it will shrink away from the cut. A broken tendon retracts away; the lung tissue is in tension at all times. Ligaments and tendons display time-dependent and history-dependent mechanical behavior characteristic of viscoelastic materials. This evidence by long-standing mechanical test in which stress(strain) are hold constant over long interval of time and strain(stress) is measured. Viscoelastic behavior has been observed and studied in cells (Bausch et al. 1999; Guilak 2000; Guilak et al. 1999, 2000; Heidemann et al. 1999; Trickey et al. 2000) and a number of biologic tissues such as articular cartilage (Mak 1986; Woo et al. 1980), bone (Lakes and Katz 1979; Lakes et al. 1979), skele-

tal muscle (Best et al. 1994), cardiovascular tissue (Rousseau et al. 1983; Sauren et al. 1983), tendon (Atkinson et al. 1999; Graf et al. 1994), and ligament (Haut and Little 1969; Provenzano et al. 2001; Thornton et al. 1997; Woo 1982, Woo et al. 1981). Structural, phenomenological, and continuum models have been formulated to describe these viscoelastic behaviors (Bingham and DeHoff 1979; Corr et al. 2001; Decraemer et al. 1980; Dehoff 1978; Egan 1987; Fung 1972; Johnson et al. 1996; Lakes and Vanderby 1999; Lanir 1979, 1980, 1983; Sanjeevi et al. 1982; Shoemaker et al. 1986; Viidik 1968). The most commonly applied model of viscoelastic behavior in biomechanics has been the Quasi-linear Viscoelasticity (QLV) model of (Fung, 1972). This model has been particularly useful in describing experimental behavior in soft tissues (Best et al. 1994; Carew et al. 1999, 2000; Fung 1972; Sauren and Rousseau 1983; Sauren et al. 1983; Thornton et al. 1997; Woo 1982; Woo et al. 1980, 1981) and has been shown to describe ligament relaxation behavior at a single fixed strain level very well (Woo 1982; Woo et al. 1981).

A recent study (Provenzano et al. 2001) in rat medial collateral ligament revealed that within the strain-stiffening "toe" region and early portions of the linear region of the stress–strain curve, stress relaxation, and creep behavior are nonlinear functions of strain and stress, respectively. The rate of stress relaxation decreases with increasing strain and the rate of creep decreases with increasing stress. Similar strain-dependent relaxation rate behavior has been reported in the fibrocartilage zone of rabbit tendon tested in compression (Haridas et al. 2001). The behavior in these data sets cannot be robustly described using QLV, since in the separable formulation the time-dependent behavior is independent of stress or strain. Hence, the same rate of relaxation or creep would be predicted regardless of strain or stress level (Provenzano et al. 2001). Although each curve in the data set could be individually fit with separate moduli and a range obtained (as was demonstrated by Haridas et al. 2001), with QLV a single modulus cannot describe the stress- or strain-dependent rate behavior.

Thornton et al. (1997) reported that stress relaxation proceeds more rapidly than creep and demonstrated that neither a linear nor a QLV theory was able to phenomenologically model both behaviors with interrelated constitutive coefficients. Such behaviors can be described, however, using the single integral form of nonlinear superposition with interrelated coefficients for relaxation and creep as shown by Lakes and Vanderby (1999), or by incorporating collagen fiber recruitment when predicting creep from stress relaxation as shown by Thornton et al. (2001). These studies examined the relaxation–creep interrelation at only one level of coupled strain–stress, therefore it is not yet known if these models can account for the strain- or stress- dependent behavior described above, or if a more general formulation

is required.

Many reasonably general constitutive models such those by Schapery (1969), Lai and Findley (1968), Christensen (1980), Pipkin and Rogers (1968) and the modified superposition (also commonly referred to as nonlinear superposition) method (Findley et al. 1976; Lai and Findley 1968; Lakes 1998) have been proposed to describe nonlinearly viscoelastic materials. The Schapery single integral approach has been shown to be accurate and adaptable (Dillard et al. 1987; Lou and Schapery 1971; Touti and Cederbaum 1997) and modified superposition is general and also allows the relaxation function to depend on strain. These models have not been used to describe ligaments, but some have been used for polymers, and their formulations show potential for ligament mechanics.

Specific studies, ACL involving stress-relaxation were found in recent studies (Delcroix, 2013, Pioletti, 2000, McLean, 2015, Skelley, 2016, and Castile, 2016). In some of these (Delcroix, 2013), ACL was strained between 3% and 10% and the various curves were averaged. Interestingly, fitting the mean curve until 100 s results in an exponent parameter around 0.03, similar to other recent studies. In more detail (McLean, 2015), authors present stress-relaxation of the ACL antero-medial bundle alone. They stated that material presents a nonlinear viscous behaviour because responses were graphically (but it is not known if statistically) different at various strain levels, precisely 6-9-12-18%, much above the strain range investigated by this study. In other researches (Skelley, 2016) and (Castile, 2016), antero-medial and postero-lateral ACL bundles were separated and compared during stress-relaxation at 5% strain. Other authors (Castile, 2016, McLean, 2015 and Pioletti, 2000) reported a greater relaxation (around 30%) respect to the present study, but at longer time-scales where relaxation becomes faster (McLean, 2015). At beginning of the century (Pioletti, 2000), relaxation curves on patellar tendon were also presented. The authors stated that for strain values lower than 16% in the case of ACL and 12% for patellar tendon, the hypothesis of variable separation was valid, as it was confirmed here on the same tissues.

Stress-relaxation curves for patellar tendon were also found in studies of (Johnson, 1994, Johnson, 1996, and Rupp, 2000). In more detail (Johnson 1994, 1996) tests on patellar tendon stress-relaxation at around 1% and 2% of imposed strain have been conducted and it has been found that results were similar, thus the relaxation function was modelled as independent by strain. Fitting their curves until 100 s resulted in an exponent parameter around 0.06, not too distant from the data reported here. Some research as (Rupp, 2000), test relaxation lasted 15 min. The imposed strain level is not clear, but stress relaxed to 80% of the starting value at 120 s, while in this work

it was around 85% at 100s. In other studies as (Atkinson, 1999), patellar tendons were transversally sectioned and relaxed with a 2% imposed strain. Even if relaxation strongly depended by the sample transversal section, the authors presented a rate of relaxation in the range 0.02-0.06, very close to what reported here. Other authors (Donahue, 2001, 2002 and Abramovitch, 2010) report stress-relaxation curves for hamstring tendons. In more detail (Donahue, 2001, 2002), hamstring tendon graft was stretched to 2.5% strain for about 15 min. Fitting the first 100 s with a power-law, it comes out an exponent parameter around 0.04, very close to what found here. Research as (Abramovitch, 2010), shown imposed strain of 2.2% and the tissues at 1h were completely relaxed. With only one strain level, the authors simply assumed a separation between strain and relaxation function. This study can support their assumption in the 1-5% strain range. Moreover, it is stated that human patellar tendon appears to relax more than hamstring tendon, which is more similar to ACL. This study observed a major similarity between tendons, which both relaxed more than ACL, with only a slight faster relaxation in the patellar tendon respect to the hamstring one.

ACL curves for creep were found from in studies of this century (Chu, 2003 and Delcroix, 2013). In more detail (Delcroix, 2013), test was carried out by application of a constant 200 N load, about two times the maximum load reached here for ACL samples, and lasted 300 s. Nevertheless, fitting their data until 100 s resulted in an exponent parameter around 0.03, consistent with the results of this study, as for stress-relaxation. Even if a static load was applied also in research (Chu, 2003), the experimental set-up (in-vivo study, ACL creep estimated via anterior tibial displacement) was too different to compare their results with those found here. It was found only a static creep plot for patellar tendon, specifically some research (Rasmussen, 1994). The tendon was loaded at a constant 90 N load, close to those experienced here at 2% of strain level, for 600 s. Fitting the curve until 100 s results in a exponent parameter around 0.017, inside the deviation range revealed in this study for the corresponding strain level.

Hamstring tendon creep curves were found in the studies (Donahue, 2001) and (Donahue, 2002). Some research (Donahue, 2001, 2002), hamstring tendons underwent creep at a constant 250 N load for about 15 min. Because samples were double looped grafts, that load corresponds approximately to the 2% strain condition of this study. From the curves it comes out a creep rate higher than the one revealed here, even if, on those graphs, the fitting is exposed to a wide margin of error.

Static stress-relaxation and creep were presented in the same study only for ACL and hamstring tendon, respectively in more details (Delcroix, 2013) and (Donahue, 2001, 2002). In none of them there was a correspondence

between loading conditions in stress-relaxation and creep phases, differently from this work. In more detail (Delcroix, 2013), stress-relaxation followed creep, the opposite to this study, and no relation between the two phenomena appears to be investigated. Other researches (Donahue, 2001, 2002) creep followed stress-relaxation, but also there no relation between them was searched.

The literature introduced so far is entirely based on tests on animal tissues and also with a differently significant scale factor compared to human tendons and ligaments.

Therefore in this thesis human tissues were investigated, and it was necessary to develop a specific test protocol. We first attempted to interpret the experimental data with a linear model and only after having confirmed the non-linearity of the creep and relaxation curves obtained did we go in search of a non-linear mathematical model.

The inter-group comparison has a direct impact on the clinical outcome, specifically for what regards the intra-articular graft tissue response. The results from the intra-group comparison (ACL, Hamstring, Patellar, Synthetic) and relaxation-creep interrelation have important impacts on modelling. In particular for the non-linear hereditariness behavior.

The proposed model is discussed in the Chapter 3 sec.3.3 and Chapter 4.

1.3 Results

In this thesis we discussed in detail the non-linear hereditariness of materials, described by means of non-linear fractional calculus, with a single-integral approach. As far as time-varying power-law is considered as integral kernel, then a fractional-order single integral non-linear model is obtained with a three parameters generalized springpot, namely: *i*) non-linear exponent α_c; *ii*) decaying exponent β_c and *iii*) the characteristic time τ_c. The model is completely equivalent to the Nutting relations observed for rubbers and polymers. The single integral model allows for the use of effect superposition of auxiliary state variables, in terms of stress and strain, that account for the position of some equivalence relations among creep and relaxations parameters, namely *i*) non-linear exponent α_r; *ii*) decaying exponent β_r and *iii*) characteristic time; τ_r observed, and verified with a large experimental campaign on several materials. The generalized springpot possesses an equivalent mechanical hierarchy, totally analogous to the well-known mechanical hierarchy already established for the linear springpot, with non-linear internal springs and dashpots. Some numerical examples reporting the behavior of the non-linear hierarchy have been reported in the paper. These aspect are

investigated in Chapter 3.

Based on this observation in the thesis to the introduction of an analytical model to describe creep and relaxation showing that some closed-form expression relating creep and relaxation parameters could be established.

Direct inspection of the results of the analytical estimates and the measured values showed excellent matches with slight coefficient of variations. The match among the values of parameters for creep and relaxation has been found, only for long-standing stress/strain and in order to show that such relations hold whatever kind of test is considered a numerical validation has been introduced with other than constant value of the applied strain (stress), namely linear and harmonically varying strain (stress).

The obtained results showed excellent match among the initial and the recovered value of the applied stress (strain) leading to conclude that the proposed relations represent a benchmark to provide a clinical support to the clinicians that apply pre-stress to the tendons before surgical replacement to reconstruct anterior cruciate ligaments functionality. These aspect are investigated in Chapter 4.

A structural micromechanics corresponding to the non-linear model has been developed previous a physical explanation of the experimental results and the non-linear behavior found in these tissues.

Additionaly, data scattering involved in the experimental measures have been represented with a random model assuming that the characteristic times in creep and relaxation are modelled as random variables with prescribed probability density. The parameters of the density may be obtained by the measured first and second-order statistics of the creep and relaxation obtained from the experimental campaign. Monte-Carlo simulation conducted with the proposed random model shows that first-order statistics obtained with the proposed approach coalesces with the measured data allowing to use the random approach introduced in sec.3.3 for the prediction of the mechanical outcomes in terms of increments of the strain and the decaying of the stress in tendons and ligaments.

Some additional recent findings still in course of investigations have been also reported to show that the non-linear hereditariness of biological fibrous tissue still deserves deep investigations.

Chapter 2

Biomechanics of the Knee

2.1 Anatomical and biomechanical description

The knee is a modified hinge joint,synovial type, which is composed of three functional compartments: the patellofemoral articulation, consisting of the patella, or "kneecap", and the patellar groove on the front of the femur through which it slides; and the medial and lateral tibiofemoral articulations linking the femur, or thigh bone, with the tibia, the main bone of the lower leg [6]. The joint is bathed in synovial fluid which is contained inside the synovial membrane called the joint capsule. The knee permits flexion and extension about a virtual transverse axis, as well as a slight medial and lateral rotation about the axis of the lower leg in the flexed position. The knee joint is called "mobile" because the femur and lateral meniscus move[17] over the tibia during rotation, while the femur rolls and glides over both menisci during extension-flexion [8]. The center of the transverse axis of the extension/flexion movements is located where both collateral ligaments and both cruciate ligaments intersect. This center moves upward and backward during flexion, while the distance between the center and the articular surfaces of the femur changes dynamically with the decreasing curvature of the femoral condyles. The total range of motion is dependent on several parameters such as soft-tissue restraints, active insufficiency, and hamstring tightness It has got six degrees of freedom: three traslations and three rotations. In sagittal axis it has flexion-extension movement, in frontal axis, it has a varus-valgus rotation and whereas in transverse axis there is internal-external rotation; for Flexion-Extension, 3 degrees of hyperextension to 155 degrees of flexion; Varus-valgus, 6-8 deg in extension; Internal-external rotation, 25-30 deg in flexion; Translation Anterior-posterior, 5–10 mm; Compression: 2–5 mm (patellar compression); Medio-lateral, 1-2 mm.

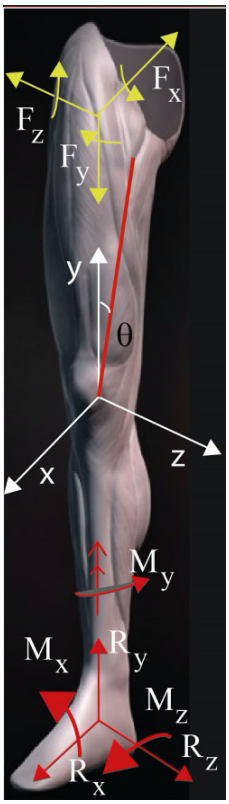

Figure 2.1: Schematic representation of six degree of freedom of the knee

2.2 Soft Tissues

In this section essential features of solid tissues will be discussed. This aspect represents a preliminary illustration of the mechanics of soft tissues discussed in this thesis.

2.2.1 Structure-function properties

The mechanics of biological material is mostly done to its arrangement at molecular level i.e the kind of specific protein that sustains the applied loads. In this regard the the most frequent elements produced by eukaryotic cells are: actin, elastin, and collagen. Collagen will be discussed in greater detail because of its extreme importance to human physiology. Then we shall consider the thermodynamics of elastic deformation, and discuss that there are two sources of elasticity: one associated wit change of internal energy, and another associated with change of entropy. Following this, we move to word the constitutive equations of soft tissues.

Actin molecules are present in all muscles, leukocytes, red blood cells, endothelial cells, and many other cells. The strength of a single actin filament were measured by Kishino and Yanagida (1988). The measurement is based on the fact that a single actin filament ($\sim$ 7 nm in diameter) can be clearly seen by video-fluorescence microscopy. Actin monomers are globular. They polymerize into filaments. Actin filaments labelled with phalloidintetramethyl-rhodamine are stable. Both ends of a single actin filament were caught using two kinds of microneedles connected to micromanipulators under a fluorescence microscope. One of the needles, used for measuring force, was very flexible, and the other, used for pulling actin filaments, was stiff. Before the experiments, the needles were coated with monomeric myosin to increase their affinity with actin. The stiff needle was pulled until the filament broke. Force was calculated from the bending of the flexible needle. For filaments of length 4 to 32 pm, the tensile force of the actin filament was found to be 108 $\pm$ 5 (s.d., $n = 61$) pN without breaking, and almost independent of the filament length. This force is comparable with the force exerted on a single thin element in muscle cells during isometric contraction. The tensile strength of the actin filament is, on assuming a force of 108 pN sustained by a fiber of diameter 7 nm, at least $2.2 \cdot 10^6$ N/m^2, or 2.2 MPa.

Elastin is a protein found in vertebrates. It is present as thin strands in the skin and in areolar connective tissue. It forms quite a large proportion of the material in the walls of arteries and veins, especially near the heart. It is a prominent component of the lung tissue. Elastin is the most "linearly" elastic biosolid materials known. If a cylindrical specimen of elastin is prepared and subjected to uniaxial load in a tensile testing machine, a tension-elongation curve as shown in fig. 2.2: 1 is obtained. The abscissa is the tensile strain defined as the change of length divided by the initial (unloaded) length of the specimen. The ordinate is the stress defined as the load divided by the initial cross-sectional area of the specimen at zero stress: Note that the loading curve is almost a straight line. Loading and unloading do lead to two different curves, showing the existence of an energy dissipation mechanism in the material; but the difference is small. Such elastic characteristics remain at least up to strain, $\lambda = 1.6$.

An example of fibrous tissue involving elastin as main element is the ligamentum nuchae, which runs along the top of the neck of horses and cattle. Specimens for laboratory testing can be prepared from the ligamentum nuchae of ungulates (but cat, dog, and man have very small ligamentum nuchae). These ligaments also contain a small amount of collagen, which can be denatured by heating to $66°C$ or above. Heating to this degree and cooling again does not change the mechanical properties of elastin.

The function of the ligamentum nuchae in the horse is clear: it holds up

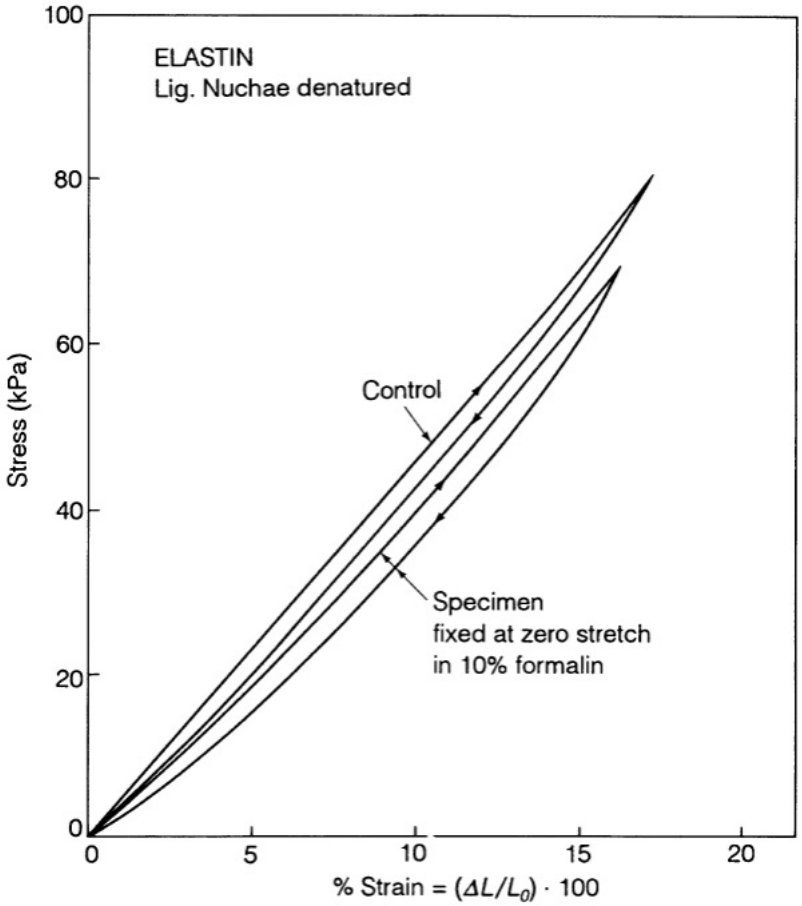

Figure 2.2: The stress-strain curve of elastin

the heavy head and permits its movement with little energy cost. If the horse depended entirely on muscles to hold its head up, energy for maintaining tension in the muscle would be needed. Elastin in the arteries and lung parenchyma provides elasticity to these tissues. In skin it keeps the tissue smooth. In humans it is known that the gene responsible for synthesizing elastin is turned off at puberty.

One particular property of elastin has probably had a profound influence on our knowledge of anatomy and histology. In the microscopic examination of a tissue, the tissue is usually fixed by formalin, formaldehyde, or glutaraldehyde; then embedded, sectioned, and stained. Elastin cannot be fixed: when elastin is soaked in these fixation agents for a long period of time, (hours, days, or weeks), it retains its elasticity. If an elastin specimen is stretched under tension and then soaked in these agents, upon release of the tension the specimen does not return to its stretched length entirely, but it can recover $40\% - 70\%$ of its stretch (depending on the degree of stretch), and then still behave elastically.

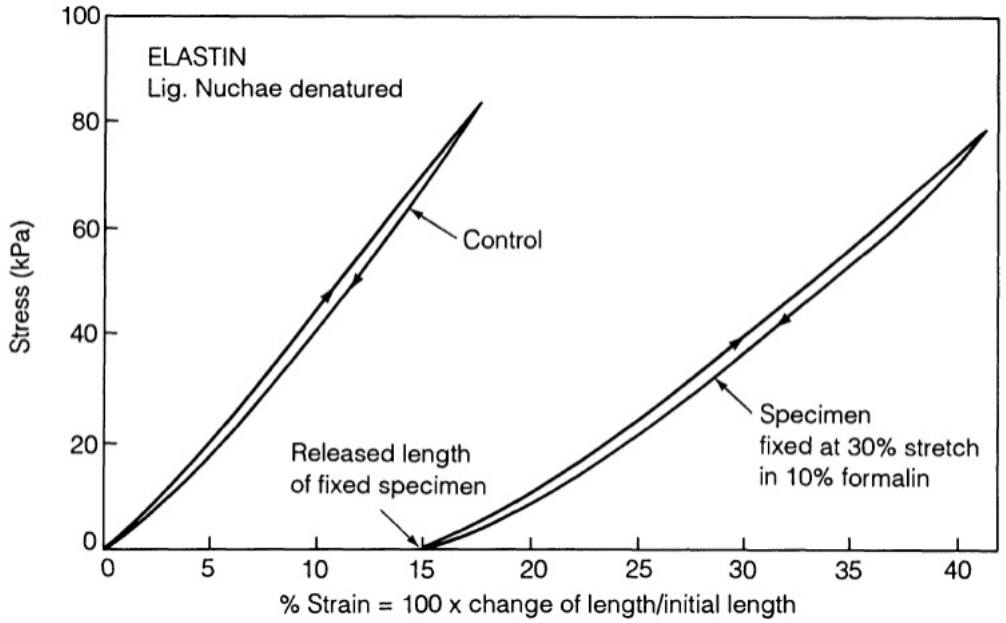

Figure 2.3: The stress-strain curve of a specimen of elastin that was first stretched 30% and then soaked in 10% formalin for two weeks.

An example is shown in fig.2.3 which refers to a specimen that was stretched to a length 1.3 times its unstressed length, soaked in formalin for two weeks, and released and tested for its stress-strain relationship. It is seen that the "fixed" specimen behaves elastically, although its Young's modulus

is somewhat smaller. If the strain (stretch ratio minus one) at which a specimen is stretched while soaked in the fixative agent is plotted against the retained strain after the "fixed" specimen is released (stress-free), we obtain fig.2.4. In this figure the abscissa shows the initial stretch during fixation, and the ordinate shows the retained stretch upon release. It is seen that elastic recovery occurs in elastin at all stretch ratios. In other words, what is commonly believed to be "fixed" is not fixed at all.

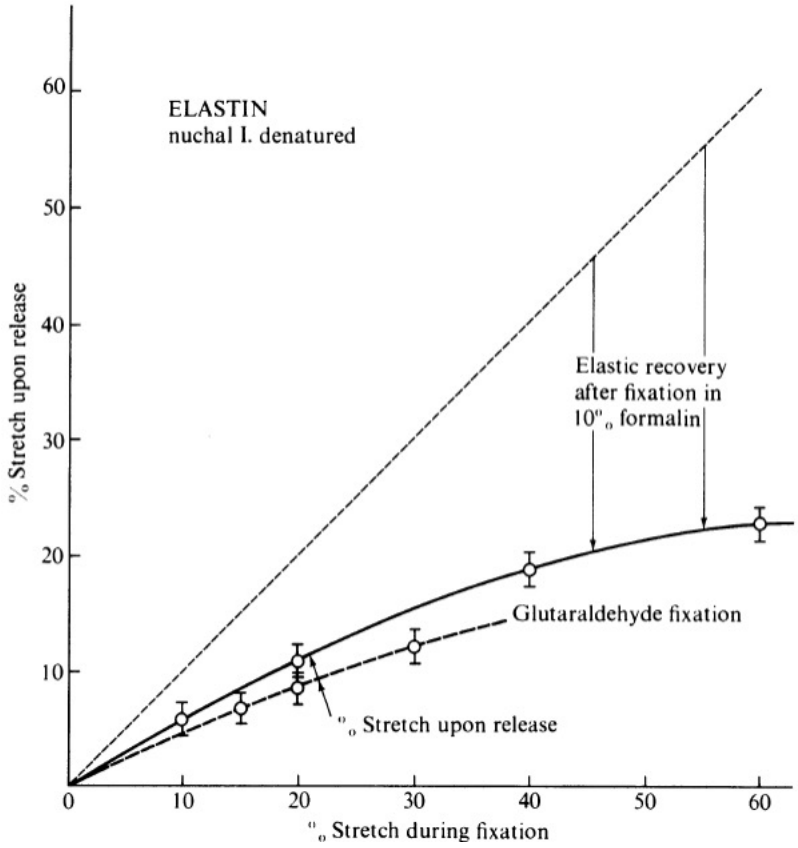

Figure 2.4: Elastic recovery of elastin after fixation in formalin and glutaraldehyde solutions.

Now if a tissue is fixed in one of these fixing agents in a state of tension, e.g., an inflated lung, or a distended artery (as these organs are usually fixed by perfusion), and then sectioned under no load, the residual stress in the elastin fibers will be released, and the length of the elastic fibers will be shortened to its length at zero stress state. The fixed part of the tissue, which is inextensible, will be buckled (wrinkled) by the shortening of the elastin. As a consequence the tissue would appear buckled and un-

even. The molecular structure of the tropoelastin, a precursor molecule of elastin, has been sequenced (Bressan et aI., 1987; Deak et aI., 1988; Indik et aI., 1987; Raju et aI., 1987; Tokimitsu et aI., 1987; Yeh et aI., 1987). Mecham and Heuser (1991) have shown that tropoelastin is formed intracellularly and then crosslinked extracellularly. The mature, cross-linked elastin molecule is inert and so stable that in normal circumstances it lasts in the body for the entire life of the organism. Repeating sequences in elastin molecule have been noted, and some of their analogs have been prepared chemically, and studied thermo-mechanically. Of these, poly (V PG VG), poly (V PG F GV GAG), and poly (VPGG) on y-irradiation cross-linking have been shown to be elastic. Urry (1991, 1992) and his associates have shown that these polypeptides will self-assemble into more ordered molecular assemblies on raising temperature, i.e., they exhibit inverse temperature transitions. The molecular proocesses that correspond to the entropic elastomeric force in the self-assembling (nonrandom) systems have been studied in detail. Urry has invented some new bioelastic proteinbased polymers on the basis of this research. He has also broadened the view that this inverse temperature transitions is a basic mechanism of biological free energy transduction.The sources of elasticity of elastin, like those of other soft tissues, must be a decrease of entropy, or an increase of internal energy with increasing strain.Hoeve and Flory (1958) explained elastin elasticity on the entropy theory. Urry (1985,1986) identified a mechanism of libration or rocking of some peptide segments that contributes to the entropy. The selfassembling mechanism discussed by Urry (1991) has a critical temperature in the order of 25°C, above which more ordered aggregation forms. Hence Urry predicts a decrease of elasticity at temperature lower than about 25°C. He verified the phenomenon in the synthesized polypentapeptide named above. Debes and Fung (1992) examined the critical temperature problem very carefully in the lung tissue (parenchyma) of the rat, and did not find any critical temperature associated with a sudden change of mechanical properties. One may conclude that the inverse temperature transition phenomenon identified by Urry for a synthetic analog of a part of the elastin molecule may not be a major mechanism for the whole elastin. Other models of elastin elasticity are proposed by Partridge (1969), Gray (1970), Weisfogh and Anderson (1970), Gosline (1978), and Fleming et al. (1980).

2.2.2 Mechanical properties of tissue components

Elastin, resilin, and abductin, like rubber, are constituted of long flexible molecules that are joined together here and there by cross-linking to form three-dimensional networks. The molecules are convoluted and thermal en-

ergy keeps them in constant thermal motion. The molecular configurations, hence the entropy, change with the strain. With this interpretation, Treloar (1967) showed that the shear modulus, G, is related to the density of the material, ρ, the average value of the weight of the piece of molecule between one cross-link and the next, M, and the absolute temperature, T, according to the formula

$$G = \frac{\rho RT}{M} \tag{2.1}$$

where R =gas constant $= 8.3 \cdot 107$ erg/deg mol. The Young's modulus is related to the shear modulus G by the formula

$$E = 2(1 + \nu)G \tag{2.2}$$

where ν is the Poisson's ratio. If the material is volumetrically incompressible so that $\nu = \frac{1}{2}$, then $E = 3G$. In using the formula above for rubbery protein, ρ is the concentration of the protein in g/cm^3 of material. Water contributes to density, but not to shear modulus, hence its weight should be excluded from p. This formula is probably correct for those proteins which are already diluted with water at the time they were cross-linked. There is a different rule for materials that were not diluted until after they had been cross-linked. In the latter case, the dilution then stretches out the molecules so that they are no longer randomly convoluted. Rubber swollen with paraffin is such an example. Crystalline materials derive their elastic stress from changes in internal energy. Their elastic moduli are related to the strain of their crystal lattices. Equation (2.1) does not apply to crystalline materials, neither does it apply to fibers whose elasticity comes partly from internal energy changes and partly from entropy changes. Most biological materials that can sustain finite strain have rubbery elasticity. For example, hair can be stretched to 1.7 times its initial length, and will spring back, but this is because the protein keratin, of which it is made, can exist in two crystalline forms-one with tight α helices, and one with looser, β helices [23, 44]. When hair is stretched, some of the α helices are changed into β helices.

Material	Young's modulus (MPa)	Tensile strength (MPa)
Resilin	1.8	3
Abduction	1–4	
Elastin	0.6	
Collagen (along fiber)	1×10^3	50–100
Bone (along osteones)	1×10^4	100
Lightly vulcanized rubber	1.4	
Oak	1×10^4	100
Mild steel	2×10^5	500

Figure 2.5: Mechanical Properties of Some Common Materials

Table in fig. 2.5 gives the average values of the Young's modulus and tensile strength for several common materials.

Collagen is a basic structural element for soft and hard tissues in animals. It gives mechanical integrity and strength to our bodies. It is present in a variety of structural forms in different tissues and organs. Collagen is the main load carrying element in blood vessels, skin, tendons, cornea, sclera, bone, fascia, dura mater, the uterian cervix, etc. The mechanical properties of collagen are therefore very important to biomechanics. We must study not only collagen molecules, but also how the molecules wind themselves together into fibrils, how the fibrils are organized into fibers, and fibers into various tissues. In each stage of structural organization, new features of mechanical properties are acquired. Since in physiology and biomechanics, our major attention is focused on the organ and tissue level, we must study the relationship between function and morphology of collagen in different organs. A collagen is defined as a protein containing sizable domains of triple-helical conformation and functioning primarily as supporting elements in an extracellular matrix. The individual chains are left-handed helices with approximately three residues per turn. The chains are, in turn, coiled around each other following a right-handed twist with a pitch of approximately 8.6 nm. The three α chains are arranged with slight longitudinal displacements. The amino acids within each chain are displaced by a distance of 0.291 nm, with a relative twist of $-110°$, making the distance between each third glycine 0.873 nm. To date 12 types of collagen have been identified. Figure 2.7 shows three types of collagen. The α chains of Type I are designated as $\alpha 1$(I), $\alpha 2$(I), etc.

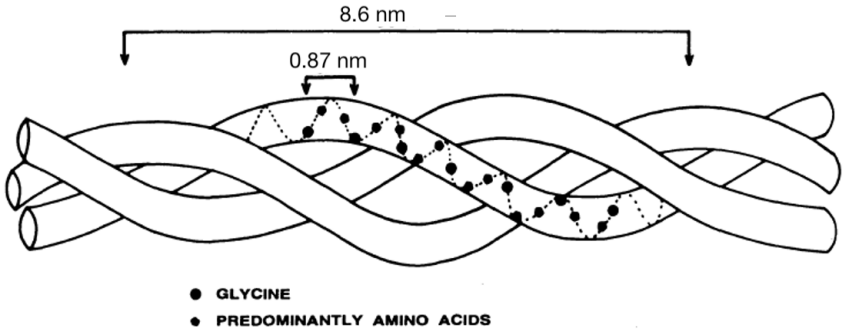

Figure 2.6: Schematic drawing of collagen triple helix

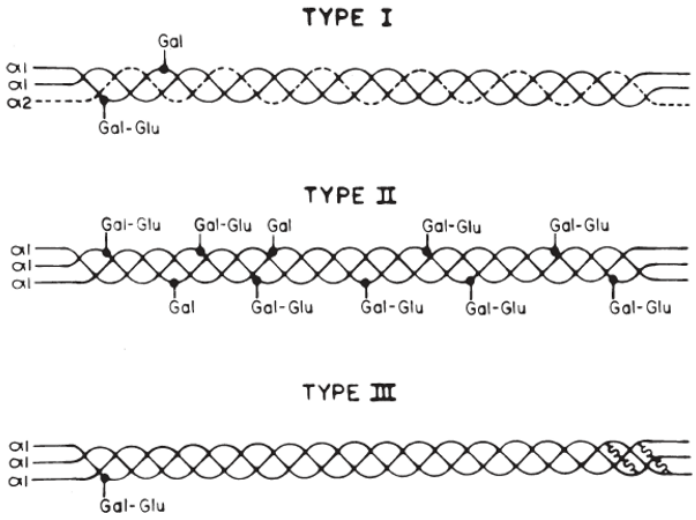

Figure 2.7: three types of collagen that differ in the arrangement of the chains, where Gal is galanin and Glu is glutamic acid

The close relation of function and structure of collagen aggregates, according to E. J. Miller (1988), is shown in fig. 2.8. (A) shows the fiber-forming collagens of Types I, II, III, V, and K. (B) shows Type IV collagen, which is a major constituent of basement membranes. (C) shows type VI collagen, which is prevalent in placental villi. (D) shows Type VII collagen, whose distribution is unknown, but has been isolated from placental membranes.

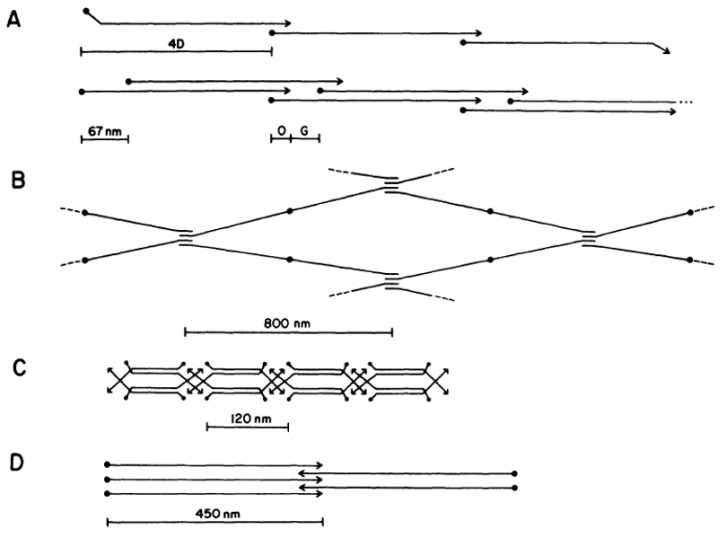

Figure 2.8: Molecular architecture of the aggregates

Type I collagen is virtually ubiquitous in distribution. It can be isolated from virtually any tissue or organ, especially the bone, dermis, placental membranes, and tendon. Type II is located chiefly in hyaline cartilag, and cartilage-like tissues such as the nucleus pulposus of the vertebral body, and vitreous body of the eye. Type III collagen, along with Type I, is a major constituent of tissues such as the dermis and blood vessel walls, and other more distensible connective tissues. It is also ubiquitous. Type V is a relatively minor constituent in any tissue or organ, but has a distribution similar to that of Type I. Type K, which is XI, is distributed like Type II, chiefly in cartilage. Two ofthe chains of Type K collagen are highly homologous to those of Type II. The collagens of Types IX and X are minor constituents of hyaline cartilages. The are called short-chain collagens because their polypeptide chains are shorter than those of fibrillar procollagens. Type IX collagen molecules contain three relatively short triple-helical domains connected by non triplehelical sequences, instead of a single, long triple-helical domain found in fibrillar collagens. Type IX collagen is also a proteoglycan in that one of its polypeptide subunits serve as the core protein for a chondroitin sulfate side chain. A collagen homologous to Type IX [50] and is named collagen Type XII. The structure, function, and distribution of Type IX/XII [14]. It is suspected that the Type IX/XII class of molecules playa major role in the assembling of collagen fibrils.

Consider first the fiber-forming collagen molecules. A collection of tropocollagen molecules forms a collagen fibril. In an electron microscope, the colla-

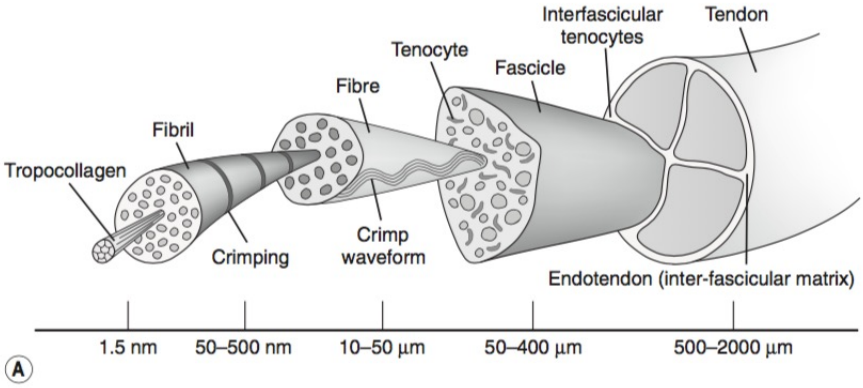

Figure 2.9: Tendon hierarchical structure

gen fibrils appear to be cross-striated. The periodic length of the striation, D, is 64 nm in native fibrils and 68 nm in moistened fibrils. The diameter of the fibrils varies within a range of 20 to 40 nm, depending on the animal species and the tissue. Bundles of fibrils form fibers, which have diameters ranging from 0.2 to 12 μm. Packaging of collagen fibers has many hierarchies, depending on the tissue. In parallel-fibered structures such as tendon, the fibers are assembled into primary bundles, or fascicles, and then several fascicles are enclosed in a sheath of reticular membrane to form a tendon.

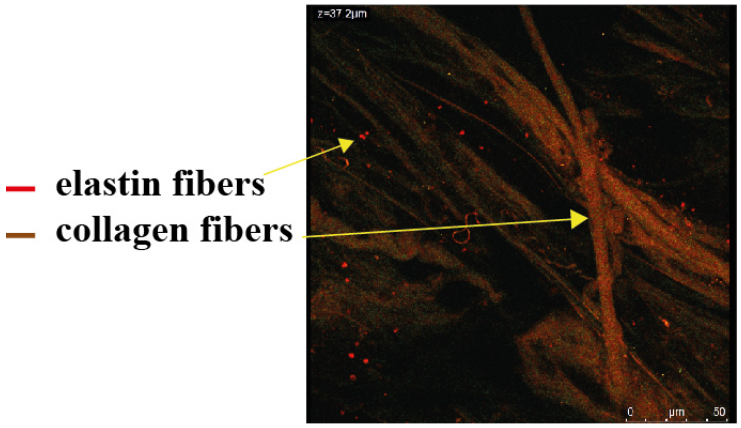

Figure 2.10: Multiphoton imaging of human patellar tendon at the tibial insection, Bioimaging lab, @ATen Center

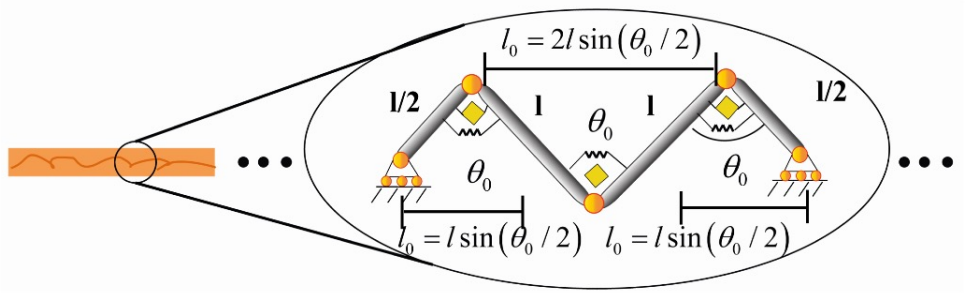

Figure 2.12: schematic crimping of the fiber

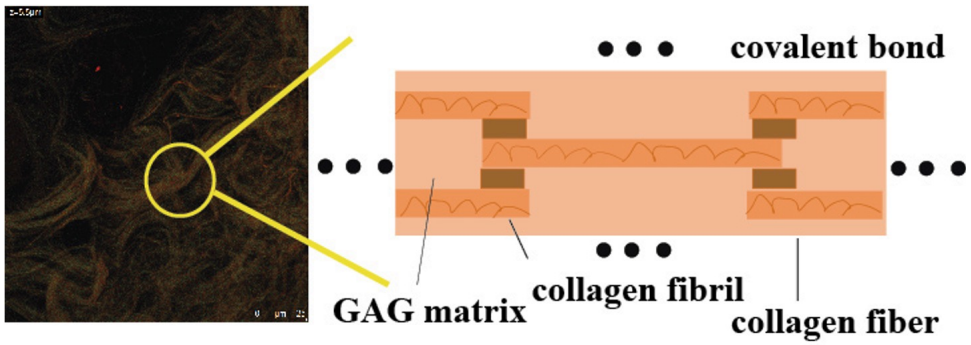

Figure 2.11: hierarchical structure of the fiber

When the tendon was teased down to fine bundles, it was observed that the physical outlines of these subbundles followed the waveform that was deduced from the polarizing optics of the intact tendon bundle. As the fiber is stretched, the "bending angle," θ_0, decreases and tends to zero when the fiber is straight.

Thus the basic mechanical units of a tendon are seen to be bent collagen fibers. The question arises whether the fibers are intrinsically bent because of some fine structural features of the fibrils. Gathercole (1974), using SEM to resolve the individual collagen fibrils about 100 nm in diameter as they follow the waveform in a rat's tail tendon, failed to find any specific changes in morphology and fine structure along the length of the waveform. It is then suggested that the curvature of the fibers might be caused by the shrinking of the noncollagen components or "ground substance" of the tendon, i.e., that the curvature is caused by the buckling of the fibers. This suggestion is consistent with the experience that the integrity of the ground substance is of great importance to the mechanical integrity of the tendon. Enzymatic

digestion directed at the noncollagen components can greatly change the mechanical properties of the tendon. The buckling model was investigated [27], and it was suggested that hyaluronic acid, which is a major space filling material and which has a fairly high metabolic turnover rate, may be responsible for the buckling of the collagen fibers. In some connective tissues, it has been suggested that elastin and collagen together form a unit of composite material. The straight elastic fibers are attached to the bent collagen fibers.

An original contribution in the field of fibril mechanics developed in the course of the thesis involved hyaluronic acid with mechanical test and imaging analysis. Hyaluronic acid (HAHMW, 1025 kDa) was purchased from Altergon (Italy). HA (Mw, 280 kDa, PDI, 1.9) and its tetrabutylammonium salt were produced as reported elsewhere [76]. HA-EDA-C_{18} derivative (Mw 320 kDa PDI 1.8) having 12±3 mol % of EDA and 30±0.5 mol % of C_{18} was synthesized and characterized as elsewhere reported Mechanical characterization of fibers bundles was performed by using a Nanotensil T150 UTM instrument. Fibers were observed by using an Zeiss Axiovert Microscope and by a confocal microscope Olympus FluoViewFV10i. Live and Dead assay was performed by using the Calcein AM, ethidiumhomodimer-III (Eth-III). SEM images of freeze-dried fibers bundles was performed by using a Phenom Tabletop SEM apparatus, while SEM pictures of AoSMC seeded fibers bundles was performed by using a SEM Quanta feg 650 FEI. In this latter case fibers were gold sputtered before the analysis. HPLC analysis was performed using an Agilent 1260 Infinity. Just after production circular bundles were transferred into a NaCl 0.9 % w/v 0.15 M and left overnight. Bundles, were stored into NaCl 0.9 % w/v if used for further characterization as wetted fibers, otherwise were cut and outstretched longitudinally to maintain fibers alignment, then freeze dried. Dried aligned fibers were then stored until their utilization. Mechanical properties of bundles were evaluated by elongation tests at rupture using a Nanotensil T150 UTM equipment. In particular unfunctionalized HA-EDA-C_{18}, composite HA-EDA-C_{18}/fibronectin, cyRGDC functionalized bundles were all collected as described before then cut and elongated to obtain cylindrical shaped bundles of about 8 cm in length with a diameter comprised between 1 and 1.3 mm. Bundles were then fixed at rhomboidal specimens maintaining a distance between grips of about 60 mm. Elongation was performed at 5 x 10-3 1/s to a maximal deformation 0.4 mm/mm. Results were expressed as a mean of n=6 different measurements indicating mean bundles diameter and mean elastic modulus (E; KPa) ± standard deviation. Bundles were characterized from a mechanical point of view comparing elastic moduli of the three different batches, i.e. non-functionalized, fibronectin loaded and cyRGDC functionalized bundles. The mechanical characterization has involved a sequence of mechanical tests with

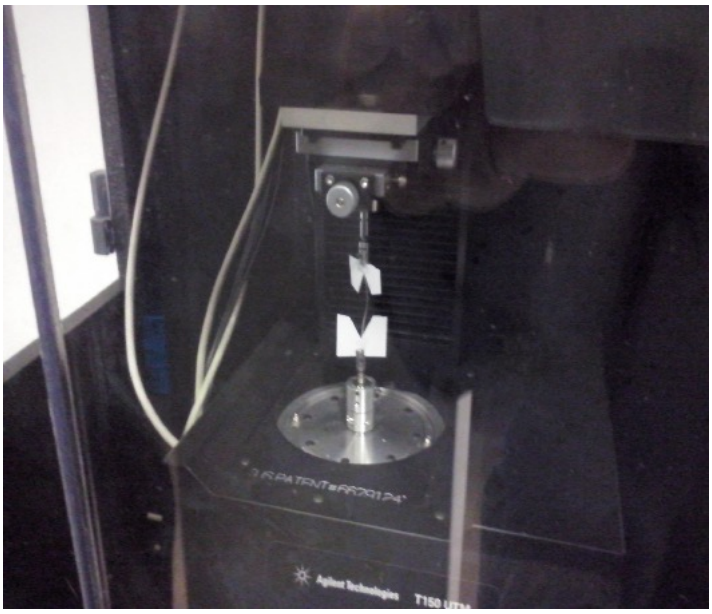

Figure 2.13: Nanotensile T150 UTM equipment with sample. @ATen Center, Bio/nano Mechanics laboratory for medical science

six samples for each kind and measuring the diameter of the fibers, assumed with circular cross-section, with a digital caliper. The fibers have been glued to paper-based templates to achieve the prescribed initial length and to avoid fiber damage close to the clamps of the machine. A specific picture of the apparatus and experimental set-up employed for the mechanical test has been reported in fig.2.13. The mechanical properties have been measured in terms of engineering stress and strains obtained as $\varepsilon = D_0/L_0$ and $\sigma = F/A_0$ where D_0 is the displacements among the clamps that is prescribed and F is the load measured by the force transducer of the equipment. The geometrical parameters, namely the reference length L_0 and the nominal cross-section A_0 have been measured at the beginning of the test. The graphical results of the mean monotone stress-strain curves have been reported in fig 2.15 for all investigated samples. Data of the stress-strain test reported in fig.2.14 show that the presence of fibronectin caused a decrease in the elastic modulus of the HA-EDA-C_{18} fibers; on the contrary cyRGDC functionalization caused a sharp increase in the elastic modulus (E= 76.7 kPa compared to 9.1 kPa of the non-functionalized bundle).

As shown in Figure 2.16, according to previous results [23,24] the HA-EDA-C_{18} non-functionalized bundles were poorly suitable to allow cell adhesion. AoSMCs remained round shaped on nonfunctionalized and fibronectin loaded bundles, moreover after 6 days cells became detached. Optical micro-

Batch of Bundle	*Mean Diameter (n=6)*	*Elastic Modulus (KPa)*
HA-EDA-C_{18}	1225 ± 83	9.1 ± 2.3
HA-EDA-C_{18}/fibronectin	1141 ± 123	2.4 ± 1.5
cyRGDC functionalized	1150 ± 198	76.7 ± 20

Figure 2.14: Values of elastic modulus (E) found for microfibrillar bundles unfunctionalized HA-EDA-C_{18}, fibronectin loaded and cyRGDC functionalized. Palumbo, F. S., et al. "Multifibrillar bundles of a self-assembling hyaluronic acid derivative obtained through a microfluidic technique for aortic smooth muscle cell orientation and differentiation." Biomaterials science 6.9 (2018): 2518-2526.

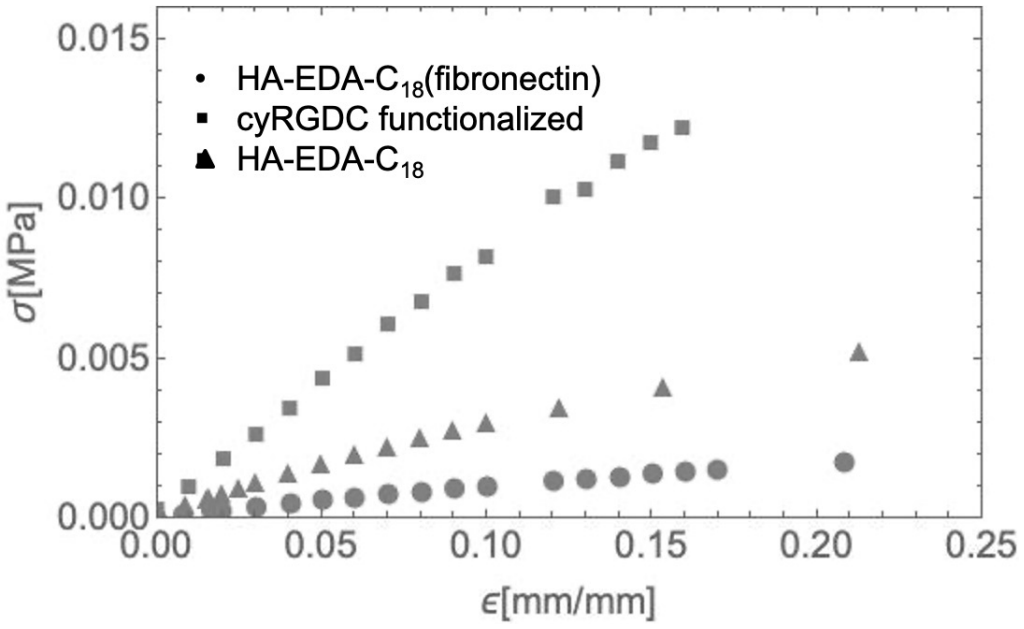

Figure 2.15: Stress/strain curves for microfibrillar bundles unfunctionalized HA-EDA-C_{18}, fibronectin loaded and cyRGDC functionalized. Palumbo, F. S., et al. "Multifibrillar bundles of a self-assembling hyaluronic acid derivative obtained through a microfluidic technique for aortic smooth muscle cell orientation and differentiation." Biomaterials science 6.9 (2018): 2518-2526.

scope images showed that microfibers of non-functionalized and fibronectin loaded bundles swelled significantly from 1 to 6 days of culture. AoSMCs became instead attached and elongated on microfibers of cyRGDC functionalized bundles already after 2 days of culture. These Confocal microscopy of elongated cells on cyRGDC functionalized bundles performed after 6 days, confirmed attachment, elongation and alignment of AoSMCs, fig.2.16 Taking into account these preliminary interesting results, a long term biological characterization has been also performed for cyRGDC functionalized bundles. In particular, viability of AoSMCs during 21 days of culture on cyRGDC functionalized bundles was qualitatively evaluated by a Live and Dead cell assay. Before cell seeding, pieces of bundles were messed up to allow maximum interaction with the seeded cells. Cells appeared almost all viable (green) and just few dead cells (red) were observed after 1 day from seeding fig.2.18A. Hence viable cells attached to microfibers, maintained their viability after 7, 14 and 21 days. The distribution of cells and their alignment were evaluated by confocal microscopy on individual microfibers fig.2.18B). After 7 days, the cells appeared randomly distributed on microfibers, most of which appeared aligned while other cells were crossing between adjacent microfibers. Already after 14 days fibers appeared uniformly covered by elongated cells having a quite good orientation. After 21 days cells increased their stretching and actin myofilament were well visible and elongated; multinucleate muscle fibers were visible and Z stack analysis, fig.2.17, showed a uniform distribution of cells along the fiber. As evidenced by SEM analysis fig.2.19 after 21 days of culture with AoSMCs, cyRGDC functionalized HA-EDA-C_{18} bundles appeared compact with well-aligned microfibers attached one another. On the surface of the fibers it is possible to observe several elongated and aligned AoSMCs. Another batch of bundle was cut longitudinally into two hemicylinders using a surgical blade and observed. Each fiber appears uniformly colonized by AoSMCs elongated and aligned with the orientation of the fibers. Immunostaining on bundles cultured for 21 days with AoSMCs showed desmin and HC-myosin positive cells, thus suggesting the maintenance of contractile phenotype of differentiated myotubes fig.2.20. Confocal analysis confirmed the quite good orientation of cells.

To reproduce the organization of muscle tissue, these scaffolds should be organized into 3D microfibrillary constructs, in which each microfiber should allow the orientation of the SMCs. Several production techniques have been proposed for the engineering of complex 3D biomaterials and to meet the requirements for regenerative medicine of smooth muscles, tendons and ligaments. The strong reduction of the elastic modulus observed for the fibronectin/HA-EDA-C18 bundle suggests that a homogeneous interpenetration of the protein and the polysaccharide derivative has occurred. It

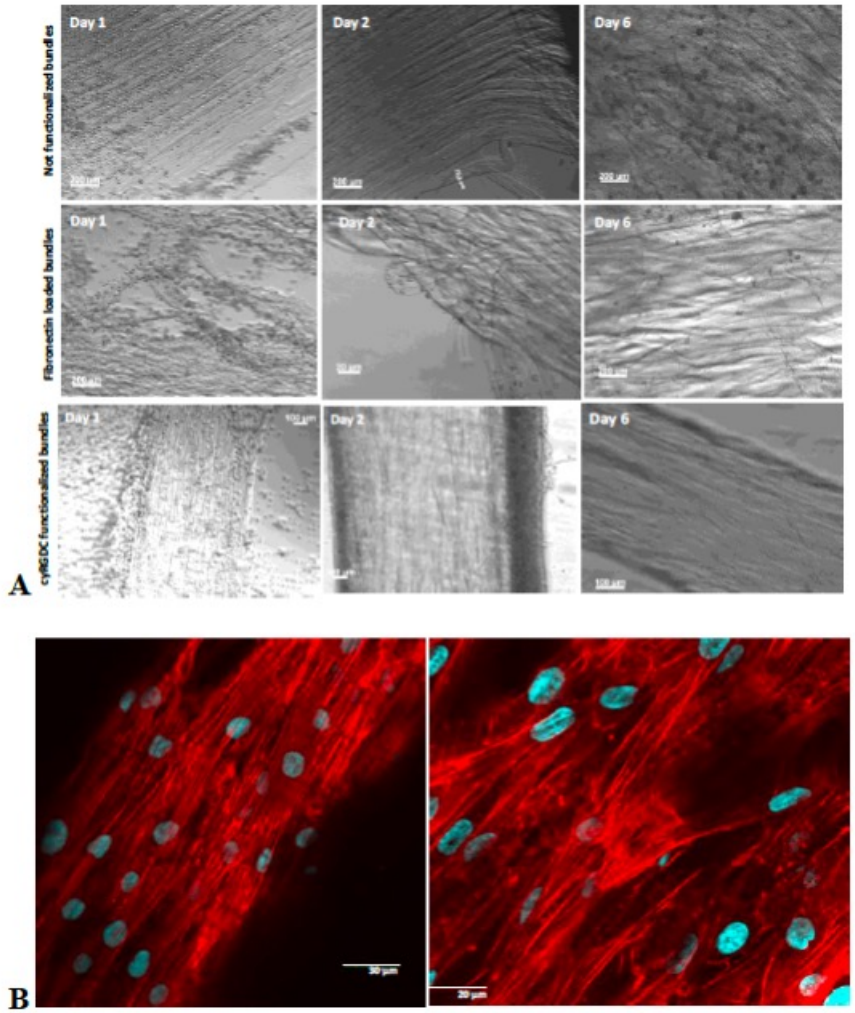

Figure 2.16: A. Optical microscope images taken on non-functionalized, fibronection loaded, cyRGDC functionalized HAEDA- C_{18} bundles after AoSMCs seeding at 1, 2 and 6 days of culture. B. Confocal microscope images of AoSMCs on cyRGDC functionalized HA-EDA-C_{18} bundle after DAPI and Alexa fluor-Phalloidin staining after 6 days of culture. Palumbo, F. S., et al. "Multifibrillar bundles of a self-assembling hyaluronic acid derivative obtained through a microfluidic technique for aortic smooth muscle cell orientation and differentiation." Biomaterials science 6.9 (2018): 2518-2526.

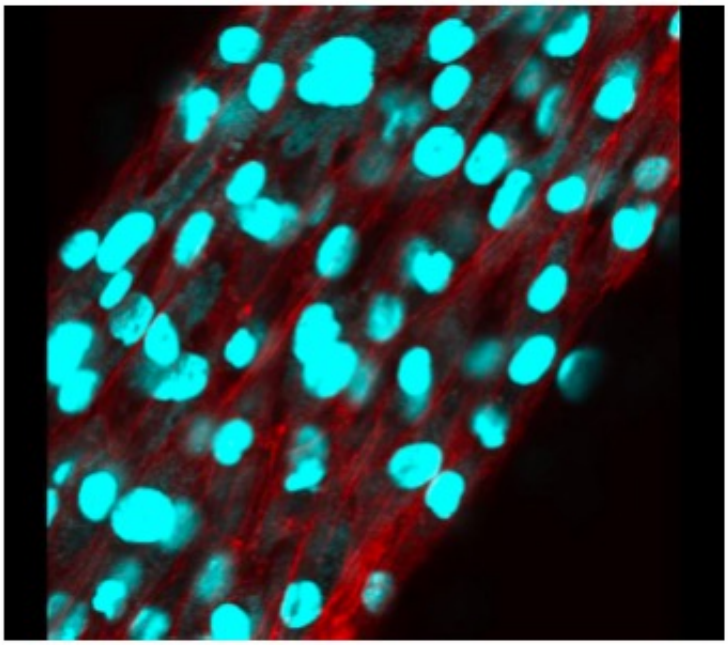

Figure 2.17: Z stack analysis performed after 6 days. Palumbo, F. S., et al. "Multifibrillar bundles of a self-assembling hyaluronic acid derivative obtained through a microfluidic technique for aortic smooth muscle cell orientation and differentiation." Biomaterials science 6.9 (2018): 2518-2526.

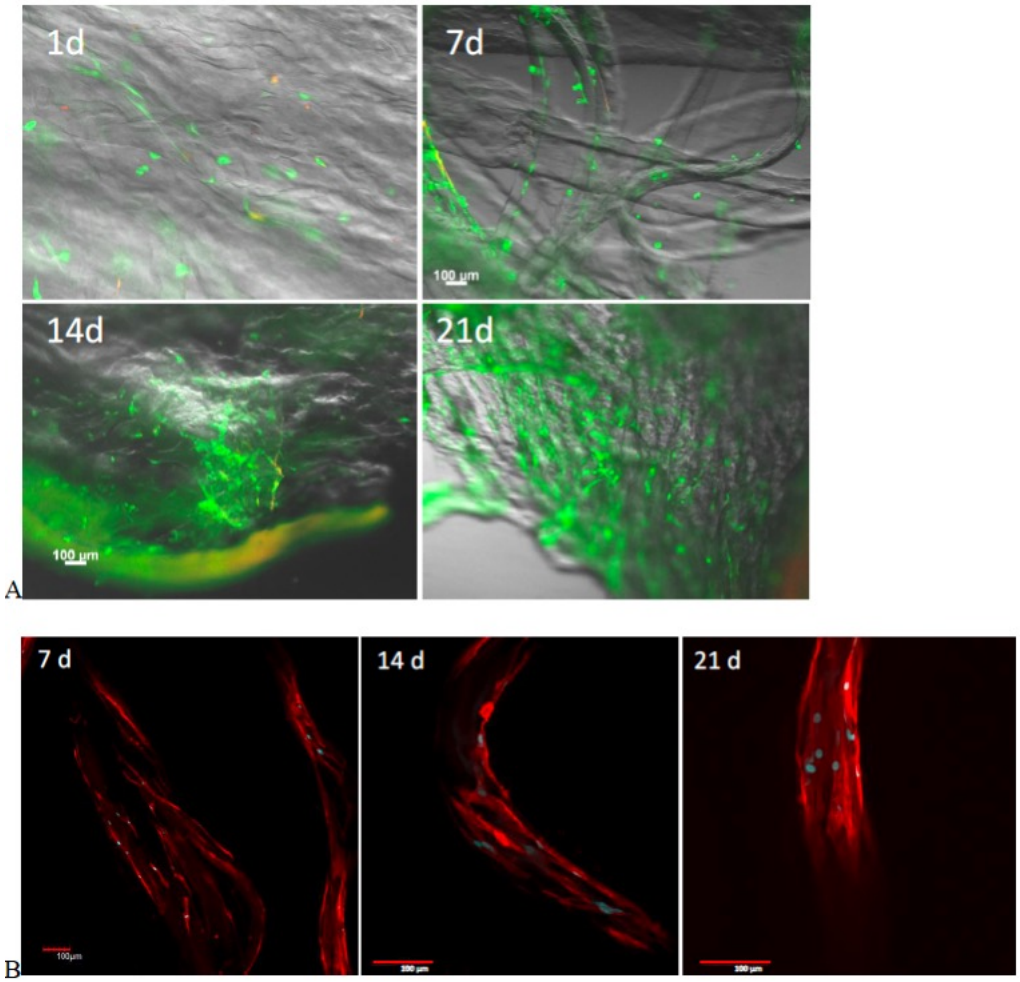

Figure 2.18: A. Live and Dead assay on cyRGDC functionalized HA-EDA-C18 bundles. Viability of AoSMCs assayed after 1, 7, 14 and 21 days from culture; viable (green) and dead (red) cells are visible. B. Confocal microscopy images performed on cyRGDC functionalized bundles after 7, 14 and 21 days of culture. Palumbo, F. S., et al. "Multifibrillar bundles of a self-assembling hyaluronic acid derivative obtained through a microfluidic technique for aortic smooth muscle cell orientation and differentiation." Biomaterials science 6.9 (2018): 2518-2526.

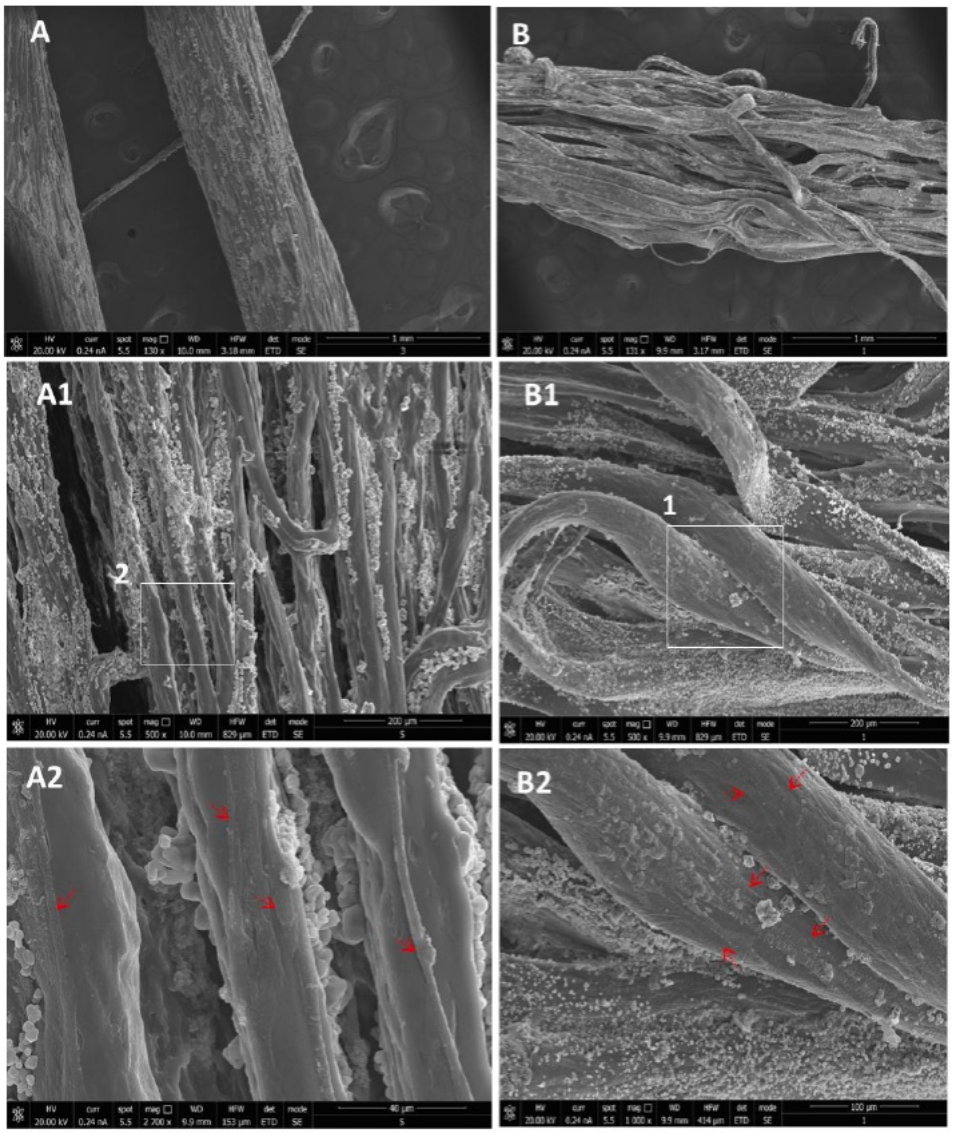

Figure 2.19: SEM analysis on cyRGDC functionalized HA-EDA-C_{18} bundles after 21 days of culture with AoSMCs. Images at different magnifications. of the external surface of bundle (A, A1 and A2) or its internal fibers (B, B1 and B2) after longitudinal sectioning. The arrows highlight some AoSMCs.Palumbo, F. S., et al. "Multifibrillar bundles of a self-assembling hyaluronic acid derivative obtained through a microfluidic technique for aortic smooth muscle cell orientation and differentiation." Biomaterials science 6.9 (2018): 2518-2526.

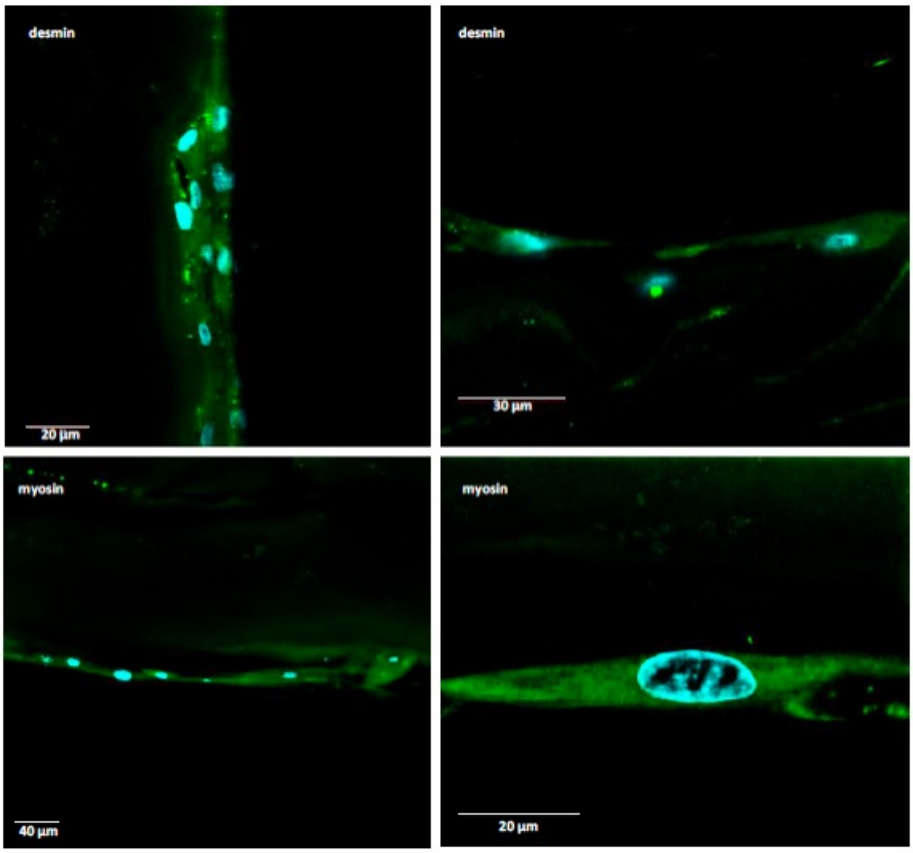

Figure 2.20: Desmin and HC-myosin staining of aligned AoSMCs on cyRGDC functionalized HAEDA- C_{18} bundle after 21 days of culture. Palumbo, F. S., et al. "Multifibrillar bundles of a self-assembling hyaluronic acid derivative obtained through a microfluidic technique for aortic smooth muscle cell orientation and differentiation." Biomaterials science 6.9 (2018): 2518-2526.

is presumable to suppose that the interpenetration decreases the stiffness of the fibers by increasing the extensibility of the bundle and decreasing the elastic modulus. The interpenetration of fibronectin with HA-EDA-C_{18} was also confirmed by the very low release of protein observed in vitro. The elastic modulus of cyRGDC functionalized bundle significantly increases when compared with the non-functionalized and fibronectin loaded samples. This result can be attributed to the partial inter-chain crosslinking that occurs between parts of the maleimido functionalities with pendent amino groups of the HA. Moreover, even the interpenetration of fibronectin did not produce improvements on cell attachment, in fact only a few round-shaped cells remained on the fibers after 2 days. Like the nonfunctionalized samples, the bundles loaded with fibronectin appeared visibly swollen, reaching after 6 days diameters up to 100 μm. The amount of interpenetrated fibronectin was not sufficient to mediate cell adhesion and, more importantly, did not improve fiber stability when compared to non- functionalized bundles. Instead, cyRGDC functionalized bundles have improved cell attachment according to previous results.

Collagen fibers are integrated with cells and intercellular substance in a tissue. In a dense connective tissue, the cells are mostly fibrocytes; the intercellular substance consists of fibers of collagen, elastin, reticulin, and a hydrophilic gel called ground substance. Dense connective tissues contain a very small amount of ground substance; loose connective tissues contain a lot. The composition of the ground substance varies with the tissue, but it contains mucopolysaccharides (or glycosaminoglycans), and tissue fluid. The mobility of water in the ground substance is a problem of profound interest in biomechanics, but it is an extremely complex one. The hydration of collagen, i.e., the binding of water to the collagen molecules, fibrils, and fibers, is also an important problem in biomechanics with respect to the problem of movement of fluid in the tissues, as well as to the mechanical properties of the tissue.

Depending on how the fibers, cells, and ground substance are organized into a structure, the mechanical properties of the tissue vary. The simplest structure, from the point of view of collagen fibers, consists of parallel fibers, as in tendon and ligaments. The two- and three-dimensional networks of the skin are more complex, whereas the most complex are the structures of blood vessels, intestinal mucosa, and the female genital tracts. Let us consider these briefly. The most rigorously parallel-fibered structure of collagen is found in each lamina of the cornea. In adjacent laminae of the cornea, the fiber orientation is varied. The transparency of the cornea depends on the strict parallelism of collagen fibers in each lamina. Tissues whose function is mainly to transmit tension can be expected to adopt the parallel-fiber stru-

cure. Tendon functions this way, and is quite regularly parallel fibered. The fiber bundles appear somewhat wavy in the relaxed condition, but become more straight under tension. A joint ligament has a similar structure, but is less regular, with collagen fibers sometimes curved and often laid out at an angle oblique to the direction of motion. Different collagen fibers in the ligament are likely to be stressed differently in different modes of function of the ligament. Most ligaments are purely collagenous, the only elastin fibers being those that accompany the blood vessels. But the ligamenta flava of the spine and ligamentum nuchae of some mammals are mostly elastin. A ligament has both ends inserted into bones, whereas a tendon has only one insertion. The transition from ligament to bone is gradual; the rows offibrocytes are transformed into groups of osteocytes, first arranged in rows and then gradually dispersed into the pattern of the bone, by way of an intermediate stage, in which the cells resemble chondrocytes. The collagen fibers are continuous and can be followed into the calcified tissue. The transition from a tendon into a bone is usually not so distinct; the tendon inserts broadly into the main fibrous layer of the periosteum. The other end of a tendon is joined to muscle. Generally the tendon bundles are invaginated into the ends of the muscle fibers in the many terminal indentations of the outer sarcolemmal layer. Recent investigation suggests that collagenous fibrils, which are bound to the plasma membranes as well as to the collagen fibers, provide the junction. Parallel fibers that are spread out in sheet form are found in those fasciae into which muscle inserts, or in those expanded tendons called aponeuroses, which are membraneous sheets serving as a means of attachment for flat muscles to the bone. The tendinous center of the diaphragm is similarly structured. These sheets appear white and shiny because of their tight structure. Other membranes that contain collagen but the fibers of which are not so regularly structured are opaque. To this group belong the periosteum, perichondrium, membrana fibrosa of joint capsules, dura mater, sclera, some fasciae, and some organ capsules. The cells in these membranes are irregular both in shape and in arrangement.

The structure of collagen fibers in the skin is more complex, and must be considered as a three-dimensional network of fibrils, although the predominant fiber direction is parallel to the surface. These fibers are woven into a more or less rhombic parallelogram pattern, which allows considerable deformation without requiring elongation of the individual fibers. In the dermis, collagen constitutes 75% of skin dry weight, elastin about 4%. The female genital tract is a muscular organ, with smooth muscle cells arranged in circular and spiral patterns. Actually, in the human uterus only 30%-40% of its wall volume is muscle, and in the cervix only 10%; the rest is connective tissue. In the connective tissue of the genital tract the ground substance

dominates, as the ratio of ground substance to fiber elements is 1.5: 1 in the nonpregnant corpus and 5: 1 in the cervix near full term. During pregnancy, the ground substance grows at the rate of the overall growth, while collagen increases more slowly, and elastin and reticulin almost not at all. Hence the composition of the connective tissue changes. This brief sketch shows that collagen fibers are organized into many different kinds of structures, the mechanical properties of which are different.

2.3 The mechanical behavior of soft tissues

In this study the mechanics of soft tissues is discussed for those composed by collagen, elastin and ground substances. Biomechanics paradigm sets that the property of a tissue is known if the constitutive equations have been established on the experimental basis involving static (kinematic) action and measured kinematic (static) variables. The simplest experiment that can be done on a biosolid is the uniaxial tension test. For this purpose a specimen of cylindrical shape is prepared and stretched in a testing machine. The load and elongation are recorded for prescribed loading or stretching histories. From these records we can deduce the stress-strain relationship of the material under uniaxial loading. The stress response , for biological tissues, will show a hysteresis loop with each cycle, but the loop decreases with succeeding cycles, rapidly at first, then tending to a steady state after a number of cycles. The existence of such an initial period of adjustment after a large disturbance seems common to all tissues. From the point of view of mechanical testing, the process is called preconditioning. Generally, only mechanical data of preconditioned specimens are presented.

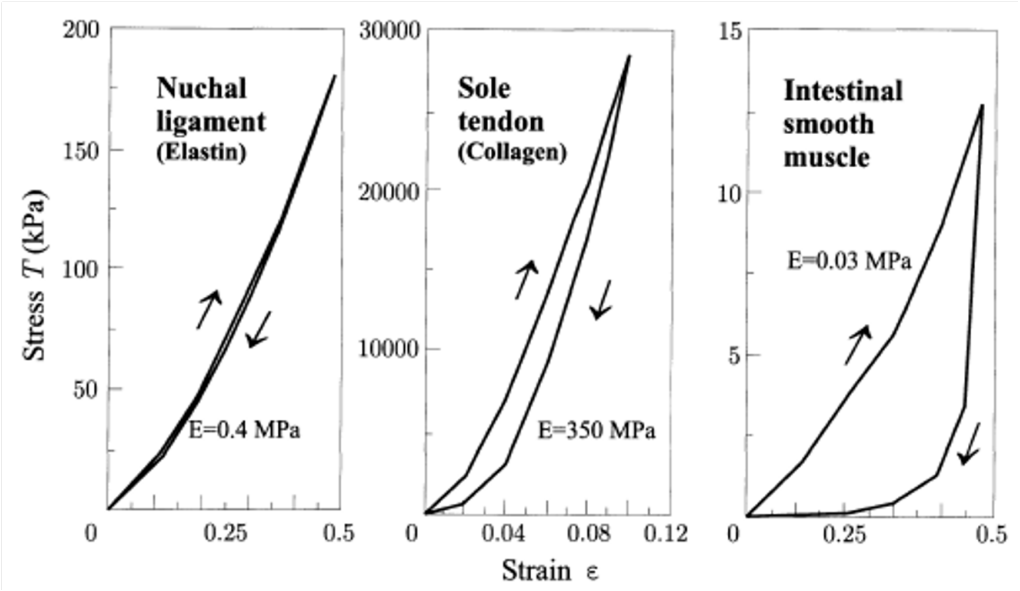

Figure 2.21: Tensile properties of elastin-rich canine nuchal ligament, collagen-rich sole tendon, and intestinal smooth muscle (Hasegawa and Azuma (1974)).

Figure 2.21 shows stress-strain relations for the canine nuchal ligament, sole tendon, and intestinal smooth muscle, which are rich in collagen, elastin,

and smooth muscle (cell), respectively [56]. The elastin-rich nuchal ligament has much less strength and much more flexibility than the collagen-rich sole tendon. The intestinal smooth muscle is much softer than the other two tissues, and its stress-strain curve has a wide hysteresis loop, which indicates that the tissue is viscoelastic.

Most biological soft tissues exhibit open hysteresis loops in their load-deformation curves, that correspond to energy dissipation in the material. Such energy dissipation is often referred as material hereditariness whose more popular evidence is the material relaxation. Indeed the patellar tendon is elongated and maintained at some length, the load does not stay at a specific level but decreases rather rapidly at first and then gradually as in fig. 2.21

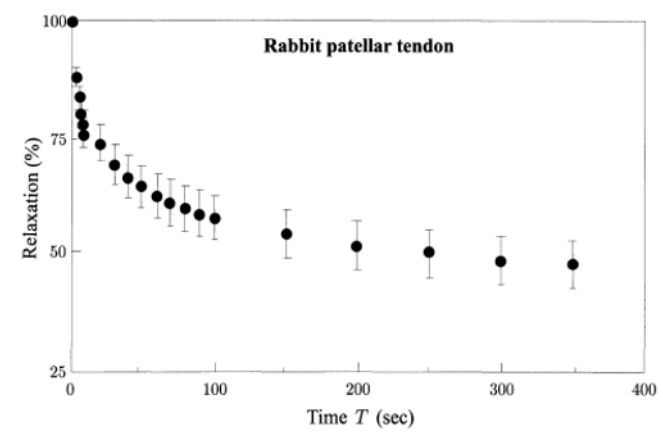

Figure 2.22: Relaxation behavior of patellar tendon (Yamamoto et al. (1999)).

A typical load-elongation curve for a tendon tested in simple elongation at a constant strain rate is shown in fig. 2.23. It is seen that the curve may be divided into three parts. In the first part, from 0 to A, the load increases exponentially with increasing elongation. In the second part, from A to B, the relationship is fairly linear. In the third part, from B to C, the relationship is nonlinear and ends with rupture. The "toe" region, from 0 to A, is usually the physiological range in which the tissue normally functions. The other regions, AB and BC, correspond to reserve strength of the tendon. The ultimate stress of human tendon at C lies in the range 50-100 MPa. The maximum elongation at rupture is usually about 10%-15%. α is the angle between the linear part of the curve and the deformation axis. The slope, $tan\alpha$, is taken as the "elastic stiffness," Young's modulus. In terms of structure function relationships, the toe-in region represents "un-crimping"

of the crimp in the collagen fibrils. Since it is easier to stretch out the crimp of the collagen fibrils, this part of the stress strain curve shows a relatively low stiffness. As the collagen fibrils become uncrimped, then we see that the collagen fibril backbone itself is being stretched, which gives rise to a stiffer material. As individual fibrils within the ligament or tendon begin to fail damage accumulates, stiffness is reduced and the ligament/tendons begins to fail, BC is an elastc damage model. Thus a key concept is that the overall behavior of ligaments and tendons depends on the individual crimp structure and failure of the collagen fibrils

Figure 2.23 shows the monotone test of patellar tendon and hamstring and ACL ligaments outline the well-known j-shaped curve.

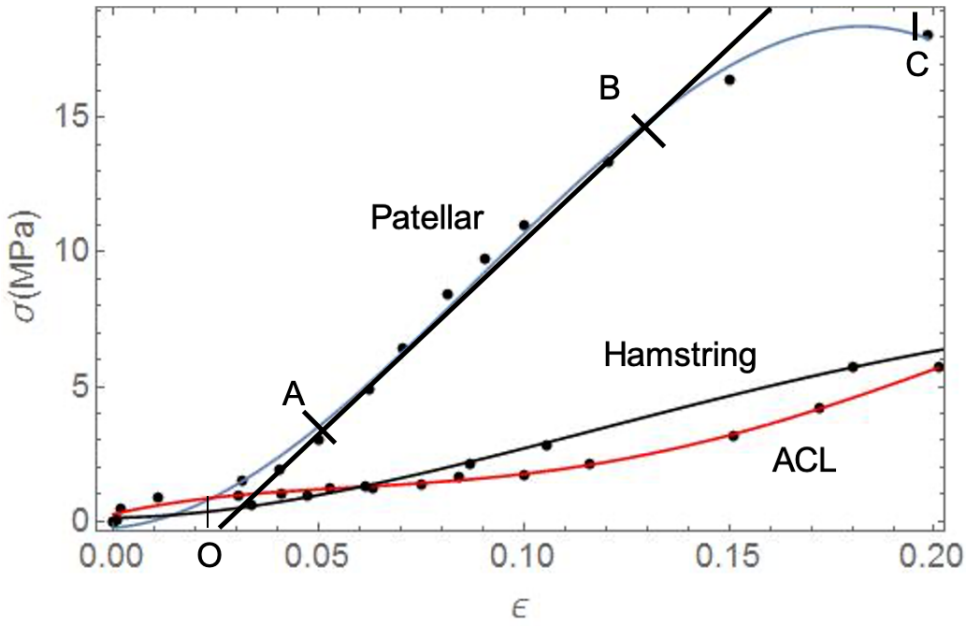

Figure 2.23: monotone test on human ligaments and tendon conduced at Aten Center. $\sigma = F/A_0$ and $\varepsilon = \Delta l/l_0$. Bologna E. et al. ESB-Ita Roma, Settembre 2017.

A J-shaped curve can be compared to an S-shaped curve in which the material has been pre-stressed, causing the effective origin of the graph to be further along the curve. This is shown in the fig. 2.23 Patellar. Arteries and other biological tissue are naturally pre-stressed but in general an s-shaped curve characterizes the stress-strain response of the rubber.

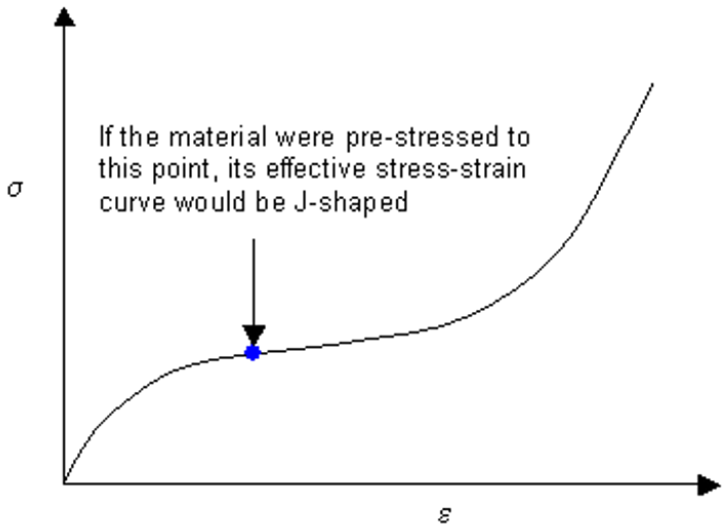

Figure 2.24: stress-strain curve called S-shaped

Comparing j-shaped and s-shaped curve, we can say that many biological tissues corresponding to j-shaped curve have an important characteristic is the initial large extension achieved with relatively low levels of stress and the subsequent stiffening at higher levels of extension. This aspect is associated with the recruitment of collagen fibres as they become uncrimped and reach their natural lengths, whereupon their significant stiffness comes into play and overrides that of the underlying matrix material.

Finally we must consider, that most biological soft tissues have a water content of more than 70%. Therefore, they hardly change their volume (isovolumic) even if load is applied, and they are almost incompressible. The incompressibility assumption is applicable to most biological soft tissues. However, it is not the case in the articular cartilage, because the tissue is micro-porous and, therefore, water can enter and leave pores depending upon load [95].

2.4 Fundamentals of continuum mechanics for soft tissue modelling

We presents the concepts for the kinematics of a body that underlie the study of viscoelasticity. Bodies occupy configurations, which are regions of the three-dimensional Euclidean point space. A one-to-one correspondence can be set between points of a body and the points they occupy in the Euclidean space. Thus, we will treat a body as a closed set of points occupying a

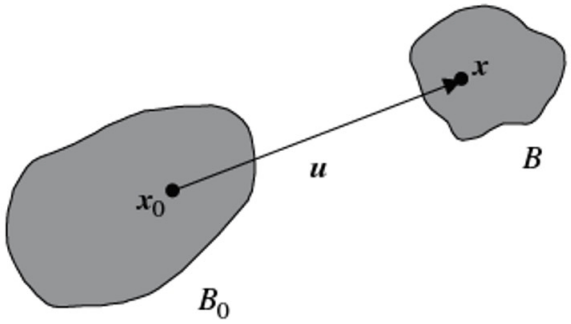

Figure 2.25: Deformation of a body

regular1 region B, called the 'current' configuration, of the three-dimensional Euclidean point space. The displacement u of these points may be measured only with respect to a reference2 configuration, which will be denoted with B_0. Points x ($x0$) defined in $B(B_0)$ are called 'spatial' (material). Therefore, with reference to fig.2.25 the displacement u is defined as

$$\mathbf{u} = \mathbf{x} - \mathbf{x}_0 \tag{2.3}$$

or

$$\mathbf{u} = \mathbf{g}(\mathbf{x}_0) - \mathbf{x}_0 \tag{2.4}$$

where the function $\mathbf{g} : B_0 \to B$ is the deformation, relating material points to spatial points. This function is invertible, with inverse $\mathbf{g}^-$, so

$$\mathbf{x} = \mathbf{g}(\mathbf{x}_0), \quad \mathbf{x}_0 = \mathbf{g}^{-\mathbf{1}}(\mathbf{x}) \tag{2.5}$$

Let us now consider two material points $\mathbf{x}_0$ and $\mathbf{x}_0 + \omega_0\boldsymbol{\omega}_0$, the latter obtained by adding to $\mathbf{x}_0$ the unit vector $\boldsymbol{\omega}_0$ multiplied by the scalar ω_0. The two points are mapped forward to

$$\mathbf{x} = \mathbf{g}(\mathbf{x}_0) \quad \text{and} \quad \mathbf{x} + \omega\boldsymbol{\omega} = \mathbf{g}(\mathbf{x}_0 + \omega_0\boldsymbol{\omega}_0) \tag{2.6}$$

so the embedded vector $\omega_0\boldsymbol{\omega}_0$ transforms to $\omega\boldsymbol{\omega}$. The Taylor series expansions of $\mathbf{g}$ and $\mathbf{g}^{-1}$ around $\mathbf{x}_0$ and $\mathbf{x}$, respectively, yield

$$\omega\boldsymbol{\omega} = \mathbf{g}(\mathbf{x}_0 + \omega_0\boldsymbol{\omega}_0) - \mathbf{g}(\mathbf{x}_0) = \mathbf{F}(\omega_0\boldsymbol{\omega}_0) + \mathbf{O}(\omega_0^2) \tag{2.7a}$$

$$\omega_0\boldsymbol{\omega}_0 = \mathbf{g}^{-1}(\mathbf{x} + \omega\boldsymbol{\omega}) - \mathbf{g}^{-1}(\mathbf{x}) = \mathbf{F}^{-1}(\omega\boldsymbol{\omega}) + \mathbf{O}(\omega^2) \tag{2.7b}$$

where $\mathbf{F}$ is the deformation gradient and $\mathbf{F}^{-1}$ its inverse $\mathbf{F}^{-1}\mathbf{F} = \mathbf{F}\mathbf{F}^{-1} = \mathbf{I}$. It is worth noting that $\mathbf{F}$ represents a gradient of a material field, whereas

$\mathbf{F}^{-1}$ is the gradient of a spatial field, namely,

$$\mathbf{F} = \frac{\partial \mathbf{g}(\mathbf{x}_0)}{\partial \mathbf{x}_0} \quad \text{and} \quad \mathbf{F}^{-1} = \frac{\partial \mathbf{g}^{-1}(\mathbf{x})}{\partial \mathbf{x}} \tag{2.8}$$

Note that tensor $\mathbf{F}$ is a two-point tensor in the sense that $\boldsymbol{\omega}_0$ and $\boldsymbol{\omega}$ are, respectively, defined in the material and spatial configurations. In order to highlight that the two gradients are taken with respect to different fields, the following convention will be used:

$$\mathbf{F} = Grad\mathbf{g} \quad \text{and} \quad \mathbf{F}^{-1} = Grad\mathbf{g}^{-1} \tag{2.9}$$

to rewrite eq.(2.8) in an alternative way and where $Grad\mathbf{f}(x,y,z) = \frac{\partial f}{\partial x}\mathbf{i} + \frac{\partial f}{\partial y}\mathbf{j} + \frac{\partial f}{\partial z}\mathbf{k}$. More in general, when an operator will be written with an initial capital (minuscule) letter, it will be referred to a material (spatial) field.

Eqs.(2.7a)(2.7b) make transparent the fundamental property of the deformation gradient $\mathbf{F}(\mathbf{F})^{-1}$: It transforms the embedded material (spatial) oriented line element into a corresponding embedded spatial (material) oriented line element. In particular, eqs. (2.7a)(2.7b) yield, when truncated at the first order:

i) The change in the modulus of the embedded oriented line element:

$$\lambda(\mathbf{x}_0, \boldsymbol{\omega}_0) = \frac{\omega}{\omega_0} = |\mathbf{F}\boldsymbol{\omega}_0| \qquad \frac{1}{\lambda(\mathbf{x}, \boldsymbol{\omega})} = \frac{\omega_0}{\omega} = |\mathbf{F}^{-1}\boldsymbol{\omega}| \tag{2.10}$$

where λ is the stretch at the material point $\mathbf{x}_0$ (or, equivalently, at the spatial point $\mathbf{x}$) relative to the material direction $\boldsymbol{\omega}_0$ (or, equivalently, spatial direction $\boldsymbol{\omega}$). Note that if $\mathbf{F}$ were singular, there would be fibres transformed into points, a situation clearly non admissible. Therefore, it is assumed that $det\mathbf{F} > 0$, so the stretch always results strictly positive: greater (smaller) than one when the fibre elongates (contracts) deforming from B_0 to B.

ii) The change in the orientation of an embedded oriented line element:

$$\boldsymbol{\omega}_0 = \frac{\mathbf{F}^{-1}\boldsymbol{\omega}}{|\mathbf{F}^{-1}\boldsymbol{\omega}|} = \lambda(\mathbf{x}, \boldsymbol{\omega})\mathbf{F}^{-1}\boldsymbol{\omega} \qquad \boldsymbol{\omega} = \frac{\mathbf{F}\boldsymbol{\omega}_0}{|\mathbf{F}\boldsymbol{\omega_0}|} = \frac{\mathbf{F}\boldsymbol{\omega_0}}{\lambda(\mathbf{x}_0, \boldsymbol{\omega}_0)} \tag{2.11}$$

It is expedient now to introduce the right and left Cauchy-Green (symmetric and positive definite) deformation tensors

$$\mathbf{C} = \mathbf{F}^T\mathbf{F} \quad \text{and} \quad \mathbf{B} = \mathbf{F}\mathbf{F}^T \tag{2.12}$$

Since the stretch is always strictly positive and, consistently, the two Cauchy-Green deformation tensors are positive definite, we may use the definition of square root of a tensor to define the right and left stretch tensors

$$\mathbf{U} = \mathbf{C}^{1/2} \quad \text{and} \quad \mathbf{V} = \mathbf{B}^{1/2} \tag{2.13}$$

which are symmetric and positive definite tensors admitting the spectral representation

$$\mathbf{U} = \lambda_1 \mathbf{u}_1 \otimes \mathbf{u}_1 + \lambda_2 \mathbf{u}_2 \otimes \mathbf{u}_2 + \lambda_3 \mathbf{u}_3 \otimes \mathbf{u}_3 \tag{2.14a}$$

$$\mathbf{V} = \lambda_1 \mathbf{v}_1 \otimes \mathbf{v}_1 + \lambda_2 \mathbf{v}_2 \otimes \mathbf{v}_2 + \lambda_3 \mathbf{v}_3 \otimes \mathbf{v}_3 \tag{2.14b}$$

where $\otimes$ is the tensor product and $\lambda_i, \mathbf{u}_i$ and $\mathbf{v}_i$ $(i = 1, 2, 3)$ are, respectively, the principal stretches (the stretches in the direction of the eigenvectors of $\mathbf{C}$ and $\mathbf{F}$. It is therefore reasonable to understand that the effect of $\mathbf{F}(\mathbf{F}^{-1})$ on a material (spatial) fibre results in a stretch given by $\mathbf{U}(\mathbf{V}^{-1})$ and a rotation $\mathbf{R}$. Defining this rotation as

$$\mathbf{v}_i = \mathbf{R}\mathbf{u}_i \tag{2.15}$$

we find the polar representation theorem that we rewrite here

$$\mathbf{F} = \mathbf{R}\mathbf{U} = \mathbf{V}\mathbf{R} \tag{2.16}$$

where $\mathbf{R} \in Orth^+$.

U and V provides a local measure of deformation because their principal components represent the stretch of the three orthogonal fibres (aligned with the eigenvectors). In particular, $\mathbf{U}(\mathbf{V}$ is a Lagrangean (Eulerian) measure of deformation because it transforms material (spatial) quantities into spatial (material). In the absence of strain, the stretch tensors reduce to the identity $\mathbf{U} = \mathbf{V} = \mathbf{I}$. All the tensors $\mathbf{C}$, $\mathbf{B}$, $\mathbf{U}$ and $\mathbf{V}$ can be chosen to quantify the strain, and more in general, we may conclude that there are infinite possibilities of choice. It therefore may be convenient to introduce the Lagrangean and Eulerian strain measures

$$\mathbf{E}^{(m)} = \begin{cases} \dfrac{\mathbf{U}^m - \mathbf{I}}{m} & m \neq o \\ \log \mathbf{U} & m = 0 \end{cases} \qquad \mathbf{G}^{(m)} = \begin{cases} \dfrac{\mathbf{V}^m - \mathbf{I}}{m} & m \neq o \\ \log \mathbf{V} & m = 0 \end{cases} \tag{2.17}$$

defined for every (positive, negative or null) integer m so that they vanish in an undeformed situation. The logarithm of a tensor is defined for symmetric positive definite tensors taking the logarithm of the eigenvalues in its spectral decomposition so that

$$log\mathbf{U} = \sum_{i=1}^{3} \varepsilon_i \mathbf{u}_i \otimes \mathbf{u}_i \quad \text{and} \quad log\mathbf{V} = \sum_{i=1}^{3} \varepsilon_i \mathbf{v}_i \otimes \mathbf{v}_i \tag{2.18}$$

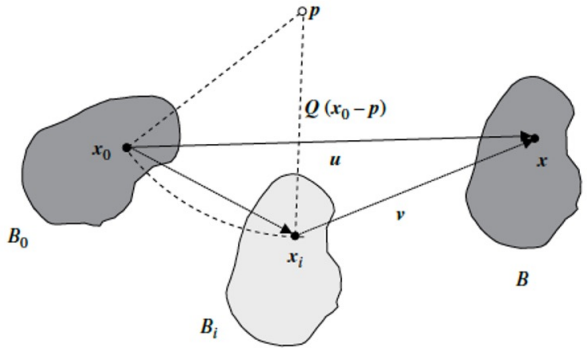

Figure 2.26: Rigid-body deformation

where

$$\varepsilon_i = log\lambda_i \tag{2.19}$$

are the so-called logarithmic strains. The logarithmic strain ε may be introduced with reference to a fibre of initial length l_0 stretched until it reaches the final length l_f so the stretch is $\lambda_f = \frac{l_f}{l_0}$. certain stage of the process of straining, the fibre has a length l, so the increment in deformation $d\varepsilon$ for an increment dl in length is

$$d\varepsilon = \frac{dl}{l} \tag{2.20}$$

which, integrated between l_0 and l_f, provides

$$\varepsilon = log\frac{l_f}{l_0} = log\lambda_f \tag{2.21}$$

an expression corresponding to the definition to eq.(2.20). Note that the two notations

$$\mathbf{T}^m = \mathbf{T}\mathbf{T}...\mathbf{T} \quad \text{and} \quad \mathbf{T}^m \tag{2.22}$$

when $m = 2$, we obtain the Green-Lagrange strains

$$\mathbf{E}^{(2)} = \frac{1}{2}(\mathbf{C} - \mathbf{I}) \quad \text{and} \quad \mathbf{G}^{(2)} = \frac{1}{2}(\mathbf{B} - \mathbf{I}) \tag{2.23}$$

homogeneous deformation occurring with constant gradient, a rigid-body rotation about the point $\mathbf{p}$ and a rigid-body translation of displacement v is illustrated in fig.2.26 The rotation about point $\mathbf{p}$ moves the solid from the reference configuration B_0 to the 'intermediate' configuration B_i, so point $\mathbf{x}_0$ is transformed into point $\mathbf{x}_i$ as

$$\mathbf{x}_i = \mathbf{p} + \mathbf{Q}(\mathbf{x}_0 - \mathbf{p}) \tag{2.24}$$

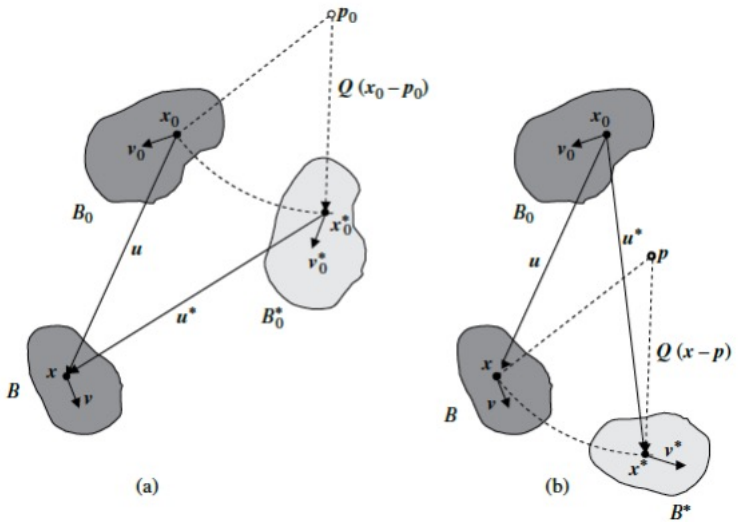

Figure 2.27: Effects of a rigid-body deformation: two rotated reference configurations to describe the same current configuration (a) and two rotated final configurations corresponding to the same reference configuration (b).

where $\mathbf{Q} \in Ortho^+$ describes the rigid-body rotation, constant for all material points in B_0. Finally, point $\mathbf{x}_i$ is translated to $\mathbf{x}$ simply by adding a vector $\mathbf{v}$, constant for all points in B_i. The result is

$$\mathbf{x} = \mathbf{q} + \mathbf{Q}(\mathbf{x}_0 - \mathbf{p}) \tag{2.25}$$

where $\mathbf{q} = \mathbf{p} + \mathbf{v}$, so the deformation gradient for a rigid-body rotation and translation is $\mathbf{F} = \mathbf{Q}$. The deformation described by eq.(2.25) is rigid because the distance between every pair of points in B_0 is preserved. Since the choice of the reference configuration is arbitrary, two reference configurations, B_0 and B_0^*, are sketched in fig. 2.27 both transformed into the same final configuration B. The difference between B_0 and B_0^* lies in a rigid-body rotation. The transformation of oriented line elements provides the following equations:

$$\mathbf{v} = \mathbf{F}\mathbf{v}_0 \quad \text{and} \quad \mathbf{v} = \mathbf{F}^*\mathbf{v}_0^* \tag{2.26}$$

where $\mathbf{F}$ and $\mathbf{F}^*$ are the two deformation gradients relative to the two reference configurations B_0 and B_0^*, respectively. Since eq.(2.26) must hold true for every vector $\mathbf{v}_0$, and $\mathbf{v}_0^* = \mathbf{Q}\mathbf{v}_0$, it may be concluded that

$$\mathbf{F}^* = \mathbf{F}\mathbf{Q}^T \tag{2.27}$$

showing how a change in the reference configuration by a rigid-body transformation affects the deformation gradient.

A motion is an ordered sequence of mappings of a reference configuration into current configurations, or in other words, a motion is a smooth one-parameter family of deformations, ordered by the time t, so that

$$\mathbf{x} = \boldsymbol{g}(\mathbf{x}_0, t) \quad \text{and} \quad \mathbf{x}_0 = \boldsymbol{g}^{-1}(\mathbf{x}, t) \tag{2.28}$$

The velocity and acceleration of particle at time t are given by

$$\dot{\mathbf{x}}(\mathbf{x}_0, t) = \frac{\partial \mathbf{g}(\mathbf{x}_0, t)}{\partial t} \quad \text{and} \quad \mathbf{v}(\mathbf{x}, t) = \dot{\mathbf{x}}\left(\mathbf{g}^{-1}(\mathbf{x}, t), t\right) \tag{2.29}$$

and material $\ddot{\mathbf{x}}$ and spatial $\mathbf{a}$ descriptions of the acceleration

$$\ddot{\mathbf{x}}(\mathbf{x}_0, t) = \frac{\partial^2 \mathbf{g}(\mathbf{x}_0, t)}{\partial^2 t} \quad \text{and} \quad \mathbf{a}(\mathbf{x}, t) = \ddot{\mathbf{x}}\left(\mathbf{g}^{-1}(\mathbf{x}, t), t\right) \tag{2.30}$$

The gradient of the material description of the velocity is

$$Grad\dot{\mathbf{x}}(\mathbf{x}_0, t) = \dot{\mathbf{F}} \tag{2.31}$$

whereas, by definition, the gradient of the spatial description of velocity is denoted by $\mathbf{L}$

$$\mathbf{L}(\mathbf{x}, t) = grad\mathbf{v} \tag{2.32}$$

the gradient with respect $\mathbf{x}_0$ and using the chain rule of differentiation,

$$\dot{\mathbf{F}} = \mathbf{L}\mathbf{F} \tag{2.33}$$

An other relation is

$$\left(\mathbf{F}^{-1}\right) = \mathbf{F}^{-1}\dot{\mathbf{F}}\mathbf{F}^{-1} \tag{2.34}$$

Introduction of the concept of force requires specification that we will refer to an inertial frame. In the current configuration, a body interacts with the environment through forces, which may act on the surface, denoted by $\boldsymbol{\sigma}$ (defined per unit surface) or, at interior points, denoted by b (defined per unit volume). The Cauchy theorem states that if $\boldsymbol{\sigma}$ and b^* (body forces) are a system of forces for B during a motion, a necessary and sufficient condition for to hold for any part $P \in B$ is the existence of a spatial tensorial field $\mathbf{T}$ the so-called Cauchy stress tensor such that
i) The traction is a linear function of the unit normal n through the Cauchy stress:

$$\mathbf{s}(\mathbf{n}) = \mathbf{T}\mathbf{n} \tag{2.35}$$

transforming the spatial unit normal to the spatial vector $\mathbf{s}$.
ii) The Cauchy stress is symmetric:

$$\mathbf{T} \in Sym \tag{2.36}$$

iii) $\mathbf{T}$ satisfies the local equations of motion

$$div\mathbf{T} + \mathbf{b}^* = \mathbf{0} \tag{2.37}$$

where $div\mathbf{f} = \dfrac{\partial f_1}{\partial x} + \dfrac{\partial f_2}{\partial y} + \dfrac{\partial f_3}{\partial z}$

Stress is the internal counterpart to forces applied by the environment to the body in its actual configuration: It intrinsically represents, therefore, a spatial quantity.

$$\mathbf{T}\mathbf{n}da = \mathbf{S}\mathbf{n}_0 da_0 \tag{2.38}$$

where

$$\mathbf{S} = J\mathbf{T}\mathbf{F}^T \tag{2.39}$$

is the first Piola-Kirchhoff stress tensor, and $\mathbf{S}\mathbf{n}_0$ is the nominal traction. Tensor S is in general un-symmetric but satisfies

$$\mathbf{S}\mathbf{F}^T = \mathbf{F}\mathbf{S}^T \tag{2.40}$$

because $\mathbf{T}$ is symmetric. Note that by introducing the so-called Kirchhoff stress,

$$\mathbf{K} = J\mathbf{T} \tag{2.41}$$

Eq.(2.39) can be rewritten in the short form as

$$\mathbf{S} = \mathbf{K}\mathbf{F}^T \tag{2.42}$$

The nomenclature 'Kirchhoff stress' to denote eq.(2.41). The first Piola-Kirchhoff stress tensor is the transpose of the nominal stress tensor (note that it is denoted by a bold minuscule letter, but it is a second-order un-symmetric tensor), that is

$$\mathbf{t} = \mathbf{S}^T = \mathbf{F}^{-1}\mathbf{K} \tag{2.43}$$

used, among others, by Hill and Ogden. Note that the nominal traction is $\mathbf{S}\mathbf{n}_0 = t^T\mathbf{n}_0$ is a measure of the surface force per unit area in the reference configuration. Therefore, the first Piola-Kirchhoff stress satisfies

$$\int_{\partial P} \mathbf{T}\mathbf{n} = \int_{\partial P_0} \mathbf{S}\mathbf{n}_0 \tag{2.44}$$

Thus, introducing the body force in the reference configuration

$$\mathbf{b}_0 = J\mathbf{b} \tag{2.45}$$

and noting that

$$\int_{\partial P} \dot{\mathbf{v}}\rho = \int_{\partial P_0} \ddot{\mathbf{x}}\rho_0 \tag{2.46}$$

we can write the balance laws

$$\int_{\partial P_0} \mathbf{S}\mathbf{n}_0 = \int_{P_0} \mathbf{b}_0 = \int_{P_0} \ddot{\mathbf{x}}\rho_0 \tag{2.47a}$$

$$\int_{\partial P_0} (\mathbf{x}-\mathbf{o})\mathbf{S}\mathbf{n}_0 + \int_{P_0} (\mathbf{x}-\mathbf{o})\mathbf{b}_0 = \int_{\partial P_0} (\mathbf{x}-\mathbf{o})\ddot{\mathbf{x}}\rho_0 \tag{2.47b}$$

Equation (2.47a) localises into a local balance expressed in the reference configuration

$$div\mathbf{S} + \mathbf{b}_0 = \rho_0\ddot{\mathbf{x}} \tag{2.48}$$

representing, when the inertia is neglected, translational equilibrium of a spatial element imposed on the reference configuration. However, symmetry of $\mathbf{S}$ does not follow from (2.47b), equivalent to the symmetry of the Kirchhoff (and thus Cauchy) stress.

To prove that eq.(2.47b) which means the symmetry of the Kirchhoff stress $\mathbf{K}$, we can proceed as follows. For every constant vector $\mathbf{a}$, we may write

$$\mathbf{a}\cdot(\mathbf{x}-\mathbf{o})\times\mathbf{S}\mathbf{n}_0 = -\left[\mathbf{S}^T(\mathbf{x}-\mathbf{o})\mathbf{a})\right]\cdot\mathbf{n}_0 \tag{2.49}$$

so the divergence theorem gives

$$\int_{\partial P_0} \mathbf{a}\cdot(\mathbf{x}-\mathbf{o})\times\mathbf{S}\mathbf{n}_0 = -\int_{P_0}\left[\mathbf{S}^T(\mathbf{x}-\mathbf{o})\times\mathbf{a})\right] \tag{2.50}$$

Using, now the property

$$div\left[\mathbf{S}^T(\mathbf{x}-\mathbf{o})\times\mathbf{a})\right] = \mathbf{S}\cdot grad[(\mathbf{x}-\mathbf{o})\times\mathbf{a}] + [(\mathbf{x}-\mathbf{o})\times\mathbf{a}]\cdot div\mathbf{S} \tag{2.51}$$

and the mixed product equality

$$((\mathbf{x}-\mathbf{o})\times\mathbf{a})\cdot div\mathbf{S} = -\mathbf{a}\cdot(\mathbf{x}-\mathbf{o})\times div\mathbf{S} \tag{2.52}$$

we can rewrite the scalar product of eq.(2.47b) with $\mathbf{a}$ as

$$\int_{\partial P_0} \mathbf{S}\cdot grad((\mathbf{x}-\mathbf{o})\times\mathbf{a}) = -\mathbf{a}\int_{P_0}(\mathbf{x}-\mathbf{o})\times[div\mathbf{S}+\mathbf{b}_0-\ddot{\mathbf{x}}\rho_0] \tag{2.53}$$

so that through (2.48) we arrive at

$$\int_{P_0} \mathbf{S}\cdot grad[(\mathbf{x}-\mathbf{o})\times\mathbf{a}] = 0 \tag{2.54}$$

which, holding for every part P_0 (and vector $\mathbf{a}$), implies the integrand to be null, which may be rewritten [using the definition of the first Piola-Kirchhoff stress and the polar decomposition of $\mathbf{F}$, as

$$[grad(\mathbf{x}-\mathbf{o})\times\mathbf{a}]\mathbf{u}=\lim_{\beta\to 0}\frac{\mathbf{g}(\mathbf{x}_0+\beta\mathbf{u})-\mathbf{g}(\mathbf{x}_0)}{\beta}\mathbf{a}=-\mathbf{aFu} \tag{2.55}$$

the spectral representation of $\mathbf{U}^{-1}$ allows us to write

$$tr\left[(\mathbf{a}\times\mathbf{v}_1)\otimes\mathbf{K}\mathbf{v}_1+(\mathbf{a}\times\mathbf{v}_2)\otimes\mathbf{K}\mathbf{v}_2+(\mathbf{a}\times\mathbf{v}_3)\otimes\mathbf{K}\mathbf{v}_3\right]=\mathbf{0} \tag{2.56}$$

which developing the scalar product and invoking arbitrariness of $\mathbf{a}$ yields

$$\mathbf{v}_1\times\mathbf{K}\mathbf{v}_1+\mathbf{v}_2\times\mathbf{K}\mathbf{v}_2+\mathbf{v}_3\times\mathbf{K}\mathbf{v}_3=\mathbf{0} \tag{2.57}$$

Thus, using the representation of $\mathbf{K}$ in the reference system $\mathbf{v}_i$, that is

$$\mathbf{K}=\sum_{i,j=1}^{3}K_{ij}\mathbf{v}_i\otimes\mathbf{v}_j \tag{2.58}$$

we finally conclude the symmetry of $\mathbf{K}$ (note that the symmetry of a tensor in one reference system implies symmetry in every reference system):

$$(K_{12}-K_{21})\mathbf{v}_2\times\mathbf{v}_1+(K_{13}-K_{31})\mathbf{v}_3\times\mathbf{v}_1+(K_{23}-K_{32})\mathbf{v}_3\times\mathbf{v}_2=\mathbf{0} \tag{2.59}$$

the subsequent application of the divergence theorem yields the theorem of power expended in the spatial description

$$\int_{\partial P}\mathbf{s}(\mathbf{n})\cdot\mathbf{v}+\int_P\mathbf{b}\cdot\mathbf{v}=\int_P\mathbf{T}\cdot\mathbf{D}+\frac{d}{dt}\int_P\frac{\rho}{2}v^2 \tag{2.60}$$

and referential description

$$\int_{\partial P_0}\mathbf{S}(\mathbf{n}_0)\cdot\dot{\mathbf{x}}+\int_{P_0}\mathbf{b}_0\cdot\dot{\mathbf{x}}=\int_{\partial P_0}\mathbf{S}\cdot\dot{\mathbf{F}}+\frac{d}{dt}\int_{P_0}\frac{\rho}{2}\dot{\mathbf{x}}^2 \tag{2.61}$$

which, in other words, represent the equation of energy balance for isothermal deformation (when temperature effects are kept into account, the internal energy, the heat flux and supply come into play.

Note that the stress power per unit volume in the reference configuration is

$$\mathbf{K}\cdot\mathbf{D}=\mathbf{S}\cdot\dot{\mathbf{F}} \tag{2.62}$$

but it also can be expressed as

$$\mathbf{T}^{(2)}\cdot\dot{\mathbf{E}}^{(2)}=\mathbf{S}\cdot\dot{\mathbf{F}} \tag{2.63}$$

where

$$\mathbf{T}^{(2)} = \mathbf{F}^{-1}\mathbf{K}\mathbf{F}^{-T} = \mathbf{F}^{-1}\mathbf{S} \tag{2.64}$$

is the second Piola-Kirchhoff (symmetric) stress tensor. Since its scalar product with the Green-Lagrange rate of strain gives the stress power per unit volume (in B_0), the second Piola-Kirchhoff stress and the Green-Lagrange strain tensor are said to be 'work conjugate'. More in general, we can define the Lagrangean and Eulerian stress measures $\mathbf{T}^{(m)}$ and $\mathbf{Z}^{(m)}$ work-conjugate to the strain measures so that

$$\mathbf{K} \cdot \mathbf{D} = \mathbf{Z}^{(m)} \cdot \dot{\mathbf{G}}^{(m)} = \mathbf{S} \cdot \dot{\mathbf{F}} = \mathbf{T}^{(m)} \cdot \dot{\mathbf{E}}^{(m)} \tag{2.65}$$

A conjugate pair of stress and strain that will become useful later is formed by the Biot stress tensor $\mathbf{T}^{(1)}$ and the right stretch-strain tensor $\mathbf{E}^{(1)}$, defined as

$$\mathbf{E}^{(1)} = \mathbf{U} - \mathbf{I} \quad \text{conjugate to} \quad \mathbf{T}^{(1)} = \frac{1}{2}\left(\mathbf{T}^{(2)}\mathbf{U} + \mathbf{U}\mathbf{T}^{(2)}\right) \tag{2.66}$$

whereas another pair is the Almansi strain $\mathbf{E}^{(2)}$ and its conjugate stress $\mathbf{T}^{(-2)}$, defined as

$$\mathbf{E}^{(-2)} = \frac{1}{2}\left(\mathbf{U}^{(-2)} - \mathbf{I}\right) \quad \text{conjugate to} \quad \mathbf{T}^{(-2)} = \mathbf{F}^{T}\mathbf{K}\mathbf{F} \tag{2.67}$$

where $\mathbf{U}^{(-2)} = \mathbf{C}^{-1} = \mathbf{F}^{-1}\mathbf{F}^{-T}$ To better understand the material or spatial nature of the stress measures that we have introduced, let us consider the effects of a rigid-body rotation of the current configuration, represented by the rotation tensor $\mathbf{Q} \in Orth^{+}$. Since the unit normal $\mathbf{n}^{*}$ and the stress vector $\mathbf{s}^{*}$ in the rotated configuration B^{*} are related to the corresponding vectors in B via

$$\mathbf{n}^{*} = \mathbf{Q}\mathbf{n}, \quad \mathbf{s}^{*} = \mathbf{Q}\mathbf{s} \tag{2.68}$$

it is concluded that the Cauchy stress transforms as an Eulerian quantity

$$\mathbf{T}^{*} = \mathbf{Q}\mathbf{T}\mathbf{Q}^{T} \tag{2.69}$$

expressing the fact that the two stress vectors $\mathbf{T}\mathbf{n}$ and $\mathbf{T}^{*}\mathbf{n}^{*}$ are related by

$$\mathbf{T}^{*}\mathbf{n}^{*} = \mathbf{Q}(\mathbf{T}\mathbf{n}) \tag{2.70}$$

We can find the transformation laws of the first and second Piola-Kirchhoff tensors through transformation rules of kinematic fields for rigid-body rotations of the current configuration $\mathbf{Q}\mathbf{S}$ and $\mathbf{T}^{(2)}$ showing that the latter remains unchanged as $\mathbf{E}^{(2)}$, whereas the former behaves as $\mathbf{F}$. Let us now consider a rigid-body rotation of the reference configuration such as that sketched in fig.2.26a, whereas the current configuration remains fixed. The Cauchy stress does not change. Therefore, the first and the second Piola-Kirchhoff tensors transform as $\mathbf{S}\mathbf{Q}^{T}$ and $\mathbf{Q}\mathbf{T}^{(2)}\mathbf{Q}^{T}$ showing that they behave again as $\mathbf{F}$ and $\mathbf{E}^{(2)}$, respectively.

Chapter 3

Material hereditariness

The mechanical behavior of materials discussed in previous chapter have been shown to depend on the specific kind of tissue considered. Such observation led to two limit cases: i) In presence of a complete recovery in cycle tensile tests the concept of material elasticity is introduced; ii) In presence of mechanical behavior such that complete energy dissipation (no recovery) is observed, then the concept of viscous material is reported. Real-type of materials show an intermediate behavior and the term material hereditariness is reported. The term hereditariness indicates the behavior of an intermediate material between elastic solid and viscous liquid, this behavior is typical of polymers [43], of human bones, of various mortars and resins used in construction, of some families of rocks [53] and other materials. The hereditariness material therefore it is characterized by having two asymptotic behaviors, that of the solid elastic and that of the viscous liquid. From previous considerations it is evident that time dependence of biological materials is a crucial aspect in understanding their function and performance.

Hereditariness has been studied in numerous biological materials such as bone, articular cartilage, skeletal muscle, ligament, tendon,cardiovascular tissues [5, 6]. Ligaments are hereditariness and thus, display time- dependent and load-history-dependent mechanical behavior. Recently, ligament hereditariness has been studied in healing, damaged, grafted, and prosthetic ligaments. It is axiomatic that a repaired or replaced ligament must possess the same hereditary characteristics as a normal ligament to provide the same function. It is also of interest to know the difference in performance between healthy and damaged ligament. For these reasons it is important to understand hereditary behavior throughout its functional range. To describe the history of stress and strain two functions are intertwined $\phi_r(\varepsilon, t)$ and $\phi_c(\sigma, t)$. In general, these functions are assumed to be non-linear functions. To investigate on the nature of $\phi_r(\varepsilon, t)$ and $\phi_c(\sigma, t)$, experimental creep and

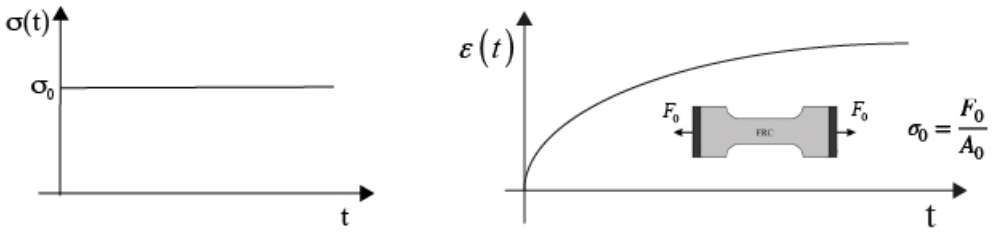

Figure 3.1: Creep test

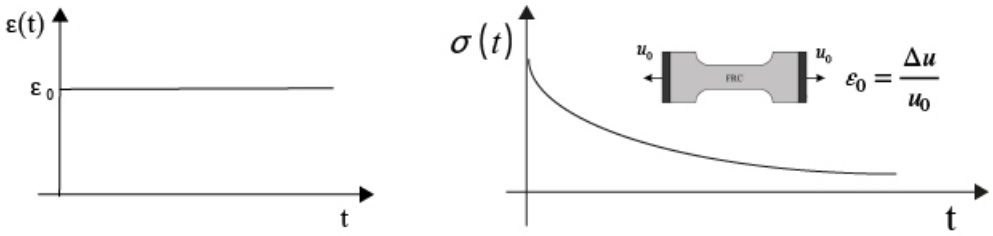

Figure 3.2: Relaxation test

relaxation testing is required.

Prior studies of ligament hereditariness often consist of a creep or relaxation test at one load or strain level.

Let a specimen be subjected to a step stress history fig.3.1, in which the stress is instantaneously increased to some value σ_0 at $t = 0$ and then held fixed. The typical strain response consists of i) an instantaneous increase in strain at $t = 0$ followed by ii) continued straining in time at a non-constant rate and (iii) an asymptotic approach to some limit value at time increases. The behavior is called creep. Let $\phi_c(\sigma_0, t) = J(t, \sigma_0)$ denote the strain at time t when the value of the stress is σ_0. Then, $J(t, \sigma_0) = 0$ when $t < 0$; ii) jumps to value $J(0, \sigma_0)$ at $t = 0$ and iii) $J(t, \sigma_0)$ monotonically increases to the limit value denoted by $J(\infty, \sigma_0)$ as $t \to \infty$. The jump in strain $J(0, \sigma_0)$ at $t = 0$ indicates instantaneous springiness or elasticity. The fact that the material reaches a non-zero limit value of strain indicates solid behavior. If the strain were to increase without bound, it would indicate fluid behavior, which is not considered here. The relations σ_0 vs $J(0, \sigma_0)$ and σ_0 vs $J(\infty, \sigma_0)$ describe, respectively, instantaneous elastic response and the long-time or equilibrium elastic response. $J(t, \sigma_0)$ has a different dependence on time t and stress σ_0 for each material, and is therefore considered to be material property called the creep function.

Let a specimen be subjected to a step strain history fig.3.2, in which the strain is instantaneously increased to some value ε_0 at $t = 0$ and then

held fixed. The typical stress history required to produce this strain history consists of i) an instantaneous increase in stress at $t = 0$ followed by ii) a gradual monotonic decrease of stress at a non-constant rate and iii) an asymptotic approach to some non-zero limit value as time increases. The behavior is called stress relaxation. Let $\phi_r(\varepsilon_0, t) = G(t, \varepsilon_0)$ denote the stress at time t when the value of the strain is fixed at ε_0. Then, i) $G(t, \varepsilon_(0, \varepsilon_0) = 0$ when $t < 0$, ii) $G(t, \varepsilon_0)$ jumps to the value $G(0, \varepsilon_0)$ at $t = 0$, and iii) $G(t, \varepsilon_0)$ monotonically decreases to the non-zero limit value denoted by $G(\infty, \varepsilon_0)$ as $t \to \infty$. The jump in stress $G(t, \varepsilon_(0, \varepsilon_0)$ at $t = 0$ is another indication of instantaneous springiness or elasticity. That fact that a non-zero stress $G(\infty, \varepsilon_0)$ is required to maintain the strain at ε_0 is another indication that the material is a solid. If $G(\infty, \varepsilon_0) = 0$, then no stress would be required to hold the material in a strained state, a characteristic of the response of fluids. The relations$G(0, \varepsilon_0)$ vs ε_0 and $G(\infty, \varepsilon_0)$ vs. ε_0 also describe, respectively, instantaneous elastic response and the long-time or equilibrium elastic response. $G(t, \varepsilon_0)$ has a different dependence on time t and strain ε_0 for each material, and is therefore considered a material property called the stress relaxation function.

Let $H(t)$ denote the Heavidide step function, $H(t) = 0$, $t \in (\infty, 0)$ and $H(t) = 1$, $t \in [0, \infty)$. When there is linearity, the stress response to the step strain history $\varepsilon(\bar{t}) = \varepsilon_0 H(t)$ is

$$\sigma(t) = G(t, \varepsilon_0) = \varepsilon_0 G(t) \tag{3.1}$$

$G(t)$ is called the stress relaxation modulus. It is convenient to introduce the notation $G(0) = G_0$ and G_∞ for the limit of $G(t)$ as $t \to \infty$.

In a similar manner, the strain response to the step stress history $\sigma(\bar{t}) = \sigma_0 H(T)$ is

$$\varepsilon(t) = J(t, \sigma_0) = \sigma_0 J(t) \tag{3.2}$$

$J(t)$ is called the creep compliance. It is assumed that $J(0) > 0$ and $J(t)$ monotonically increases to a finite limit $J_\infty > 0$ as $t \to \infty$. It is convenient to introduce the notation $J(0) = J_0$ and J_∞ for the limit of $J(t)$ as $t \to \infty$.

For these reason creep and relaxation also illustrate the duality of responses, strain is found under stress control conditions, or stress is found under strain control conditions. This further raises the question of how to determine the strain response when the stress varies with time or the stress response when the strain varies with time.

Force versus displacement curves at constant strain rates demonstrate that ligament is non-linear. The reason is that [30] collagen fibers are recruited as load increases. The stress–strain curves, as in fig.2.8, of liga-

ment display a "toe" region where fibers straighten and elongate in a strain-stiffening fashion until the fibers are no longer crimped. At that point the fibers elongate, giving rise to the linear segment of the stress–strain curve. For these reasons, this chapter is divided into sec. 3.1 and sec.3.2 on linear hereditariness e non-linear hereditariness, respectively. Sec. 3.1 describing the models present in the literature and the limits of these, attention will be paid to the link between creep and relaxation in the linear hereditary field, the monoaxial model will be extended to the triaxial model, finally, isotropic material will show why in the tendons and ligaments of the human knee the linear model does not agree with the experimental data. The sec. 3.2 will analyze the non-linear hereditariness, from the junction of the Quasi-linear hereditariness to some of the nonlinear models proposed in the literature, finally an original model will be proposed as the subject of the doctoral thesis which for the first time proposes a link between creep and relaxation in non-linear models.

3.1 Linear hereditariness

Around 1921, Nutting [74] focused his attention on hereditariness materials behavior. He conducted several experiments that did led to assert that the two equations used to describe solids perfectly rubber bands and perfectly viscous fluids were actually special cases of a single general law. Also since best-fitting of the experimental data he noticed that the deformation-time bond, it was not well described by laws in which dependence on the temporal variable it was given by an exponential type function (as obtained from the models classics), but the curve that interpolated the points well must necessarily be a power-law. The experimentation provided two types of curves, one of the u in displacement as a function of time t and one of the displacement as a function of the applied force F (constant time). The time-displacement curves u-t showed a proportionality link between the displacement and the n-th power of the temporal variable t^n; there or implied a relationship of linearity between the logarithm of the displacement and the logarithm of the time, that is:

$$log\, u \propto log\, t \tag{3.3}$$

moreover, n was independent of the force value. From the displacement-force curves u - F a relationship similar to previous one:

$$log\, u \propto log\, F \tag{3.4}$$

hence the displacement resulted or proportional to the real power of the force applied F^m. By virtue of the aforementioned observations Nutting proposed

a power- law able to express the link between the three quantities in play u, F and t. This law, of a purely empirical nature, with a simple and mathematical structure general validity, and shown below:

$$u = at^n F^m \tag{3.5}$$

it expresses the law of variation of displacement as a function of time at vary the force applied. Parameters are n and m, characteristic of the single material, they are independent of u, t, F and the geometry of the specimen but result variable as the temperature changes. The constant a is instead independent from u, t and F, but dependent on the type of test. If we consider keeping in small displacements we can consider keeping in the linear field.

In the framework of linear hereditariness an important assumption in this regard is that the material response is linear. The property of linearity of response consists of two conditions: scaling and superposition. These are discussed here only for the stress response to a strain history. Analogous comments apply to the strain response to a stress history. In this regard the material function for creep test satisfies the linearity conditions, namely:

$$\phi_c(\lambda\sigma, t) = \lambda\phi_c(\sigma, t) \quad \forall\lambda \in R \quad ; \quad \phi_c(\sigma_1 + \sigma_2, t) = \phi_c(\sigma_1, t) + \phi_c(\sigma_2, t) \tag{3.6}$$

A similar consideration holds true for the material function for relaxation test that satisfies the linearity conditions in 3.6 as:

$$\phi_r(\lambda\varepsilon, t) = \lambda\phi_r(\varepsilon, t) \quad \forall\lambda \in R \quad ; \quad \phi_r(\varepsilon_1 + \varepsilon_2, t) = \phi_r(\varepsilon_1, t) + \phi_r(\varepsilon_2, t) \tag{3.7}$$

In other terms, the assumption of linearity of response states that if a strain history $\varepsilon(\bar{t})$ is scaled by constant λ, then the corresponding stress $\sigma(t)$ is also scaled by λ and if two strain histories are superposed, then the corresponding stresses are also superposed. It is important to note that the property of linearity of response does not refer to the shape of any material response curve. It refers to a method of constructing the stress response to a composite strain history by scaling and superposing the stress responses to the component strain histories. The linearity assumptions for the creep and relaxation functions allow to introduce material hereditariness for unitary value of applied stress, and strain, namely $\sigma = 1$, $\varepsilon = 1$ resulting in stress and strain independent material hereditary functions as $\phi_c(1, t) = \sigma J(t) = 1J(t)$, and $\phi_r(1, t) = \varepsilon G(t) = 1G(t)$, respectively.

Time-varying functions $[G(t)] = F/L^2$ and $[J(t)] = L^2/F$ are the well-known relaxation and creep functions, respectively.
Linear superposition applied to a generic stress/strain history, namely $\sigma(\tau)$ and $\varepsilon(\tau)$ with $\tau \leq t$, yields:

$$\sigma(t) = \int_0^t G(t-\tau)d\varepsilon(\tau) + \varepsilon_0 G(t) = \int_0^t G(t-\tau)\dot{\varepsilon}(\tau)d\tau + \varepsilon_0 G(t) \quad (3.8a)$$

$$\varepsilon(t) = \int_0^t J(t-\tau)d\sigma(\tau) + \sigma_0 J(t) = \int_0^t J(t-\tau)\dot{\sigma}(\tau)d\tau + \sigma_0 J(t) \quad (3.8b)$$

Eqs.(3.6a, b) are defined in terms of Boltzman superposition with $d\sigma = \dot{\sigma}dt$ and $d\varepsilon = \dot{\varepsilon}dt$ increments, where $[\cdot] = \frac{d}{dt}$. Laplace transform of eqs.(3.8a),(3.8b) with $\sigma_0 = 0$ and $\varepsilon_0 = 0$ yields the fundamental relation between creep and relaxation of linear hereditariness in the Laplace domain as:

$$\hat{J}(s)\hat{G}(s) = \frac{1}{s^2} \quad (3.9)$$

where $\hat{G}(s)$ and $\hat{J}(s)$ are the Laplace transform of relaxation and creep functions, respectively. This fundamental relationship expresses the circumstance that $G(t)$ and $J(t)$ are functions related to each other in the domain of Laplace. It follows that if it is determined through experimental tests $G(t)$, the function $J(t)$ is determined accordingly and vice versa.

The specific functional class of creep and relaxation functions reported in may be guessed from experimental data collected in the course of experimental campaigns and they are very often expressed as single or linear combinations of exponential functions by means of Prony representation theorem [77] as:

$$J(t) = \sum_{r=1}^{M} J_r \left(1 - \exp\left(-\frac{t}{\tau_j^{(c)}}\right)\right) \quad (3.10a)$$

$$G(t) = \sum_{r=1}^{N} G_r \exp\left(-\frac{t}{\tau_j^{(r)}}\right) \quad (3.10b)$$

where the coefficients of the expansions have physical measures $[G_r] = \dfrac{F}{L^2}$ and $[J_r] = \dfrac{L^2}{F}$ and the material characteristic times in creep and relaxations, namely, $\tau_j^{(c)}$ and $\tau_j^{(r)}$ are additional material parameters that may be estimated by best fitting procedures together with the expansion coefficients. The integer numbers in the expansions, namely, M and N are respectively, the order of the Prony series used for creep and relaxation.

The expressions for creep and relaxation functions reported in eqs.(3.10a) (3.10b) can not, however, satisfy the fundamental relation of linear hereditariness, and, henceforth they must be used separately in stress-based and strain based constitutive relations. Some attempts to introduce analogous formulations joint in creep and relaxation led to unphysical negative values of the material relaxation times in the Prony expansion [77].

For this reason, the use of the power-law is preferred, and in the early twentieth century through the experimental campaign of Nutting on concrete and ceramic polymers, it showed how the power-law best-fitting the experimental data.

3.1.1 Rheological Models

Another approach used to develop constitutive equations for linear hereditary response involves mechanical analogs. These are mechanical devices formed by combining linear elastic springs and linear viscous dampers in series or parallel. The devices can be shown to exhibit a time dependent response that is similar to that observed in hereditary materials, namely, creep under constant load and force relaxation under constant deformation. For this reason these devices are treated as mechanical analogs of hereditariness response. Since the springs and dampers are described by linear equations, as are the equations for the kinematics of deformation and force transmission, there is a linear relation between the overall force and deformation. These approach are known as rheological models and they will discussed in the following. The spring in Fig.3.3a is the elastic (or storage) element, as for it the force is proportional to the extension; it represents a perfect elastic body obeying the Hooke law. This model is thus referred to as the Hooke model. We denote by m the pertinent elastic modulus In this case we have no creep and no relaxation so the creep compliance and the relaxation modulus are constant functions $J(t) \equiv 1/E$, $G(t) \equiv E$

The dashpot in fig.3.3b is the viscous (or dissipative) element, the force being proportional to rate of extension; it represents a perfectly viscous body obeying the Newton law. Denoting by ν the pertinent viscosity coefficient. We note that the Hooke and Newton models represent the limiting cases of viscoelastic bodies.

A branch constituted by a spring in parallel with a dashpot is known as the Voigt model, see fig.3.3c where τ_ε is referred to as the retardation time.

A branch constituted by a spring in series with a dashpot is known as the Maxwell model, see fig.3.3d, where τ_σ is is referred to as the the relaxation time. The Voigt model exhibits an exponential (reversible) strain creep but no stress relaxation; it is also referred as the retardation element. The

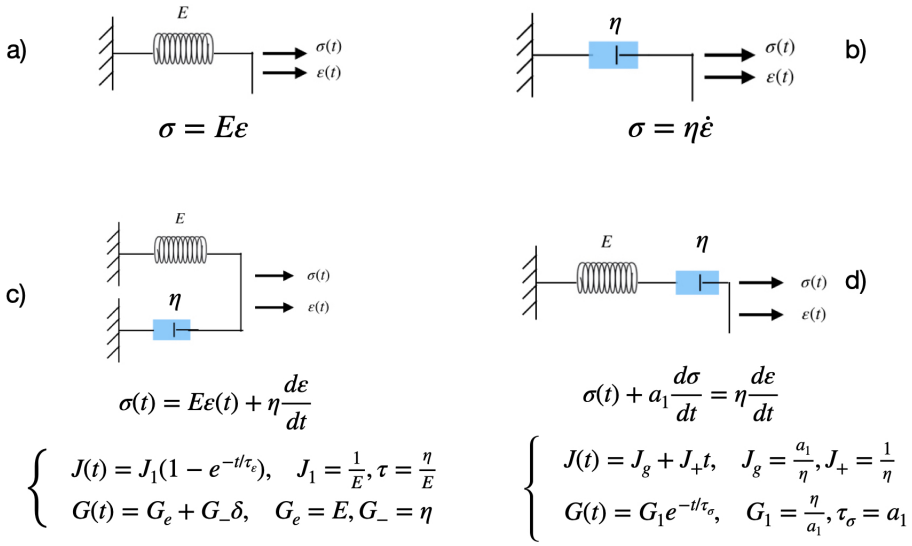

Figure 3.3: classic viscoelastic models: a) Hooke model, b) Newton model, c) Kelvin-Voigt model, d)Maxwell model

Maxwell model exhibits an exponential (reversible) stress relaxation and a linear (non reversible) strain creep; it is also referred to as the relaxation element.

By increasing the number of simple elements to the Kelvin-Voigt model they are obtained other more accurate models in the simulation of viscoelastic behavior. Such models are called SLS (Standard Linear Solid) or Zener.

The simplest viscoelastic model is obtained by adding a spring either in series to a Voigt model or in parallel to a Maxwell model, respectively. In this way, according to the combination rule, we add a positive constant both to the Voigt-like creep compliance and to the Maxwell-like relaxation modulus so that $J_g > 0$ and $G_e > 0$. Such a model was considered by Zener with the denomination SLS and will be referred here also as the Zener model. We have for the model in fig.3.4a The model shown in fig.3.4b, consisting of a Hooke in model parallel with a Maxwell model with α and β the same for both.

In similar fashion the functional stress-strain relations reported in eqs.(3.10a) (3.10b) possess an equivalent differential formulation in terms of elastic (Hookean) and viscous (Newtonian) elements.

In more details, the differential formulation of the Prony series expansion for the creep function $J(t)$ in eqs.(3.10a) (3.10b) is provided in fig.3.3. Similarly the mechanical arrangements springs and dashpots reported in fig. (3.3

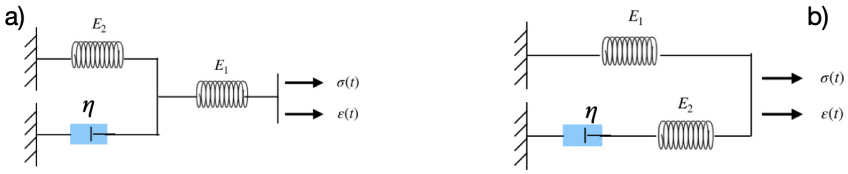

$$\dot{\sigma}(t) + \alpha\sigma(t) = E_1\left[\dot{\varepsilon}(t) + \beta\varepsilon(t)\right] \qquad \dot{\sigma}(t) + \beta\sigma(t) = \alpha\eta\dot{\varepsilon}(t) + \beta E_1\varepsilon(t)$$

$$\alpha = \frac{E_1 + E_2}{\eta} \qquad \beta = \frac{E_2}{\eta}$$

Figure 3.4: a)Zener model:a spring in series to a Voigt model; b) Zener model: a spring in parallel to a Maxwell model

b) corresponds to the rheological representation of the relaxation function $G(t)$ reported in eqs.(3.10a) (3.10b). with $\tau_c = \tau_r = \dfrac{\eta_1}{E_1}$. Direct comparisons of figs.(3.3 a and b) shows that the mechanics beyond the creep and relaxation functions described by Prony series expansion is quite different as shown by the series and parallel arrangements of springs and dashpots that correspond to the prescribed analytical expression in eqs.(3.10a) (3.10b). Such a consideration is a direct consequence to the lack of mathematical consistency of creep and relaxation functions expressed in terms of Prony series expansions. In passing we observe that, as far as $N = M = 1$ the well-known Maxwell elements representing relaxation and Kelvin-Voigt element for creep are obtained.

3.1.2 1D Fractional-order linear hereditariness

Linear hereditariness is certainly the field of the most extensive applications of fractional calculus, in view of its ability to model hereditary phenomena with long memory. The analysis start from the power-law creep to justify the introduction of the operators of fractional calculus into the stress-strain relationship.

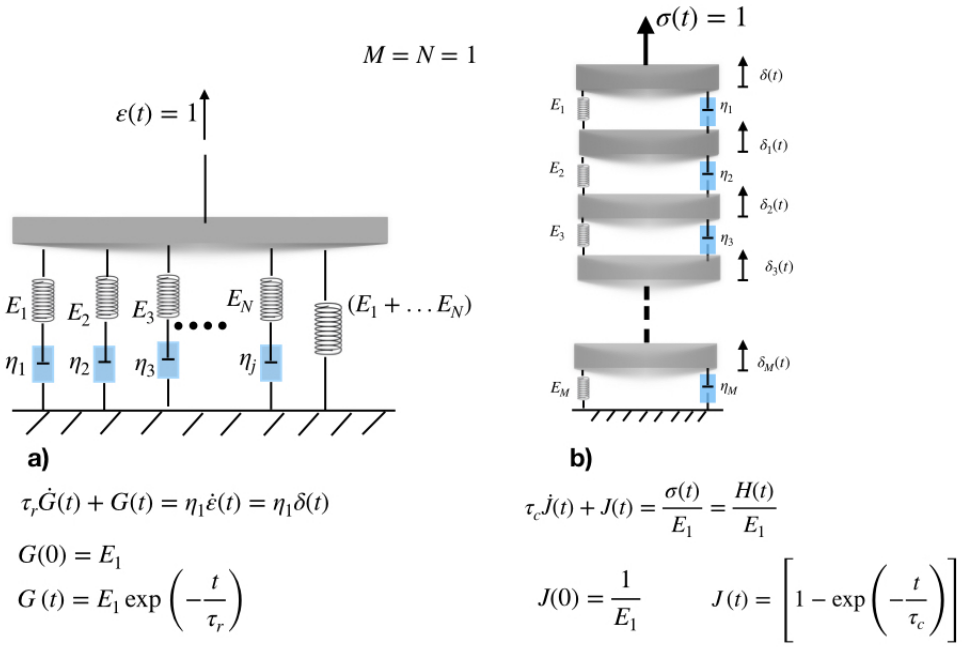

Figure 3.5: a) Rheological model for exponential relaxation; b) Rheological model for exponential creep

Let us consider the hereditariness of a material with creep compliance,

$$J(t) = \frac{1}{G_0\Gamma(1+\beta)}\left(\frac{t}{\tau_0}\right)^{\beta} \tag{3.11}$$

where $\Gamma(\cdot)$ is the Euler-Gamma function, β, and $[\tau_0] = T$ are material parameters that may be estimated through a best-fitting procedure of experimental data and G_0 the elastic modulus of the material. Such creep behaviour is found to be of great interest in a number of creep experiments; usually it is referred to as the power-law creep. In virtue of the reciprocity relationship eq.(3.9) in the Laplace domain we can find for such hereditariness solid its relaxation modulus,and then the corresponding relaxation spectrum. After simple manipulations we get

$$G(t) = \frac{G_0}{\Gamma(1-\beta)}\left(\frac{t}{\tau_0}\right)^{-\beta} \tag{3.12}$$

For our hereditariness solid exhibiting power-law creep, the stress/strain relationship in the creep representation can be easily obtained by inserting the creep law eq.(3.11) into the integral eq.(3.9). Straightforward manipulations

show that the power-law functional class in eqs.(2a, b) satisfies the conjugation relation and it yields, upon substitution in eqs. (1a, b) the following constitutive relations:

$$\sigma(t) = \frac{G_0\tau_0^\beta}{\Gamma(1-\beta)}\int_0^t (t-\tau)^{-\beta}\dot{\varepsilon}(\tau)d\tau = G_0\tau_0^\beta\left(D_{0^+}^\beta\varepsilon\right)(t) \tag{3.13a}$$

$$\varepsilon(t) = \frac{1}{G_0\tau_0^\beta\Gamma(\beta+1)}\int_0^t (t-\tau)^{\beta}\dot{\sigma}(\tau)d\tau = \frac{1}{\tau_0^\beta G_0}\left(I_{0^+}^\beta\sigma\right)(t) \tag{3.13b}$$

where $\left[{}_C D_0^{+\beta}\right]$ is the Fractional Caputo derivative and $[I_{o^+}^\beta]$ is the Riemann-Liouville fractionalintegral, The constitutive equation eqs. (3.13a)(3.13b) have been modelled with the introduction of a new rheological element, the springpot, fig.3.5 after Scott-Blair. Springpot is a mechanical element with mechanical properties are intermediate between those of a pure elastic solid (Hooke model) and a pure viscous fluid (Newton model). The use of fractional calculus in linear hereditariness leads us to generalize the classical mechanical models, in that the basic Newton element (dashpot) is substituted by springpot. The springpot, fig.3.6 defined in terms of two parameters, i.e. $C_\beta = G_0\tau_0^\beta \geq 0$ and β, with $\beta \in [0,1]$ whose constitutive relation is reported in eqs.(3a,b). Such element is widely used nowadays to define several types of materials including as limiting cases, elastic ($\beta = 0$) and viscous elements ($\beta = 1$). More precisely, a simple spring corresponds to $\beta = 0$ and $\dfrac{d^\beta f}{dt^\beta} = \dfrac{d^0 f}{dt^0} = f$; whilst the case of $\beta = 1$ corresponds to a first order derivative, i.e. $\dfrac{d^\beta f}{dt^\beta} = \dfrac{df}{dt} = \dot{f}$, which is a Newtonian dashpot.

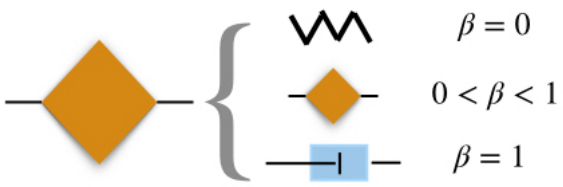

Figure 3.6: Springpot element

3.1.3 Three dimensional isotropic fractional-order nonlinear hereditariness

In such a context, uniaxial hereditariness [32, 37, 43, 65] involving fractional order stress-strain relations has been reported since the beginning of the 20th

century [74, 49] defining the so-called springpot element [16], as discussed in previus section.

In presence of the multi axial stress/strain state as that usually encountered in usual application the 3D constitutive relation describing material hereditariness is discussed in the context of power-laws functional classes of the relaxation/creep functions.

In such case an extension of the constitutive relation presented in section 3.1.2 and tensorial strain/stress state are discussed in this section by means of effect superposition.

Let us consider a 2nd-order stress tensor $\boldsymbol{\sigma}$ with the symmetries $\sigma_{ij} = \sigma_{ji}$ for $i \neq j$. In the following we introduce the Voigt representation of the state variables of the material in terms of vector representation of stress and strains tensors as:

$$\boldsymbol{\sigma}^T(t) = [\sigma_{11}(t)\,\sigma_{22}(t)\,\sigma_{33}(t)\,\sigma_{32}(t)\,\sigma_{31}(t)\,\sigma_{12}(t)] \tag{3.14}$$

$$\boldsymbol{\varepsilon}^T(t) = [\varepsilon_{11}(t)\,\varepsilon_{22}(t)\,\varepsilon_{33}(t)\,2\varepsilon_{32}(t)\,2\varepsilon_{31}(t)\,2\varepsilon_{12}(t)] \tag{3.15}$$

where t is the current time and the mixed index stress and strain components, namely $\sigma_{ij}(t)$ and $\varepsilon_{ij}(t)$ with $i \neq j$ denote shear stress and strain, respectively. Let us assume that $\sigma_{ij}(t) = \delta_{ij}$ and let us consider a single normal stress $\sigma_{ii} = 1$ for (i = 1,2,3).

In such a context the evolution of the strain $\varepsilon_{ii}(t)$ along the stress direction $\sigma_{ii}(t)$ and in the orthogonal planes reads:

$$\varepsilon_{ii}(t) = J_L(t)\,\sigma_{ii} = J_L(t) \tag{3.16a}$$

$$\varepsilon_{kk}(t) = \varepsilon_{jj}(t) = -J_v(t)\,\sigma_{ii} \tag{3.16b}$$

with $i \neq j \neq k$ and $i,\ j,\ k = 1, 2, 3$. In eqs.(3.16a)(3.16b) $J_L(t)$ and $J_v(t)$ are the axial and the transverse creep functions with respect to the stress direction, respectively. Under the assumption of smooth load process $\sigma_{ij}(t)$ the presence of contemporaneous stress $\sigma_{ij}(t) = \sigma_{ij}(t)\delta_{ij}$, with $i = 1, 2, 3$, may be accounted for by the integral

$$\varepsilon_{ii}(t) = \int_0^t J_L(t-\tau)\,\dot{\sigma}_{ii}(\tau) - J_v(t-\tau)\,[\dot{\sigma}_{jj}(\tau) + \dot{\sigma}_{kk}(\tau)]\,d\tau \tag{3.17}$$

with $i \neq j \neq k$ and i,j,k=1,2,3, respectively.

In the context of material isotropy shear strains $2\varepsilon_{ij}(t)$, $(i \neq j)$, are not involved by the axial stress $\sigma_{ii}(t)$, but only by the shear stress as $\sigma_{ij}(t)$ with $i \neq j$. The evolution of the shear strain $2\varepsilon_{ij}(t)$ due to a generic shear stress

history $\sigma_{ij}(t)$ may be obtained by superposition integrals by means of the shear creep function $J_T(\cdot)$ as:

$$2\varepsilon_{ij}(t) = \int_0^t J_T(t-\tau)\dot{\sigma}_{ij}(\tau)\, d\tau \tag{3.18}$$

with $i \neq j$ and $i, j = 1, 2, 3$. The constitutive equations reported in eqs.(3.17),(3.18) may be reported in Voigt notation as:

$$\boldsymbol{\varepsilon}(t) = \int_0^t \mathbf{J}(t-\tau)\dot{\boldsymbol{\sigma}}(\tau)\, d\tau \tag{3.19}$$

where $\mathbf{J}(t)$ is the creep functions matrix that is described as:

$$\mathbf{J}(t) = \begin{bmatrix} \mathbf{J}^{(A)}(t) & \mathbf{0} \\ \mathbf{0} & \mathbf{J}^{(T)}(t) \end{bmatrix} \tag{3.20}$$

where the elements of the axial creep matrix $\mathbf{J}^{(A)}(t)$ are:

$$J_{ij}^{(A)}(t) = J_L(t)\,\delta_{ij} - (1-\delta_{ij})\,J_\upsilon(t) \tag{3.21}$$

with $i, j = 1, 2, 3$. The shear creep matrix $\mathbf{J}^{(T)}(t)$ is a diagonal matrix gathering the shear creep functions $J_T(t)$ as:

$$J_{ij}^{(T)}(t) = J_T(t)\,\delta_{ij} \tag{3.22}$$

The three creep functions $J_L(t)$,$J_\upsilon(t)$ and $J_T(t)$ are related by a linear relation that reads:

$$J_T(t) = 2J_L(t) - J_\upsilon(t) \tag{3.23}$$

that may be obtained, with straightforward manipulations, by introducing a shear stress state $\sigma_{ij}(t)$ that involves a shear strain state under isotropy assumption, namely $\gamma_{ij} = 2\varepsilon_{ij}(t)$, and as evaluating the elongation and the stress along the principal axes at angles of $\pi/4$.

Under the assumption of linear elasticity, the creep functions coincide with the material compliance, which reads $J_T = 1/G$, $J_L = 1/E$ and $J_\upsilon = \upsilon/E$. After substitution in eq.(3.23), this yields:

$$\frac{1}{G} = 2\left(\frac{1}{E} + \frac{\upsilon}{E}\right) = \frac{2(1+\upsilon)}{E} \tag{3.24}$$

that is the well-known relation among elasticity moduli.

Knowledge of the creep function matrix $\mathbf{J}(t)$ in eq.(3.20) allows for the definition of the relaxation matrix $\mathbf{G}(t)$ by means of the coniugation relation as:

$$\hat{\mathbf{G}}(s)\hat{\mathbf{J}}(s) = \frac{1}{s^2}\mathbf{I} \tag{3.25}$$

where $\mathbf{I}$ is the identity matrix and $\hat{\boldsymbol{G}}(s)$, $\hat{\boldsymbol{J}}(s)$ are the Laplace transforms of the relaxation $\mathbf{G}(t)$ and the creep functions $\mathbf{J}(t)$ matrices.

With straightforward manipulations of eq.(3.25) and inverse Laplace transform, the relaxation matrix may be written as: With straightforward manipulations of eq.(3.25) and inverse Laplace transform, the relaxation matrix may be written as:

$$\mathbf{G}(t) = \begin{bmatrix} \mathbf{G}^{(A)}(t) & \mathbf{0} \\ \mathbf{0} & \mathbf{G}^{(T)}(t) \end{bmatrix} \tag{3.26}$$

where:

$$G_{ij}^{(A)}(t) = \mathcal{L}^{-1}\left[\frac{1}{s^2\left(\hat{J}_L + \hat{J}_v\right)\left(\hat{J}_L - 2\hat{J}_v\right)}\right]\left[\left(\hat{J}_L - \hat{J}_v\right)\delta_{ij} + (1-\delta_{ij})\,\hat{J}_v\right] \tag{3.27a}$$

$$G_{ij}^{(T)}(t) = \mathcal{L}^{-1}\left[\frac{1}{s^2\left(\hat{J}_L + \hat{J}_v\right)}\right]\delta_{ij} \tag{3.27b}$$

Eqs.(3.27a),(3.146b) show that in the presence of material fading memory, the relaxation matrix $\mathbf{G}(t)$ is obtained as a combination of creep functions relative to uniaxial creep tests. Similar considerations may be also withdrawn from the observation that in uniaxial relaxation tests, the relaxation function $G_L(t)$ is obtained in lateral free conditions, that is the strain state involves $\varepsilon_{11} \neq \varepsilon_{22} \neq 0$ and $\varepsilon_{33} = 1$ and measuring only $\sigma_{33}(t) = G_L(t)$ relaxation with $\sigma_{11} = \sigma_{22} = 0$. Knowledge of the relaxation matrix of the material $\mathbf{G(t)}$ allows to evaluate the stress vector as:

$$\boldsymbol{\sigma}(t) = \int_0^t \mathbf{G}(t-\tau)\dot{\boldsymbol{\varepsilon}}(\tau)\,d\tau \tag{3.28}$$

The longitudinal shear and transverse relaxation functions $G_T(t)$,$G_L(t)$ and $G_v(t)$ are linearly related by an equation that is similar to the one involving creep functions in eq.(3.23), reading:

$$G_T(t) = \frac{1}{2}\left(G_L(t) - G_v(t)\right). \tag{3.29}$$

The latter allows for the evaluation of the transverse relaxation $G_v(t)$, as:

$$G_v(t) = G_L(t) - 2G_T(t) \tag{3.30}$$

In the following section, we derive the thermodynamic restrictions among the material parameters used in power-law representation of isotropic material hereditariness.

3.1.4 Power-law isotropic hereditariness: Thermodynamic restrictions

Let us assume that relaxation functions in laterally restrained axial and torsion shear tests may be captured, respectively, by power-laws with different order ($\alpha \neq \beta$) as:

$$G_L(t) = G_L^{(\alpha)} t^{-\alpha} + \bar{G}_L; \quad G_T(t) = G_T^{(\beta)} t^{-\beta} + \bar{G}_T \tag{3.31a}$$

$$G_v(t) = 2\left({G_T}^{(\beta)} t^{-\beta} + \bar{G}_T\right) - \left({G_L}^{(\alpha)} t^{-\alpha} + \bar{G}_L\right) \tag{3.31b}$$

with eq.(3.31b) obtained from the application of eq.(3.26). The physical dimensions of the coefficients are $[C_L] = [C_T] = F/L^2$, $\left[C_L^{(\alpha)}\right] = \dfrac{F}{L^2 T^{-\alpha}}$, $\left[C_L^{(\alpha)}\right] = \dfrac{F}{L^2 T^{-\beta}}$.

The expressions of the relaxation functions in eqs.(3.31a),(3.31b) yield the relaxation matrix of the material in eq.(3.26), with elements in the block matrices $\mathbf{G^{(A)}}(\mathbf{t})$ and $\mathbf{G^{(T)}}(\mathbf{t})$ reading:

$$G_{ij}^{(A)} = G_L(t)\,\delta_{ij} + (1 - \delta_{ij})\,G_v(t) \tag{3.32a}$$

$$G_{ij}^{(T)}(t) = G_T(t)\,\delta_{ij} \tag{3.32b}$$

We see that the relaxation matrix involves elements decaying with different power-laws of order β and α ($\alpha, \beta \in [0, 1]$).

The coefficients and parameters involved in the power-law descriptions of the material relaxation, namely, $G_L(t)$, $G_v(t)$ and $G_T(t)$ are related by thermodynamical restrictions to ensure the requirement of positive entropy rate increment [28]. Indeed, a dissipative simple solid is defined only if the restrictions:

$$\mathbf{G}(0) \geq \mathbf{G}(\infty) \geq 0 \tag{3.33}$$

$$\dot{\mathbf{G}}(0) \geq 0 \tag{3.34}$$

are fulfilled by the relaxation matrix of the material as reported in basic references on material hereditariness [24, 92, 28].

Eqs.(3.33)(3.34)are always satisfied by assuming positive values of the coefficients $\bar{G}_L$, $\bar{G}_T$ and $G_L^{(\alpha)}$ and $G_T^{(\beta)}$, whereas eq.(3.34)) alone is satisfied as the eigenvalues of the first derivative of the matrix, namely, $\dot{\mathbf{G}}(0)$ are all

negative. This requirement may be verified by introducing a one-parameter family of relaxation matrices defined on a real parameter δ as $\mathbf{G}_\delta(t) = \mathbf{G}(t+\delta)$, and by studying the behavior of $\dot{\mathbf{G}}_\delta(t)$ for the limiting case $\delta \to 0$.

The parameter-dependent family of matrices $\dot{\mathbf{G}}_\delta(t)$ is defined as:

$$\dot{\mathbf{G}}_\delta(t) = \begin{bmatrix} \dot{\mathbf{G}}_\delta^{(A)}(t+\delta) & \mathbf{0} \\ \mathbf{0} & \dot{\mathbf{G}}_\delta^{(T)}(t+\delta) \end{bmatrix} \tag{3.35}$$

where the elements read:

$$\dot{G}_\delta^{(A)}(t+\delta) = -G_L^{(\alpha)}\alpha(t+\delta)^{-\alpha-1} \tag{3.36a}$$

$$\dot{G}_\delta^{(T)}(t+\delta) = -G_T^{(\beta)}\beta(t+\delta)^{-\beta-1} \tag{3.36b}$$

$$\dot{G}_\delta^{(\upsilon)}(t+\delta) = -2G_T^{(\beta)}\beta(t+\delta)^{-\beta-1} + G_L^{(\alpha)}\alpha(t+\delta)^{-(\alpha+1)} \tag{3.36c}$$

Observe that the one-parameter family $\dot{\mathbf{G}}_\delta(t)$ tends to the limit:

$$\lim_{\delta\to 0} \dot{\mathbf{G}}_\delta(t) = \dot{\mathbf{G}}(t) \tag{3.37}$$

We can infer the behavior of $\dot{\mathbf{G}}(t)$ from that of $\mathbf{G}_\delta(t)$, and by letting $\delta \to 0$. In this regard, the requirement in eq.(3.37) may be recast as:

$$-\dot{G}(0) = -\lim_{\delta\to 0} \dot{G}_\delta(t) \geq 0 \tag{3.38}$$

that is we evaluate the eigenvalues $\lambda_i(\delta)$ $(i = 1, 2, ...6)$ of the matrix $\dot{\mathbf{G}}_\delta(0)$ and with the additional constraints $-\lambda_i(\delta) \geq 0$ $(i = 1, 2, ...6)$ as $\delta \to 0$.

The evaluation of the eigenvalues $\lambda_i(\delta)$ gives:

$$-\lambda_1(\delta) = -\lambda_2(\delta) = -2\left(\dot{G}_L(\delta) - \dot{G}_T(\delta)\right) \geq 0 \tag{3.39a}$$

$$-\lambda_3(\delta) = -\lambda_4(\delta) = -\lambda_5(\delta) = -\dot{G}_T(\delta) \geq 0 \tag{3.39b}$$

$$-\lambda_6(\delta) = -4\dot{G}_T(\delta) + \dot{G}_L(\delta) \geq 0 \tag{3.39c}$$

Substitution of eqs.(3.36a),(3.36b) into eq.(3.39b) shows that the inequality is fulfilled for $G_T^{(\beta)} \geq 0$ and $0 \leq \beta \leq 1$. The inequalities eqs.(3.39a),(3.39c) read, after substitution:

$$\alpha G_\alpha \delta^{-(\alpha+1)} - \beta G_\beta \delta^{-(\beta+1)} \geq 0 \tag{3.40a}$$

$$4\beta G_\beta \delta^{-(\beta+1)} - \alpha G_\alpha \delta^{-(\alpha+1)} \geq 0 \tag{3.40b}$$

that, after some straightforward manipulation, may be cast in a more suitable form, taking natural logarithms as:

$$\ln\left(A_{\alpha\beta}\right) \geq (\alpha - \beta)\ln\delta \tag{3.41a}$$

$$\ln\left[\frac{\left(A_{\alpha\beta}\right)}{4}\right] \leq (\alpha - \beta)\ln\delta \tag{3.41b}$$

where $A_{\alpha\beta} = \alpha G_L^{(\alpha)} / \left(\beta G_T^{(\beta)}\right)$. Inequalities in eqs.(3.41a)(3.41b) must be fulfilled for any value of the parameter δ yielding that $\alpha = \beta$. Moreover, in this latter case the additional thermodynamical restriction holds true.

$$G_T^{(\beta)} \leq G_L^{(\beta)} \leq 3G_T^{(\beta)}. \tag{3.42}$$

In passing, we observe that the condition $\alpha = \beta$ holds true only for the two terms (or one term) description of the relaxation function in eq.(3.32a). Indeed, as we assume that the relaxation functions $G_L(t)$ and $G_T(t)$ involve linear combinations of power-laws as:

$$G_L\left(t\right) = \sum_{j=1}^{n} G_L^{(\alpha_j)} t^{-\alpha_j}; \quad G_T\left(t\right) = \sum_{i=1}^{m} G_T^{(\beta_i)} t^{-\beta_i} \tag{3.43}$$

with n and m the number of power-laws involved. Under such circumstances, the thermodynamical arguments proposed in this study yield the same conditions among the order of the power-laws as:

$$\max_{j=1,N}\left(\alpha_j\right) = \max_{i=1,M}\left(\beta_j\right) \tag{3.44a}$$

$$\min_{j=1,N}\left(\alpha_j\right) = \min_{i=1,M}\left(\beta_j\right) \tag{3.44b}$$

Substitution of eqs.(3.32a),(3.32b) into the constitutive equations for the three-axial hereditariness yields a relation among the stress vector and the history of the strain vector $\boldsymbol{\varepsilon}(t)$ as:

$$\boldsymbol{\sigma}\left(t\right) = \mathbf{G}_\beta \int_0^t \left(t-\tau\right)^{-\beta} \dot{\boldsymbol{\varepsilon}}\left(\tau\right) d\tau + \bar{\mathbf{G}} = \mathbf{G}_\beta \left(D_{0^+}^{\beta} \boldsymbol{\varepsilon}\right)\left(t\right) + \bar{\mathbf{G}} \tag{3.45}$$

where we have embraced the Voigt representation of the relaxation tensor $\mathbf{G}\left(\mathbf{t}\right)$ in matrix form and we have used the notation:

$$\mathbf{G}\left(t\right) = \mathbf{G}_\beta \frac{t^{-\beta}}{\Gamma\left(1-\beta\right)} + \bar{\mathbf{G}} \tag{3.46}$$

with the matrices:

$$\mathbf{G}_{\beta}(t) = \begin{bmatrix} G_{\beta}^{(L)} & G_{\beta}^{(\upsilon)} & G_{\beta}^{(\upsilon)} & 0 & 0 & 0 \\ G_{\beta}^{(\upsilon)} & G_{\beta}^{(L)} & G_{\beta}^{(\upsilon)} & 0 & 0 & 0 \\ G_{\beta}^{(\upsilon)} & G_{\beta}^{(\upsilon)} & G_{\beta}^{(L)} & 0 & 0 & 0 \\ 0 & 0 & 0 & G_{\beta}^{(T)} & 0 & 0 \\ 0 & 0 & 0 & 0 & G_{\beta}^{(T)} & 0 \\ 0 & 0 & 0 & 0 & 0 & G_{\beta}^{(T)} \end{bmatrix} \tag{3.47a}$$

$$\overline{\mathbf{G}} = \begin{bmatrix} \bar{G}_L & \bar{G}_{\upsilon} & \bar{G}_{\upsilon} & 0 & 0 & 0 \\ \bar{G}_{\upsilon} & \bar{G}_L & \bar{G}_{\upsilon} & 0 & 0 & 0 \\ \bar{G}_{\upsilon} & \bar{G}_{\upsilon} & \bar{G}_L & 0 & 0 & 0 \\ 0 & 0 & 0 & \bar{G}_T & 0 & 0 \\ 0 & 0 & 0 & 0 & \bar{G}_T & 0 \\ 0 & 0 & 0 & 0 & 0 & \bar{G}_T \end{bmatrix} \tag{3.47b}$$

The stress vector obtained as a functional of the strain vector $\boldsymbol{\varepsilon}(t)$ in eq.(3.45) is the generalization of the constitutive equation reported in eq.(3.8a) under the assumption of material isotropy.

In the next section the multiaxial fractional-order hereditariness will be further discussed by introducing a mechanical hierarchy that yields the constitutive model reported in eq.(3.45)

3.1.5 Exact mechanical description of fractional-order isotropic hereditariness

The stress/strain tensor outlined in section (2) requires a multiaxial constitutive relation, as in eq.(3.45), that under the assumption of $\bar{\mathbf{G}} = 0$ generalizes eq.(3.8a).

The rheological element, namely the springpot, corresponding to eq.(3.8a) can not, however, be defined also for the isotropic description, namely for the presence of shear stress/strain. A mechanical model that may be involved in the presence of normal and shear stress to be used in experimental test is represented in Fig.3.8

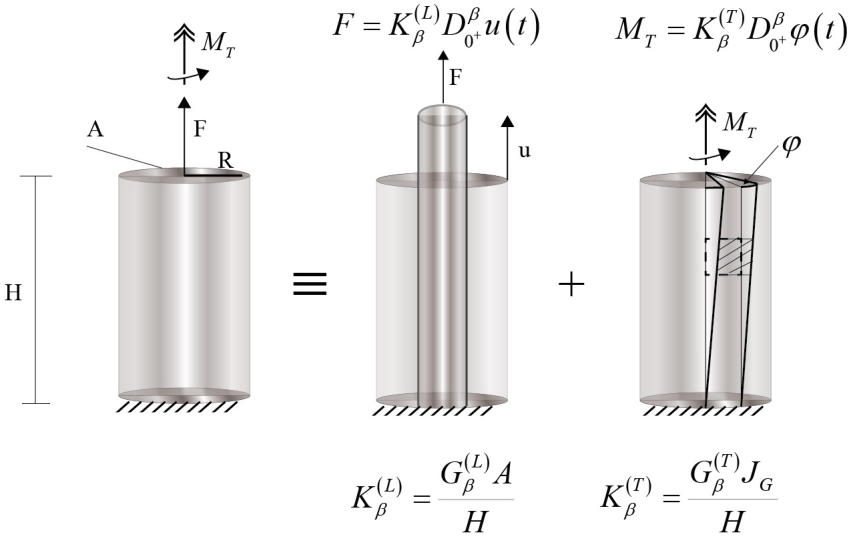

Figure 3.7: Rheologic elements

Under such conditions, the circular column of height H, cross section A and radius R under axial stress and shear stress related to the measured relative displacements $u(t)$ and twist angle $\varphi(t)$ provides these equilibrium equations:

$$\begin{aligned} F &= K_\beta^{(L)} (D_{0+}^\beta u)(t) \\ M_T &= K_\beta^{(T)} (D_{0+}^\beta \varphi)(t) \end{aligned} \tag{3.48}$$

where $J_G = \pi R^4/4$ is the polar moment of inertia of the circular cross-section represented in Fig.3.8. The constitutive equation(3.48) involve for limiting cases: i) a linear elastic spring ($\beta = 0$); and ii) a linear viscous element ($\beta = 1$), respectively.

In the following, we introduce a hierarchic mechanical model to capture the axial and shear hereditariness assuming power-law description of the creep and relaxation functions for axial and shear stress/strain, respectively [37, 32]. The obtained mechanical hierarchy corresponds exactly to an axial and shear springpots with the same order of time evolution/decay.

To this aim let us introduce an elastic column of unbounded length with circular cross section of radius R. The elastic features of the column are non-costant along the column axis and vary with the coordinate as:

$$E(z) = \frac{E_\alpha}{\Gamma(1-\alpha)} z^{-\alpha}; \quad G(z) = \frac{G_\alpha}{\Gamma(1-\alpha)} z^{-\alpha} \quad -1 \le \alpha \le 1 \tag{3.49}$$

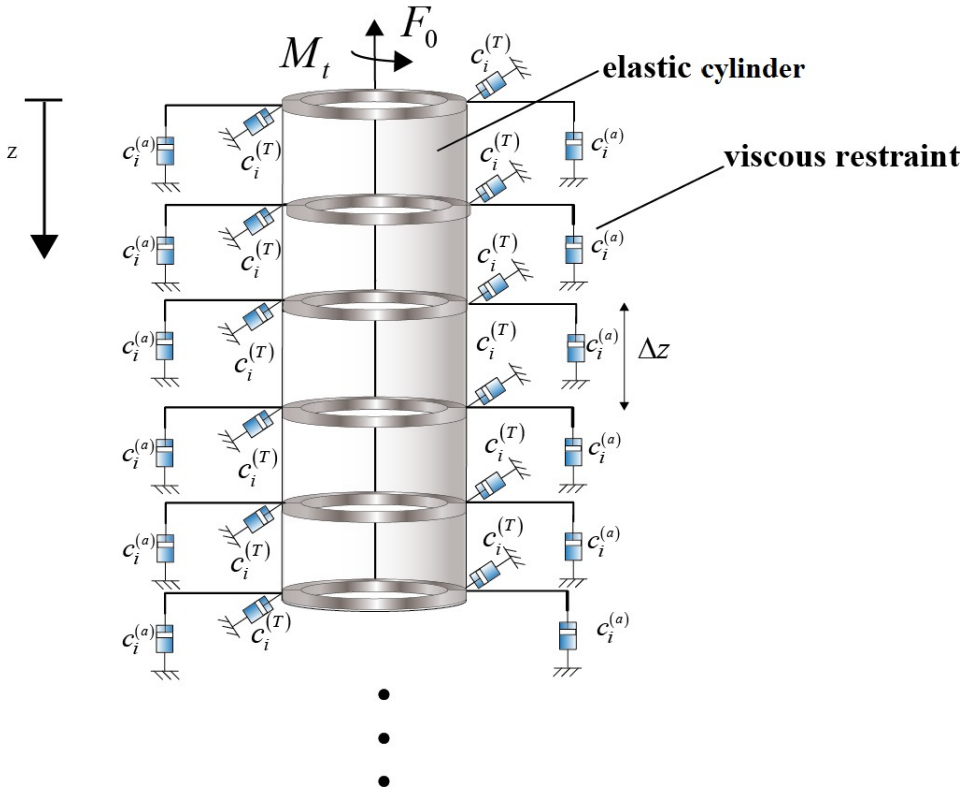

Figure 3.8: column with non-homogeneous viscosity

The column is externally restrained by a set of torsional and axial viscous dashpots Fig.3.9 with non-homogeneous viscosity $\eta(z)$ as:

$$\eta\left(z\right)=\frac{\eta_{\alpha}}{\Gamma\left(1+\alpha\right)}z^{-\alpha}\qquad-1\leq\alpha\leq1 \tag{3.50}$$

Axial and torsional equilibrium along the column axis reads:

$$\frac{\eta_{\alpha}}{\Gamma\left(1+\alpha\right)}z^{-\alpha}2\pi R\Delta z\dot{u}\left(z,t\right)=\frac{E_{\alpha}\pi R^{2}s(z+\Delta z)^{-\alpha}}{\Gamma\left(1-\alpha\right)}\left[u\left(z+\Delta z,t\right)-u\left(z,t\right)\right]+$$

$$+\frac{E_{\alpha}\pi R^{2}sz^{-\alpha}}{\Gamma\left(1-\alpha\right)}\left[u\left(z,t\right)-u\left(z-\Delta z,t\right)\right] \tag{3.51a}$$

$$\frac{\eta_{\alpha}}{\Gamma\left(1+\alpha\right)}z^{-\alpha}2\pi R^{2}\Delta z\dot{\varphi}\left(z,t\right)=G_{\alpha}\pi R^{4}(z+\Delta z)^{-\alpha}\left[\varphi\left(z+\Delta z,t\right)-\varphi\left(z,t\right)\right]+$$

$$+G_{\alpha}\pi R^{4}(z+\Delta z)^{-\alpha}\left[\varphi\left(z,t\right)-\varphi\left(z-\Delta z,t\right)\right] \tag{3.51b}$$

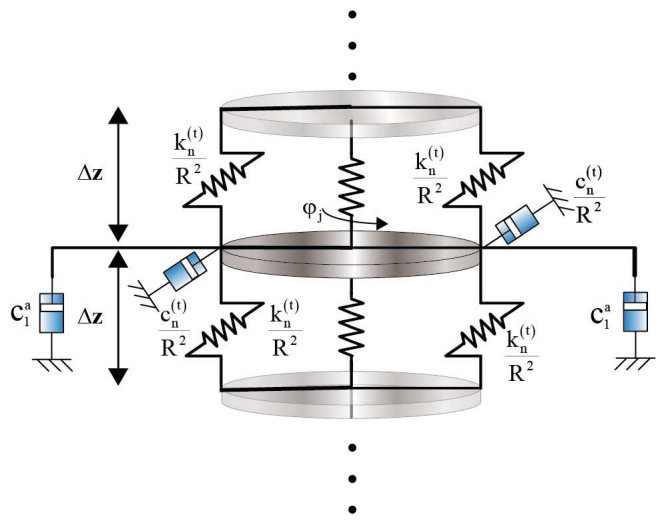

Figure 3.9: elements of the column with non-homogeneous viscosity

that, can be rewritten in differential form, by letting $\Delta z \to 0$ as:

$$\frac{\eta_\alpha z^{-\alpha}}{\Gamma(1+\alpha)}\frac{\partial u(z,t)}{\partial t} = \frac{E_\alpha R s}{\Gamma(1-\alpha)}\frac{\partial}{\partial z}\left(z^{-\alpha}\frac{\partial u(z,t)}{\partial z}\right) \tag{3.52a}$$

$$\frac{\eta_\alpha z^{-\alpha}}{\Gamma(1+\alpha)}\frac{\partial \varphi(z,t)}{\partial t} = \frac{G_\alpha R}{\Gamma(1-\alpha)}\frac{\partial}{\partial z}\left(z^{-\alpha}\frac{\partial \varphi(z,t)}{\partial z}\right) \tag{3.52b}$$

The boundary conditions involving the differential fields $u(z,t)$ and $\varphi(z,t)$ in eqs.(3.52a),(3.52b) read, respectively.

$$\lim_{z\to\infty} u(z,t) = 0 \tag{3.53a}$$

$$\lim_{z\to 0} \frac{E_\alpha}{\Gamma(1-\alpha)} z^{-\alpha}\frac{\partial u}{\partial z} = F_0 \tag{3.53b}$$

$$\lim_{z\to\infty} \varphi(z,t) = 0 \tag{3.54a}$$

$$\lim_{z\to 0} \frac{G_\alpha}{\Gamma(1-\alpha)} z^{-\alpha}\frac{\partial \varphi}{\partial z} = M_0 \tag{3.54b}$$

Mathematical operators and boundary conditions in eqs.(3.54a)(3.54b) are completely equivalent to those of a previous differential problem that has been solved by resorting to a non- linear mapping followed by Laplace transforms [37, 31]. Such a procedure yields a Bessel differential equation of second kind in terms of the anomalous Laplace parameters. The position of

the boundary conditions and inverse Laplace transform provides the solution in the form:

$$u_0(t) = u_0(z,t) = \lim_{z\to\infty} u(z,t) = \frac{t^{-\beta}}{k_\beta^{(L)}} F_0 = J_L(t) F_0 \tag{3.55}$$

$$\varphi_0(t) = \varphi_0(z,t) = \lim_{z\to\infty} \varphi(z,t) = \frac{t^{-\beta}}{k_\beta^{(T)}} M_0 = J_T(t)_0 \tag{3.56}$$

with:

$$k_\beta^{(L)} = \frac{\Gamma(2\beta)\left(\tau_L^\beta\right)}{E_\alpha 2^{1-2\beta}\Gamma(\beta)\Gamma(1-\beta)} \tag{3.57}$$

$$k_\beta^{(T)} = \frac{\Gamma(2\beta)\left(\tau_L^\beta\right)}{G_\alpha 2^{1-2\beta}\Gamma(\beta)\Gamma(1-\beta)} \tag{3.58}$$

with $\beta = \dfrac{1+\alpha}{2}$ and the relaxation times:

$$\tau_L = \frac{\eta_\alpha}{E_\alpha}\frac{\Gamma(1-\alpha)}{\Gamma(1+\alpha)} \tag{3.59}$$

$$\tau_T = \frac{\eta_\alpha}{G_\alpha}\frac{\Gamma(1-\alpha)}{\Gamma(1+\alpha)} \tag{3.60}$$

The Superposition principle provides, by resorting to the fundamental equations of linear viscoelasticity, the constitutive equations of the macroscopic variables, as:

$$F_0(t) = k_\beta^{(L)}\left(D_{0^+}^\beta u_0\right)(t) \tag{3.61}$$

$$M_T(t) = k_\beta^{(T)}\left(D_{0^+}^\beta \varphi_0\right)(t) \tag{3.62}$$

Eqs.(3.61),(3.62) are the constitutive equation at the macro-scale and, by recalling that $F_0 = \sigma_{33} A$ and $|\tau| = \sqrt{|t_{31}|^2 + |t_{32}|^2} = \dfrac{M_0}{2As}$, the constitutive equations of the material read:

$$\sigma_{33} = G_\beta^{(L)}\left(D^\beta \varepsilon_{33}\right)(t) \tag{3.63}$$

$$|\tau| = G_\beta^{(T)}\left(D^\beta |\gamma|\right)(t) \tag{3.64}$$

where the coefficients $G_\beta^{(L)}$ and $G_\beta^{(T)}$ read:

$$G_\beta^{(L)} = \frac{\bar{k}_\beta^{(L)}\bar{l}}{A} \qquad G_\beta^{(T)} = \frac{\bar{k}_\beta^{(T)}}{2As}\frac{R}{\bar{l}} \tag{3.65}$$

and where $\bar{l}$ is an internal length of the material. Eqs.(3.63),(3.64) are the multiaxial constitutive relations of the isotropic material and, henceforth, correspond to the hierarchy introduced by the fractional-order isotropy.

3.2 Non-Linear Viscoelasticity

Many materials or structures are called soft in the sense that they are able to undergo large displacements / rotations, possibly in addition to large strains: rubbery materials and soft living tissues are typical examples, but truss-like structures also display such behaviors due to some internal mechanisms. The mechanical response of soft materials during their service life is very seldom linear (unless restricted to the small strains regime in some specific use), and most of the time, non-linearities are present; an intuitive idea of a nonlinear response is provided by the crushing of a soft ball, with the ball returning to its initial shape when the pressure is released. Non-linearities in continuum mechanics can be classified as geometrical non-linearities and material non-linearities: the first type (geometrical non-linerarities)occur when the displacement or rotation of material elements of the structure are large in comparison to its size; this may occur for slender structures having a small bending stiffness compared to their in-plane properties. The second type (material non-linearities) are due to the occurrence of large strains.

The experimental results illustrated show that biological tissues are not elastic [5, 7]. The history of strain affects the stress. In particular, there is a considerable difference in stress response to loading and unloading. Most authors discuss soft tissue experiments in the framework of the linear theory of viscoelasticity relating stress and strain on the basis of the Voigt, Maxwell, and Kelvin models,formulated a continuous relaxation spectrum that corresponds to a combination of an infinite number of Voigt and Maxwell elements. A non-linear theory of the Kelvin type was proposed by Viidik (1966) on the basis of a sequence of springs of different natural length, with the number of participating springs increasing with increasing strain. It is reasonable to expect that for oscillations of small amplitude about an equilibrium state, the theory of linear viscoelasticity should apply. For finite deformations, however, the non-linear stress-strain characteristics of the living tissues must be accounted for.

For a viscoelastic solid the constitutive assumption states that the stress σ, internal energy "e" and specific entropy η at time t depend on histories of the deformation gradient $\boldsymbol{F}$, temperature θ and temperature gradient. Thermodynamic arguments show that the stress, internal energy, and specific entropy it is assumed that do not depend on the temperature gradient $grad\theta$. Temperature, being a scalar will not be explicitly mentioned.

As in the case of linear viscoelasticity, it is assumed that the solid is in its reference configuration for $t < 0$, i.e. $\boldsymbol{F}(t) = \boldsymbol{I}$, $t < 0$. It is further assumed that the material does not age and the stress at the current time t depends on the history of the deformation gradient,$\bar{t} \in (-\infty, t]$, thereby allowing for

jump discontinuities at $t = 0$. This constitutive equation expressing this dependence is denoted by

$$\boldsymbol{\sigma} = \mathcal{F}\left[\boldsymbol{F}(t-\bar{t})|_{\bar{t}=0}^{\infty}\right] \tag{3.66}$$

$\mathcal{F}$ is called a tensor-valued response functional and plays the rule of the material response function $\phi_r(\varepsilon, t)$ observed in previous chapter. There are three main sources of restrictions on $\mathcal{F}$: (a) the influence of superposed rigid body motions, (b) material symmetry, (c) restrictions due to thermodynamics.

Consider the motion $\boldsymbol{x}(\bar{t}) = \boldsymbol{\chi}(\boldsymbol{X}, \bar{t})$, $\bar{t} \in [0, t]$ and suppose that the body undergoes a second motion $\boldsymbol{x}(\bar{t}) = \boldsymbol{\chi}^*(\boldsymbol{X}, \bar{t})$ that is obtained from the first by a superposed rigid body motion,

$$\boldsymbol{\chi}^*(\boldsymbol{X}, \bar{t}) = \boldsymbol{Q}(\bar{t})\left[\boldsymbol{\chi}(\boldsymbol{X}, \bar{t}) - \boldsymbol{d}(\bar{t})\right], \quad \bar{t} \in [0, t] \tag{3.67}$$

Vector $\boldsymbol{d}(\bar{t})$ represents a rigid body translation. $\boldsymbol{Q}(\bar{t})$ represents a rigid body rotation and satisfies the orthogonal condition as:

$$\boldsymbol{Q}(\bar{t})\boldsymbol{Q}(\bar{t})^T = \boldsymbol{Q}(\bar{t})^T\boldsymbol{Q}(\bar{t}) = \boldsymbol{I} \tag{3.68}$$

It is assumed that the superposed rigid body motion affects the stress at time t by only its rotation at time $\bar{t}$. This leads to the condition that

$$\mathcal{F}[\boldsymbol{Q}(t-\bar{t})\boldsymbol{F}(t-\bar{t})|_{\bar{t}=0}^{\infty}] = \boldsymbol{Q}(\bar{t})\mathcal{F}[\boldsymbol{F}(t-\bar{t})|_{\bar{t}=0}^{\infty}]\boldsymbol{Q}(\bar{t})^T \tag{3.69}$$

for any rotation history $\boldsymbol{Q}(\bar{t})$ as long as it satisfies eq.(3.68). This, when combined with the Polar Decomposition of $\boldsymbol{F}(\bar{t})$ leads to the statement that eq.(3.66) is of the form

$$\boldsymbol{\sigma} = \boldsymbol{R}(t)\mathcal{F}\left[\boldsymbol{U}(t-\bar{t}|_{\bar{t}=0}^{\infty}\right]\boldsymbol{R}(t)^T \tag{3.70}$$

Because $\boldsymbol{U}$ and $\boldsymbol{C}$ contain essentially the same information about the local deformation and $\mathcal{F}$ is as yet arbitrary, eq. (3.70) is usually restated without loss in generality in the form

$$\boldsymbol{\sigma} = \boldsymbol{F}(t)\mathcal{G}\left[\boldsymbol{C}(t-\bar{t})|_{\bar{t}=0}^{\infty}\right]\boldsymbol{F}(t)^T \tag{3.71}$$

where $\mathcal{G}$ is a new response functional.

The concept of material symmetry arises from the fact that a material has some physical microstructure in its reference configuration, such as a crystalline structure or a randomly oriented macromolecular network. Consider a sample of material in its reference configuration and its microstructure. Suppose there is a transformation of this reference configuration to a new configuration such that the material appears to have the same microstructure as

before. Let both the original and transformed configurations be subjected to the same homogeneous deformation history with deformation gradient $\boldsymbol{F}(\bar{t})$. The underlying microstructures, which appear to be the same in their respective reference configurations, are distorted in the same way. The stresses are assumed to be the same at each time t and these configurations are said to be mechanically equivalent.

A transformation of the original reference configuration to one that is mechanically equivalent is a linear transformation denoted by $\boldsymbol{H}$. One restriction on $\boldsymbol{H}$ is that it produce no volume change and this leads to the condition that $|det\boldsymbol{H}| = 1$. In addition, for most equivalent microstructures of interest, $\boldsymbol{H}$ is a rotation or a reflection and satisfies

$$\boldsymbol{H}\boldsymbol{H}^T = \boldsymbol{H}^T\boldsymbol{H} = \boldsymbol{I} \tag{3.72}$$

Symmetries of a material are described by specifying the set of transformations $\boldsymbol{H}$ that lead to equivalent microstructures. These form a mathematical entity called a material symmetry group. The material symmetries commonly used to describe nonlinear viscoelastic materials are isotropy, transverse isotropy and orthotropy

The possible motions of a body may be limited by constraints such as incompressibility or inextensibility in certain directions. Such constraints impose restrictions on the constitutive equations. Discussion here is restricted to the constraint of incompressibility, this leads to an idealized material model for which any possible motion must satisfy the constraint,

$$det\boldsymbol{F}(\bar{t}) = 1, \quad \bar{t} \in [0, t] \tag{3.73}$$

Consideration of the restrictions of the thermodynamics for materials with constraint eq.(3.73) leads to a modified form for constitutive equation eq.(3.66),

$$\boldsymbol{\sigma}(t) = -p(t)\boldsymbol{I} + \mathcal{F}[\boldsymbol{F}(t - \bar{t})|_{\bar{t}=0}^{\infty}] \tag{3.74}$$

in which $p(t)$ is an arbitrary scalar function. The restriction imposed by consideration of the influence of superposed rigid body motions must still be satisfied so that $\mathcal{F}$ in eq.(3.74) still must satisfy eq.(3.69).

There is an interesting result for isotropic nonlinear viscoelastic solids that does not depend on the form of the response functional $\mathcal{F}$. Since (3.69) must hold for arbitrary rotation transformations $\boldsymbol{H}$ and rotation histories $\boldsymbol{Q}(\bar{t})$, $\bar{t} \in [0, t]$, in [72] it has shown that the constitutive equation can be written in the form

$$\boldsymbol{\sigma} = \hat{\mathcal{G}}[\boldsymbol{B}(t); \boldsymbol{C}_t(t - \bar{t})|_{\bar{t}=0}^{\infty}] \tag{3.75}$$

where $\boldsymbol{B}(t)$ is defined by $\boldsymbol{B}(t) = \boldsymbol{F}(t)\boldsymbol{F}(t)^T$ and is called the left Cauchy–Green tensor, and $\boldsymbol{C}_t(\bar{t})$ was defined by $\boldsymbol{C}_t(\bar{t}) = \boldsymbol{F}_t(\bar{t})^T\boldsymbol{F}_t(\bar{t})$, where $\boldsymbol{F}_t$ is called the relative deformation gradient. The response functional $\hat{\mathcal{G}}$ satisfies

$$\hat{\mathcal{G}}[\boldsymbol{H}^T\boldsymbol{B}(\boldsymbol{H};\boldsymbol{H}^T\boldsymbol{C}_t(t-\bar{t}))\boldsymbol{H}|_{\bar{t}=0}^{\infty}] = \boldsymbol{H}^T\hat{\mathcal{G}}[\boldsymbol{B};\boldsymbol{C}_t(t-\bar{t})|_{\bar{t}=0}^{\infty}]\boldsymbol{H} \tag{3.76}$$

for all orthogonal transformations $\boldsymbol{H}$. $\hat{\mathcal{G}}$ is said to be an isotropic functional. If, in addition, the material is incompressible and isotropic, the constitutive equation can be written as

$$\boldsymbol{\sigma}(t) = -p(t)\boldsymbol{I} + \hat{\mathcal{G}}[\boldsymbol{B};\boldsymbol{C}_t(t-\bar{t})|_{\bar{t}=0}^{\infty}] \tag{3.77}$$

where $\hat{\mathcal{G}}$ satisfies eq.(3.76).

A number of specific representations for the response functionals $\mathcal{F}$ and $\mathcal{G}$ have appeared in the literature and these are for example in the book by Lockett [64] as well as recent review article [40]. Some models proposed in the literature will be summarized below, and finally the model developed in this thesis will be presented.

3.2.1 Rate and Differential Type Constitutive Equations

One class of constitutive equations is that in which stress and its first "n" time derivative and the deformation gradient and its first "m" time derivatives, all evaluated at the current time t, are linked. We get for the functional

$$\mathcal{R}\left[\boldsymbol{\sigma}, \frac{d\boldsymbol{\sigma}}{dt}, \frac{d^2\boldsymbol{\sigma}}{dt^2}, ..., \frac{d^n\boldsymbol{\sigma}}{dt^n} : \boldsymbol{F}, , \frac{d\boldsymbol{F}}{dt}, \frac{d^2\boldsymbol{F}}{dt^2}, ..., \frac{d^m\boldsymbol{F}}{dt^m}\right] \tag{3.78}$$

where $\mathcal{R}$ is a function of $m + n + 2$ arguments. When subjected to the restrictions imposed by the considerations of superposed rigid body motions, the constitutive equation has the form [73].

$$\boldsymbol{R}_1\left[\boldsymbol{R}^T\boldsymbol{\sigma}\boldsymbol{R}, \boldsymbol{R}^T\frac{d^j}{d\bar{t}^j}\left[\boldsymbol{R}_t(\bar{t})^T\boldsymbol{\sigma}(\bar{t})\boldsymbol{R}_t(\bar{t})\right]_{\bar{t}=t}\boldsymbol{R}; \boldsymbol{U}, \boldsymbol{R}^T\left[\frac{d^k}{d\bar{t}^k}\boldsymbol{U}_t(\bar{t})\right]_{\bar{t}=t}\boldsymbol{R}\right] = \boldsymbol{0} \tag{3.79}$$

in which $J = 1, ..., n$ and $k = 1, ..., m$. Such constitutive equations are said to be of rate type and the j-th derivative

$$\frac{d^j}{d\bar{t}^j}\left[\boldsymbol{R}_t(\bar{t})^T\boldsymbol{\sigma}(\bar{t})\boldsymbol{R}_t(\bar{t})\right]_{\bar{t}=t} \tag{3.80}$$

is called the jth invariant stress rate. The orthogonal tensor $\boldsymbol{R}(\bar{t})$ is the rigid body rotation. Equation (3.79) can be solved, in concept, for the stress in terms of the deformation history or for the deformation in terms of the stress history. A special case of (3.79) is explicit in the stress and does not depend on the stress rates,

3.2.2 Green–Rivlin Multiple Integral Constitutive Equations

Previous considerations holds true as we do not specify the kinematic class of the deformations undergone by the solid.

In the following we may consider on attention measure of the strain with the introduction of the Green–St. Venant strain tensor defined by

$$\boldsymbol{E}(\bar{t}) = \frac{1}{2}\left(\boldsymbol{C}(\bar{t}) - \boldsymbol{I}\right) \tag{3.81}$$

Note $\boldsymbol{F} = \dfrac{\partial \boldsymbol{x}(\bar{t})}{\partial \boldsymbol{X}}$ that $\boldsymbol{E}(\bar{t}) = 0$, $\bar{t} \in (-\infty, 0)$. Let $\boldsymbol{E}(\bar{t})$ be introduced into eq.(3.71), which then becomes

$$\boldsymbol{\sigma}(\bar{t}) = \boldsymbol{F}(t)\mathcal{G}_1\left[\boldsymbol{E}(t-\bar{t})|_{\bar{t}=0}^{\infty}\right]\boldsymbol{F}(t)^T \tag{3.82}$$

Green and Rivlin [51] assumed that the response functional $\mathcal{G}_1$ is continuous in a $\boldsymbol{E}(\bar{t})$ in a sense described in [40]. By expressing $\boldsymbol{E}(\bar{t})$, $\bar{t} \in (0, t)$ as a Fourier series and then using the Stone–Weierstrass theorem, Green and Rivlin obtained a representation for eq.(3.82) as a multiple integral series,

$$\begin{aligned}
\mathcal{G}_1\left[\boldsymbol{E}(t-\bar{t})|_{\bar{t}=0}^{\infty}\right] &= \int_{-\infty}^{t} \boldsymbol{K}_1(t-\bar{t})d\boldsymbol{E}(t_1) + \\
&+ \int_{-\infty}^{t}\int_{-\infty}^{t} \boldsymbol{K}_2(t-t_1, t-t_2)d\boldsymbol{E}(t_1)d\boldsymbol{E}(t_2) \\
&+ \int_{-\infty}^{t}\int_{-\infty}^{t}\int_{-\infty}^{t} \boldsymbol{K}_3(t-t_1, t-t_2, t-t_3)d\boldsymbol{E}(t_1)d\boldsymbol{E}(t_2)d\boldsymbol{E}(t_3) + \ldots
\end{aligned} \tag{3.83}$$

in order to account for a jump discontinuity in $\boldsymbol{E}(\bar{t})$. $\boldsymbol{K}_1(t-\bar{t})d\boldsymbol{E}(t_1)$, $\boldsymbol{K}_2(t-t_1, t-t_2)$, $\boldsymbol{K}_3(t-t_1, t-t_2, t-t_3)$ are tensor-valued functions of order four, six and eight, respectively. The dual assumption can also be made. As discussed in Lockett [64], it has the form

$$\boldsymbol{E} = \mathcal{I}_1\left[\left(\boldsymbol{F}(\bar{t})^{-1}\boldsymbol{\sigma}(\bar{t})\boldsymbol{F}(\bar{t})^T\right)\|_{0^-}^{t}\right] \tag{3.84}$$

$\mathcal{I}_1$ has a multiple integral series representation analogous to eq.(3.83) with $\boldsymbol{E}(\bar{t})$ replaced by $\boldsymbol{F}(\bar{t})^{-1}\boldsymbol{\sigma}(\bar{t})\boldsymbol{F}(\bar{t})^T$. In applications, only the truncation of

eq.(3.83) or the series representation of eq. (3.84) up to triple integrals has been considered.

Coleman and Noll [25] developed a constitutive equation based on the assumption of fading memory, i.e. the current stress depends more on recent deformations than past deformations. They also assumed that deformation of the current configuration with respect to the reference configuration is large, and that the deformation of recent configurations relative to the current configuration changes slowly, in a sense made precise in [25]. This led to Taylor series–like approximations to eq.(3.71), the leading terms of which are

$$\boldsymbol{\sigma}(t) = \boldsymbol{R}(t)\Big\{\boldsymbol{k}_1\big[\boldsymbol{C}(t)\big] + \int_{-\infty}^{t} \boldsymbol{K}_1\big[\boldsymbol{C}(t), t-\bar{t}\big]\big[\boldsymbol{R}(t)^T(\boldsymbol{C}_t(\bar{t}) - \boldsymbol{I}\boldsymbol{R}(t))\big]d\bar{t}\Big\}\boldsymbol{R}(t)^T \tag{3.85a}$$

$$\boldsymbol{\sigma}(t) = \boldsymbol{F}(t)\Big\{\boldsymbol{k}_2\big[\boldsymbol{C}(t)\big] + \int_{-\infty}^{t} \boldsymbol{K}_2\big[\boldsymbol{C}(t), t-\bar{t}\big]\big[\boldsymbol{F}(t)^T(\boldsymbol{C}_t(\bar{t}) - \boldsymbol{I})\boldsymbol{F}(t)\big]d\bar{t}\Big\}\boldsymbol{F}(t)^T \tag{3.85b}$$

The integrands in eqs.(3.85a)(3.85b) are linear in the tensors $\boldsymbol{R}(t)^T(\boldsymbol{C}_t(\bar{t}) - \boldsymbol{I}\boldsymbol{R}(t)$ and $\boldsymbol{F}(t)^T(\boldsymbol{C}_t(\bar{t}) - \boldsymbol{I})\boldsymbol{F}(t)$. $\boldsymbol{K_1}$ and $\boldsymbol{K_2}$ are fourth-order tensor functions of $\bar{t}$ and $\boldsymbol{C}(t)$ and have the property, made precise in [25], that they monotonically decay to zero as $\bar{t}$ increases. Dependence on the finite strain tensor $\boldsymbol{C}(t)$ expresses the notion that deformation of the current configuration with respect to the reference configuration can be large. The linear dependence of the integrand on $\boldsymbol{C}_t(\bar{t}) - \boldsymbol{I}$ arises from the assumption that the deformation occurs slowly. If the material is assumed to be incompressible, then the assumption of fading memory imposed on eqs.(3.85a)(3.85b) leads

to

$$\boldsymbol{\sigma}(t) = -p(t)\boldsymbol{I} + \boldsymbol{R}(t)\Big\{\boldsymbol{k}_1\big[\boldsymbol{C}(t)\big] +$$

$$\int_0^t \boldsymbol{K}_1\big[\boldsymbol{C}(t), t-\bar{t}\big]\big[\boldsymbol{R}(t)^T(\boldsymbol{C}_t(\bar{t}) - \boldsymbol{I}\boldsymbol{R}(t))\big]d\bar{t}\Big\}\boldsymbol{R}(t)^T \tag{3.86a}$$

$$\boldsymbol{\sigma}(t) = -p(t)\boldsymbol{I} + \boldsymbol{F}(t)\Big\{\boldsymbol{k}_2\big[\boldsymbol{C}(t)\big] +$$

$$+ \int_0^t \boldsymbol{K}_2\big[\boldsymbol{C}(t), t-\bar{t}\big]\big[\boldsymbol{F}(t)^T(\boldsymbol{C}_t(\bar{t}) - \boldsymbol{I})\boldsymbol{F}(t)\big]d\bar{t}\Big\}\boldsymbol{F}(t)^T \tag{3.86b}$$

When there is no deformation, then $\boldsymbol{x}(t) = \boldsymbol{X}$, $t > 0$. All of the tensorial variables appearing in eqs.(3.86a)(3.86b) reduce to $\boldsymbol{I}$ and the stress reduces to $\boldsymbol{\sigma}(t) = \boldsymbol{k}_1(\boldsymbol{I})$ or $\boldsymbol{\sigma}(t) = \boldsymbol{k}_2(\boldsymbol{I})$. It is assumed that the material is stress free in its reference configuration so that $\boldsymbol{k}_1(\boldsymbol{I}) = \boldsymbol{k}_2(\boldsymbol{I}) = \boldsymbol{0}$. The dual form of this constitutive equation in which the deformation is expressed in terms of the stress history has not been considered.

3.2.3 Pipkin–Rogers Constitutive Theory

Pipkin and Rogers [79] developed a constitutive theory for nonlinear viscoelastic solids based on a set of assumptions about the response to step strain histories. The response functional in eq.(3.71) has the form of a series in which the first term gives the best approximation to measured mechanical response using single step strain histories. The next level of approximation uses the response to double step strain histories, and so on. The leading terms terms that make up the whole formulation

$$\boldsymbol{\sigma}(t) = \boldsymbol{F}(t)\Big\{\boldsymbol{K}_3\big[\boldsymbol{C}(t), 0\big] + \int_0^t \frac{\partial}{\partial(t-\bar{t})}\boldsymbol{K}_3\big[\boldsymbol{C}(t), t-\bar{t}\big]d\bar{t}\Big\}\boldsymbol{F}(t)^T \tag{3.87}$$

If the material is assumed to be incompressible, then

$$\boldsymbol{\sigma}(t) = -p(t)\boldsymbol{I} + \boldsymbol{F}(t)\Big\{\boldsymbol{K}_3\big[\boldsymbol{C}(t), 0\big] + \int_0^t \frac{\partial}{\partial(t-\bar{t})}\boldsymbol{K}_3\big[\boldsymbol{C}(t), t-\bar{t}\big]d\bar{t}\Big\}\boldsymbol{F}(t)^T \tag{3.88}$$

where the motion must be such that $det\boldsymbol{F}(t) = det\boldsymbol{C}(\bar{t}) = 1$. At a fixed value $\boldsymbol{C}$ of the strain tensor argument, $\boldsymbol{K}_3[\boldsymbol{C}, \bar{t}]$ is assumed to monotonically

decrease with $\bar{t}$ to a non-zero limit. This, in effect, incorporates the notion of fading memory into the Pipkin–Rogers constitutive theory. If the material does not deform from its reference configuration, then eq.(3.87) reduces to $\boldsymbol{\sigma}(t) = \boldsymbol{K}_3(\boldsymbol{I}, t)$. It is assumed that the material is stress free and hence $\boldsymbol{K}_3(\boldsymbol{I}, t) = 0$. Pipkin and Rogers discussed the dual to eq.(3.87). Although the dual formulation gives an expression that is convenient for modeling the results of creep experiments. Consequently, only eqs.(3.87)(3.88) are considered here.

3.2.4 Material Symmetry Restriction

The forms for the constitutive equations presented reduce the problem of finding material symmetry restrictions on the response functional $\mathcal{G}$ in eq.(3.71) to that of finding material symmetry restrictions on the tensor valued functions in eqs.(3.79),(3.83), (3.85a), (3.85b),(3.86a),(3.86b) or (3.87). Each of these is a tensor valued function of a set of tensors $\boldsymbol{M}_i$, $i = 1, 2...N$, that is, of the form $\boldsymbol{\Phi}(\boldsymbol{M}_1.\boldsymbol{M}_2, ...\boldsymbol{M}_N)$. The material symmetry condition

$$\boldsymbol{H}^T \mathcal{G}[\boldsymbol{C}(t-\bar{t})|_{\bar{t}=0}^{\infty}]\boldsymbol{H} = \mathcal{G}[\boldsymbol{H}^T\boldsymbol{C}(t-\bar{t})|_{\bar{t}=0}^{\infty}\boldsymbol{H}] \tag{3.89}$$

imposed on the functions $\boldsymbol{\Phi}$ has the form

$$\boldsymbol{H}\boldsymbol{\Phi}(\boldsymbol{M}_1, \boldsymbol{M}_2, ...\boldsymbol{M}_N)\boldsymbol{H}^T = \boldsymbol{\Phi}(\boldsymbol{H}\boldsymbol{M}_1\boldsymbol{H}^T, \boldsymbol{H}\boldsymbol{M}_2\boldsymbol{H}^T, ...\boldsymbol{H}\boldsymbol{M}_N\boldsymbol{H}^T) \tag{3.90}$$

The method for determining the form of $\boldsymbol{\Phi}(\boldsymbol{M}_1, \boldsymbol{M}_2, ...\boldsymbol{M}_N)$ satisfying eq.(3.90) has been presented in the review article [85]. It is shown in [85]that for each type of material symmetry,
1. there is a set of basic scalar functions $I_k(\boldsymbol{M}_1, \boldsymbol{M}_2, ...\boldsymbol{M}_N)$, $k = 1, ...k$, called invariants, that have the property

$$I_k(\boldsymbol{M}_1, \boldsymbol{M}_2, ...\boldsymbol{M}_N) = I_k(\boldsymbol{H}\boldsymbol{M}_1\boldsymbol{H}^T, \boldsymbol{H}\boldsymbol{M}_2\boldsymbol{H}^T, ...\boldsymbol{H}\boldsymbol{M}_N\boldsymbol{H}^T) \tag{3.91}$$

for each transformation $\boldsymbol{H}$ of the material symmetry group under consideration;
2. there is a set of basic tensor valued functions, $\boldsymbol{P}_m(\boldsymbol{M}_1, \boldsymbol{M}_2, ...\boldsymbol{M}_N)$, $m = 1, ...M$ that satisfy (3.90) for each transformation $\boldsymbol{H}$ of the material symmetry group under consideration.
3. A function $\boldsymbol{\Phi}(\boldsymbol{M}_1, \boldsymbol{M}_2, ...\boldsymbol{M}_N)$ that satisfies (3.90) can be represented in the form

$$\boldsymbol{\Phi} = \sum_{m=1}^{M} \tilde{\Phi}\boldsymbol{P}_m \tag{3.92}$$

where $\tilde{\Phi}$ is a scalar function of the basic scalar invariants, i.e. $\tilde{\Phi}_m = \tilde{\Phi}_m(I_1, ..., I_N)$. It is straightforward to show that eq.(3.92) satisfies eq.(3.90).

The representation eq.(3.92) shows that material symmetry restrictions determine the basic functions $\boldsymbol{P}_m(\boldsymbol{M}_1, \boldsymbol{M}_2, ...\boldsymbol{M}_N)$ and hence the general tensorial structure of$\boldsymbol{\Phi}(\boldsymbol{M}_1, \boldsymbol{M}_2, ...\boldsymbol{M}_N)$. Material symmetry restrictions also determine the arguments of the scalar coefficients $\tilde{\Phi}_m$, but provide no information as to how $\tilde{\Phi}_m$ depends on these arguments.

The constitutive theories above involve only second order tensors. In this case, there is no distinction between proper or full isotropy because eq.(3.71) is identically satisfied by central reflection transformations. The rate type constitutive equation in eq.(3.79) becomes

$$\mathcal{R}_2\Big[\boldsymbol{\sigma}, \boldsymbol{\sigma}_1, \boldsymbol{\sigma}_2, ..., \boldsymbol{\sigma}_n; \boldsymbol{A}_1, \boldsymbol{A}_2, ..., \boldsymbol{A}_m; \boldsymbol{B}\Big] = \boldsymbol{0} \tag{3.93}$$

The tensors $\boldsymbol{A}_k$, known as Rivlin–Ericksen tensors [82], are defined recursively by

$$\boldsymbol{A}_1 = (\boldsymbol{L} + \boldsymbol{L})^T -, \qquad \boldsymbol{A}_{k+1} = \frac{D\boldsymbol{A}_k}{Dt} + \boldsymbol{A}_k\boldsymbol{L} + \boldsymbol{L}^T\boldsymbol{A}_k \tag{3.94}$$

where $\boldsymbol{L} = \boldsymbol{F}\boldsymbol{F}^{-}1$. $\boldsymbol{\sigma}_n$ is defined recursively by

$$\boldsymbol{\sigma}_0 = \boldsymbol{\sigma}, \qquad \boldsymbol{\sigma}_{(n+1)} = \frac{D\boldsymbol{\sigma}_n}{Dt} + \boldsymbol{\sigma}_n\boldsymbol{L} + \boldsymbol{L}^T\boldsymbol{\sigma}_n \tag{3.95}$$

$\mathcal{R}_2$ is an isotropic function of its arguments.

The form of each integrand in eq.(3.83) can be constructed by identifying it with $\boldsymbol{\Phi}$. For isotropic materials, the Green–Rivlin constitutive equation eq. (3.83) becomes [64]

$$\begin{aligned}
\mathcal{G}_1\left[\boldsymbol{E}(t-\bar{t})|_{\bar{t}=0}^{\infty}\right] &= \int_{-\infty}^{t}[\psi_1 T_1\boldsymbol{I} + \psi_2\boldsymbol{M}_1]+ \\
&+ \int_{-\infty}^{t}\int_{-\infty}^{t}[\boldsymbol{I}\psi_3 T_1T_2 + \boldsymbol{I}\psi_4 T_{12} + \psi_5 T_1\boldsymbol{M}_2 + \psi_6\boldsymbol{M}_1\boldsymbol{M}_2] \\
&+ \int_{-\infty}^{t}\int_{-\infty}^{t}\int_{-\infty}^{t}[\boldsymbol{I}\psi_7 T_{123} + \boldsymbol{I}\psi_8 T_1T_{23} + \psi_9 T_1T_2\boldsymbol{M}_3+ \\
&+ \psi_{10}T_{12}\boldsymbol{M}_3 + \psi_{11}T_1\boldsymbol{M}_2\boldsymbol{M}_3 + \psi_{12}\boldsymbol{M}_1\boldsymbol{M}_2\boldsymbol{M}_3] + ...
\end{aligned} \tag{3.96}$$

where $\psi_i = \psi_i(t-t_1)$, $i = 1,2$, $\psi_i = \psi_i(t-t_1, t-t_2)$, $i = 3,4,5,6$, $\boldsymbol{M}_a = d\boldsymbol{E}(t_a)$, $T_a = tr(\boldsymbol{M}_a)$, $T_{a,b} = tr(\boldsymbol{M}_a\boldsymbol{M}_b)$ and $T_{a,b,c} = tr(\boldsymbol{M}_a\boldsymbol{M}_b\boldsymbol{M}_c)$

This constitutive theory received a great deal of attention when first proposed. An extensive discussion of experimental and analytical work based on this theory is provided in [45]. Most of the experimental work makes use of the dual form eq.(3.84) because it is experimentally more feasible to apply step stresses and measure creep. There is little current interest in the model for several reasons. The triple integral truncation of eq.(3.2.4) is adequate for strains of about 0.1. However, larger strains require integrals of higher multiplicity. This rapidly increases the number of experiments and functions of time to be measured and the cost of the numerical evaluation of the integrals.

Instead, when the material is isotropic eqs.(3.85a)(3.85b) can be written as eq.(3.75)

$$\boldsymbol{\sigma}(t) = \hat{\boldsymbol{k}}[\boldsymbol{B}(t)] + \int_{-\infty}^{t} \hat{\boldsymbol{K}}\big[\boldsymbol{B}(t), t-\bar{t}\big](\boldsymbol{C}_t(\bar{t}) - \boldsymbol{I})d\bar{t} \tag{3.97}$$

in which the forms of $\hat{\boldsymbol{k}}$ and $\hat{\boldsymbol{K}}$ are found using the precedent results. $\hat{\boldsymbol{K}}[\boldsymbol{B}, \bar{t}]$ has the property that it monotonically decreases with $\bar{t}$ to zero for fixed $\boldsymbol{B}$. In order to discuss the response to step changes in deformation, it is usually written in the alternate form obtained by integrating by parts,

$$\boldsymbol{\sigma}(t) = \tilde{\boldsymbol{k}}[\boldsymbol{B}(t)] + \int_{-\infty}^{t} \tilde{\boldsymbol{K}}\big[\boldsymbol{B}(t), t-\bar{t}\big]\frac{d\boldsymbol{C}_t(\bar{t})}{d\bar{t}}d\bar{t} \tag{3.98}$$

The form of $\tilde{\boldsymbol{k}}$ is

$$\tilde{\boldsymbol{k}} = a_0\boldsymbol{I} + a_1\boldsymbol{B} + a_2\boldsymbol{B}^2 \tag{3.99}$$

The scalar coefficients a_i are functions of the invariants $I_a(\boldsymbol{B})$ of $\boldsymbol{B}(t)$ defined by

$$I_1(\boldsymbol{B}) = tr(\boldsymbol{B}), \qquad I_2(\boldsymbol{B}) = \frac{1}{2}[tr(\boldsymbol{B})^2 - tr(\boldsymbol{B^2})], \qquad I_3(\boldsymbol{B}) = det(\boldsymbol{B}) \tag{3.100}$$

The properties of $\tilde{\boldsymbol{K}}[\boldsymbol{B}, \bar{t}]$ are similar to those of $\hat{\boldsymbol{K}}[\boldsymbol{B}, \bar{t}]$. The integrand of

eq.(3.98) is given

$$\tilde{\boldsymbol{K}}[\boldsymbol{B}(t), t-\bar{t}]\frac{d\boldsymbol{C}_t(\bar{t})}{d\bar{t}} = \sum_{a=0}^{2}\phi_a(t-\bar{t})\left[\boldsymbol{B}^a\frac{d\boldsymbol{C}_t(\bar{t})}{d\bar{t}} + \frac{d\boldsymbol{C}_t(\bar{t})}{d\bar{t}}\boldsymbol{B}^a\right] + \\ + \sum_{a=0}^{2}\sum_{b=0}^{2}\phi_{ab}(t-\bar{t})\boldsymbol{B}^a tr\left[\boldsymbol{B}^b\frac{d\boldsymbol{C}_t(\bar{t})}{d\bar{t}}\right] \qquad (3.101)$$

The scalar coefficients ϕ_a and ϕ_{ab} are functions of $(t-\bar{t})$ and the invariants $I_a(\boldsymbol{B})$. If the material is assumed to be incompressible and isotropic, eq.(3.97) and eq.(3.98) are replaced, respectively, by

$$\boldsymbol{\sigma}(t) = -p(t)\boldsymbol{I} + \hat{\boldsymbol{k}}[\boldsymbol{B}(t)] + \int_0^t \hat{\boldsymbol{k}}[\boldsymbol{B}(t), t-\bar{t}](\bar{C}_t(\bar{t}) - \boldsymbol{I})d\bar{t} \qquad (3.102)$$

or

$$\boldsymbol{\sigma}(t) = -p(t)\boldsymbol{I} + \hat{\boldsymbol{k}}[\boldsymbol{B}(t)] + \int_0^t \hat{\boldsymbol{k}}[\boldsymbol{B}(t), t-\bar{t}]\frac{d\boldsymbol{C}_t(\bar{t})}{d\bar{t}}d\bar{t} \qquad (3.103)$$

$\hat{\boldsymbol{k}}[\boldsymbol{B}(t)]$ and $\tilde{\boldsymbol{k}}[\boldsymbol{B}(t)]$ have the same form as in eq.(3.99). However, since $I_3(\boldsymbol{B}) = 1$, the scalar coefficients i now depend only on $I_1(\boldsymbol{B})$ and $I_2(\boldsymbol{B})$. Several authors carried out an extensive experimental program to determine $\tilde{\boldsymbol{k}}$ and $\tilde{\boldsymbol{K}}$ for a styrene-butadiene rubber. The result of their program, summarized in [69], is the following specific form of eq.(3.103),

$$\boldsymbol{\sigma} = -p(t)\boldsymbol{I} + \left[d + \frac{e}{(I_1-2)^2} + I_1[f + g(I_2-3)]\right]\boldsymbol{B}(t) - [f + g(I_2-3)]\boldsymbol{B}(t)^2 +$$

$$+ 2\int_{-\infty}^{t}\left[\phi_0(t-\bar{t}) + (I_2-3)\boldsymbol{\Phi}_0(t-\bar{t})\right]\frac{d\boldsymbol{C}_t(\bar{t})}{d\bar{t}}d\bar{t} +$$

$$+ \int_{-\infty}^{t}\left[\phi_1(t-\bar{t}) + \frac{\bar{\phi}_1(t-\bar{t})}{(I_1-2)^2}\right]\left[\boldsymbol{B}(t)\frac{d\boldsymbol{C}_t(\bar{t})}{d\bar{t}} + \frac{d\boldsymbol{C}_t(\bar{t})}{d\bar{t}}\boldsymbol{B}(t)\right]d\bar{t} \qquad (3.104)$$

In eq.(3.104), I_1, I_2 are the invariants of $\boldsymbol{B}$, d, e, f, g are constants and $\phi_0(t)$, $\boldsymbol{\Phi}_0(t)$ $\phi_1(t)$, $\bar{\phi}_0(t)$ are monotonically decreasing functions of time.

While for Pipikin and Rogers Theory the tensor valued function $\boldsymbol{K}_3[\boldsymbol{C}, \bar{t}]$ in eq. (3.87) and eq.(3.88) has the form

$$\boldsymbol{K}_3[\boldsymbol{C}, \bar{t}] = a\boldsymbol{I} + b\boldsymbol{C} + c\boldsymbol{C}^2 \qquad (3.105)$$

where a, b, c are functions of $\bar{t}$ and the invariants of $\boldsymbol{C}$,

$$I_1(\boldsymbol{C}) = tr(\boldsymbol{C}), \qquad I_2(\boldsymbol{C}) = \frac{1}{2}[tr(\boldsymbol{C})^2 - tr(\boldsymbol{C^2})], \qquad I_3(\boldsymbol{C}) = det(\boldsymbol{C}) \qquad (3.106)$$

For notational convenience, let $I_(\boldsymbol{C}$ denote the set $(I_1(\boldsymbol{C}), I_2(\boldsymbol{C}), I_3(\boldsymbol{C}))$. By eq.(3.105) and the assumed dependence of $\boldsymbol{K}_3[\boldsymbol{C}, \bar{t}]$ on $\bar{t}$, the scalar coefficients a, b, c also monotonically decrease with $\bar{t}$ to non-zero limit values. For an isotropic material, eq. (3.87) can be written as

$$\boldsymbol{\sigma}(t) = \boldsymbol{F}(t)\boldsymbol{\Pi}\boldsymbol{F}(t)^T \tag{3.107}$$

where

$$\begin{aligned}\boldsymbol{\Pi}(t) = a(I(\boldsymbol{C}(t),0)\boldsymbol{I} + b(I(\boldsymbol{C}(t),0)\boldsymbol{C}(t) + c(I(\boldsymbol{C}(t),0)\boldsymbol{C}^2(t) + \\ + \int_0^t \frac{\partial}{\partial(t-\bar{t})}\big[a(I(\boldsymbol{C}(\bar{t}), t-\bar{t})\boldsymbol{I} + \\ + b(I(\boldsymbol{C}(\bar{t}), t-\bar{t})\boldsymbol{C}(\bar{t}) + c(I(\boldsymbol{C}(\bar{t}), t-\bar{t})\boldsymbol{C}^2(\bar{t})\big]d\bar{t}\end{aligned} \tag{3.108}$$

If the material is assumed to be incompressible, then eq.(3.107) is modified by the addition of the term $-p\boldsymbol{I}$, as in the case of eq.(3.88) , and $I(\boldsymbol{C})$ now represents $(I_1(\boldsymbol{C}), I_2(\boldsymbol{C}))$since deformations are restricted by eq.(3.73) to satisfy the constraint $I_3(\boldsymbol{C}) = 1$. Recalling the assumption that the material is stress free in the reference configuration and hence $\boldsymbol{K}_3(\boldsymbol{I}, t) = 0$, it follows from eq.(3.105) that

$$a_0(I(\boldsymbol{I}), \bar{t}) + a_1(I(\boldsymbol{I}), \bar{t}) + a_2(I(\boldsymbol{I}), \bar{t}) = 0 \tag{3.109}$$

When the material is incompressible, $I(\boldsymbol{I}) = (3, 3, 1)$ and when it is incompressible $I(\boldsymbol{I}) = (3, 3)$.

The terms outside the integral can be expressed in terms of $\boldsymbol{B}(t)$ by use of $\boldsymbol{B}(t) = \boldsymbol{F}(t)^T$ and the observation that $I_a(\boldsymbol{C}) = I_a(\boldsymbol{B})$, $a = 1, 2, 3$. The integrand cannot be expressed in terms of $\boldsymbol{B}(t)$ because it depends on $\boldsymbol{C}(\bar{t}$ for all times $\bar{t} \in [0, t]$. It is possible to express $\boldsymbol{F}(t)\boldsymbol{C}(\bar{t})\boldsymbol{F}(t)^T$ in terms of $\boldsymbol{B}(t)$ and $\boldsymbol{C}_t(\bar{t})$.

Kaye and Bernstein, Kearsley and Zapas [62, 15] proposed a constitutive equation for polymer fluids of the form

$$\boldsymbol{\sigma} = -p\boldsymbol{I} + \int_{-\infty}^{t} \left\{ \frac{\partial U(I_1, I_2, t-\bar{t})}{\partial I_1}\boldsymbol{C}_t(\bar{t})^{-1} - \frac{\partial U(I_1, I_2, t-\bar{t})}{\partial I_2}\boldsymbol{C}_t(\bar{t}) \right\} d\bar{t} \tag{3.110}$$

in which $U(I_1, I_2, \bar{t})$ is a material property that depends on time $\bar{t}$ and the scalar invariants of the relative right Cauchy–Green strain tensor $\boldsymbol{C}_t(\bar{t}) = \boldsymbol{F}_t^T(\bar{t})\boldsymbol{F}_t(\bar{t})$,

$$I_1(\boldsymbol{C}) = tr((\boldsymbol{C}_t(\bar{t}))^{-1}), \qquad I_2(\boldsymbol{C}) = tr(\boldsymbol{C}_t(\bar{t})) \tag{3.111}$$

This constitutive equation, is mentioned here for several reasons. It is a nonlinear single integral constitutive equation whose integrand is expressed in terms of finite strain tensors, just as in eq.(3.97) or eq.(3.108). In addition, with it a number of boundary value problems involving viscoelastic fluids can be approached in a manner similar to problems involving viscoelastic solids.

3.2.5 Transversely isotropic and orthotropic material restriction

For many materials, such as biological tissue, it is appropriate to use a constitutive equation for an anisotropic viscoelastic solid, several authors have addressed this aspect [4] . The restrictions due to transverse isotropy and orthotropy on the functions appearing in the rate and differential constitutive equations, the Green–Rivlin constitutive equation and the finite linear viscoelastic constitutive equation lead to very complicated expressions. In the case of the Pipkin–Rogers constitutive equation eqs.(3.87) and (3.88), the expressions are more tractable and have been discussed by [81] For a material that is transversely isotropic with respect to the $\boldsymbol{E}_3$ direction, the invariants are

$$I_1(\boldsymbol{C}) = tr(\boldsymbol{C}), \qquad I_2(\boldsymbol{C}) = \frac{1}{2}[tr(\boldsymbol{C})^2 - tr(\boldsymbol{C^2})], \qquad I_3(\boldsymbol{C}) = det(\boldsymbol{C})$$

$$I_4(\boldsymbol{C}) = C_{33} \qquad I_5(\boldsymbol{C}) = C_{13}^2 + C_{23}^2 \tag{3.112}$$

Let $I(\boldsymbol{C})$ denote the set $(I_1(\boldsymbol{C}), ..., I_5(\boldsymbol{C}))$,eq.(3.87) becomes:

$$\begin{aligned}
\boldsymbol{\sigma}(t) = \boldsymbol{F}(t)\{&a_1(I(\boldsymbol{C}(t)),0)\boldsymbol{I} + a_2(I(\boldsymbol{C}(t)),0)[I_1(\boldsymbol{C}(t))I - \boldsymbol{C}(t)]+ \\
&+ a_3(I(\boldsymbol{C}(t)),0)\boldsymbol{E}_3 \otimes \boldsymbol{E}_3 + a_4(I(\boldsymbol{C}(t)),0)[C_{12}(t)(\boldsymbol{E}_1 \otimes \boldsymbol{E}_3 + \boldsymbol{E}_3 \otimes \boldsymbol{E}_1)+ \\
&+ C_{23}(t)(\boldsymbol{E}_2 \otimes \boldsymbol{E}_3 + \boldsymbol{E}_3 \otimes \boldsymbol{E}_2)] + \int_0^t \frac{\partial}{\partial(t-\bar{t})}\big[a_1(I(\boldsymbol{C}(\bar{t})(t-\bar{t})\boldsymbol{I} \\
&+ a_2(I(\boldsymbol{C}(\bar{t})),t-\bar{t})(I_1(\boldsymbol{C}(\bar{t}))I - \boldsymbol{C}(\bar{t})) + a_3(I(\boldsymbol{C}(\bar{t})),t-\bar{t})\boldsymbol{E}_3 \otimes \boldsymbol{E}_3+ \\
&+ a_4(I(\boldsymbol{C}(\bar{t})),t-\bar{t})[]C_{13}(\bar{t})(\boldsymbol{E}_1 \otimes \boldsymbol{E}_3 + \boldsymbol{E}_3 \otimes \boldsymbol{E}_1)+ \\
&+ C_{23}(\bar{t})(\boldsymbol{E}_2 \otimes \boldsymbol{E}_3 + \boldsymbol{E}_3 \otimes \boldsymbol{E}_2)]\big]d\bar{t}\}\boldsymbol{F}(t)^T
\end{aligned}$$

For a material that is orthotropic, the invariants are:

$$I_1(\boldsymbol{C}) = C_{11} \qquad I_2(\boldsymbol{C}) = C_{22} \qquad I_3(\boldsymbol{C}) = C_{33} \tag{3.113}$$
$$I_4(\boldsymbol{C}) = C_{12}^2 \qquad I_5(\boldsymbol{C}) = C_{23}^2 \qquad I_6(\boldsymbol{C}) = C_{31}^2 \tag{3.114}$$

Let $I(\boldsymbol{C})$ denote the set $(I_1(\boldsymbol{C}), ..., I_6(\boldsymbol{C}))$,eq.(3.87) becomes

$$\begin{aligned}
\boldsymbol{\sigma}(t) = \boldsymbol{F}(t)\{&a_1(I(\boldsymbol{C}(t)),0)\boldsymbol{E}_1 \otimes \boldsymbol{E}_1 + a_2(I(\boldsymbol{C}(t)),0)\boldsymbol{E}_2 \otimes \boldsymbol{E}_2 + \\
&+ a_3(I(\boldsymbol{C}(t)),0)\boldsymbol{E}_3 \otimes \boldsymbol{E}_3 + 2a_4(I(\boldsymbol{C}(t)),0)C_{12}(\boldsymbol{E}_1 \otimes \boldsymbol{E}_2 + \boldsymbol{E}_2 \otimes \boldsymbol{E}_1) + \\
&+ 2a_5(I(\boldsymbol{C}(t)),0)C_{23}(t)(\boldsymbol{E}_2 \otimes \boldsymbol{E}_3 + \boldsymbol{E}_3 \otimes \boldsymbol{E}_2) + \\
&2a_6(I(\boldsymbol{C}(t)),0)C_{31}(t)(\boldsymbol{E}_3 \otimes \boldsymbol{E}_1 + \boldsymbol{E}_1 \otimes \boldsymbol{E}_3)] + \\
&+ \int_0^t \frac{\partial}{\partial(t-\bar{t})}\big[a_1(I(\boldsymbol{C}(\bar{t})(t-\bar{t})\boldsymbol{E}_1 \otimes \boldsymbol{E}_1 + \\
&+ a_2(I(\boldsymbol{C}(\bar{t})),t-\bar{t})\boldsymbol{E}_2 \otimes \boldsymbol{E}_2 + a_3(I(\boldsymbol{C}(\bar{t})),t-\bar{t})\boldsymbol{E}_3 \otimes \boldsymbol{E}_3 + \\
&+ 2a_4(I(\boldsymbol{C}(\bar{t})),t-\bar{t})C_{12}(\bar{t})(\boldsymbol{E}_1 \otimes \boldsymbol{E}_2 + \boldsymbol{E}_2 \otimes \boldsymbol{E}_1) + \\
&+ 2a_5(I(\boldsymbol{C}(\bar{t})),t-\bar{t})C_{23}(\boldsymbol{E}_2 \otimes \boldsymbol{E}_3 + \boldsymbol{E}_3 \otimes \boldsymbol{E}_2) + \\
&+ 2a_6(I(\boldsymbol{C}(\bar{t})),t-\bar{t})C_{31}(\boldsymbol{E}_1 \otimes \boldsymbol{E}_3 + \boldsymbol{E}_3 \otimes \boldsymbol{E}_1)\big]d\bar{t}\}\boldsymbol{F}(t)^T
\end{aligned} \tag{3.115}$$

3.2.6 Homogeneous deformation:Triaxial stretch histories

Let an isotropic nonlinear viscoelastic solid block undergo the triaxial stretch motion

$$x_i(\bar{t}) = \lambda_i(\bar{t})X_i \qquad \bar{t} \in (-\infty, t] \qquad i = 1,2,3 \tag{3.116}$$

with

$$\lambda_1(\bar{t}) = \lambda_2(\bar{t}) = \lambda_3(\bar{t}) = 1 \qquad \bar{t} \in (-\infty, 0) \tag{3.117}$$

$\lambda_i(\bar{t})$is a stretch ratio in the X_i direction. It can have a jump discontinuity at $\bar{t} = 0$ and then vary arbitrarily for $\bar{t} \in [0, t]$. The deformation gradient history is

$$\boldsymbol{F}(\bar{t}) = \boldsymbol{I} \qquad \bar{t} \in (-\infty, 0)$$

$$\boldsymbol{F}(\bar{t}) = diag[\lambda_1(\bar{t}), \lambda_2(\bar{t}), \lambda_3(\bar{t})] \qquad \bar{t} \in [0, t] \tag{3.118}$$

from which the kinematical quantities needed for use in the constitutive equations are found to be given by

$$\boldsymbol{C}(\bar{t}) = \boldsymbol{I} \qquad \bar{t} \in (-\infty, 0)$$

$$\boldsymbol{C}(\bar{t}) = diag[\lambda_1(\bar{t})^2, \lambda_2(\bar{t})^2, \lambda_3(\bar{t})^2] \qquad \bar{t} \in [0, t] \tag{3.119}$$

$$\boldsymbol{B}(t) = diag[\lambda_1(t)^2, \lambda_2(t)^2, \lambda_3(t)^2] \tag{3.120}$$

$$\boldsymbol{C}_i(\bar{t}) = diag[1/\lambda_1(t)^2, 1/\lambda_2(t)^2, 1/\lambda_3(t)^2] \qquad \bar{t} \in (-\infty, 0)$$

$$\boldsymbol{C}_i(\bar{t}) = diag[(\lambda_1(\bar{t})/\lambda_1(t))^2, (\lambda_2(\bar{t})/\lambda_2(t))^2, (\lambda_3(\bar{t})/\lambda_3(t))^2] \qquad \bar{t} \in [0, t] \tag{3.121}$$

In addition

$$I_1(\boldsymbol{C}(\bar{t})) = \lambda_1(\bar{t})^2 + \lambda_2(\bar{t})^2 + \lambda_3(\bar{t})^2$$

$$I_2(\boldsymbol{C}(\bar{t})) = \lambda_1(\bar{t})^2\lambda_2(\bar{t})^2 + \lambda_2(\bar{t})^2\lambda_3(\bar{t})^2 + \lambda_3(\bar{t})^2\lambda_1(\bar{t})^2$$

$$I_3(\boldsymbol{C}(\bar{t})) = \lambda_1(\bar{t})^2\lambda_2(\bar{t})^2\lambda_3(\bar{t})^2 \tag{3.122}$$

Note that $I_k(\boldsymbol{B}(t)) = I_k(\boldsymbol{C}(t))$, $k = 1, 2, 3$. Finally,

$$\frac{d\boldsymbol{C}_i(\bar{t})}{d\bar{t}} = \boldsymbol{0} \qquad \bar{t} \in (-\infty, 0)$$

$$\frac{d\boldsymbol{C}_i(\bar{t})}{d\bar{t}} = diag\left[\left(\frac{\lambda_1(0)}{\lambda_1(t)}\right)^2 - \left(\frac{1}{\lambda_1(t)}\right)^2, \left(\frac{\lambda_2(0)}{\lambda_2(t)}\right)^2 - \left(\frac{1}{\lambda_2(t)}\right)^2,\right.$$

$$\left.\left(\frac{\lambda_3(0)}{\lambda_3(t)}\right)^2 - \left(\frac{1}{\lambda_3(t)}\right)^2\right]\delta(\bar{t}) \tag{3.123}$$

$$\frac{d\boldsymbol{C}_i(\bar{t})}{d\bar{t}} = diag\left[2\frac{\lambda_1(\bar{t})}{\lambda_1(t)^2}\frac{d\lambda_1(\bar{t})}{d\bar{t}}, 2\frac{\lambda_2(\bar{t})}{\lambda_2(t)^2}\frac{d\lambda_2(\bar{t})}{d\bar{t}}, 2\frac{\lambda_3(\bar{t})}{\lambda_3(t)^2}\frac{d\lambda_3(\bar{t})}{d\bar{t}}\right] \qquad \bar{t} \in [0,t] \tag{3.124}$$

Substituting eqs.(3.120)-(3.124) into eqs.(3.98)-(3.101) gives an expression for the stress $\sigma_{ii}(t)$,

$$\sigma_{ii}(t) = a_0 + a_1\lambda_i(t)^2 + a_3\lambda_i(t)^4 + 2\sum_{a=0}^{2}\phi_a(t)\left[\lambda_i(t)^{2a}\left[\left(\frac{\lambda_i(0)}{\lambda_i(t)}\right)^2 - \left(\frac{1}{\lambda_i(t)}\right)^2\right]\right] +$$

$$+ 4\int_0^t \sum_{a=0}^{2}\phi_a(t-\bar{s})\lambda_i(t)^{2a}\frac{\lambda_i(\bar{t})}{\lambda_i(t)^2}\frac{d\lambda_i(\bar{t})}{d\bar{t}}d\bar{t}$$

$$2\sum_{a=0}^{2}\sum_{b=0}^{2}\phi_{ab}(t)\lambda_i(t)^{2a}\sum_{k=1}^{3}\left[\lambda_k(t)^{2b}\left[\left(\frac{\lambda_k(0)}{\lambda_k(t)}\right)^2 - \left(\frac{1}{\lambda_k(t)}\right)^2\right]\right] +$$

$$+ 4\int_0^t \sum_{a=0}^{2}\sum_{b=0}^{2}\phi_{ab}(t-\bar{t})\lambda_i(t)^{2a}\left(\sum_{k=1}^{3}\lambda_k(t)^{2b}\frac{\lambda_k(\bar{t})}{\lambda_k(t)^2}\frac{d\lambda_k(\bar{t})}{d\bar{t}}\right)d\bar{t} \tag{3.125}$$

For an incompressible material, $\sigma_{ii}(t)$ is replaced by $\sigma_{ii}(t)+p$ and the motion is such that $\lambda_1(\bar{t})\lambda_2(\bar{t})\lambda_3(\bar{t}) = 1$, $\bar{t} \in [0,t]$. For the constitutive equation

(3.104)

$$\sigma_{ii} = -p(t) + \left[d + \frac{e}{(I_1-2)^2} + I_1[f + g(I_2-3)]\right]\lambda_i(t)^2 - [f + g(I_2-3)]\lambda_i(t)^4 +$$

$$+ 2\left[\phi_0(t) + (I_2-3)\Phi_0(t)\right]\left[\left(\frac{\lambda_i(0)}{\lambda_i(t)}\right)^2 - \left(\frac{1}{\lambda_i(t)}\right)^2\right] +$$

$$+ 4\int_0^t \left[\phi_0(t-\bar{t}) + (I_2-3)\Phi_0(t-\bar{t})\right]\lambda_i(\bar{t})\frac{\lambda_i(\bar{t})}{\lambda_i(t)^2}\frac{d\lambda_i(\bar{t})}{d\bar{t}}d\bar{t} +$$

$$+ 4\left[\phi_1(t) + \frac{\bar{\phi}_1(t)}{(I_1-2)^2}\right]\left[\left(\frac{\lambda_i(0)}{\lambda_i(t)}\right)^2 - \left(\frac{1}{\lambda_i(t)}\right)^2\right]\lambda_i(t)^2 +$$

$$+ 4\int_0^t \left[\phi_1(t-\bar{t}) + \frac{\bar{\phi}_1(t-\bar{t})}{(I_1-2)^2}\right]\lambda_i(t)^2\lambda_i(\bar{t})\frac{\lambda_i(\bar{t})}{\lambda_i(t)^2}\frac{d\lambda_i(\bar{t})}{d\bar{t}}d\bar{t} \qquad (3.126)$$

From eq.(3.107)

$$\sigma_{ii}(t) = \lambda_i(t)^2\{a_0(I(\boldsymbol{C}(t),0) + a_1(I(\boldsymbol{C}(t),0)\lambda_i(t)^2 +$$

$$+ a_2(I(\boldsymbol{C}(t),0)\lambda_i(t)^4 + \int_0^t \frac{\partial}{\partial(t-\bar{t})}\big[a_0(I(\boldsymbol{C}(\bar{t}),t-\bar{t}) +$$

$$+ a_1(I(\boldsymbol{C}(\bar{t}),t-\bar{t})\lambda_i(t)^2 + a_2(I(\boldsymbol{C}(\bar{t}),t-\bar{t})\lambda_i(t)^4\big]d\bar{t}\} \qquad (3.127)$$

in which $I(\boldsymbol{C})$ denotes the set of invariants eq.(3.122). For an incompressible material, $\sigma_{ii}(t)$ is replaced by $\sigma_{ii}(t) + p$, the motion is such that $\lambda_1(\bar{t})\lambda_2(\bar{t})\lambda_3(\bar{t}) = 1$, $\bar{t} \in [0,t]$ or $I_3(\boldsymbol{C}) = 1$ and $I(\boldsymbol{C}) = (I_1(\boldsymbol{C}), I_2(\boldsymbol{C}))$.

3.2.7 Homogeneous deformation: Uniaxial stretch histories

Uniaxial stretch is the special case of triaxial stretch when there is only one non-zero stress component. As in other areas of solid mechanics such as elasticity and plasticity, an understanding of uniaxial stretch is essential to an understanding of the material. Thus, this subsection contains a detailed

discussion of uniaxial stretch for nonlinear viscoelasticity. Many of the features of the uniaxial response introduced for linear viscoelastic response are re-visited here. Let the reference configuration of an isotropic nonlinear viscoelastic solid be a block with edges along the X_1, X_2, X_3 axes of a cartesian coordinate system. The block undergoes uniaxial extension along the X3-axis. The motion is described by eq.(3.117) and the stresses are given by eq.(3.127) with $\sigma_{11}(t) = \sigma_{22}(t) = 0$, $t > 0$. For notational convenience, let $\lambda_3(t) = \lambda(t)$ and $\sigma_{33}(t) = \sigma(t)$. Equations (3.127) become

$$0 = -p(t) + a_0(I(\boldsymbol{C}(t),0))\lambda(t)^2 + a_1(I(\boldsymbol{C}(t),0)\lambda(t)^4 + a_2(I(\boldsymbol{C}(t),0)\lambda(t)^6 +$$

$$+ \int_0^t \frac{\partial}{\partial(t-\bar{t})}\big[a_0(I(\boldsymbol{C}(\bar{t}),t-\bar{t})\lambda(t)^2 +$$

$$+ a_1(I(\boldsymbol{C}(\bar{t}),t-\bar{t})\lambda_(t)^2\lambda(\bar{t})^2 + a_2(I(\boldsymbol{C}(\bar{t}),t-\bar{t})\lambda(t)^2\lambda(\bar{t})^4\bar{t}\big]d\bar{t} \qquad (3.128a)$$

$$0 = -p(t) + a_0(I(\boldsymbol{C}(t),0))\lambda_1(t)^2 + a_1(I(\boldsymbol{C}(t),0)\lambda_1(t)^4 + a_2(I(\boldsymbol{C}(t),0)\lambda_1(t)^6 +$$

$$+ \int_0^t \frac{\partial}{\partial(t-\bar{t})}\big[a_0(I(\boldsymbol{C}(\bar{t}),t-\bar{t})\lambda_1(t)^2 +$$

$$+ a_1(I(\boldsymbol{C}(\bar{t}),t-\bar{t})\lambda_1(t)^2\lambda_1(\bar{t})^2 + a_2(I(\boldsymbol{C}(\bar{t}),t-\bar{t})\lambda_1(t)^2\lambda_1(\bar{t})^4\bar{t}\big]d\bar{t} \qquad (3.128b)$$

$$0 = -p(t) + a_0(I(\boldsymbol{C}(t),0))\lambda_2(t)^2 + a_1(I(\boldsymbol{C}(t),0)\lambda_2(t)^4 + a_2(I(\boldsymbol{C}(t),0)\lambda_2(t)^6 +$$

$$+ \int_0^t \frac{\partial}{\partial(t-\bar{t})}\big[a_0(I(\boldsymbol{C}(\bar{t}),t-\bar{t})\lambda_2(t)^2 +$$

$$+ a_1(I(\boldsymbol{C}(\bar{t}),t-\bar{t})\lambda_2(t)^2\lambda_2(\bar{t})^2 + a_2(I(\boldsymbol{C}(\bar{t}),t-\bar{t})\lambda_2(t)^2\lambda_2(\bar{t})^4\bar{t}\big]d\bar{t} \qquad (3.128c)$$

It is intended that eqs.(3.128a)(3.128b)(3.128c) apply to both compressible and incompressible materials in a single expression. When the material is compressible, $p = 0$ and when it is incompressible. Equations (3.128a)(3.128b) (3.128c) are supplemented by the condition $\lambda_1(\bar{t})\lambda_2(\bar{t})\lambda_3(\bar{t}) = 1$, $\bar{t} \in [0,t]$. Suppose that the material is compressible. If the history

$\lambda_3(\bar{t}) = \lambda(\bar{t})$, $\bar{t} \in [0,t]$ is specified, then eqs.(3.128b) (3.128c) become a system of nonlinear Volterra integral equations for $\lambda_1(\bar{t})$ and $\lambda_2(\bar{t})$, $\bar{t} \in [0,t]$. Once these are known, eq.(3.128a) is used to determine $\sigma(t)$,$t > 0$. If the stress history, $\sigma(t)$, $t > 0$, is specified, eqs.(3.128b) (3.128c) becomes a system of nonlinear Volterra integral equations for $\lambda_1(\bar{t}), \lambda_2(\bar{t}), \lambda_3(\bar{t})$, $\bar{t} \in [0,t]$.

Suppose that the material is incompressible. If the history $\lambda_3(\bar{t}) = \lambda(\bar{t})$, $\bar{t} \in [0,t]$ is specified, then eqs.(3.128b) (3.128c) along with $\lambda_1(\bar{t})\lambda_2(\bar{t})\lambda_3(\bar{t}) = 1$, $\bar{t} \in [0,t]$ become a system of nonlinear Volterra integral equations for $p, \lambda_1(\bar{t})$ and $\lambda_2(\bar{t})$, $\bar{t} \in [0,t]$. Once these are known, eq.(3.128a) is used to determine $\sigma(t)$, $t > 0$. If the stress history,$\sigma(t)$, $t > 0$, is specified, eqs.(3.128b) (3.128c) along with $\lambda_1(\bar{t})\lambda_2(\bar{t})\lambda_3(\bar{t}) = 1$, $\bar{t} \in [0,t]$ becomes a system of nonlinear Volterra integral equations for p,$\lambda_1(\bar{t}), \lambda_2(\bar{t}), \lambda_3(\bar{t})$, $\bar{t} \in [0,t]$. These can be solved using the numerical method.

For determination of $\lambda_1(\bar{t})$ and $\lambda_2(\bar{t})$, $\bar{t} \in [0,t]$, For both compressible and incompressible materials, subtraction of eqs. (3.128b) (3.128c) gives:

$$
\begin{aligned}
0 = {} & (\lambda_2(t)^2 - \lambda_1(t)^2)[]a_0(I(\boldsymbol{C}(t),0)) + a_1(I(\boldsymbol{C}(t),0)(\lambda_2(t)^2 + \lambda_1(t)^2) + \\
& + a_2(I(\boldsymbol{C}(t),0)(\lambda_2(t)^4 + \lambda_2(t)^2\lambda_1(t)^2 + \lambda_1(t)^4)] + \\
& + \int_0^t \frac{\partial}{\partial(t-\bar{t})}\big[a_0(I(\boldsymbol{C}(\bar{t}),t-\bar{t})(\lambda_2(t)^2 - \lambda_1(t)^2) + \\
& + a_1(I(\boldsymbol{C}(\bar{t}),t-\bar{t})(\lambda_2(t)^2\lambda_2(t)^2 - \lambda_1(t)^2\lambda_1(t)^2) + \\
& + a_2(I(\boldsymbol{C}(\bar{t}),t-\bar{t})(\lambda_2(t)^2\lambda_2(t)^4 - \lambda_1(t)^2\lambda_1(t)^4)\big]\,d\bar{t}
\end{aligned}
\tag{3.129}
$$

Eq.(3.129) leads to a relation between $\lambda_1(\bar{t})$ and $\lambda_2(\bar{t})$. Let $t = t_1 = 0$. The integral becomes zero and eq.(3.129) reduces to:

$$
\begin{aligned}
0 = {} & (\lambda_2(t_1)^2 - \lambda_1(t_1)^2)[a_0(I(\boldsymbol{C}(t_1),t_1)) + a_1(I(\boldsymbol{C}(t_1),t_1)(\lambda_2(t_1)^2 + \lambda_1(t_1)^2) + \\
& + a_2(I(\boldsymbol{C}(t_1),t_1)(\lambda_2(t_1)^4 + \lambda_2(t_1)^2\lambda_1(t_1)^2 + \lambda_1(t_1)^4)]
\end{aligned}
\tag{3.130}
$$

It is assumed that the expression in square brackets is not zero. Then the only physically meaningful solution to eq.(3.130) is $\lambda_2(t_1)^2 = \lambda_1(t_1)^2$. Next, evaluate eq.(3.129) at $t = t_2$, introduce the notation ${}_i(t-\bar{t})/\partial(t-\bar{t}) = \dot{a}_i(t-\bar{t})$ and approximate the integral using the trapezoidal rule. Since $\lambda_2(t_1)^2 =$

$\lambda_1(t_1)^2$, eq. (3.129) reduces to:

$$
\begin{aligned}
0 = {} & (\lambda_2(t_2)^2 - \lambda_1(t_2)^2)[a_0(I(\boldsymbol{C}(t_2), t_1)) + a_1(I(\boldsymbol{C}(t_2), t_1)(\lambda_2(t_2)^2 + \lambda_1(t_2)^2) + \\
& + a_2(I(\boldsymbol{C}(t_2), t_1)(\lambda_2(t_2)^4 + \lambda_2(t_2)^2\lambda_1(t_2)^2 + \lambda_1(t_2)^4)] + \\
& + \frac{1}{2}(t_2 - t_1)\{[\dot{a}_0(I(\boldsymbol{C}(t_2), t_1)) + \dot{a}_0(I(\boldsymbol{C}(t_1), t_2 - t_1)](\lambda_2(t_2)^2 - \lambda_1(t_2)^2) + \\
& + [\dot{a}_1(I(\boldsymbol{C}(t_2), t_1)(\lambda_2(t_2)^2 + \lambda_1(t_2)^2) + \dot{a}_1(I(\boldsymbol{C}(t_1), t_2 - t_1)]\lambda_1(t_2)^2] \\
& (\lambda_2(t_2)^2 - \lambda_1(t_2)^2) + [\dot{a}_2(I(\boldsymbol{C}(t_1), t_2 - t_1) + \dot{a}_2(I(\boldsymbol{C}(t_1), t_2 - t_1) \\
& (\lambda_2(t_1)^4 + \lambda_2(t_1)^2\lambda_1(t_1)^2 + \lambda_1(t_1)^4])]\lambda_1(t_1)^4](\lambda_2(t_2)^2 - \lambda_1(t_2)^2)\}
\end{aligned}
\tag{3.131}
$$

Since each term in eq.(3.131) has the factor $\lambda_2(t_1)^2 = \lambda_1(t_1)^2$, this equation admits the solution $\lambda_2(t_2)^2 = \lambda_1(t_2)^2$. It is assumed that this is the only physically meaningful solution. Next, let eq.(3.129) be evaluated at $t = t_n$ and assume that $\lambda_2(t_k)^2 = \lambda_1(t_k)^2$, $k = 1, 2, ..., n-1$.

Approximating eq.(3.129) by use of the trapezoidal rule gives:

$$0 = (\lambda_2(t_n)^2 - \lambda_1(t_n)^2)[a_0(I(\boldsymbol{C}(t_n), t_1)) + a_1(I(\boldsymbol{C}(t_n), t_1)(\lambda_2(t_n)^2 + \lambda_1(t_n)^2)+$$

$$+ a_2(I(\boldsymbol{C}(t_n), t_1)(\lambda_2(t_n)^4 + \lambda_2(t_n)^2\lambda_1(t_n)^2 + \lambda_1(t_n)^4)]+$$

$$+ \sum_{i=1}^{i=n-2} \frac{1}{2}(t_{i+1} - t_1)\{[\dot{a}_0(I(\boldsymbol{C}(t_i), t_n - t_{i+1})) + \dot{a}_0(I(\boldsymbol{C}(t_i), t_n - t_{i+1})]$$

$$(\lambda_2(t_n)^2 - \lambda_1(t_n)^2) + [\dot{a}_1(I(\boldsymbol{C}(t_{i+1}), t_n - t_{i+1})(\lambda_2(t_{i+1})^2+$$

$$+ \dot{a}_1(I(\boldsymbol{C}(t_i), t_n - t_i)(\lambda_1(t_i)^2](\lambda_2(t_n)^2 - \lambda_1(t_n)^2)+$$

$$+ [\dot{a}_2(I(\boldsymbol{C}(t_{i+1}), t_n - t_{i+1})\lambda_1(t_{i+1})^4 + \dot{a}_2(I(\boldsymbol{C}(t_i), t_n - t_i)\lambda_1(t_i)^4]$$

$$(\lambda_2(t_n)^2 - \lambda_1(t_n)^2)\} + \frac{1}{2}(t_n - t_{n-1})\{[\dot{a}_0(I(\boldsymbol{C}(t_n), t_1))+$$

$$+ \dot{a}_0(I(\boldsymbol{C}(t_{n-1}), t_n - t_{n-1})](\lambda_2(t_n)^2 - \lambda_1(t_n)^2)+$$

$$+ [\dot{a}_1(I(\boldsymbol{C}(t_n), t_1)(\lambda_2(t_n)^2 + \lambda_1(t_n)^2) + \dot{a}_1(I(\boldsymbol{C}(t_{n-1}), t_n - t_{n-1})(\lambda_1(t_{n-1})^2]$$

$$(\lambda_2(t_n)^2 - \lambda_1(t_n)^2) + [a_2(I(\boldsymbol{C}(t_n), t_1)(\lambda_2(t_n)^4 + \lambda_2(t_n)^2\lambda_1(t_n)^2 + \lambda_1(t_n)^4)+$$

$$\dot{a}_2(I(\boldsymbol{C}(t_{n-1}), t_n - t_{n-1})(\lambda_1(t_{n-1})^4](\lambda_2(t_n)^2 - \lambda_1(t_n)^2)\} \tag{3.132}$$

Since each term in eq.(3.132) has the factor $\lambda_2(t_n)^2 - \lambda_1(t_n)^2$, this equation admits the solution $\lambda_2(t_n)^2 = \lambda_1(t_n)^2$. As before, it is assumed that this is the only physically meaningful solution. This solution holds as tn increases, that is, as time marches forward. In the limit as the number of time steps increases and the time increments decrease, the approximation to eq.(3.129) is expected to approach the exact equation. Thus, the numerical solution

implies that $\lambda_2(\bar{t})^2 = \lambda_1(\bar{t})^2$, $\bar{t} \in [0,t]$. The invariants in eq.(3.124) reduce to:

$$I_1(\boldsymbol{C}(\bar{t})) = 2\lambda_1(\bar{t})^2 + \lambda(\bar{t})^2$$

$$I_2(\boldsymbol{C}(\bar{t})) = \lambda_1(\bar{t})^4 + 2\lambda_1(\bar{t})^2\lambda(\bar{t})^2$$

$$I_3(\boldsymbol{C}(\bar{t})) = \lambda_1(\bar{t})^4\lambda(\bar{t})^2 \tag{3.133}$$

When the material is compressible, eq.(3.128a)(3.128b), with $p = 0$ give a system of non-linear Volterra integral equations that relate $\lambda(\bar{t}, \lambda_1(\bar{t})$ and $\sigma(\bar{t})$. When the material is incompressible, one finds from the result $\lambda_2(\bar{t})^2 = \lambda_1(\bar{t})^2$, $\bar{t} \in [0,t]$ and the condition $\lambda_1(\bar{t})\lambda_2(\bar{t})\lambda_3(\bar{t}) = 1$ $\bar{t} \in [0,t]$ that:

$$\lambda_1(\bar{t}) = \lambda(\bar{t})^{-1/2} \qquad \bar{t} \in [0,t] \tag{3.134}$$

The invariants eq.(3.133) reduce further to

$$I_1(\boldsymbol{C}(\bar{t})) = \lambda(\bar{t})^2 + \frac{2}{\lambda(\bar{t})} \qquad I_1(\boldsymbol{C}(\bar{t})) = 2\lambda(\bar{t})\frac{1}{\lambda(\bar{t})^2} \tag{3.135}$$

The scalar p is found from eq.(3.128b). Eliminating p between eq.(3.128a) and eq.(3.128b) gives:

$$\sigma(t) = \left(\lambda(\bar{t})^2 + \frac{2}{\lambda(\bar{t})}\right)\left[a_0(I(\boldsymbol{C}(t),0)) + a_1(I(\boldsymbol{C}(t),0))\left(\lambda(\bar{t})^2 + \frac{2}{\lambda(\bar{t})}\right)+\right.$$

$$\left. + a_2(I(\boldsymbol{C}(t),0))\left(\lambda(\bar{t})^4 + \lambda(t) + \frac{2}{\lambda(\bar{t})^2}\right)\right]+$$

$$+ \int_0^t \frac{\partial}{\partial(t-\bar{t})}\left[a_0(I(\boldsymbol{C}(\bar{t}), t-\bar{t})\left(\lambda(\bar{t})^4 + \lambda(t) + \frac{2}{\lambda(\bar{t})^2}\right)+\right. \tag{3.136}$$

$$a_1(I(\boldsymbol{C}(\bar{t}), t-\bar{t})\left(\lambda(t)^2\lambda(\bar{t})^2 - \frac{1}{\lambda(t)\lambda(\bar{t})}\right) \tag{3.137}$$

$$\tag{3.138}$$

$$\left. a_2(I(\boldsymbol{C}(\bar{t}), t-\bar{t})\left(\lambda(t)^2\lambda(\bar{t})^4 - \frac{1}{\lambda(t)\lambda(\bar{t})^2}\right)\right] d\bar{t} \tag{3.139}$$

the stress–stretch relation for an isotropic, incompressible nonlinear viscoelastic solid.

3.2.8 Quasi-Linear Viscoelasticity (QLV)

Let us assume that in eqs.(3.87)(3.88) the kernel $\boldsymbol{K}_3[\boldsymbol{C},\bar{t}]$ is separable, i.e.

$$\boldsymbol{K}_3[\boldsymbol{C},\bar{t}] = \boldsymbol{K}^{(e)}[\boldsymbol{C}]G(\bar{t}) \tag{3.140}$$

has become known as Quasi-linear viscoelasticity. $\boldsymbol{K}^{(e)}[\boldsymbol{C}]$ is normalized so that $G(0) = 1$. Then,eq.(3.141) becomes

$$\boldsymbol{\sigma}(t) = -p(t)\boldsymbol{I} + \boldsymbol{F}(t)\left\{\boldsymbol{K}^{(e)}\big[\boldsymbol{C}(t)\big] + \int_0^t \boldsymbol{K}^{(e)}\big[\boldsymbol{C}(t)\big]\frac{\partial G(t-\bar{t})}{\partial(t-\bar{t})}d\bar{t}\right\}\boldsymbol{F}(t)^T \tag{3.141}$$

The terminology "quasi-linear viscoelasticity" arises because $\boldsymbol{K}^{(e)}[\boldsymbol{C}]$ can be thought of as a non-linear measure of strain. The expression in braces in eq.(3.141) is linear in this nonlinear strain measure.

In 1D form as we particularize the elastic tensor $\boldsymbol{K}^{(e)}[\boldsymbol{C}] = \partial\psi_H/\partial\varepsilon$ and $G(t)$ is the relaxation function with $\psi_H(\varepsilon)$ the Helmoltz free energy function of hyperelastic materials and we may write the one-dimensional reletion for the strain histrory yielding the QLV model of non-linear hereditariness as reported in [48]:

$$\varepsilon(t) = \int_0^t J(t-\tau)\left(\frac{\partial\dot{\psi}_G}{\partial\sigma}\right)d\tau = \int_0^t J(t-\tau)\frac{\partial^2\psi_G(\sigma)}{\partial\sigma^2}\dot{\varepsilon}(\tau)\,d\tau \tag{3.142a}$$

$$\sigma(t) = \int_0^t G(t-\tau)\frac{\partial\psi_H}{\partial\varepsilon}\dot{\sigma}d\tau = \int_0^t G(t-\tau)\frac{\partial^2\psi_H(\varepsilon)}{\partial\varepsilon^2}\dot{\sigma}(\tau)\,d\tau \tag{3.142b}$$

where $\psi_G(\sigma)$ is the Gibbs free energy. It must be remarked that the specific form of QLV in eqs.(3.142a)(3.142b) has been defined independently by eq.(3.142a) [48].

3.3 Quasi-Fractional Hereditary Materials (Q-FHM)

The constitutive equation reported in eqs.(3.142a)(3.142b) have been obtained from mathematical approximation without any mechanical justification. Indeed, the behavior of the material is non-linear hereditariness, the relationship eq. (3.9) between the creep and relaxation functions is not applicable. Additionally to this point it is not possible to relate the results of the creep with those of the relaxation and vice versa.

In this paragraph we aim to show that power-laws expressed in terms of real powers of time for the material creep t^{β_c} and relaxation functions $t^{-\beta_r}$

may be used for an consistent mathematical description of non-linear models of material hereditariness.

As it has been observed in sec.3.1 for many materials power-law relation in time and in stress/strain have been observed. Under such circumstances data analysis shows that material functions for constant stress, namely $\phi_c(\sigma,t)$ and for uniform strain, namely, $\phi_r(\varepsilon,t)$ functions may be expressed in a generalized, separable form as:

$$\phi_c(\sigma,t) = J_e(\sigma)\,J(t) = \left(\frac{\sigma}{G_0}\right)^{\alpha_c}\left(\frac{t}{\tau_0}\right)^{\beta_c}\frac{1}{\Gamma(1+\beta_c)} = \frac{s^{\alpha_c}}{\Gamma(1+\beta_c)}\left(\frac{t}{\tau_0}\right)^{\beta_c} \tag{3.143a}$$

$$\phi_r(\varepsilon,t) = G_e(\varepsilon)\,G(t) = G_0\varepsilon^{\alpha_r}\left(\frac{t}{\tau_0}\right)^{-\beta_r}\frac{1}{\Gamma(1-\beta_r)} \tag{3.143b}$$

that are completely equivalent to the Nutting observation for polymers. In the latter equality in eq.(3.143a) we introduced, for simplicity, the non-dimensional stress $s = \dfrac{\sigma_0}{G_0}$.

Generalization to negative values of the stress and strain my be provide as we introduce the $sign(s)$ function as:

$$\phi_c(\sigma,t) = \frac{|s|^{\alpha_c}sign(s)}{\Gamma(1+\beta_c)}\left(\frac{t}{\tau_0}\right)^{\beta_c} \tag{3.144a}$$

$$\phi_r(\varepsilon,t) = \frac{|\varepsilon|^{\alpha_r}sign(\varepsilon)}{\Gamma(1-\beta_r)}\left(\frac{t}{\tau_0}\right)^{-\beta_r} \tag{3.144b}$$

Let us introduce in the material function the non-linear transform

$$s_n(t) = |s|^{\alpha_c}sign(s) \quad \text{and} \quad \varepsilon_n(t) = |\varepsilon|^{\alpha_r}sign(\varepsilon) \tag{3.145}$$

and let us assume that the eqs.(3.143a)(3.143b) holds true also for non-constant stress/strain histories. In this case Boltzmann superposition applies also to $s_n(t)$ and $\varepsilon(t)$ yields:

$$s(t) = \frac{(\tau_r)^{\beta_r}}{\Gamma(1+\beta_r)}\int_0^t (t-\tau)^{-\beta_r}\,\dot{\varepsilon}_n(\tau)\,d\tau = (\tau_r)^{\beta_r}\left(D_0^{\beta_r}\varepsilon_n\right)(t) \tag{3.146a}$$

$$\varepsilon(t) = \frac{(\tau_c)^{-\beta_c}}{\Gamma(1-\beta_c)}\int_0^t (t-\tau)^{\beta_c-1}\,\dot{s}_n(\tau)\,d\tau = (\tau_c)^{-\beta_c}\left(I_0^{\beta_c}s_n\right)(t) \tag{3.146b}$$

As we assume that, after the introduction of fractional calculus formalism

yields:

$$s(t) = (\tau_r)^{\beta_r} \left(D_{0^+}^{\beta_r} \left[\varepsilon(t)^{\alpha_r} \right] \right)(t) \tag{3.147a}$$

$$\varepsilon(t) = \left[\frac{1}{\tau_r^{\beta_r}} \left(I_{0^+}^{\beta_r} s \right)(t) \right]^{1/\alpha_r} \tag{3.147b}$$

or, involving the knowledge of the creep functions:

$$\varepsilon(t) = (\tau_c)^{-\beta_c} \left(I_{0^+}^{\beta_c} \left[s(t)^{\alpha_c} \right] \right)(t) \tag{3.148a}$$

$$s(t) = \left[(\tau_c)^{\beta_c} \left(D_{0^+}^{\beta_c} \varepsilon \right)(t) \right]^{1/\alpha_c} \tag{3.148b}$$

Observation of eqs.(3.146)(3.146b) shows three main features:

i) The constitutive equations for the non-dimensional stress involves a non-linear transform of the strain $\varepsilon(t) \to \varepsilon_n(t)$ a relaxation time τ_r and the time-decay order β_r;

ii) The constitutive equation for the strain evolution involves the non-linear transform of the stress $s(t) \to s_n(t)$, a creep characteristic time τ_c and an evolution order β_c, with $\beta_c \neq \beta_r$;

iii) Some specific relations among creep $(\alpha_c, \beta_c, \tau_c)$ and relaxation $(\alpha_r, \beta_r, \tau_r)$ parameters can be obtained as from the next part.

3.3.1 Relations among Creep and Relaxation parameters

The non-linear dependence of the strain and the stress observed in the experimental campaign was extensively investigated in several papers on ligaments and tendons hereditariness [80, 1, 78]. However, despite the large efforts in the description of material parameters observed in relaxation tests no relations among α_c, β_c, τ_c for the creep tests and α_r, β_r, τ_r for the relaxation could be observed as reported by several authors. This latter comment is discussed in detail in this section obtaining the fundamental conditions that must be fulfilled for fractional-order modeling of non-linear hereditariness of tendons of the knee.

To this aim let us evaluate the strain $\varepsilon(t)$ at time instant $t = \tau_c$ yielding a one-to-one relation among the applied, non dimensional, stress s and the measured strain $\varepsilon(\tau_c)$, omitting arguments:

$$s = \varepsilon^{1/\alpha_c} \left(\Gamma(\beta_c + 1) \right)^{1/\alpha_c} \tag{3.149}$$

that, after substitution in eq.(3.149) yields the equality:

$$\varepsilon^{1/\alpha_c}(\Gamma(\beta_c+1))^{1/\alpha_c} = \frac{\varepsilon^{\alpha_r}}{\Gamma(\beta_r)}\left(\frac{\tau_c}{\tau_r}\right)^{-\beta_r} \tag{3.150}$$

that may be cast as:

$$\varepsilon^{\left(\frac{1}{\alpha_c}-\alpha_r\right)}\Gamma(\beta_r)\,\Gamma(1+\beta_c)^{1/\alpha_c} = \left(\frac{\tau_c}{\tau_c}\right)^{-\beta_r} \tag{3.151}$$

that holds true, for any value of the strain ε as $\alpha_r = \dfrac{1}{\alpha_c}$ so that a relation among the material characteristic times observed in creep and relaxation may be established as:

$$\tau_r = \tau_c\Gamma(\beta_c+1)^{1/(\alpha_c\beta_r)}\Gamma(\beta_r)^{1/\beta_r} \tag{3.152}$$

that, in. conjunction with the relation $\alpha_r = \dfrac{1}{\alpha_c}$ allows to estimate the characteristic time of the relaxation upon measure of the characteristic time observed in creep once a relation among the decay β_r and the order β_c has been established.

This latter condition may be obtained as we search the estimates of creep parameters with direct measures of the relaxation parameters, namely, α_r, β_r, τ_r. Under this condition the relation among the characteristic time in creep estimate τ_c and the characteristic time observed in relaxation reads:

$$\tau_c = \tau_r\left[\Gamma(\beta_r)^{\frac{1}{\alpha_r\beta_c}}\,\Gamma(\beta_c+1)^{\frac{1}{\beta_c}}\right]^{-1} \tag{3.153}$$

yielding:

$$\tau_r = \tau_c\left[\Gamma(\beta_r)^{\frac{1}{\alpha_r\beta_c}}\,\Gamma(\beta_c+1)^{\frac{1}{\beta_c}}\right] \tag{3.154}$$

Direct comparison of eq.(3.154) with eq.(3.152) yields the relation among the orders:

$$\beta_c = \alpha_c\beta_r \qquad \text{(3.155a)} \qquad\qquad \beta_r = \alpha_r\beta_c \qquad \text{(3.155b)}$$

eqs.(3.155) allows for a relation among the decaying order of the relaxation, given the creep parameters as:

$$\beta_r = \frac{\beta_c}{\alpha_c} \tag{3.156}$$

that corresponds, in conjunction with $\alpha_r = 1/\alpha_c$, to eq.(3.155b) namely $\beta_r = \alpha_r \beta_c$.

Relaxation order β_r of the stress $s\,(t)$ yields the order of the relaxation $\beta_r \geq \beta_c$ according to the well-established paradigms that *relaxation run faster than creep* as reported by several authors [63].

3.3.2 Numerical assessment

In this section we aim to show that the proposed equivalence relations hold true also in the presence of non-constant stress or strain histories and that the constitutive equations in eqs.(3.147a)(3.147b) (3.148a)(3.148b) are completely general.

we can shown the numerical results for a polynomial class of stress and strain. In the first application a function s (t) of type has been assigned:

$$s(t) = 5t \tag{3.157}$$

we have studied the problem by applying the eqs.(3.148a)(3.148b), and we have considered three different value of α_c, in particular $\alpha_{c=}1$ to show the particular case of linear behavior, $\beta_c = \beta_r = \beta = 0.45$, and $\alpha_c = 1, 1.4, 1.7$ and other parameters are fixed, $\tau_c = 4.5$; The solutions were obtained developed a numerical code implementing Grünwald-Letnikov's diferintegral, we considered 2000 steps with a time step of 0.1.

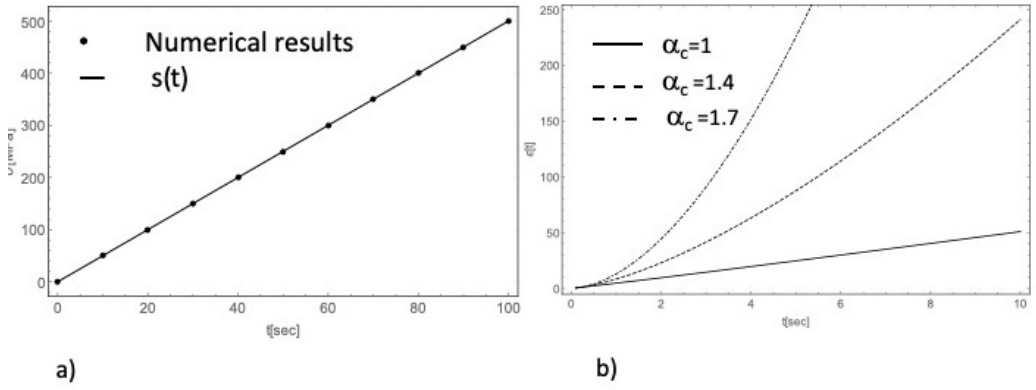

Figure 3.10: Numerical results between $s(t)$ assigned and Numerical results

The figs.(3.10a,b) showed the numerical results respectively of eq.(3.148a) and eq.(3.148b). Fig.3.10a and fig.3.10b shown the perfect match between assigned function of stress history and numerical results of eq.(3.148a) Fig.3.10b highlight the effect of non-linearity in the $\varepsilon(t)$ function, that increase for increasing values α_c.

If now we consider harmonic-type stress and strain histories function, for example s (t) of type has been assigned

$$s(t) = s_i Sin(\omega_j t) \quad with \quad i, j = 0, 1, 2 \tag{3.158}$$

where $s_0 = 10, s_1 = 15, s_2 = 20$. In the first application, we have considered to show the effect of amplitude on the non linearity of the function $s(t)$ eq.(3.148a), so we fixed the value of ω, in particular $\omega_0 = 1$ and also we established values for $\beta_c = 0.045$, $\tau_c = 7.5$ and $\alpha_c = 0.77$. A numerical code has been developed for solving the eqs.(3.148a) and (3.148b), in particular we used the solution of Fractional Integral and fractional derivative by Grünwald-Letnikov's differintegral, we considered 5000 steps with a time step of 0.01. The fig.3.11a shows that numerical application of eq.(3.148a) perfectly overlaps the assigned functions of $s(t)$ and the effect of the non-linearity in the $\varepsilon(t)$ function for three different values of s_i. while the fig.3.11b shows the perfectly overlaps between assigned stress history and the stress functions from eq.(3.148a) for each value of ω.

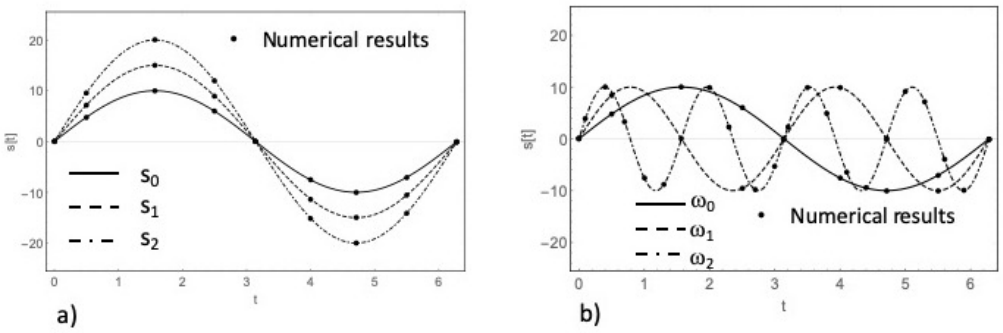

Figure 3.11: a) Numerical results between s(t) assigned ad s(t) obtained for 3 different amplitude; b) Numerical results between s(t) assigned ad s(t) obtained for 3 different frequency levels

In the following, the we have fixed the values of amplitude and have change ω_j, the three parameters chosen are $\omega_0 = 1, \omega_1 = 2, \omega_2 = 4$. The function $s(t)$ is calculated considering $\beta_c = 0.045$, $\tau_c = 7.5$ and $\alpha_c = 0.77$. The fig.3.11b shows the evaluation of

$$s(t) = s_1 Sin(\omega_j t) \tag{3.159}$$

To further highlight the effect of non-linearity in the case of non-linear viscoelastic behaviour, the value of the function to $\varepsilon(t)$ eq.(3.148b) was also

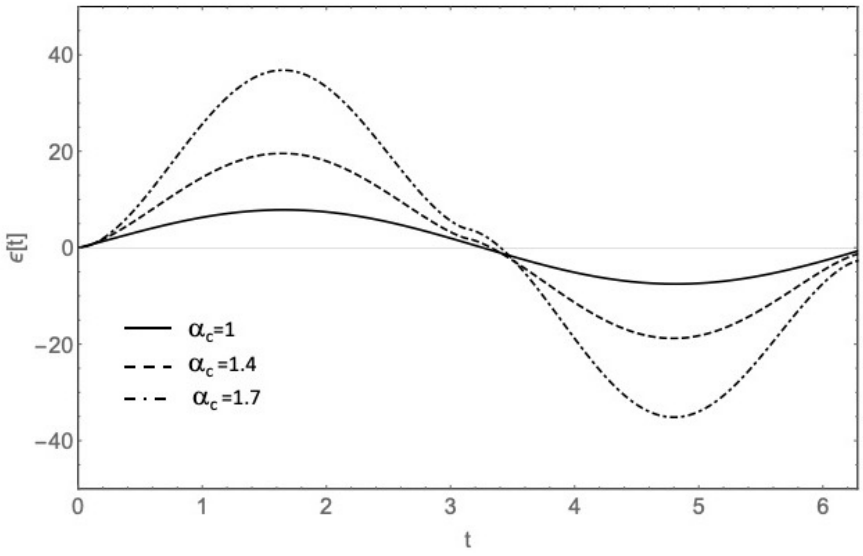

Figure 3.12: Numerical results of strain for assigned amplitude $s_0 = 10$ and frequency ω_1 and 3 different value of α_c

calculated for three different values of α_c, in particular $\alpha_c = 1$ to show the particular case of linear behavior, $\beta_c = \beta_r$, and $\alpha_c = 1.4$ and $\alpha_c = 1.7$. For each analysis we have considered fixed value of amplitude and ω. In following figs.(3.12,3.13 and 3.14) show the results of eq.(3.148b) was calculated by implementing Grünwald-Letnikov's differintegral for the calculation of the fractional integral, in which 5000 steps were carried out with a time step of 0.01. In the numerical tests carried out the effect of the non-linearity on the strain function both by keeping the amplitude constant and by keeping the frequency constant, the amplitude of the function is increased in both cases as the parameter increases α_c

In the next subsection we aim to show that the quasi-linear model of fractional-order material hereditariness is exactly modeled by a rheological assembly of internal linear springs and internal linear dashpots depending on the level of the external agency.

3.3.3 The rheological model of Fractional-order Quasi-linear Hereditary Materials (FQHM)

The original study aim to show that the proposed approach to fractional model of FQHM possess an equivalent rheological model totally analogous to a mechanical hierarchy that has been proposed for the linear fractional-

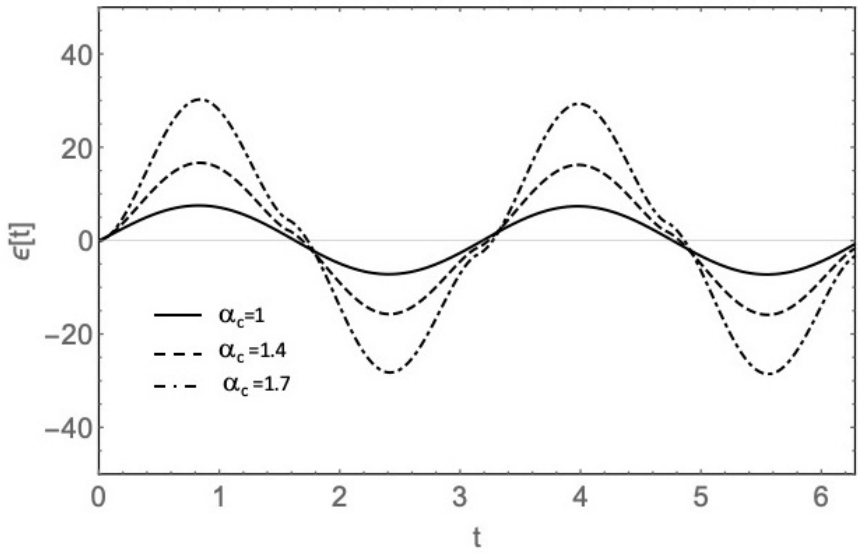

Figure 3.13: Numerical results of strain for assigned amplitude $s_0 = 10$ and frequency ω_2 and 3 different value of α_c

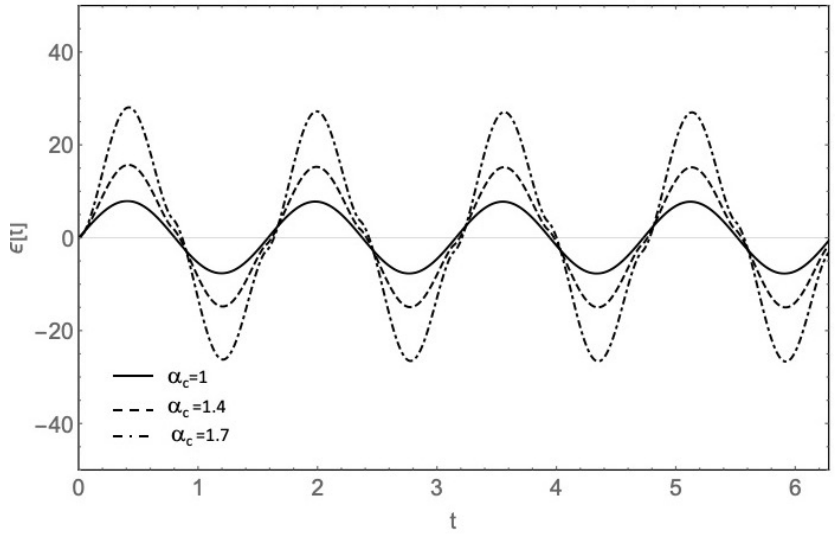

Figure 3.14: Numerical results of strain for assigned amplitude $s_0 = 10$ and frequency ω_3 and 3 different value of α_c

order hereditary material (FHM).

Rheological description of the non-linear dependence of the power-law in previous section may be captured as we introduce an unbounded linearly elastic bar that is externally restrained by a bed of viscous element along the column length as in Fig.3.15.

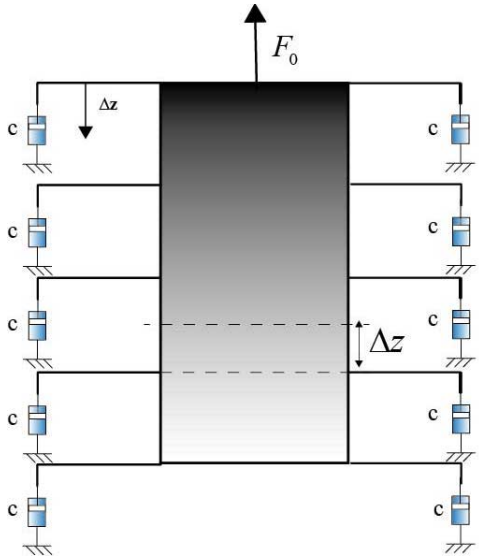

Figure 3.15: Linear elastic bar externally restrained by viscous elements and equilibrium representation of the single element

The equilibrium of the generic element reads:

$$N_e(z+\Delta z) - N_e(z) = -N_v \tag{3.160}$$

where N_v is the overall force of the dashpots along the column and it reads:

$$N_v(z) = -C\left(z, F_0\right)\Delta z \frac{\partial u}{\partial t}\left(z,t\right) \tag{3.161}$$

and the elastic axial stress along the column reads:

$$N_e\left(z\right) = K(z,F_0)\left[u\left(z,t\right) - u\left(z-\Delta z,t\right)\right] \tag{3.162a}$$

$$N_e\left(z+\Delta z\right) = K(z+\Delta z,F_0)\left[u\left(z+\Delta z,t\right) - u\left(z,t\right)\right] \tag{3.162b}$$

and with $u(z,t)$ the axial displacement along the column. Substitutions of eqs.(3.161),(3.162a),(3.162b) into eq.(3.160) yields the equilibrium equation in terms of the kinematic field $u(z,t)$ along the column as:

$$K(z+\Delta z,F_0)\Delta u\left(z+\Delta z,t\right) - K(z,F_0)\Delta u\left(z,t\right) = C\left(z,F_0\right),,taz\frac{\partial u}{\partial t} \tag{3.163}$$

that, after some algebraic manipulation may be written as:

$$\frac{\Delta}{\Delta z}\left[K\left(z,F_0\right)\Delta u\right]=C\left(z,F_0\right)\frac{\partial u}{\partial t} \tag{3.164}$$

and introducing the relation $K\left(z,F_0\right)=\dfrac{K_a(z,F_0)}{\Delta z}$ with $[K_a]=F$ and letting $\Delta z\to 0$ eq.(3.164) reads:

$$\frac{\partial}{\partial z}\left[K_a\left(z,F_0\right)\frac{\partial u}{\partial z}\right]=C\left(z,F_0\right)\frac{\partial u}{\partial t} \tag{3.165}$$

with the relevant boundary conditions:

$$\lim_{z\to\infty}u\left(z,t\right)=0;\qquad \lim_{z\to 0}K_a\left(z,t\right)\frac{\partial u}{\partial z}=F_0\quad\forall t \tag{3.166}$$

and for the initial condition $u(z,0)=0\ \forall z$. The mechanical hierarchy that corresponds to the non-linear creep function in eq.(3.165) is obtained assuming that the applied force F_0 is constant as in standard creep test. In the following we assume that the axial stiffness and axial damping are expressed by the relation:

$$K_a\left(z,F_0\right)=K_{\alpha_c}\frac{F_0 z^{-\delta}}{\Gamma\left(1-\alpha_c\right)}=K_0\frac{F_0^{(1-\alpha_c)}z^{-\delta}}{\Gamma\left(1-\delta\right)} \tag{3.167}$$

with $[K_0]=L^{\delta}F^{(2+\alpha_c)}$ and $\Gamma(\cdot)$ is the Euler-Gamma function and $\delta\in[-1,1]$ and . The non-linear damping coefficient reads:

$$C\left(z,F_0\right)=C_0\frac{F_0^{(1-\alpha_c)}z^{-\delta}}{\Gamma\left(1-\delta\right)} \tag{3.168}$$

with $[C_0]=F^{(2+\alpha_c)}TL^{\delta}$. Substituting of eqs.(3.167),(3.168) into eq.(3.165) yields:

$$\frac{\partial}{\partial z}\left[K_0 z^{-\delta}\frac{\partial u}{\partial z}\right]=C_0 z^{-\delta}\frac{\partial u}{\partial t} \tag{3.169}$$

that has the same mathematical structures of the governing equation of the linear hereditary hierarchy described in [30, 35] Laplace transform $\mathcal{L}[u]=\widehat{u}(s)$ of eq.(3.169) yields; after some straightforward manipulations:

$$\frac{d}{dz}\left[z^{-\delta}\frac{d\hat{u}}{dz}\right]=s\tau_0 z^{-\delta}\hat{u} \tag{3.170}$$

with relaxation time $\tau_0 = \dfrac{C_0}{K_0}$. The solution of eq.(3.170) may be obtained in terms of the first and second modified Bessel function, $Y_{\beta_c}(z\sqrt{\tau_0 s})$ and $K_{\beta_c}(z\sqrt{\tau_0 s})$ with $\beta_c(\delta+1)/2$ as:

$$\hat{u}\,(z,s) = z^{\beta_c}\left[B_1 Y_{\beta c}\,(z\sqrt{\tau_0 s}) + B_2 K_{\beta c}\,(z\sqrt{\tau_0 s})\right] \tag{3.171}$$

yielding, after substitution in eq.(3.166) the condition $B_1 = 0$. The integration constant B_2 is obtained by the boundary condition in eq.(3.166) yields:

$$B_2 \lim_{z\to 0}\left[z^{(2\beta_c-1)}\frac{F_0^{(1-\alpha_c)}K_0}{\Gamma\,(1-\delta)}\frac{d}{dz}z_c^{\beta}K_{\beta_c}\,(z\sqrt{\tau_0 s})\right] = \frac{F_0}{s} \tag{3.172}$$

yielding the constant B_2 as:

$$B_2 = \frac{F_0^{\alpha_c}(s\tau_0)^{-\beta_c/2}}{\Gamma\,(2\beta_c)\,K_0 2^{2\beta_c-1}} \tag{3.173}$$

The the axial displacement of the hierarchy at $z \to 0$,namely, $u_0\,(t)$ corresponds to the material creep functions as:

$$\begin{aligned} u_0\,(t) &= \mathcal{L}^{-1}\left[\frac{F_0^{\alpha_c}(s\tau_0)^{-\beta_c/2}}{\Gamma\,(2\beta_c)\,K_0 2^{2\beta_c-\alpha_c}}\lim_{z\to 0} z^{\beta_c}K_{\beta_c}\left(z\sqrt{\tau_0 s}\right)\right] = \\ &= \frac{F_0^{\alpha_c}\tau_0^{-\beta_c}}{K_0\Gamma\,(2\beta_c)\,\Gamma\,(\beta_c)\,K_0 2^{2\beta_c}}t^{\beta_c} = \frac{F_0^{\alpha_c}}{K_0\Gamma\beta_c}\left(\frac{t}{\bar{\tau}_c}\right)^{\beta_c} \end{aligned} \tag{3.174}$$

where we denoted:

$$\tau_c = \tau_0^{\beta_c}\Gamma\,(2\beta_c)\,\Gamma\,(\beta)\,K_0 2^{\beta_c} \tag{3.175}$$

that is completely equivalent to the non-linear creep function introduced to capture the non-linear behavior of the tendons observed in the mechanical tests. In passing we observe that the expression of the creep function in eq.(3.175) does not allow for the use of time-superposition principle so that no convolution integrals may be defined for non-linear hereditariness provided by eqs.(3.146)(3.146b) unless the non-linear transform $F_e\,(t) \to F\,(t)^{\alpha_c}$ is introduced. Under these circumstances the effect superposition may be used and the fractional-order operators may be readily defined.

In order to find the response of the hierarchic model to a constant applied stress, the equilibrium equations of the elements of the discretized model eq.(3.164) are recast in matrix form as follows:

$$F_0^{1-\alpha_c}\left(p_V\mathbf{B}\dot{\mathbf{u}} + q_V\mathbf{A}\mathbf{u}\right) = \mathbf{v}F_0 \tag{3.176}$$

where $\mathbf{v}$ is an influence vector and

$$p_V = \frac{C_0 \Delta z^{1-\delta}}{\Gamma(1+\delta)} \tag{3.177a}$$

$$q_V = \frac{K_0 \Delta z^{-1-\delta}}{\Gamma(1-\delta)} \tag{3.177b}$$

and

$$\mathbf{A} = \begin{bmatrix} 1^{-\delta} & -1^{-\delta} & 0 & \cdot & \cdot & \cdot & 0 \\ -1^{-\delta} & 1^{-\delta}+2^{-\delta} & -2^{-\delta} & \cdot & \cdot & \cdot & 0 \\ 0 & -2^{-\delta} & 2^{-\delta}+3^{-\delta} & \cdot & \cdot & \cdot & 0 \\ \cdot & \cdot & \cdot & \cdot & & & \cdot \\ \cdot & \cdot & \cdot & & \cdot & & \cdot \\ \cdot & \cdot & \cdot & & & \cdot & -(N-1)^{-\delta} \\ 0 & 0 & 0 & \cdot & \cdot & \cdot & (N-1)^{\delta}+N^{-\delta} \end{bmatrix} \tag{3.178a}$$

$$\mathbf{B} = \begin{bmatrix} 1^{-\delta} & 0 & 0 & \cdot & \cdot & \cdot & 0 \\ 0 & 2^{-\delta} & 0 & \cdot & \cdot & \cdot & 0 \\ 0 & 0 & 3^{-\delta} & \cdot & \cdot & \cdot & 0 \\ \cdot & \cdot & \cdot & \cdot & & & \cdot \\ \cdot & \cdot & \cdot & & \cdot & & \cdot \\ \cdot & \cdot & \cdot & & & \cdot & \cdot \\ 0 & 0 & 0 & \cdot & \cdot & \cdot & N^{-\delta} \end{bmatrix} \tag{3.178b}$$

and N is the number of laminae in which the hierarchical model is discretized. In order to evaluate the solution the set of ordinary differential equations (3.176), the system is premultiplied by $\mathbf{B}^{-1/2}$ and the coordinates transformation is introduced as $\mathbf{x} = \mathbf{B}^{1/2}\mathbf{u}$; as a consequence, eq. (3.176) may be written as

$$p_V \dot{\mathbf{x}} + q_V \mathbf{D}\mathbf{x} = \tilde{\mathbf{v}} F_0^{\alpha_c} \tag{3.179}$$

being $\mathbf{D} = \mathbf{B}^{-1/2}\mathbf{A}\mathbf{B}^{-1/2}$ and $\tilde{\mathbf{v}} = \mathbf{B}^{-1/2}\mathbf{v}$. Moreover in eq. (3.179) the load terms have been simplified and the load appears only to the r.h.s. of the system; as a consequence for constant applied load history the system is linear. For this reason the matrix $\mathbf{D}$ can be easily diagonalized by the standard method of modal analysis [35]. To this purpose, let the $\mathbf{\Phi}$ be the modal matrix whose columns are the eigenvectors of the matrix $\mathbf{D}$, then

$$\mathbf{\Phi}^T \mathbf{D} \mathbf{\Phi} = \mathbf{\Lambda} \qquad \mathbf{\Phi}^T \mathbf{\Phi} = \mathbf{I} \tag{3.180}$$

being $\mathbf{I}$ the identity matrix and $\mathbf{\Lambda}$ a diagonal matrix containing the eigenvectors of $\mathbf{D}$. By introducing the modal coordinates in eq. (3.179) as

$$\mathbf{x}(t) = \mathbf{\Phi}\mathbf{y}(t) \qquad \mathbf{y}(t) = \mathbf{\Phi}^T \mathbf{x}(t) \tag{3.181}$$

the following system of uncoupled linear differential equations is obtained

$$p_V \dot{\mathbf{y}} + q_V \mathbf{\Lambda x} = \bar{\mathbf{v}} F_0^{\alpha_c} \tag{3.182}$$

The generic $j-th$ equation reads

$$\delta_j \dot{y}_j + y_j = \frac{\phi_{1,j}}{q_V \lambda_j} F_0^{\alpha_c} \tag{3.183}$$

where $\delta_j = p_V/q_V\lambda_j > 0$ and $\phi_{1,j}$ is the first component of the $j-th$ eigenvector. eq. (3.183) represents the governing equation of the well-known viscoelastic Kelvin-Voigt model with unitary stiffness coefficient and damping coefficient equal to δ_j. Since the applied force at the r.h.s. of eq. (3.183) is constant, the solution is the creep function of the Kelvin-Voigt model amplified by the value of the force in the y domain, that is

$$y_j(t) = \frac{\phi_{1,j}}{q_V \lambda_j} F_0^{\alpha_c} \left[1 - \exp(-t/\delta_j)\right] \tag{3.184}$$

The solution in the original domain related to the upper lamina, the one we are interested in, can be easily obtained by the following

$$u_1(t) = \mathbf{v}^T \mathbf{B}^{-1/2} \mathbf{\Phi y}(t) \tag{3.185}$$

Eq. (3.185) is able to reproduce the nonlinear creep behavior described by the Nutting law. To this purpose fig.3.16 shows the creep function obtained with the aid of eq. (3.185) for different values of the applied force F_0. It is evident that as the applied force increases, the creep curves do not scale linearly.

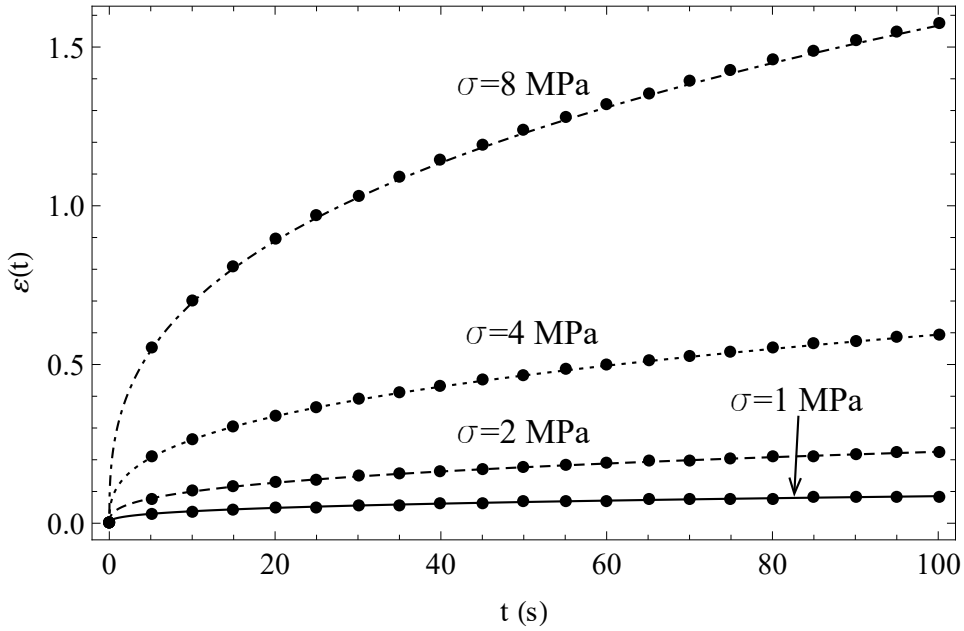

Figure 3.16: Plot of the creep curve related to the displacement of the upper lamina for different values of the applied force. Parameter values: $\alpha_c = 1.4$, $\beta_c = 0.3$, $\Delta z = 0.01$, $N = 2000$, $(\tau_c = 1)$.

Chapter 4

Non-linear hereditariness: Ligaments and Tendons of human knee

In this chapter the proposed approach to non-linear hereditariness in terms of fractional-order calculus is used for the biomechanical characterization of knee tendons and ligaments.

At first we report that in clinical biomechanics of graft used for surgical reconstruction makes wide use of terms as stress and strain. Unfortunately preconditioning of graft before surgery is usually done by means of application of forces.

In the next section we show by experimental results that a correct approach to be followed in clinical biomechanics will be the replacement the stress and strain as correct measures.

4.1 An in vitro mechanical test to mimic preconditioning/pretension protocol

In this paragraph we will assume that: i) a preconditioning protocol can be optimized with respect to the graft section, i.e. diameter, since geometrical factors affect, significatively, the results of the protocol [3]; ii) the protocol tuning on the graft diameter may be not sufficient to obtain an optimal outcome, because the grafts involves different tissue with different mechanical behaviour, although of the same size. In this experimental study these assumptions are investigated to provide the effects of an "in vitro" mechanical test, mimicking a simple preconditioning/pretensioning protocol, and apply it to several graft samples used in ACL reconstruction. Final aim of this

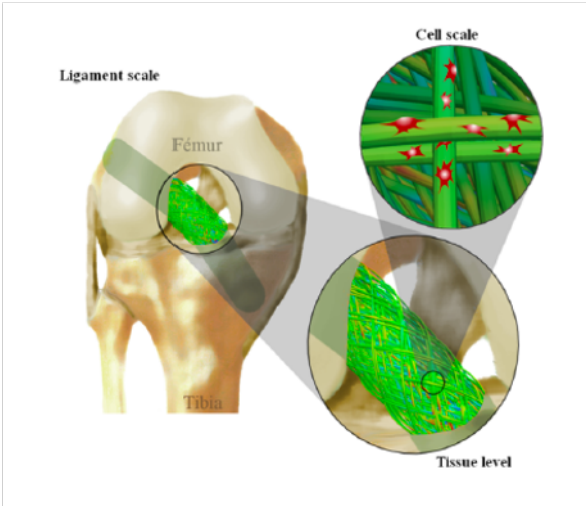

Figure 4.1: The three scales of tissue engineering in case of the cruciate anterior ligament

work is to identify reliable metrics able to support the optimal tuning of the initial loading conditions for any graft chosen in the treatment of ACL injury.

The experimental campaign involved three different types of human tissues, namely patellar (P) and hamstring (H) tendons, Anterior Cruciate Ligaments (ACL), and a commercial synthetic graft Lars (S). This choice was justified by the fact that these tissues are commonly used in ACL reconstruction [47]. They were collected from a Tissue Bank (Science Care, USA). The study was approved by the local Ethics Committee (protocol "TISS-KNEE" 8425). Tendons were stored at -80 $°C$ and thawed in a 37 $°C$ water bath for 15 min prior to testing [42] and then prepared by an experienced orthopaedic surgeon. After preparation, each specimen was cleaned and cut at the same length before clamping fig.4.2. For the first study we have prepared four different groups were prepared: - "H 32 mm^2", an H group with section 32$\pm$ 11 mm^2, with pretensioning load of 140$\pm$18 N that corresponds to 4 MPa stress, equivalent to the pretensioning load of 160 N used in [88] for 7 mm diameter grafts and indicated as good for stiffness and strength.

- "H 10 mm^2", an H group with section 10$\pm$11 mm^2, with pretensioning load of 140 N was applied.

- "P 32 mm^2", a P group with section 32$\pm$1 mm^2, with a pretensioning load of 140 N was applied.

- "S 10 mm^2", an S group as furnished by the manufacturer with section 10$\pm$1 mm^2, with pretensioning load of 140 N was applied. Each group was composed of six samples, as indicated in [58].

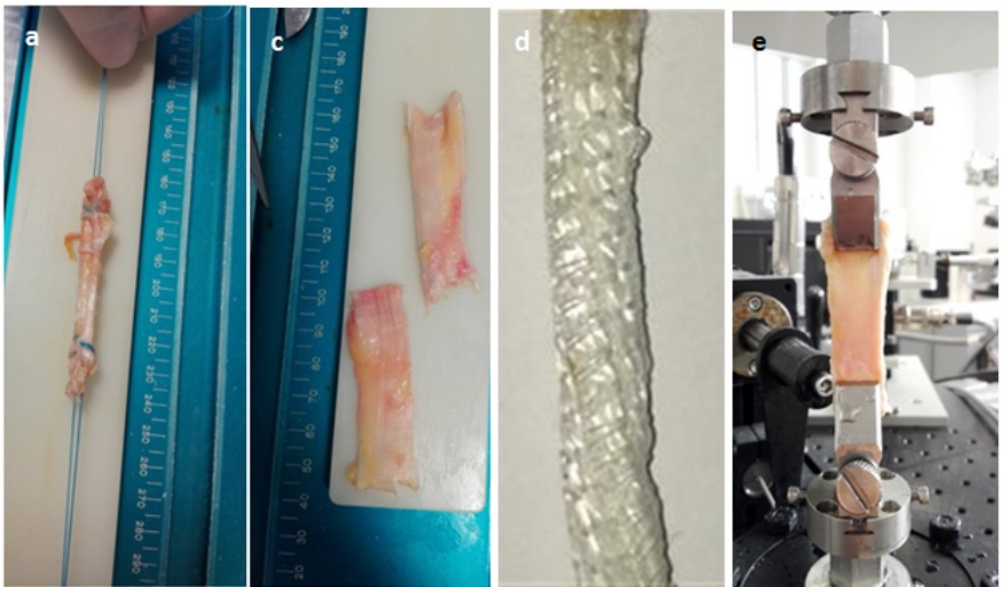

Figure 4.2: Preparation for testing of: hamstring tendon sample H (a), patellar tendon samples P (b), synthetic ligament S (c). A patellar sample clamped in the traction machine (d).

The aim of this study is the definition of an "optimal" procedure to tune the initial loading conditions of grafts. The experimental set-up used to this aim has involved the use of a single-axis electroforce dynamic system (Bose 3330, TA instruments) to perform uniaxial tensile tests. Sample principal fibres were qualitatively aligned along the machine loading axis (fig. 4.2d). Clamping was obtained with the aid of milled grips, involving sandpaper for the synthetic grafts and a surgical basting suture at the end of hamstrings grafts (fig.4.2a) [68]. In order to obtain reliable results, a specific experimental protocol consisting in four phases consecutively applied on the same sample was developed (fig. 4.3):

1. Preconditioning: specimens were preconditioned by harmonic load between 20 and 100 N, for twenty cycles at 0.25 Hz, thus to remove any crimping in the tendon fibrils caused by prolonged storage in a fixed position [55].

2. Recovery: a 20 N load was maintained for 15 min to exhaust sample elongation. After recovery, the initial length of the specimen as well as its initial width and thickness were measured along three sections of mid-substance by using a standard digital caliper; measurements were repeated three times by two different operators and values were then averaged to calculate strain and engineering stress.

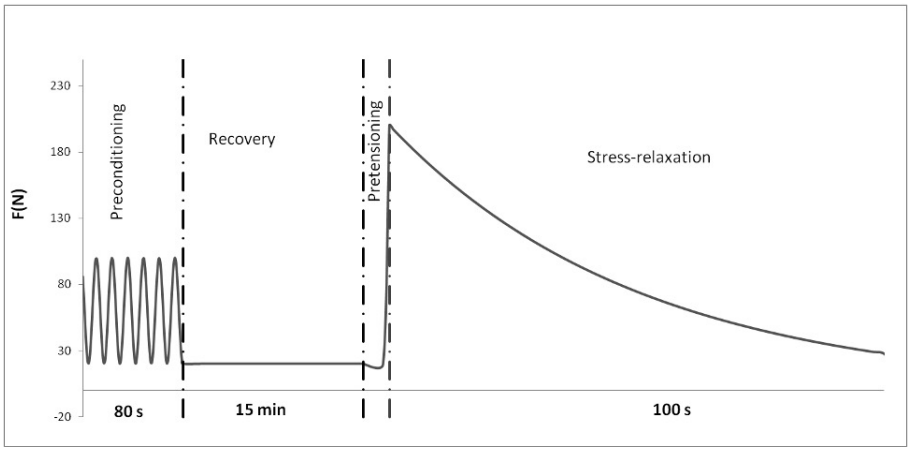

Figure 4.3: Protocol test

3. Pretensioning: a load was applied to induce pretension on the graft, considering a linear ramp with a loading rate of 315 N/s.

4. Stress relaxation: sample position reached in pretensioning was maintained for 100 s to mimic the behaviour of the grafts being implanted into the knee joint.

During the whole experimental test, specimens were continuously moistened with saline solution [54]. Stress relaxation lasted 100 s, that is an observation time chosen for accurate estimation of the phenomenon through a power-law model. The experimental data from the mechanical tests reporting the normalized stress with superimposed power-law fitting, are reported in fig. 4.4. The results about the pretension level $\sigma(t)$ are collected in fig. 4.5. The observation of the data shows that with a three times larger section A_0, the "H 32 mm^2" the group presented about a three times lower $\sigma(t)$ respect to the "H 10 mm^2" set; difference was statistically significant (p-value 0.0248). No difference was present between different materials with same section. The relaxation rates β are collected in fig.4.6. It can be observed that samples with larger section, in particular the "H 32 mm^2" set, shows faster relaxation if no statistical difference is present. Thus, the "H $32mm^2$" showed the highest decay, but no statistical difference is present.

The first assumption about the influence of the stress in the role of the ACL graft cross-section area (i.e. diameter), was specifically demonstrated by comparing grafts of the same typology, i.e. hamstring tendons, including different section areas. The second assumption, about the importance of the graft tissue, arise from the need to tune the preconditioning/pretensioning protocol for each graft. However, the protocol did not show any significantly different effect depending on the graft typology at least for the selected test

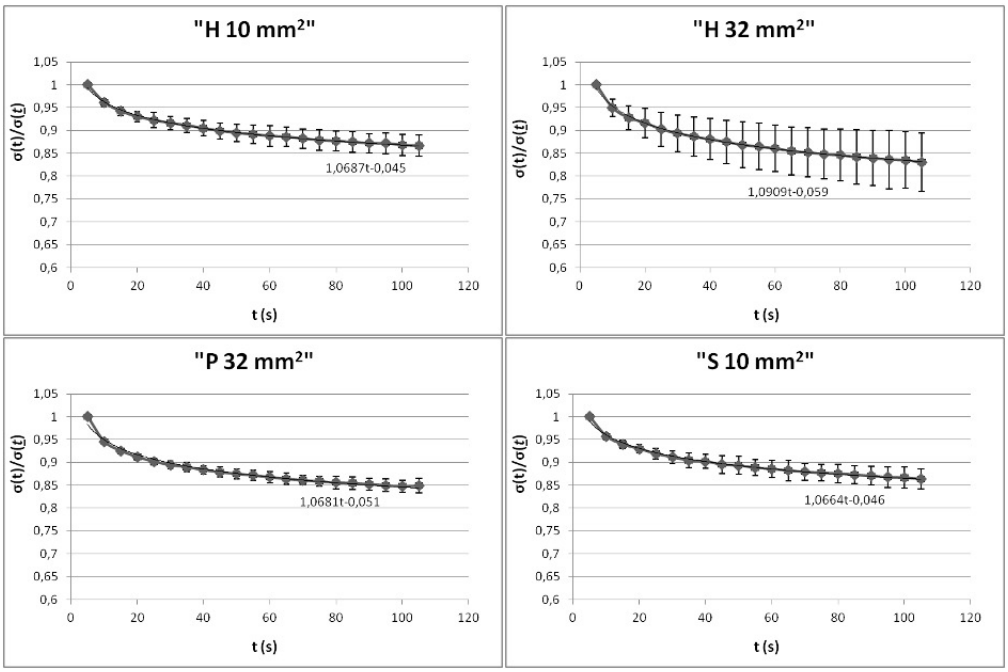

Figure 4.4: Stress relaxation dimensionless mean curves (markers) for patellar P, hamstring H and synthetic S samples with section area 32 or 10 mm^2, and relative power fitting superimposed (straight lines). $\sigma(t)$ stands for tension at time t,$\sigma(t)$ is the tension at the beginning of the relaxation (pretension). n

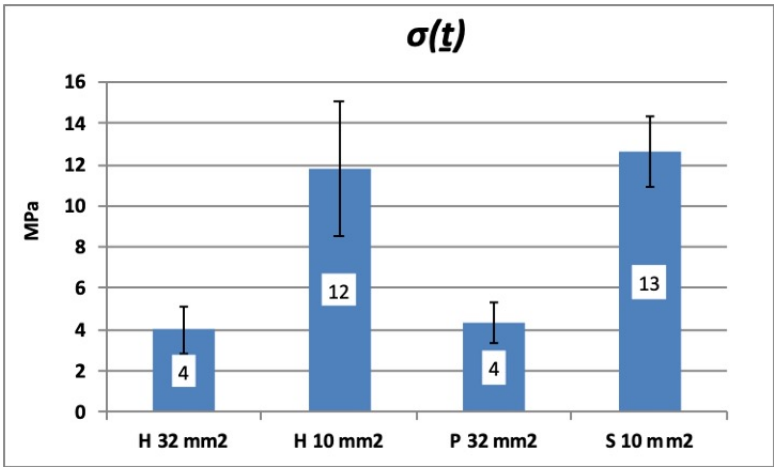

Figure 4.5: Pretension $\sigma(t)$ for patellar P, hamstring H and synthetic S samples with section area 32 or $10mm^2$.

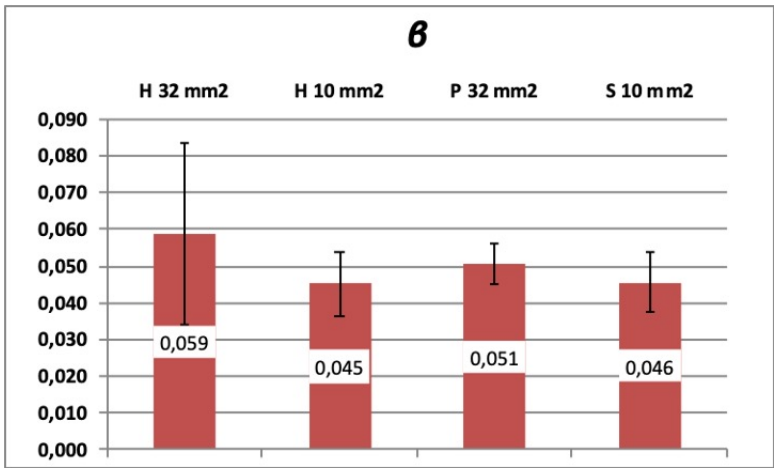

Figure 4.6: Relaxation rate β for patellar P, hamstring H and synthetic S samples with section area 32 or $10mm^2$.

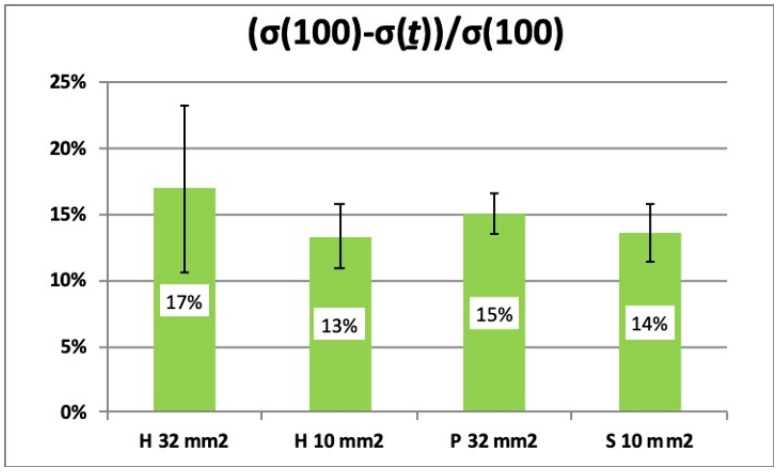

Figure 4.7: Loading loss, for patellar P, hamstring H and synthetic S samples with section area 32 or $10mm^2$.

conditions and analysis. The proposed preconditioning and based-on-stress pretensioning protocol shows comparable values of graft loss of tension after fixation, with respect to literature [70, 39]. These findings further underlines the strong effect of pretensioning and hence the need to define a proper protocol in clinical applications. The influence of the graft cross-section has been observed primarily on pretension and also, with less extend on stress relaxation. In particular for H, the test yields an inverse relationship between graft area and pretensioning and a direct relationship between graft size and relaxation. The results obtained for P are in agreement with literature. The pretensioning load influences the mechanics of the grafts to a large extend. The Stress, defined as force on section area, appears as the correct metric to take into account both the contributes, with the aim to identify an optimal approach for graft selection and preparation. In fact, the inherent definition of stress could help comparing and exploiting the results obtained in different studies. For instance, indications about a "dangerous" pretension – i.e. an excessive applied force able to introduce alterations in structure –, seem to be different if we consider a load of 340 N for a hamstring graft and a load of 500 N for a hamstring-polyethylene hybrid transplant. Nevertheless, focusing on cross-section area, we found that the first study used a graft diameter of about 7 mm, whereas the second of about 9 mm, thus both leading to a common indication in terms of stress (for both about 8 MPa). Indeed, stress is fundamental in interpreting structural-mechanical relationship. The previously reported stress value of 8 MPa represents an important basis also to interpret our results. While Hingorani et al. [60] and Vena et al. [90] showed that a higher pretension load led to a higher level of relaxation, the behaviour identified in this work appeared to be quite different, presenting lower level of relaxation when higher stress was applied; anyhow in [59] only pre-damage strains were used and it was speculated that a separate behaviour may be identified at higher levels of induced stress. This could be indeed our case, since the higher stress values are all above the critical value of 8 MPa, thus micro-damages could have impaired a full reorganization of the tissues and therefore the overall relaxation behaviour. In the analysed testing conditions, the influence of different graft materials was not that evident. Despite few differences due to the proposed testing protocols, consistency with literature was specifically identified in tension level and rate of relaxation for both P and H samples. Unfortunately, no data for comparison were found in literature concerning synthetic graft, with particular attention to the specific polyethylene terephtalate material. Despite this study did not find different macroscopic behaviours related to the several grafts tested, their specificity should not be ignored. Micro-structural differences were in fact reported between hamstring and patellar tendons. Although these grafts are of the

same typology of tissue, they were harvested from different knee anatomical locations, definitely with a specific different function. For this reason, under mechanical test conditions different from these observed in this study, some significant differences were highlighted. For the analysed synthetic solution, differences with respect to hamstring were not attended in general, as hamstring graft represents a "gold standard", thanks to a broad range of available analyses [89, 61]. Nevertheless, new materials are under development to obtain optimal ACL graft properties, therefore focusing on stress - here proposed as one possible tuning metrics - can be useful to identify the optimal graft diameter. This study presented several limitations and that may be improved in the close future. Concerning testing, despite the use of several solutions to avoid slippage of the soft tissues, further experiments should necessarily consider the clamping performed on bone insertions or the use of special gripping techniques. The obtained results show that the major limitation pertains to the small sample size and testing conditions, that did not allow us to completely generalize relationships between graft diameters and materials. Nevertheless, this study provided an important basis that can be used as a preliminary approach to optimize in particular the preconditioning/pretensioning protocol and, more in general, the choice of graft in the treatment of ACL injury.

4.2 The non-linear hereditariness of ligaments and tendons human knee

In this paragraph we investigated from each type of graft used in surgical reconstruction, behavior at different levels of imposed strain. In more details we build a specific protocol on to introduced the same specimen relaxation followed by material creep in five phases. 1. Preconditioning: specimens were preconditioned by cycling between 20 and 100 N, for twenty cycles at 0.25 Hz, thus to remove any crimping in the tendon fibrils caused by prolonged storage in a fixed position. 2. After preconditioning, the initial length of the specimen as well as its initial width and thickness were measured along three sections of mid-substance by using a standard digital caliper; measurements were repeated three times by two different operators and values were then averaged to calculate strain and engineering stress. 3. Stress relaxation testing: considering the physiological range for ACL during daily-life activities, different levels of strain, i.e. 1 %, 2 %, 3 %, 4 %, 5 %, were applied for 100 s to each specimen of each group, considering a linear ramp with a displacement rate of 250 mm/s, thus to mimic physiological loading conditions. 4.

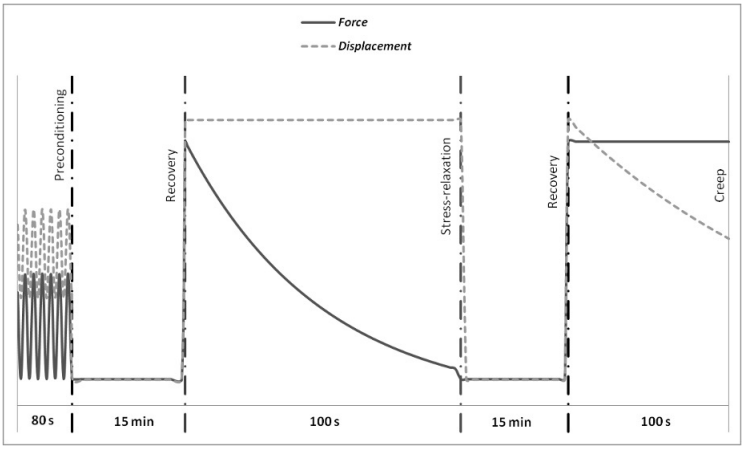

Figure 4.8: Scheme of the testing protocol, where "Force" is the vertical force read by the load cell (Newton) and "Displacement" is the distance between clamps (millimetres)

Recovery: after relaxation, the applied strain was removed, and the specimen was left untested for 15 min, thus to recover the effects of the loading history and reduce the residual stress within the material. Recovery was assessed by checking that after the unloaded period, the length of the sample was the same measured at the end of phase 1. 5. Creep testing: the load recorded at the beginning of phase 2 was applied to the sample for 100 s, considering a linear ramp with a loading rate of 315 N/s. During the whole experimental test, specimens were continuously moistened with saline solution

For each type of graft, five testing sessions which corresponded to the imposed strains of 1-2-3-4-5% These values were chosen because peak ACL strains during commonly activities range between 0% and 5%, and also because the strain at which the patellar tendon transits from the toe-region to its linear region is slightly less than 5%. During the test, the specimen was continuously moistened with saline solution. We have used the protocol test in fig.4.8

Before testing, the specimens were preconditioned by cycling between 20 and 100 N, for twenty cycles at 0.25 Hz to remove any crimping in the tendon fibrils caused by prolonged storage in a fixed position .

4.2.1 Experimental findings

The experimental data in terms of the axial engineering strain $\varepsilon(\sigma, t)$ have been averaged, for each level of applied stress. The averaged creep functions, namely $< \varepsilon^{(P)} > (\sigma_i, t) >$ and $< \varepsilon^{(H)} (\sigma_i, t) >$ are reported in tab.4.1

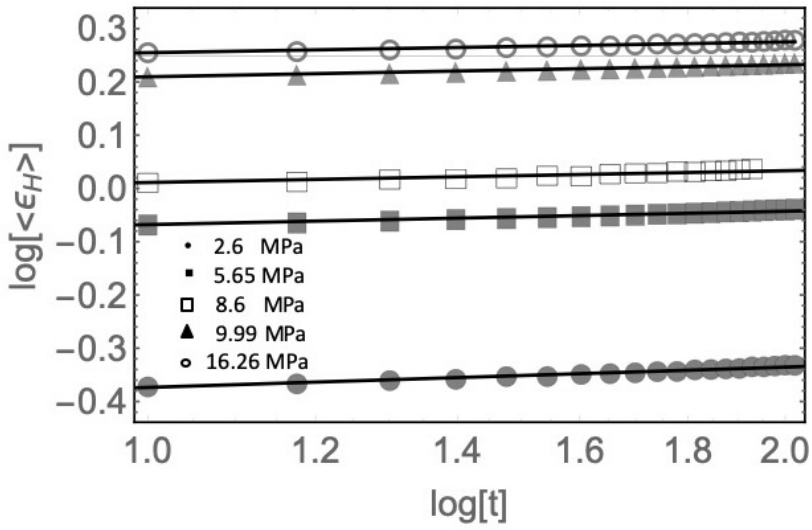

Figure 4.9: log-log plots averaged creep functions hamstring ligaments

and tab.4.2, respectively. A more detailed representation of the averaged creep functions may be observed in a $\log\left[<\varepsilon>\right] - \log\left[t\right]$ plot reported in figs.(4.9,4.10) for the patellar and hamstring tendons, respectively.

Creep							
Hamstring				Patellar			
σ	β_c	τ_c	α_c	σ	β_c	τ_c	α_c
2.61	0.1266	3.976	1.255	2.21	0.0917	4.938	0.635
5.65	0.0832	11.405	1.811	4.55	0.0902	2.742	0.717
8.61	0.0744	8. 701	1.649	5.37	0.0885	4.000	0.789
9.98	0.0735	4.052	1.591	6.88	0.011	5.799	0.672
16.26	0.067	11.29	1.568	7.57	0.058	5.22	0.729

Table 4.1: Average values for Hamstring and Patellar tendons obtained from best fitting of experimental campaigns for creep test

Data analysis reported in fig.4.2 and fig.4.3 for the log-log plots reveals that good candidate to fit averaged values of creep functions $\mu_{\varepsilon}^{(P)}\left(\bar{\sigma}_i, t\right)$ and $\mu_{\varepsilon}^{(H)}\left(\bar{\sigma}_i, t\right)$ is the a linear model with equation:

$$\log\left[<\varepsilon^{(j)}\left(\sigma, t\right)>\right] = \beta_j \log\left(\frac{t}{\Gamma\left(1-\beta_j\right)\tau_c^{(j)}}\right)^{\frac{1}{\beta_j}} + \alpha_j \log\left(\frac{\sigma_j}{G_0}\right) \qquad (4.1)$$

where $j = P, H$ denotes the specific tissue considered, $\tau_c^{(j)}$ and $\bar{\sigma}_j$ are respec-

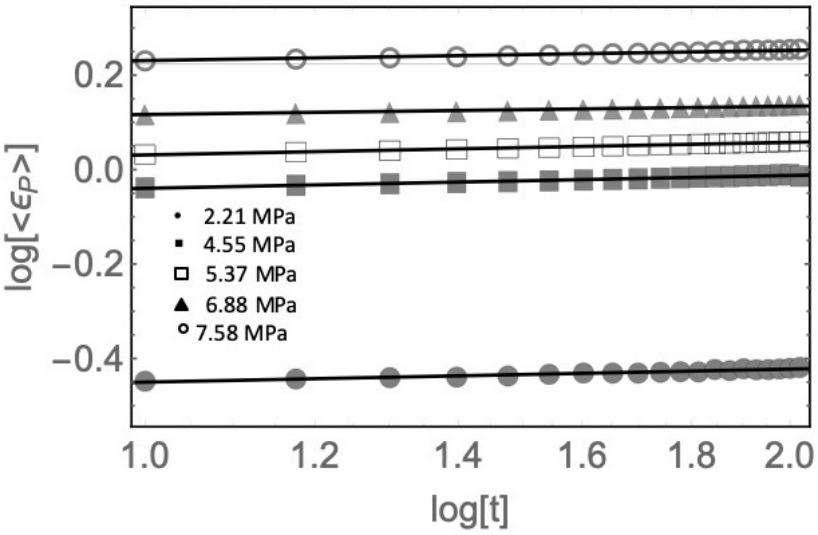

Figure 4.10: log-log plots averaged creep functions Patellar tendons

tively a characteristic time and the non-dimensional stress $\bar{\sigma}_j = \dfrac{\sigma_j}{E}$ where E is the tangent elastic modulus obtained at the origin of a monotone test.

Straightforward manipulation of eq. (4.1) yields the relation for the average of the strain omitting j-dependence:

$$< \varepsilon\left(\sigma, t\right) >= \left(\frac{\sigma}{G_0}\right)^{\alpha} \left(\frac{t}{\Gamma\left(1-\beta_c\right)^{\frac{1}{\beta}} \tau_c}\right)^{\beta} = \frac{\|s\|^{\alpha_c} sign\left(\sigma\right)}{\Gamma\left(1-\beta_c\right)} \left(\frac{t}{\tau_c}\right)^{\beta_c} \tag{4.2}$$

with $0 \leq \beta_c \leq 1$, $0 \leq \alpha_c \leq 1$ two material parameters, $[\tau_c] = [T]$ is an additional material constant representing the characteristic time of the material observed in a creep test and $sign\left(\bullet\right)$ is the signum function. It may be observed that values of α_c, β_c and τ_c are represented in tab.4.1 for the considered tissues.

Inspection of eq.(4.2) reveals that the creep function coalesces with the original formulation of Nutting obtained by experimental data conducted for rubbers, concrete, steel, but not for biological tissues as in fact $< \varepsilon(\sigma, t) >$ for an assigned value of σ, is a creep function that is $< \varepsilon(\sigma, t) >= \phi_c(s, t) = s^{\alpha_c} = J(t)$ for $s > 0$.

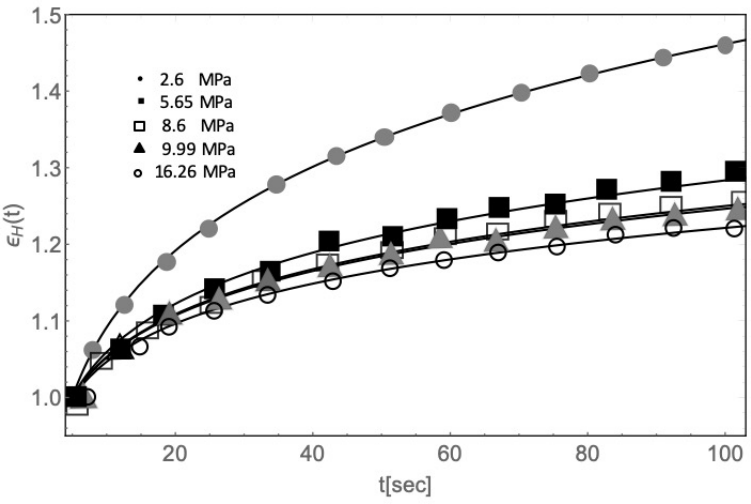

Figure 4.11: averaged creep functions hamstring ligaments

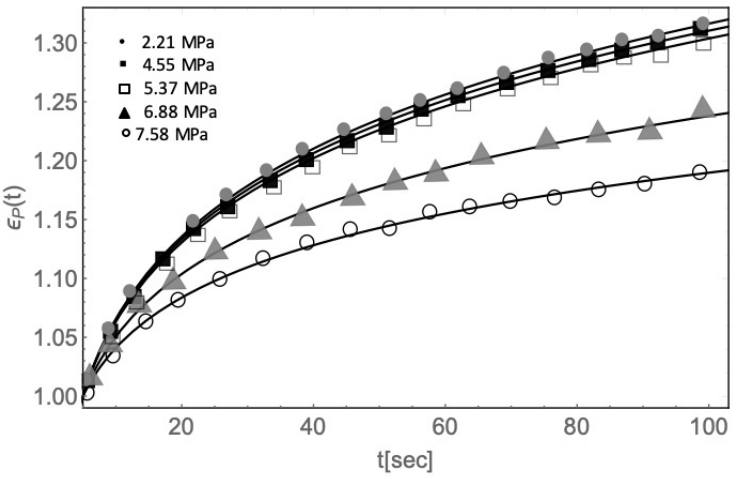

Figure 4.12: averaged creep functions Patellar tendons

Solid lines in fig.4.11 and fig.4.12 represent fits of the data with eq.(4.1) and excellent agreement among curves and data may be observed as expected for power-laws representation of ligaments and tendons hereditariness [63]. The Nutting law given in the form $|s|^{\alpha_c} sgn(\sigma) J(t)$ has been obtained by

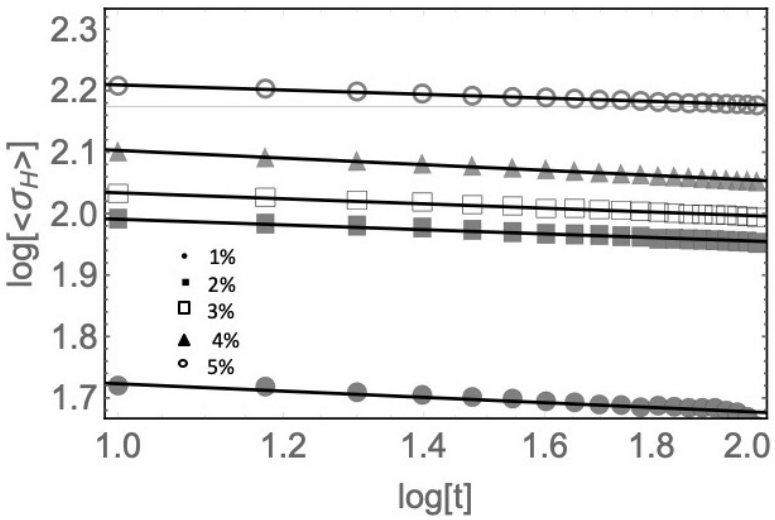

Figure 4.13: log-log plots averaged relaxation functions hamstring tendons

considering a creep test. Since eq.(4.2) is non-linear, it may be obtained the correspondent relation for the relaxation test like it happens in the linear case. In order to achive this result we proceed with the relation test on the specimen for patellar and hamstring tendons. Previous considerations about the averaged values of the creep test results may be reported for the relaxation averaged data in figs.(4.15, 4.16) and for the log-log plots reported in figs.(4.13, 4.14) for the patellar and hamstring tendons, respectively. Solid lines in figs.(4.13, 4.14) represents the linear fitting with equations (omitting j-dependence)

Relaxation							
Hamstring				Patellar			
ε	β_r	τ_r	α_r	ε	β_r	τ_r	α
1%	0.1589	5.191	0.796	1%	0.1444	5.39	1.574
2%	0.1507	5.211	0.552	2%	0.1258	5.2311	1.394
3%	0.1227	4.686	0.606	3%	0.1122	4.971	1.268
4%	0.117	4.503	0.628	4%	0.1060	4.601	1.489
5%	0.1051	4.532	0.637	5%	0.098	4.98	1.69

Table 4.2: Average values for Hamstring and Patellar tendons obtained from experimental campaigns for relaxation test

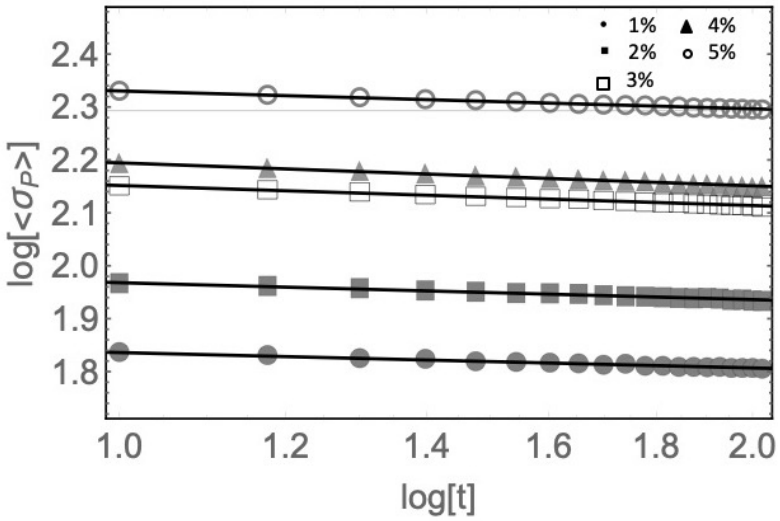

Figure 4.14: log-log plots averaged relaxation functions Patellar tendons

$$\log\left[\frac{<\sigma(\varepsilon,t)>}{G_0}\right]=\log\left[<s(t)>\right]=-\beta_r\log\left[\frac{\Gamma(\beta_r)^{\frac{1}{\beta_r}}\,t}{\tau_r}\right]+\alpha_r\log\left[\varepsilon\right] \quad (4.3)$$

that corresponds, after straightforward manipulations to the stress average relaxation expressed as:

$$<s(t)>=\frac{\varepsilon^{\alpha_r}}{\Gamma(\beta_r)}\left(\frac{t}{\tau_r}\right)^{-\beta_r}=\frac{\|\varepsilon\|^{\alpha_r}sign(\varepsilon)}{\Gamma(\beta_r)}\left(\frac{t}{\tau_r}\right)^{-\beta_r} \quad (4.4)$$

with α_r, β_r relaxation material parameters and $[\tau_r]=[T]$ the characteristic time of the tissue obtained in a relaxation test. The observation of eqs.(4.2, 4.4) shows that both creep and relaxation functions of the fibrous tissue are non-linear functions of the stress and the strain respectively. Under the assumption that $\alpha=\gamma=1$ a linear dependence is experienced so that the creep and relaxation may be expressed as:

$$<\varepsilon(t)>=\frac{s}{\Gamma(1-\beta_c)}\left(\frac{t}{\tau_c}\right)^{\beta_c}=sJ(t) \quad (4.5a)$$

$$<s(t)>=\frac{\varepsilon}{\Gamma(\beta_r)}\left(\frac{t}{\tau_r}\right)^{-\beta_r}=\varepsilon G(t)$$

with $J(t)$ and $G(t)$ the well-known creep and relaxation functions of linear hereditariness as $\tau_r=\tau_c=\tau_0$ and $\beta_r=\beta_c=\beta$.

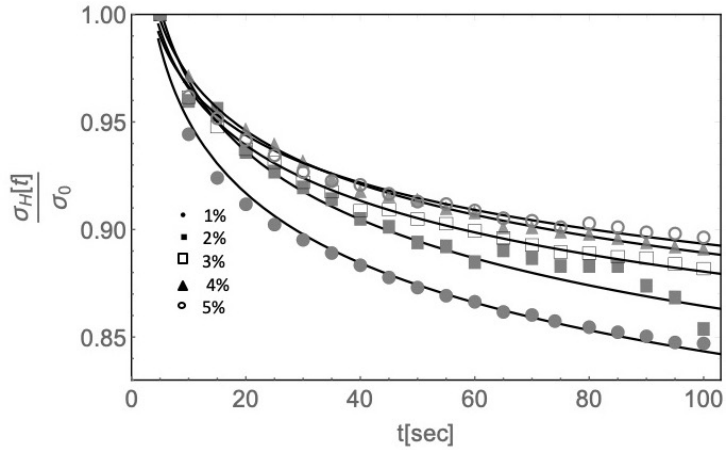

Figure 4.15: averaged relaxation functions hamstring tendons

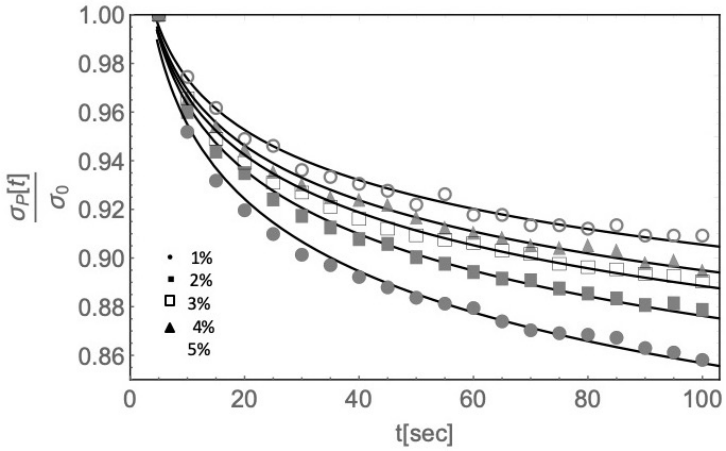

Figure 4.16: averaged relaxation functions Patellar tendons

The same considerations can be made for ACL and the LARS synthetic prosthesis

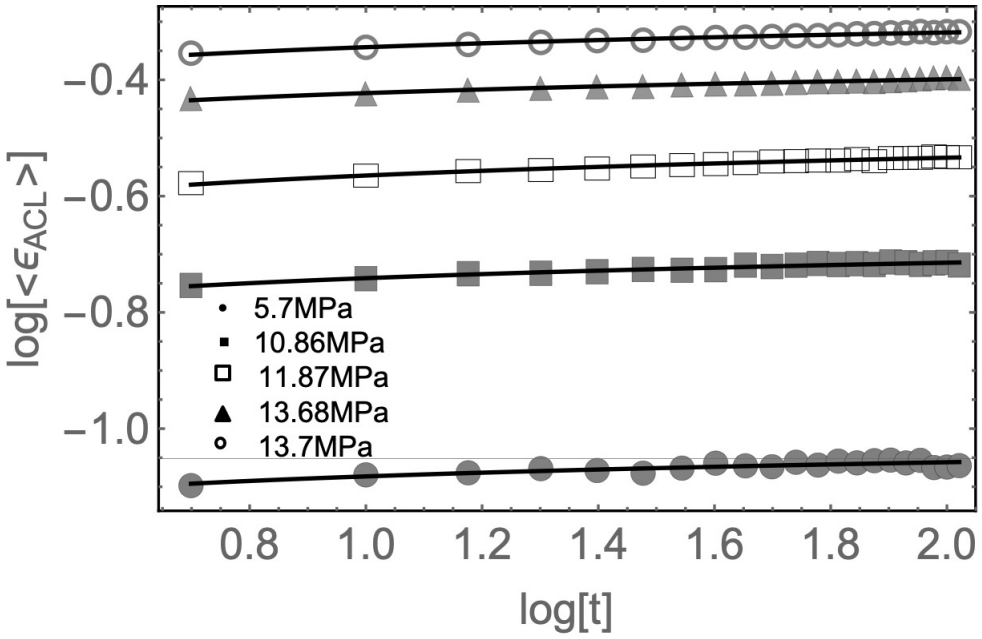

Figure 4.17: log-log plots averaged creep functions ACL

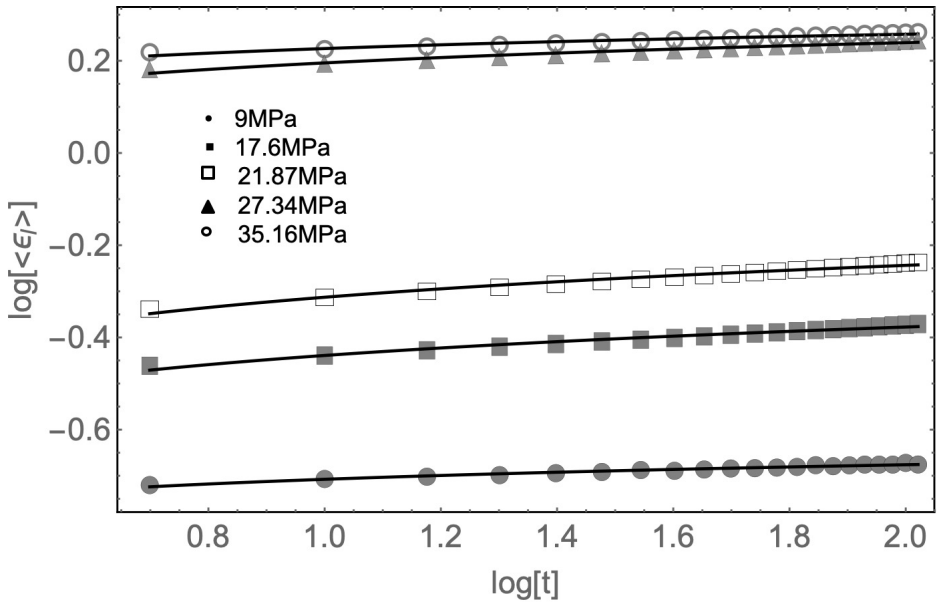

Figure 4.18: log-log plots averaged creep functions LARS graft

Creep							
ACL ligaments				Lars graft			
σ	β_c	τ_c	α_c	σ	β_c	τ_c	α_c
5,7	0.101	9.67	0.91	9	0.22	13.9	0.97
10.86	0.0883	9.34	1.017	17.6	0.203	5.98	1.021
11.87	0.084	5.19	1.025	21.87	0.14	7.24	1.07
13.68	0.08	4.75	0.96	27.34	0.101	20.83	1.31
13.7	0.0789	3.66	0.92	35.16	0.1	30	1.39

Table 4.3: Average values for ACL and LARS obtained from best fitting of experimental campaigns for creep test

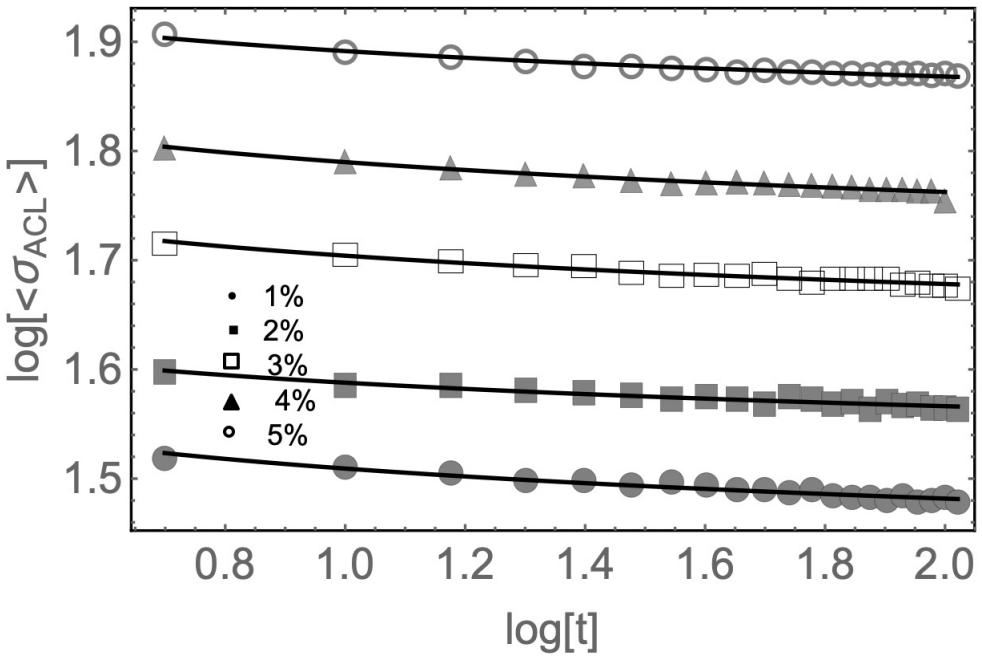

Figure 4.19: log-log plots averaged relaxation functions ACL

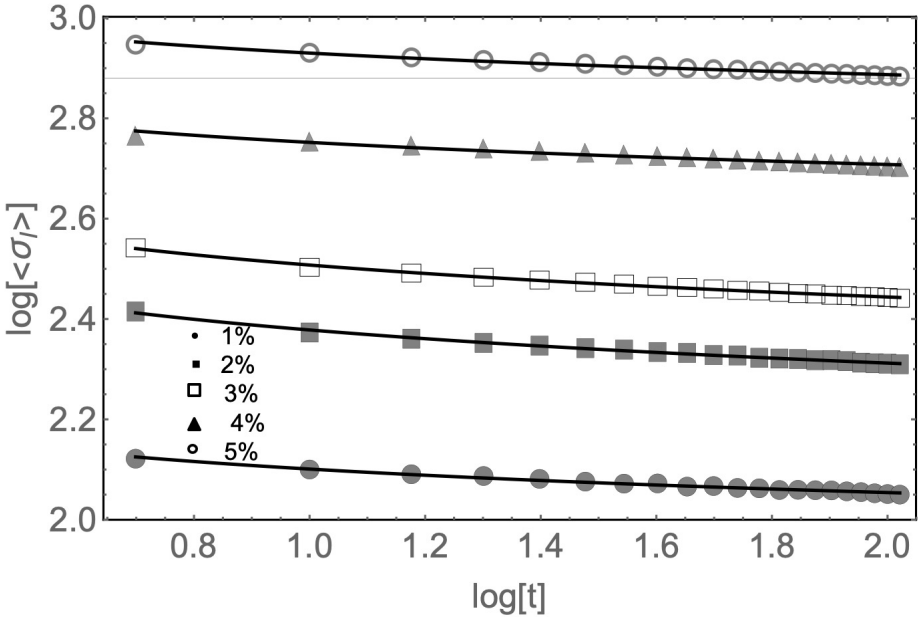

Figure 4.20: log-log plots averaged relaxation functions Lars graft

Relaxation							
ACL ligaments				Lars graft			
ε	β_r	τ_r	α_r	ε	β_r	τ_r	α_r
1%	0.091	14.1	1.11	1%	0.219	53.6	1.05
2%	0.09	19.93	0.981	2%	0.211	59.71	0.971
3%	0.086	23.86	0.99	3%	0.155	48.37	0.942
4%	0.077	4.18	1.02	4%	0.1463	63.48	0.719
5%	0.071	3.78	1.13	5%	0.1427	4.41	0.725

Table 4.4: Average values for ACL and LARS obtained from best fitting of experimental campaigns for relaxation test

4.2.2 Comparison among creep and relaxation parameters

In table(4.5,4.6,4.7) and table 4.8 values of the parameters obtained by best fitting of the experimental data in sec.(3) for creep and relaxation tests have been contrasted with the results of the proposed equations used to relate creep and relaxation parameters. The columns of the tables report the estimates of creep parameters for measured values of the relaxation parameters at different level of applied stress assuming $G_0 = 1MPa$ respectively for

hamstring (tab.4.5) and patellar tendons (tab.4.6). The table reports the percentage absolute value of the mean error e_i with $i = \beta, \alpha, \tau$, among estimated and measured parameters and direct inspections shows that errors are less than 5%.

Hamstring tendons

σ	$\beta_c = \beta_r \alpha_r$	e_β	$\alpha_c = 1/\alpha_r$	e_α	τ_c	e_τ
2.61	0.1251	0.0118	1.247	0.006	5.1	0.033
5.65	0.0833	0.0012	1.831	0.0109	3.8	0.386
8.61	0.0738	0.008	1.641	0.005	4.141	0.0352
9.98	0.0722	0.018	1.477	0.072	5.75	0.008
16.26	0.065	0.0299	1.555	0.009	5.391	0.033

Table 4.5: Average values for Hamstring tendons obtained from parameters relationships

Patellar tendons

σ	$\beta_c = \beta_r \alpha_r$	e_β	$\alpha_c = 1/\alpha_r$	e_α	τ_c	e_τ
2.21	0.1397	0.033	0.614	0.033	4.01	0.008
4.55	0.1235	0.018	0.71	0.024	11.34	0.006
5.37	0.109	0.029	0.765	0.03	8.9	0.0023
6.88	0.012	0.09	0.673	0.002	4.07	0.004
7.57	0.089	0.091	0.732	0.004	11.11	0.01

Table 4.6: Average values for Patellar tendons obtained from parameters relationships

ACL ligaments

σ	$\beta_c = \beta_r \alpha_r$	e_β	$\alpha_c = 1/\alpha_r$	e_α	τ_c	e_τ
5,7	0.102	0.009	0.9	0.009	9.55	0.012
10.86	0.083	0.063	1.019	0.002	9.39	0.005
11.87	0.081	0.037	1.021	0.001	5.22	0.006
13.68	0.078	0.026	0.962	0.003	4.6	0.031
13,7	0.075	0.052	0.899	0.022	3.69	0.008

Table 4.7: Average values for ACL obtained from parameters relationships

Lars Graft						
σ	$\beta_c = \beta_r \alpha_r$	e_β	$\alpha_c = 1/\alpha_r$	e_α	τ_c	e_τ
9	0.102	0.045	0.95	0.018	13.6	0.021
17.6	0.083	0.01	1.03	0.008	6.2	0.036
21.87	0.081	0.042	1.06	0.007	7.02	0.03
27.34	0.078	0.04	1.39	0.061	21.2	0.01
35.16	0.075	0.03	1.37	0.008	30.6	0.02

Table 4.8: Average values for LARS graft obtained from parameters relationships

The observation of the experimental data reported in tabs. (4.1,4.2,4.3,4.4) as well as of the relations among creep and relaxation coefficients, shows that the order of the power-law $[\bullet]^{-\beta_r}$ and $[\bullet]^{\beta_c}$ depends, non-linearly, by the level of the initial strain ε (relaxation) or the initially assigned stress σ (creep).

In such circumstances the multiplicative decomposition of the material functions $J(\sigma, t)$ and $G(\varepsilon, t)$ does not hold. However, statistical analysis on the experimental data shows that assuming the average value of the order $\beta_c \to \bar{\beta}_c$ and $\beta_r \to \bar{\beta}_r$ for creep and relaxation may be assumed in engineering context whereas the scattering of material-time data, namely τ_c and τ_r with respect to a mean value among the different level of strains has been modeled as random fluctuations [18].

In this case the formulation proposed for general kind of stress/strain histories, see sec.3.3, may be still used in biomechanical constitutive equation of the fibrous tissues of the knee:

$$s(t) = (\tau_r)^{\bar{\beta}_r} \left(D_{0^+}^{\bar{\beta}_r} \left[\varepsilon(t)^{\alpha_r} \right] \right)(t) \tag{4.6a}$$

$$\varepsilon(t) = \left[\frac{1}{\tau_r^{\bar{\beta}_r}} \left(I_{0^+}^{\bar{\beta}_r} s \right)(t) \right]^{1/\alpha_r} \tag{4.6b}$$

or, involving the knowledge of the creep functions:

$$\varepsilon(t) = (\tau_c)^{-\bar{\beta}_c} \left(I_{0^+}^{\bar{\beta}_c} \left[s(t)^{\alpha_c} \right] \right)(t) \tag{4.7a}$$

$$s(t) = \left[(\tau_c)^{\bar{\beta}_c} \left(D_{0^+}^{\bar{\beta}_c} \varepsilon \right)(t) \right]^{1/\alpha_c} \tag{4.7b}$$

The use of single-integral model of non-linear hereditariness in the context of fractional-order calculus has not been exploited, mainly, for the lack of equivalence among creep and relaxation parameters. Analytical and experimental arguments showed here showed that, as far as the creep parameters $(\alpha_c, \bar{\beta}_c, \tau_c)$ have been measured by experimental tests, the corresponding relaxation parameters $(\alpha_r, \bar{\beta}_r, \tau_r)$, may be estimated by means of the relations

reported in eqs.(3.153)(3.154)(3.155)(3.155b)(3.156) and viceversa. The $\bar{\beta}_c$ and $\bar{\beta}_r$ value referred to and the average value corresponding to the slope of the previously reported logarithmic curves.

Finally, to focus on the trend of the parameters, the histograms of the average β values, for each level of stress/strain, have been reported for each group considered for both the creep and the relaxation results. Moreover, the histograms of the beta values between the groups are reported both for creep and for relaxation

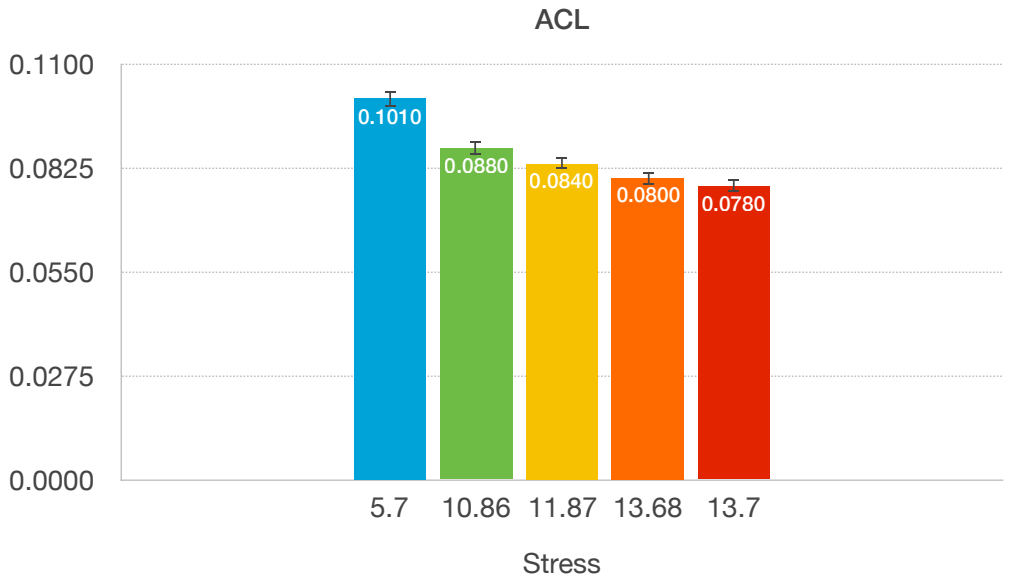

Figure 4.21: average β_c for ACL tissue

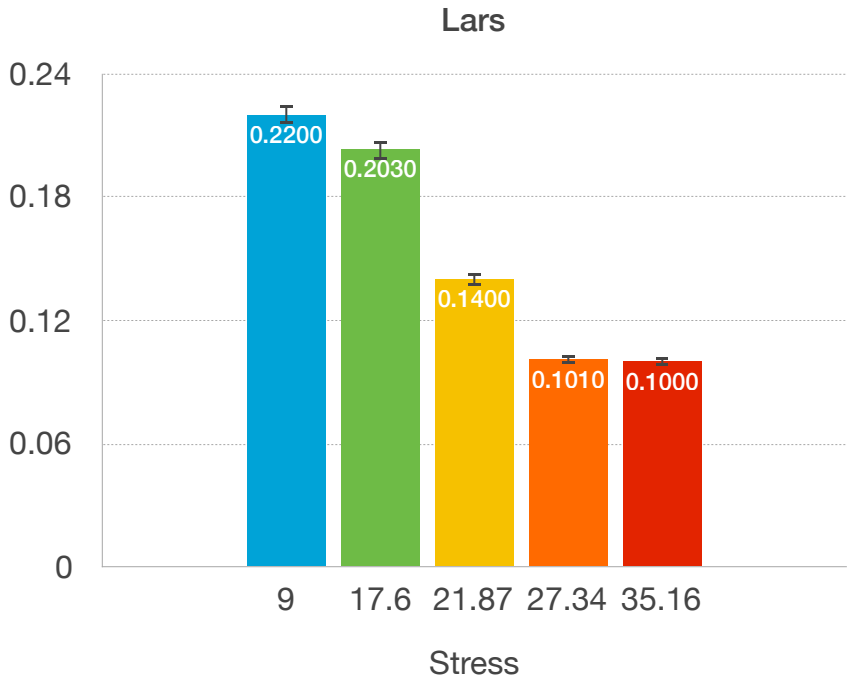

Figure 4.22: average β_c for Lars graft

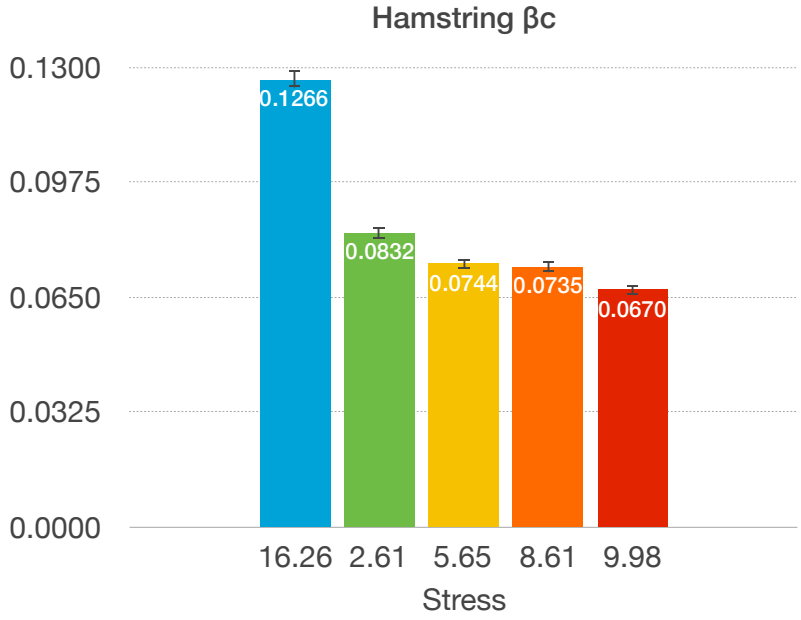

Figure 4.23: average β_c for Hamstring tissue

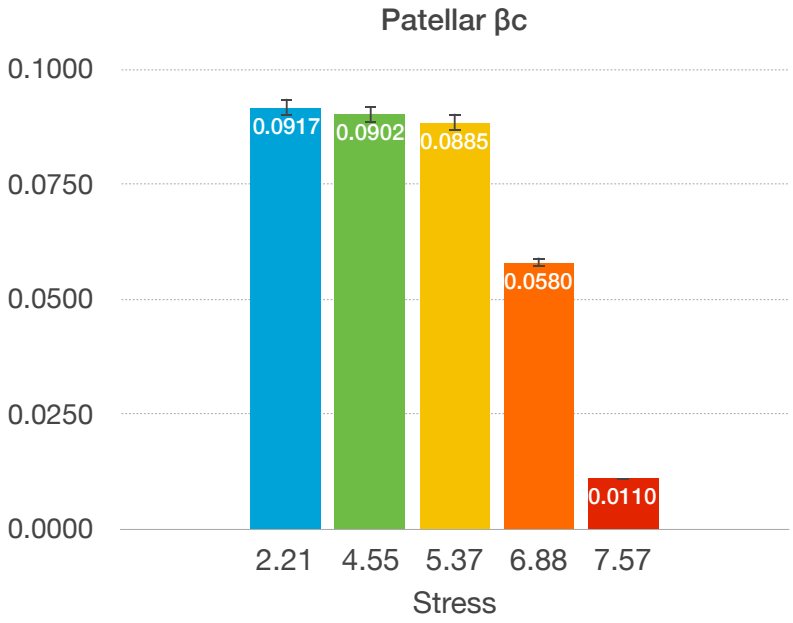

Figure 4.24: average β_c for Patellar tissue

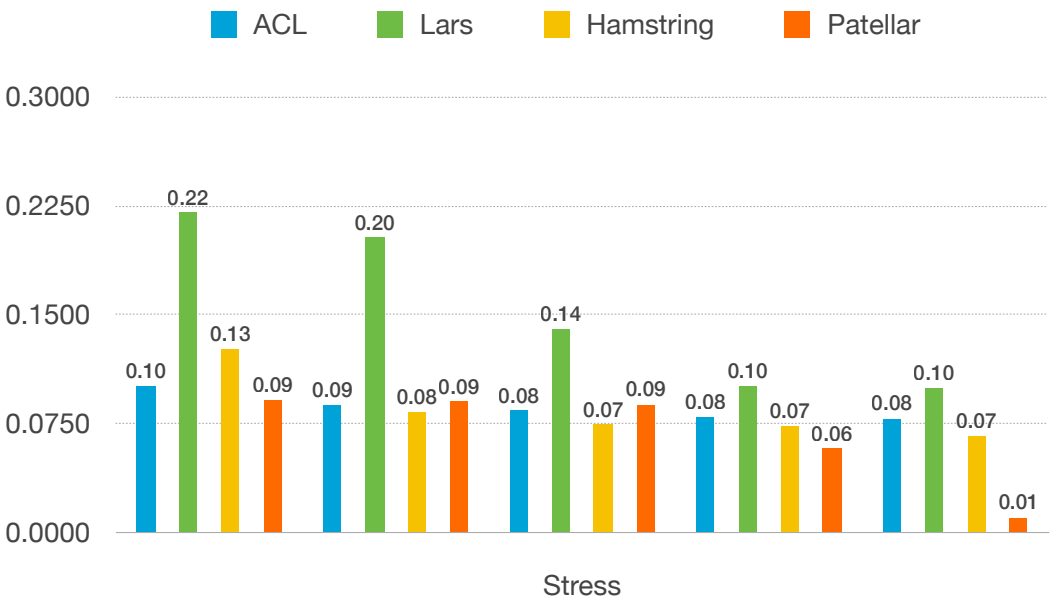

Figure 4.25: average β_c among all tissues

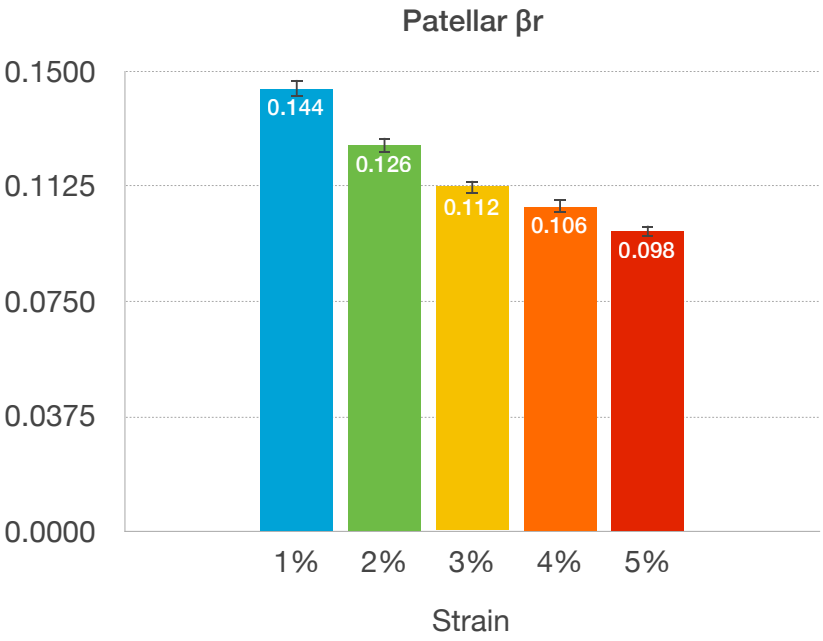

Figure 4.26: average β_r for Patellar tissue

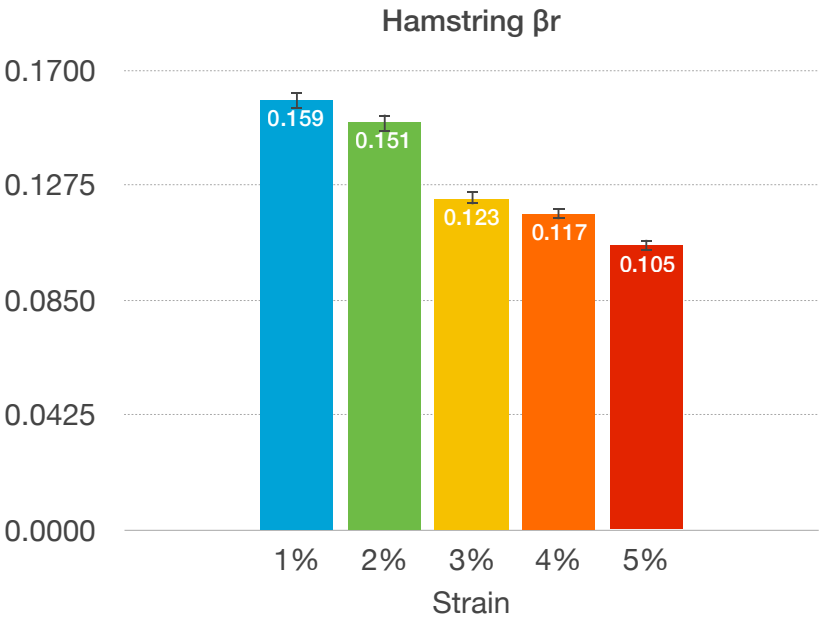

Figure 4.27: average β_r for Hamstring tissue

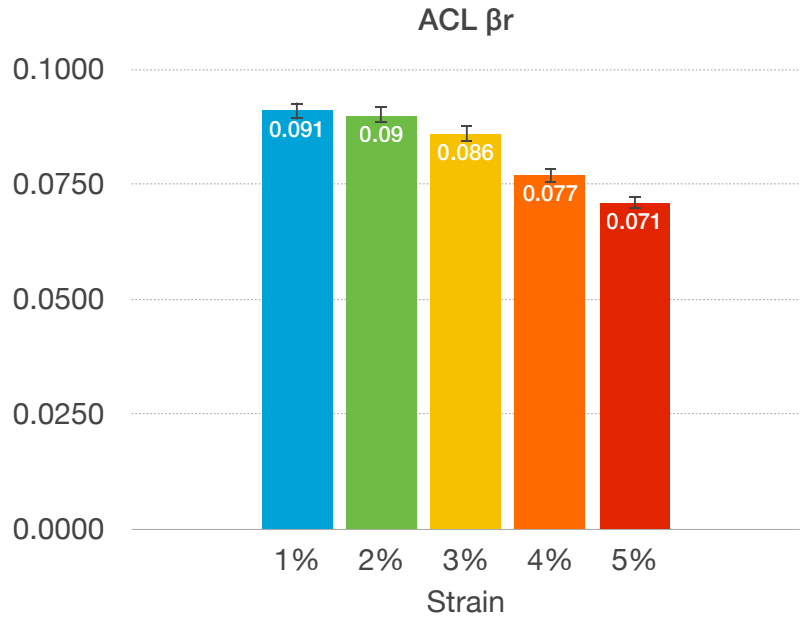

Figure 4.28: average β_r for ACL tissue

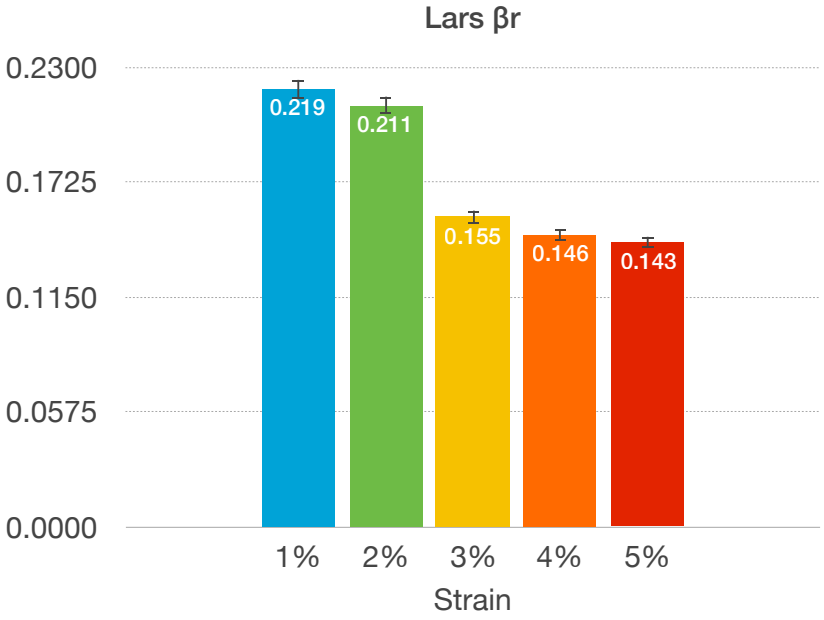

Figure 4.29: average β_c for Lars graft

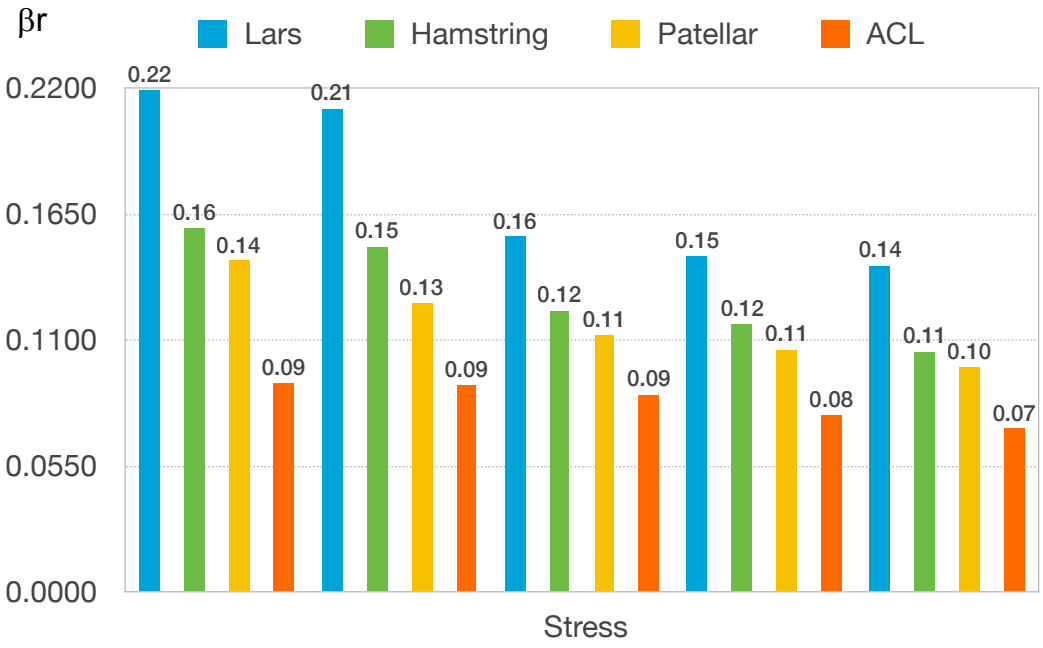

Figure 4.30: average β_r among all tissues

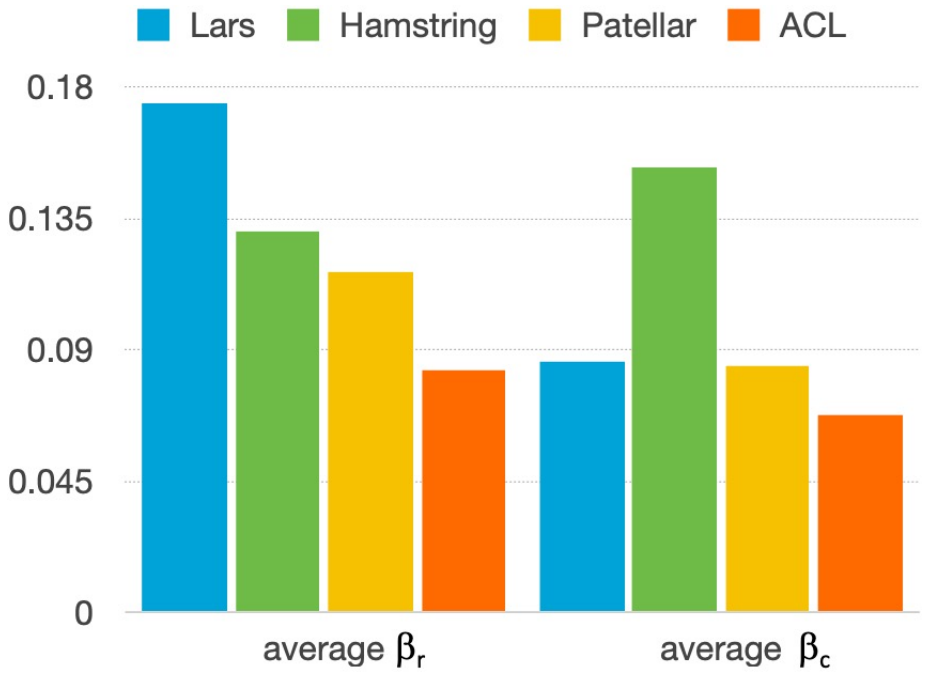

Figure 4.31: comparison between β_r and β_c

The histograms show:
i) thatβ_r is greater than β_c,
ii) β_c decreases with increasing stress level in each group
iii) β_r decreases with increasing strein level in each group
iv) histograms between tissue groups show that this trend is confirmed for both tendons and ligaments

4.2.3 Stochastic models of creep and relaxation material parameters

The analysis provided in previous approach showed the anomalous behavior of tendons and ligaments that, however, accounting for the variation of the order of the power-law careful requires the use of the single-integral approach. In this section we show that a microstructure approaching provide additional insights to the macroscopic mechanics of ligaments and tendons. In this section non-linear hereditariness of knee tendons and ligaments is framed in the context of stochastic mechanics. The proposed constitutive equations of fibrous tissues involves three material parameters for the creep tests and three material parameters for relaxation tests. One-to-one relations among material parameters estimated in creep and relaxations were established and reported in the paper. Data scattering, observed with a novel experimental protocol used to characterize the mechanics of the tissue, was modelled as the outcome of the random mechanical parameters. The numerical example proposed in this study shows that for an assigned probability density function of the material random parameters, the parameters of the probability density function (pdf) may be obtained by a statistical analysis of the experimental data.

Data analysis of the experimental campaign reported in previous section showed that constitutive equations for creep and relaxation involves three sets of parameters α, β, τ_c, and γ, δ, τ_r.

Results collected in experimental campaign showed that data scattering observed in experimental tests result in averaged expressions of the strain evolution $\mu_\varepsilon(t)$ and $\mu_{\bar{\sigma}}(t)$ as well as in standard deviation, namely $S_\varepsilon(t)$ and $S_{\bar{\sigma}}(t)$.

In this study we assumed that the source of data scattering is due to the outcomes of the characteristic times of the material, considered a random variables namely, $\tau_c \to T_c$ and $\tau_r \to T_r$ with prescribed probability density functions $p_{\tau_c}(\tau_c)$ and $p_{\tau_r}(\tau_r)$, respectively for the characteristic times in creep and relaxations.

Under these circumstances the random description of the stress/strain

evolution equations read, in creep and relaxation, respectively:

$$\mathrm{E}\,(t) = \left(\frac{1}{T_c}\right)^{\beta} \frac{\bar{\sigma}^{\alpha} t^{\beta}}{\Gamma\,(\beta+1)} \tag{4.8a}$$

$$\Sigma\,(t) = \left(\frac{1}{T_r}\right)^{-\delta} \frac{\varepsilon^{\gamma} t^{-\delta}}{\Gamma\,(\delta)} \tag{4.8b}$$

Eqs.(4.8a,4.8b)) allow for the evaluation of the averages of the stress and strain functions as:

$$\mu\,(t) =< \left(\frac{1}{T_c}\right)^{\beta} > \frac{\bar{\sigma}^{\alpha} t^{\beta}}{\Gamma\,(\beta+1)} \tag{4.9a}$$

$$\mu_{\bar{\sigma}}\,(t) =< \left(\frac{1}{T_r}\right)^{-\delta} > \frac{\varepsilon^{\gamma} t^{-\delta}}{\Gamma\,(\delta)} \tag{4.9b}$$

where $< \bullet >$ denotes the mathematical expectation operator that reads:

$$< \left(\frac{1}{T_c}\right)^{\beta} >= \int_{-\infty}^{\infty} \left(\frac{1}{\tau_c}\right)^{\beta} p_c\,(\tau_c)\,d\tau_c \tag{4.10a}$$

$$< \left(\frac{1}{T_r}\right)^{-\delta} >= \int_{-\infty}^{\infty} \left(\frac{1}{\tau_r}\right)^{\delta} p_r\,(\tau_r)\,d\tau_r \tag{4.10b}$$

Similar comments hold true also for the mean square error of the random functions $\mathrm{E}\,(\mathrm{t})$ and $\Sigma\,(t)$ resulting into:

$$S_{\varepsilon}\,(t) =< \left(\mathrm{E}\,(t) - \mu_{\varepsilon}\,(t)\right)^2 >=< \mathrm{E}(t)^2 > -\mu_{\varepsilon}(t)^2 \tag{4.11a}$$

$$S_{\bar{\sigma}}\,(t) =< \left(\Sigma\,(t) - \mu_{\bar{\sigma}}\,(t)\right)^2 >=< \Sigma(t)^2 > -\mu_{\bar{\sigma}}(t)^2 \tag{4.11b}$$

with second-order moments:

$$< \mathrm{E}(t)^2 >=< \left(\frac{1}{T_c}\right)^{2\beta} > \frac{\bar{\sigma}^{2\alpha} t^{2\beta}}{\Gamma(1+\beta)^2} \tag{4.12a}$$

$$< \Sigma(t)^2 >=< \left(\frac{1}{T_r}\right)^{-2\delta} > \frac{\varepsilon^{2\gamma} t^{-2\delta}}{\Gamma(\delta)^2} \tag{4.12b}$$

and the mathematical expectation reads:

$$< \left(\frac{1}{T_c}\right)^{2\beta} >= \int_{-\infty}^{\infty} \left(\frac{1}{\tau_c}\right)^{2\beta} p_c\left(\tau_c\right) d\tau_c \tag{4.13a}$$

$$< \left(\frac{1}{T_r}\right)^{2\delta} >= \int_{-\infty}^{\infty} \left(\frac{1}{\tau_r}\right)^{2\delta} p_r\left(\tau_r\right) d\tau_r \tag{4.13b}$$

In the following we assumed that the probability density functions $p_{\tau_c}\left(\tau_c\right)$ and $p_{\tau_r}\left(\tau_c\right)$ are described by uniform density in the interval $[\bar{\tau_c} - a_c; \bar{\tau_c} + a_C]$ and $[\bar{\tau_r} - a_r; \bar{\tau_r} + a_r]$ with $2a_r$ and $2a_c$ the amplitude of the interval representing the boundary of the characteristic times.

The results of the proposed model of random hereditariness was reported in figs.(4.32,4.33,4.34, 4.35) with solid lines for the averaged and the second-order statistics of the strain evolution and stress decay in conjunction with the amplitude of the interval of the pdf obtained by best fitting of the data to characterize the density function.

Observation of figs.(4.32,4.33,4.34,4.35) shows that the second-order moments of data scattering is well described by the proposed random model of the characteristic times reported in this section.

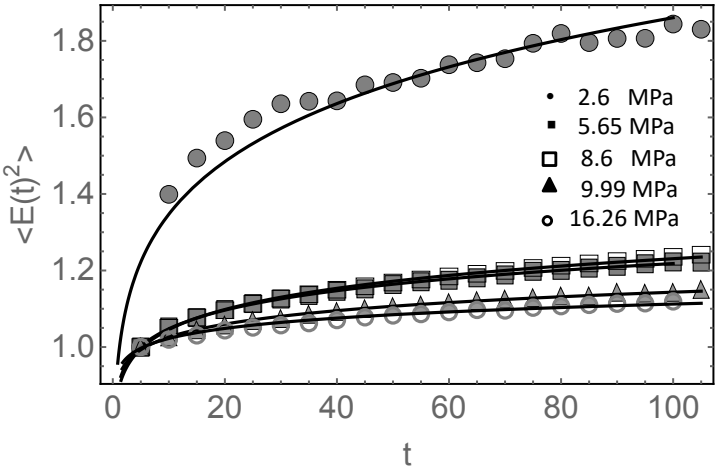

Figure 4.32: second-order moment creep hamstring ligaments

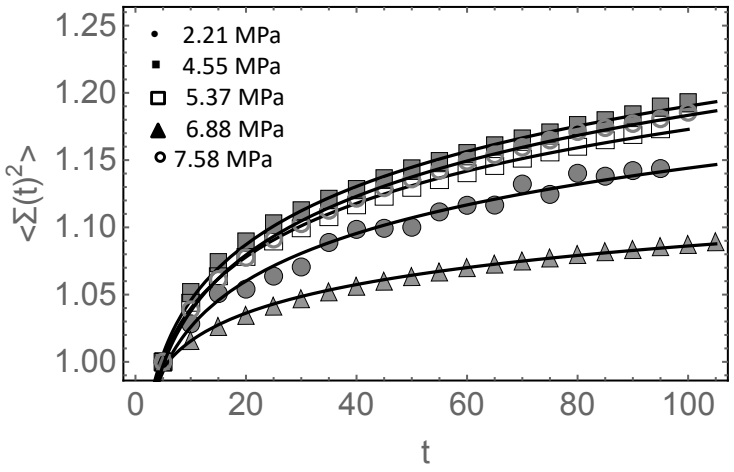

Figure 4.33: second-order moment creep Patellar tendons

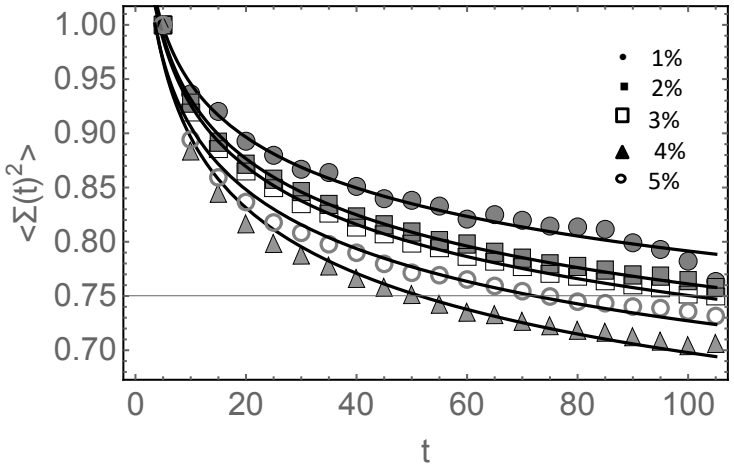

Figure 4.34: second-order moment relaxation hamstring ligaments

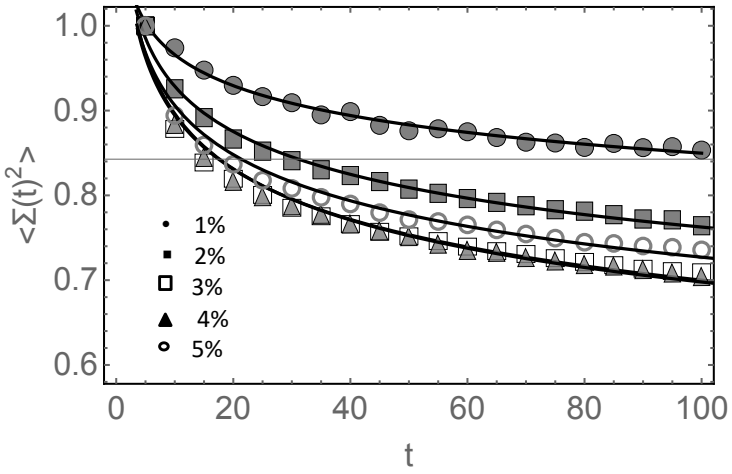

Figure 4.35: second-order moment relaxation Patellar tendons

In passing we observe also that the relation among the characteristic times τ_r and τ_c provided in sec.(3.2) holds true also with the random description of the characteristic times as:

$$< T_c >=< T_r > \Gamma(\beta+1)^{1/\alpha\delta}\Gamma(\delta)^{1/\delta} \tag{4.14a}$$

$$< {T_c}^2 >=< {T_r}^2 > \Gamma(\beta+1)^{2/\alpha\delta}\Gamma(\delta)^{2/\delta} \tag{4.14b}$$

allowing to define the statistics of the characteristic times with only the relaxation or the creep tests.

Data scattering involved in the experimental measures have been represented with a random model assuming that the characteristic times in creep and relaxation are modelled as random variables with prescribed probability density. The parameters of the density may be obtained by the measured first and second-order statistics of the creep and relaxation obtained from the experimental campaign.

A monte-carlo simulation conducted with the proposed random model shows that first-order statistics obtained with the proposed approach coalesces with the measured data allowing to use the random approach introduced for the prediction of the mechanical outcomes in terms of increments of the strain and the decaying of the stress in tendons and ligaments.

4.3 A microstructure approach to tendons non-linear hereditariness

The level of the fascicle including collagen fibers, membranes and interstitial fluid is quite representative of the structure of tendons. We presently investigate the effect of the rheology of the components of the tendon fascicles in a multiscale analysis starting from the level of individual collagenfibers organizedinto bundles, and then into fascicles at the next scale. A configuration of a collagen bundle is conceived in terms of a representative unit cell including a collagen fiber surrounded by a viscous membrane and aphysiological fluid. The mixing of solid and fluid components gives rise to an equivalent stress-strain response in tensor format highlighting a long term memory, in addition to instantaneous viscous effects. The kernel function of the hereditary response is determined thanks to the theory of homogenization, relying on the solution of the localization problem over the selected unit cell. Homogenization is the principal factor responsible for both the relaxation phenomena and the non-linearity due to recruitment of fibrils observed at the fascicle level, although none of the components present at the lower scales is endowed with these properties. The nature of the matrix surrounding the collagen fiber described as either viscous solid or a biological fluid - is shown to strongly influence the transverse response, but it has a weaker influence on the tensile response of fascicles. The initial waviness and progressive recruitment of the collagen fibers under the effect of the local strain has been integrated in the expression of the elastic and viscous stresses at the scale of the collagen fiber bundle, allowing simulating the nonlinear response of a fascicle.

Tendon exhibits a hierarchical structure with each level comprising the assembly of many finer structures at lower scales.The mechanical behavior at each level thus depends on the immediate lower level, but also on the nature of the assembly. This behavior can therefore vary from one level to the next one, and as a corollary, the whole set of responses of the inherent entities govern the tendon response itself. It is accordingly necessary to provide context for this work in relation to the structure and behavior often don at its different hierarchical levels.Tendons are natural fibrous composite materials; their complex structure has been widely described (e.g.Wang, 2006; Cowin,2000): it can be modeled as a composite tissue, with a complex. hierarchical arrangement going from collagen molecules (nano-scale) to fibrils (hundreds of nanometers),fibers (tens of micro-meters), and different levels of fascicles (hundreds of micrometers)up to the macro level of the tendon. At the different levels of this hierarchy, discontinuous aligned

structures are embedded in a hydrated matrix, and some levels (from subfascicles to the whole tendon) are surrounded by a thin membrane called the endotenon.Understanding the role and impact of the mechanics of the constituents at the separate scales on the behavior of the structure at the ultimate scale of the whole tendon is a very challenging problem, due to the combination of time-dependent (viscous) responses and geometrical as well as material nonlinear effects. Moreover, the proposition of accurate biomechanical constitutive theory ac-counting for the dynamic description of the tendinous micro-structure is crucial for the development of novel healing methods in tissue engineering (Lin et al., 2004), technical applications in biomedical and (further) improvements of surgical techniques in tissue repair (Matheson et al., 2005), or for the finite element modeling of joints within the human body.

From a physiological point of view, tendons are hierarchical structures consisting of the assembly of fibril seprincipally collagen, with a content higher than 95% -, physiological liquid and little elastin. The collagen portion is made up of 97e98% type I collagen, with small amounts of other types of collagen, including essentially hetero-typic collagens of type I, III, V, and a smaller fraction of collagens of type II, IX, XI and XII (Woo et al., 2006).This type of structure and behavior grossly appears at each level,without being the same from one scale to the next one, since a given scale level is not the mere copy of the immediately preceding one. At the fiber level, each fiber is made almost exclusively of fibrils of collagen I. Fibers are assembled to form fascicles maintained by a membrane called the endotenon, similar to a perforated net-like structure serving as an insertion site for the collagen fibers. Contrary to fibers and fascicles,fibrils are not enclosed by a membrane; they are moreover linked together only by a few proteoglycan bridges (Silver et al., 2003). It makes therefore sense to make the approximation that fibrils are nearly mutually free, also assuming they have the same geometry and mechanical properties;the mechanical behavior of fibers can then be assimilated to that of fibrils (Franchetti and col. 2002;Silver et al., 2003). Non-linear behavior of the tendons and ligaments has not been modeled through a structural scheme with a corresponding mathematical model that returns the experimental evidence on non-linearity either for elasticity and/or material hereditariness. In this study we propose a micromechanical fiber model to which to attribute the nonlinear behavior of these tissue. In particular, we want represent the phenomenon of the curling of the fibers as the main source of evidences of the deviation from the linearity of collagen fibrils bundles. The structural model of the collagen fibril is represented as lumped-mass truss with an assigned opening angle θ_0 that has a range of values reported in the literature, also a spring and a springpot are inserted. This micromechanical model with

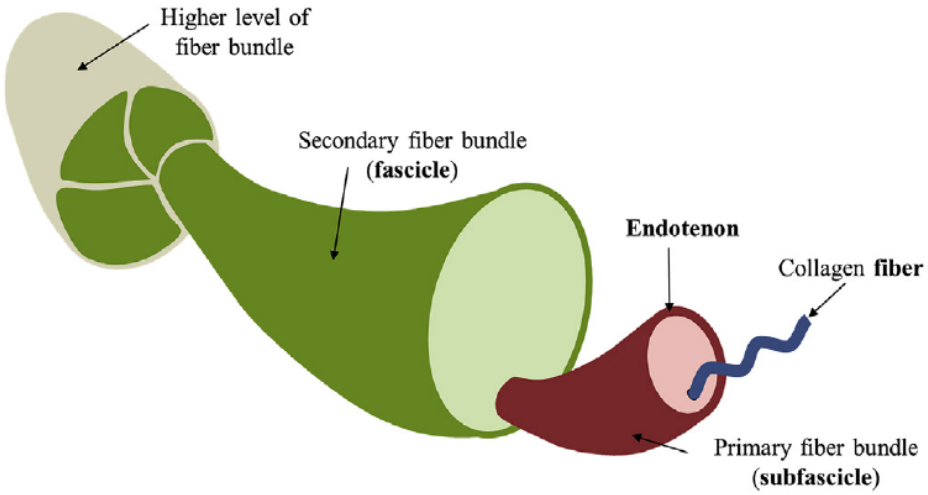

Figure 4.36: Simplified hierarchical structure of a tendon considered in the present study

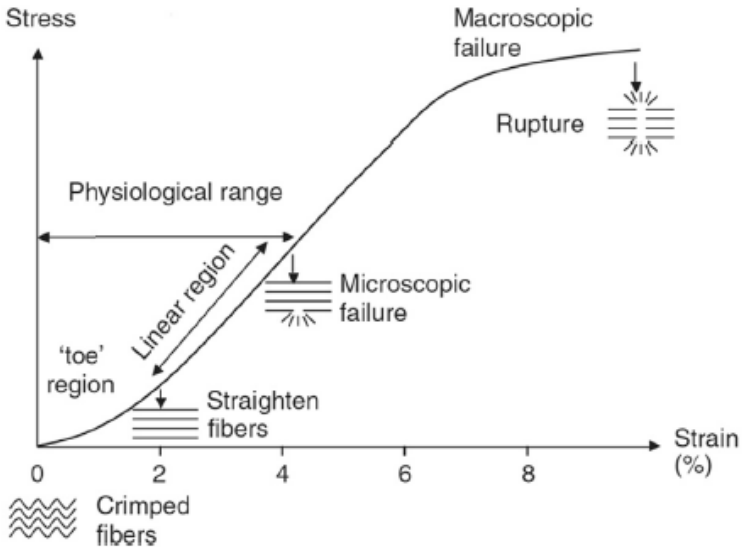

Figure 4.37: Simplified hierarchical structure of a tendon considered in the present study

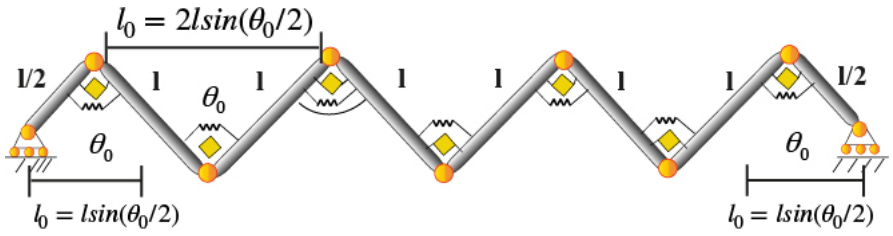

Figure 4.38: mechanical representation of tendon fiber

its governing equation captures the Q-FHM behavior introduced previously. Two different solution are observed for creep and relaxation involving the same differential equation. Let us consider the fiber in fig. 4.38 and let us isolate an element, fig. 4.39 of the truss for simplicity sake. The equilibrium equation is a non-linear fractional differential equation:

$$F(t) = \frac{1}{\tau_0 h(\theta)} \left(D^{\beta}_{0+}(\theta - \theta_0) \right)(t) + \frac{K}{h(\theta)}(\theta - \theta_0) \tag{4.15}$$

where

$$h(\theta) = l_a cotg(\theta) \quad \text{and} \quad \lambda = \frac{l_a}{l_0} = \frac{sin(\theta/2}{sin(\theta_0/2)} \tag{4.16}$$

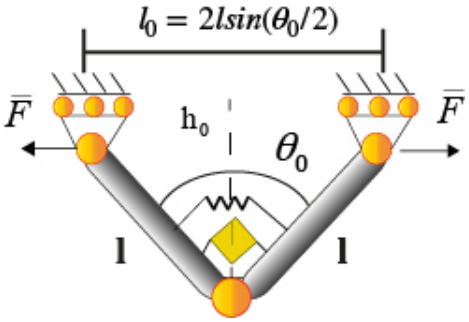

Figure 4.39: micromechanical model of fiber

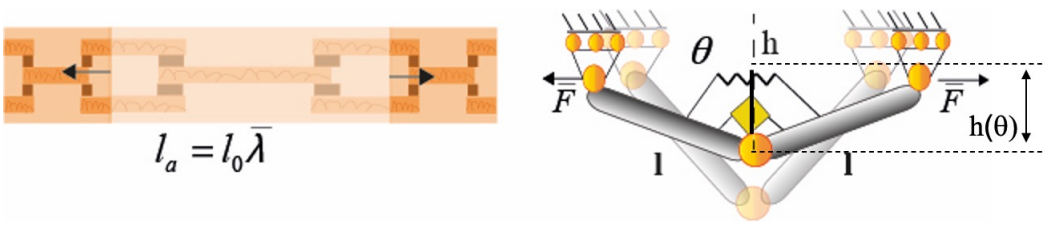

Figure 4.40: micromechanical model change configuration

with λ stretch of the fiber, θ_0 it is the angle indicating the initial opening of the fiber, K represents the bending stiffness of the collagen fiber, $h_0 = h(\theta_0)$ and β represents the order of stress decay in the collagen fiber.

Relaxation test

The numerical application on this model is carried out starting from relaxation and fixing three values of $\beta_r = 0.095, \beta_r = 0.09, \beta_r = 0.14$ and $\tau_0 = 10$ We have fixed a value of $\theta_0 = 13°$ and the value of $\lambda = 0.03$ These choices allow us to say that we are analyzing physiological conditions for these tissues. Assuming these parameters, the equation obtained is

$$F = \frac{\tau_0}{h(\bar{\theta})} \left(D_{0^+}^{\beta_r} (\bar{\theta} - \theta_0) \right) (t) + \frac{K}{h(\bar{\theta})} (\bar{\theta} - \theta_0) \tag{4.17}$$

whose solution in presents of constant $\bar{\theta} - \theta_0)$

$$F = \frac{\tau_0}{h(\bar{\theta})} \frac{(\bar{\theta} - \theta_0) U(t) t^{-\beta_r}}{\beta \Gamma(\beta + 1)} \tag{4.18}$$

where $U(t)$ is the Unit step function. By solving the equation for the relaxation, we obtained the curves represented by points are shown in fig.4.41. Subsequently a fitting of these numerical values was made using a power-law, we can see in the figure 4.41 how the points of the numerical test are perfectly superimposed on the fitting curve with the solid line.

Creep test

To simulate the creep test, the previous fixed values of β and θ_0 were inserted in the model and $F = 25N$ was imposed. Assuming these parameters, the equation obtained is

$$\bar{F} = \frac{1}{\tau_0 h(\theta)} \left(D_{0^+}^{\beta_r} (\theta - \theta_0) \right) (t) + \frac{K}{h(\theta)} (\theta - \theta_0) \tag{4.19}$$

the equation to be solved is a non-linear fractional differential equation.

Numerical solution of the non-linear differential equation, has been obtained by means of Adams algorithm that was developed and modified to solve the non-linear differential equations. In more detail the integration method uses variable step-size coefficients. Given a sequence of step sizes $h_{n-k+1}, h_{n-k+2}, ..., h_n$, where h_n is the current step to take, the coefficients

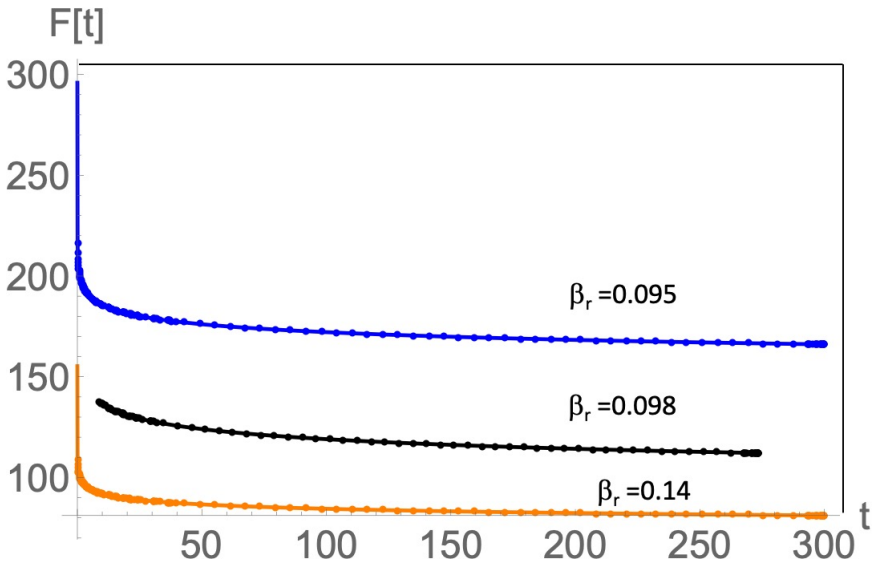

Figure 4.41: relaxation function obtained from micromechanical model

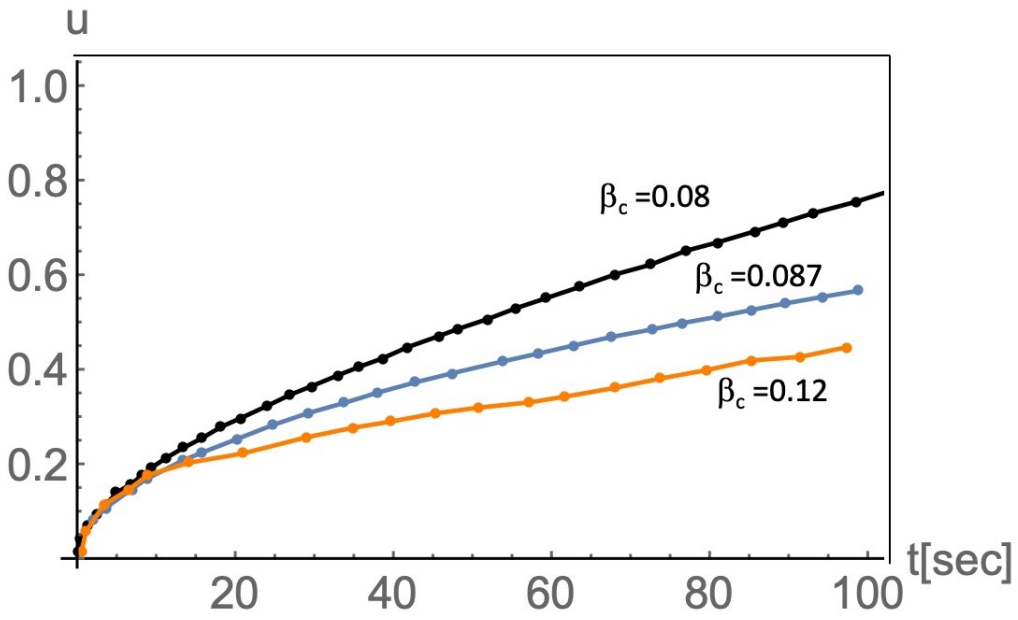

Figure 4.42: creep function obtained from micromechanical model

for the method with AdamsBashforth predictor of order k and AdamsMoulton corrector of order $k+1$, $g_j(n)$ such that

$$y_{n+1} = h_n g_k(n) \Phi_k(n+1) + p_{n+1} \tag{4.20}$$

$$p_{n+1} = y_n + h_n \sum_{j=0}^{k-1} g_j(n) \Phi_k^*(n) \tag{4.21}$$

where the $\Phi_j(n)$ are the divided differences. This defines a function that computes the coefficients that are used in error estimation. Figure4.42 shows the numerical values and the fitting curves superimposed with the solid line. The β_c values obtained with the fitting of numerical data are lower than the β_r values, as obtained from the experimental data.

Conclusions

In this thesis we provide a biomechanical analysis of ligaments and tendons of the human knee with respect to the time dependent behavior.

In more details the study involved four kind of fibrous tissues of the human knee namely Anterior Cruciate Ligaments, Patellar, Hamstring and synthetic graft named Lars (Ligament Augmentation and Reconstruction System) .

It is known that under long-standing loads the collagen structure and the ground substance composing the tissue undergoes a time-dependent behavior that deviate from elastic.

Some previous study have shown the mechanics of the time dependence for rat, rabbit ligaments but now of then focus on human fibrous tissues.

The mathematical model proposed in the thesis extend the well-know quasi-linear viscoelastic model often and used in biomechanics in the field of fractional-order calculus it has been shown that, as long as fractional order calculus is used then some specific relations among creep and relaxation parameters may be obtained.

This led to conclude that a three parameters model may capture some non-linear behavior of material obtained generalization of the springpot that is a two parameters material model. The proposed approach has been assumed by an extensive experimental campaign of fibrous tissues of the human knee with a specific testing protocol showing maximum deviate of 6% among measured and estimated parameters.

The micromechanics beyond the observed non-linearity from creep and relaxation tests have been introduced by means of the structural model the tissue at fiber level that involves bundles of waves of collagen fibrils. The geometric non-linearity of the fiber is analyzed and its mechanical behavior is good agreement with observed experimental data.

The proposed approach shows, however, some limitations related to the single-integral model used to describe the stress/strain constitutive equation that has been observed in further creep test with two step load.

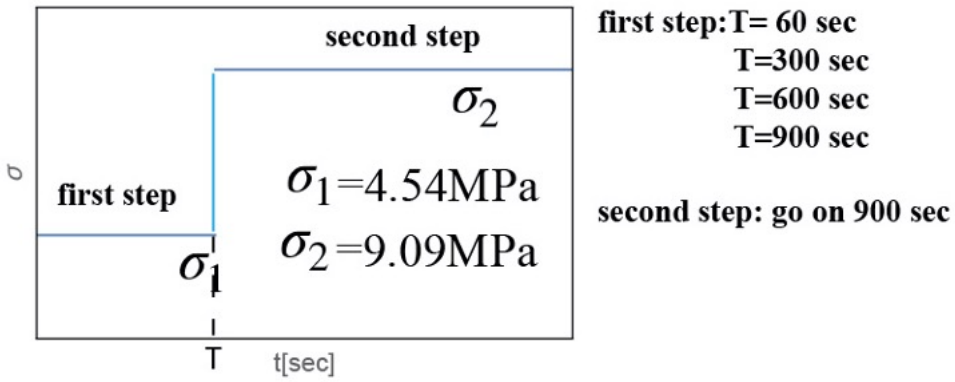

Figure 4.43: Two-step creep test protocol

Indeed we begun a new test protocol on patellar and hamstring tendons and we observed a non-linear dependence of the order of power-law $\beta_c = \beta_c(\sigma, T)$. The testing protocol has involved regularization of the samples in the dimensions of width and length. After that they have been cut by a band saw after previously placing in liquid nitrogen to induce the brittle fracture during cut.

The machine protocol involves two creep tests in succession on the same sample. Two different levels of force are applied, corresponding to two increasing tensions. After being clamped between two knurled pliers, the sample is subjected to a loading program which includes:

i) test in load control constant force through a ramp 315 N/s. The load is kept constant for 60sec for the first test, on the second sample for 300 sec, on the third sample for 600sec and on the last sample for 900sec.

ii) the test continues to be conducted in load control, with a constant force increased compared to the first, always with a ramp at 315 N/s, for 900 seconds. the figure 4.45 shows a creep test conducted with this protocol.

Data processing of the experimental findings showed that the values of β_c of the first and second steps are different. Furthermore, data showed that the second value of β_c varies according to the duration of the first phase. This result is shown in fig. 4.45 that highlights a non-linear dependence of β_c on time as well as on the stress level, which up to now was the only form of non-linearity assumed also in the current thesis.

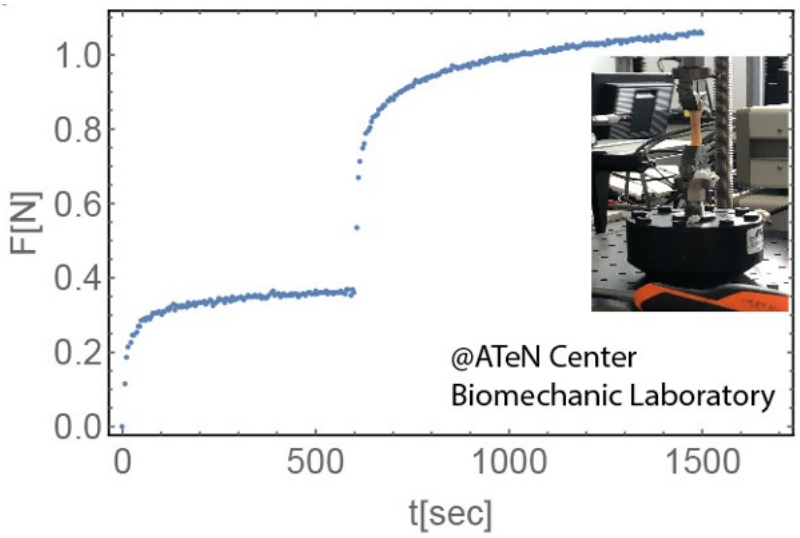

Figure 4.44: Patellar Test results

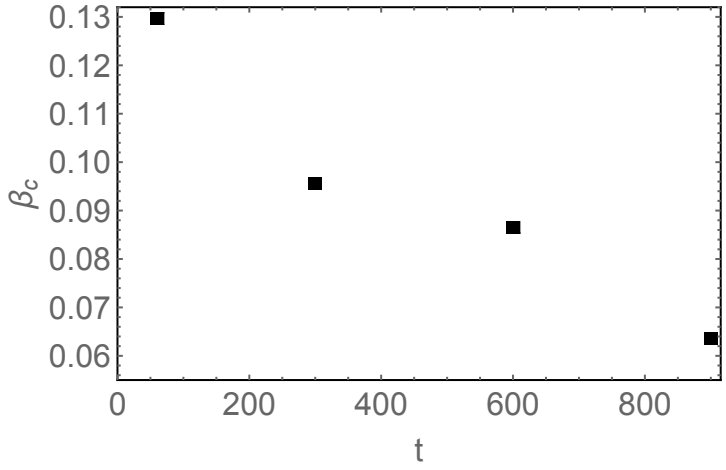

Figure 4.45: β_c trend as the duration of time t of the first step of the test protocol changes

Previous considerations lead to argue that a complete phenomenological constitutive equations describing hereditariness of ligaments and tendons requires additional terms with respect to the proposed Q-FHM. This research is underway and it will be presented elsewhere.

Appendix A

Fractional Calculus

A.1 Riemann-Liouville Fractional Integrals and Fractional Derivatives

We give the definitions of the Riemann-Liouville fractional integrals and fractional derivatives on a finite interval of the real line and present some of their properties in spaces of summable and continuous functions. More detailed information may be found in the book by Samko et al.

Let $\Omega = [a, b](-\infty < a < \infty)$ be a finite interval on the real axis $\mathbb{R}$. The Riemann-Liouville fractional integral $I^{\alpha}_{a+}f$ and $I^{\alpha}_{b-}f$ of order $\alpha \in \mathbb{C}$ $\mathcal{R}(\alpha) > 0)$ are defined by

$$\left(I^{\alpha}_{a+}f\right)(x) = \frac{1}{\Gamma(\alpha)}\int_a^x \frac{f(t)dt}{(x-t)^{1-\alpha}} \quad (x > a;\, \mathcal{R}(\alpha) > 0) \tag{A.1}$$

and

$$\left(I^{\alpha}_{b-}f\right)(x) = \frac{1}{\Gamma(\alpha)}\int_b^x \frac{f(t)dt}{(t-x)^{1-\alpha}} \quad (x > b;\, \mathcal{R}(\alpha) > 0) \tag{A.2}$$

respectively. Here $\Gamma(\alpha)$ is the Gamma function. These integrals are called the left-sided and the right-sided fractional integrals. When $\alpha = n \in \mathbb{N}$, the definitions (A.5) and (A.2) coincide with the nth integrals of the form

$$\left(I^{n}_{a+}f\right)(x) = \int_a^x dt_1 \int_a^{t_1} dt_2 ... \int_a^{t_{n-1}} f(t_n)dt_n = \tag{A.3}$$

$$= \frac{1}{(n-1)!}\int_a^x (x-t)^{n-1} f(t)dt \quad (n \in \mathbb{N}) \tag{A.4}$$

and

$$\left(I_{b-}^{n} f\right)(x) = \int_{b}^{x} dt_1 \int_{b}^{t_1} dt_2 ... \int_{b}^{t_{n-1}} f(t_n) dt_n =$$

$$= \frac{1}{(n-1)!} \int_{b}^{x} (x-t)^{n-1} f(t) dt \quad (n \in \mathbb{N}) \tag{A.5}$$

The Riemann-Liouville fractional derivatives $D_{a+}^{\alpha} y$ and $D_{b-}^{\alpha} y$ of order $\alpha \in \mathbb{C}$ $(\mathcal{R}(\alpha) \geq 0)$ are defined by

$$(D_{a+}^{\alpha} y)(x) = \left(\frac{d}{dx}\right)^{n} \left(I_{a+}^{n-\alpha} y\right)(x) =$$

$$= \frac{1}{\Gamma(n-\alpha)} \left(\frac{d}{dx}\right)^{n} \int_{a}^{x} \frac{y(t) dt}{(x-t)^{\alpha-n+1}} \quad (n = [R(\alpha)] + 1; x > a) \tag{A.6}$$

and

$$(D_{b-}^{\alpha} y)(x) = \left(-\frac{d}{dx}\right)^{n} \left(I_{b-}^{n-\alpha} y\right)(x) =$$

$$= \frac{1}{\Gamma(n-\alpha)} \left(-\frac{d}{dx}\right)^{n} \int_{x}^{b} \frac{y(t) dt}{(x-t)^{\alpha-n+1}} \quad (n = [\mathcal{R}(\alpha)] + 1; x < b) \tag{A.7}$$

respectively, where $[\mathcal{R}(\alpha)]$ means the integral part of $\mathcal{R}(\alpha)$. In particular, when $\alpha = n \in \mathbb{N}_o$, then

$$(D_{a+}^{0} y)(x) = (D_{b-}^{0} y)(x) = y(x); (D_{a+}^{n} y)(x) = y^{(n)}(x), \tag{A.8a}$$

$$(D_{b-}^{n} y)(x) = (-1)^n y^{(n)}(x) \quad (n \in \mathbb{N}) \tag{A.8b}$$

where $y^{(n)}$ is the usual derivative of$y(x)$ of order n. If $0 < \mathcal{R}(\alpha) < 1$, then

$$(D_{a+}^{\alpha} y)(x) = \frac{1}{\Gamma(1-\alpha)} \frac{d}{dx} \int_{a}^{x} \frac{y(t) dt}{(x-t)^{\alpha-[\mathcal{R}(\alpha)]}} (0 < \mathcal{R}(\alpha) < 1; x > a) \tag{A.9}$$

$$(D_{b-}^{\alpha} y)(x) = -\frac{1}{\Gamma(1-\alpha)} \frac{d}{dx} \int_{x}^{b} \frac{y(t) dt}{(t-x)^{\alpha-[\mathcal{R}(\alpha)]}} (0 < \mathcal{R}(\alpha) < 1; x < b) \tag{A.10}$$

When $\alpha \in \mathbb{R}^+$, then (A.6) and (A.7) take the following form:

$$(D^{\alpha}_{a+}y)(x) = \frac{1}{\Gamma(n-\alpha)}\left(\frac{d}{dx}\right)^n \int_a^x \frac{y(t)dt}{(x-t)^{\alpha-n+1}} (n = [\alpha]+1; x > a) \quad \text{(A.11)}$$

$$(D^{\alpha}_{b-}y)(x) = \frac{1}{\Gamma(n-\alpha)}\left(-\frac{d}{dx}\right)^n \int_a^x \frac{y(t)dt}{(t-x)^{\alpha-n+1}} (n = [\alpha]+1; x < b) \quad \text{(A.12)}$$

while (A.9) and (A.10) are given by

$$(D^{\alpha}_{a+}y)(x) = \frac{1}{\Gamma(1-\alpha)}\frac{d}{dx}\int_a^x \frac{y(t)dt}{(x-t)^{\alpha}} (0 < \alpha < 1; x > a) \quad \text{(A.13)}$$

and

$$(D^{\alpha}_{b-}y)(x) = -\frac{1}{\Gamma(1-\alpha)}\frac{d}{dx}\int_x^b \frac{y(t)dt}{(t-x)^{\alpha}} (0 < \alpha < 1; x < b) \quad \text{(A.14)}$$

respectively.

A.2 Caputo Fractional Derivatives

We introduce the definition of the Caputo fractional derivatives. Let $[a, b]$ be a finite interval of the real line $\mathbb{R}$ and let $D^{\alpha}_{a+}[y(t)](x) \equiv (D^{\alpha}_{a+}y)(x)$ and $D^{\alpha}_{b-}[y(t)](x) \equiv (D^{\alpha}_{b-}y)(x)$ be the Riemann-Liouville fractional derivatives of order $\alpha \in \mathbb{C}$ $\mathcal{R}(\alpha) \geq 0)$ defined by (A.6) and (A.7) respectively. The fractional derivatives $({}_CD^{\alpha}_{a+}y)(x)$ and $({}_CD^{\alpha}_{b-}y)(x)$ of order $\alpha \in \mathbb{C}$ $(\mathcal{R}(\alpha) \geq 0)$ on $[a, b]$ are defined via the above Riemann-Liouville fractional derivatives by

$$({}_CD^{\alpha}_{a+}y)(x) = \left(D^{\alpha}_{a+}\left[y(t) - {}^{n-1}_{k=0}\frac{y^{(k)}(a)}{k!}(t-a)^k\right]\right)(x) \quad \text{(A.15)}$$

and

$$({}_CD^{\alpha}_{b-}y)(x) = \left(D^{\alpha}_{b-}\left[y(t) - {}^{n-1}_{k=0}\frac{y^{(k)}(b)}{k!}(b-t)^k\right]\right)(x) \quad \text{(A.16)}$$

respectively, where

$$n = [\mathcal{R}(\alpha)] + 1 \quad for \quad \alpha \notin \mathbb{N}_0 \quad \text{(A.17)}$$

These derivatives are called left-sided and right-sided Caputo fractional derivatives of order α.

In particular, when $0 < \mathcal{R}(\alpha) < 1$, the relations (A.15) and (A.16) take the following forms:

$$({}_CD^{\alpha}_{a+}y)(x) = (D^{\alpha}_{a+}[y(t) - y(a)])(x) \quad \text{(A.18)}$$

$$({}_C D^{\alpha}_{b-} y)(x) = (D^{\alpha}_{b-}[y(t) - y(b)])(x) \tag{A.19}$$

If $\alpha \notin \mathbb{N}_0$ and $y(x)$ is a function for which the Caputo fractional derivatives $({}_C D^{\alpha}_{a+} y)(x)$ and $({}_C D^{\alpha}_{b-} y)(x)$ of order $\alpha \in \mathbb{C}$ $(\Re(\alpha) \geq 0)$ exist together with the Riemann-Liouville fractional derivatives $(D^{\alpha}_{a+} y)(x)$ and $(D^{\alpha}_{b-} y)(x)$, then, in accordance with (A.8a) and (A.9) they are connected with each other by the following relations:

$$({}_C D^{\alpha}_{a+} y)(x) = \left(D^{\alpha}_{a+} \left[y(t) - \sum_{k=0}^{n-1} \frac{y^{(k)}(a)}{\Gamma(k-\alpha+1)} (x-a)^k \right] \right) (x-a)^{k-a}$$
$$(n = [\Re(\alpha)] + 1) \tag{A.20}$$

and

$$({}_C D^{\alpha}_{b-} y)(x) = \left(D^{\alpha}_{b-} \left[y(t) - \sum_{k=0}^{n-1} \frac{y^{(k)}(b)}{\Gamma(k-\alpha+1)} (b-x)^k \right] \right) (x-a)^{k-a}$$

$$(n = [\Re(\alpha)] + 1) \tag{A.21}$$

In particular, when $0 < \Re < 1$, we have

$$({}_C D^{\alpha}_{a+} y)(x) = (D^{\alpha}_{a+} y)(x) - \frac{y(a)}{\Gamma(1-\alpha)} (x-a)^{-\alpha} \tag{A.22}$$

$$({}_C D^{\alpha}_{b-} y)(x) = (D^{\alpha}_{b-} y)(x) - \frac{y(b)}{\Gamma(1-\alpha)} (b-x)^{-\alpha} \tag{A.23}$$

A.3 Grünwald-Letnikov Fractional Derivatives

We give the definition of the Grünwald-Letnikov fractional derivatives. The above operation of fractional differentiation is based on a generalization of the usual differentiation of a function $y(x)$ of order $n \in \mathbb{N}$ of the form

$$y(x)^{(n)}(x) = \lim_{h \to 0} \frac{(\Delta^n_h y)(x)}{h^n} \tag{A.24}$$

Here $(\Delta^n_h y)(x)$ is a finite difference of order $n \in \mathbb{N}_0$ of a function $y(x)$ with a step $h \in \mathbb{R}$. Property (A.24) is used to define a fractional derivative by directly replacing $n \in \mathbb{N}$ in (A.24) by $\alpha > 0$. For this, h^n is replaced by h^{α}, while the finite difference while the finite difference $(\Delta^n_h y)(x)$ is replaced by the difference $(\Delta^{\alpha}_h y)(x)$ of a fractional order $\alpha \in \mathbb{R}$ defined by the following infinite series:

$$(\Delta^{\alpha}_h y)(x) = \sum_{k=0}^{\infty} (-1)^k \binom{\alpha}{k} y(x - kh) \quad (x, h \in \mathbb{R}; \quad \alpha > 0) \tag{A.25}$$

where $\begin{pmatrix} \alpha \\ k \end{pmatrix}$ are the binomial coefficients. When $h > 0$, the difference is called left-sided difference, while for for $h < 0$ it is called a right-sided difference. The series in (A.25) converges absolutely and uniformly for each $\alpha > 0$ and for every bounded function $y(x)$.

Following (A.24), the left- and right-sided Grünwald-Letnikov derivatives $y_+^\alpha(x)$ and $y_-^\alpha(x)$ are defined by

$$y_+^\alpha(x) = \lim_{h\to 0} \frac{(\Delta_h^\alpha y)(x)}{h^\alpha} \quad (\alpha > 0) \tag{A.26}$$

and

$$y_-^\alpha(x) = \lim_{h\to 0} \frac{(\Delta_{-h}^\alpha y)(x)}{h^\alpha} \quad (\alpha > 0) \tag{A.27}$$

respectively.

The definition (A.25) of the fractional difference $(\Delta_h^\alpha y)(x)$ assumes that the function $y(x)$ is given at least on the half-axis. For the function $y(x)$ given on a finite interval $[a, b]$, such a difference can be defined as follows by a continuation of $y(x)$ as a vanishing function beyond $[a, b]$:

$$(\Delta_h^\alpha y)(x) = (\Delta_h^\alpha y^*)(x) = \sum_{k=0}^{\infty} (-1)^k \begin{pmatrix} \alpha \\ k \end{pmatrix} y^*(x - kh) \quad (x, h \in \mathbb{R}; \quad \alpha > 0) \tag{A.28}$$

where

$$y^*(x) = \begin{cases} y(x), & x \in [a, b] \\ 0; & x \notin [a, b] \end{cases} \tag{A.29}$$

It is acceptable to rewrite the fractional difference (A.28) in terms of the function $y(x)$ itself, avoiding its continuation as a vanishing function, in the forms

$$(\Delta_{h,a+}^\alpha y)(x) = \sum_{k=0}^{\frac{x-a}{h}} (-1)^k \begin{pmatrix} \alpha \\ k \end{pmatrix} y^*(x - kh) \quad (x, h \in \mathbb{R}; \quad \alpha > 0) \tag{A.30}$$

and

$$(\Delta_{h,b-}^\alpha y)(x) = \sum_{k=0}^{\frac{b-x}{h}} (-1)^k \begin{pmatrix} \alpha \\ k \end{pmatrix} y^*(x + kh) \quad (x, h \in \mathbb{R}; \quad \alpha > 0) \tag{A.31}$$

Bibliography

[1] Abramowitch, Steven D.; Woo, Savio L.-Y. An improved method to analyze the stress relaxation of ligaments following a finite ramp time based on the quasi-linear viscoelastic theory. Journal of biomechanical engineering, 2004, 126.1: 92-97.

[2] Abramowitch SD, Zhang X, Curran M, Kilger R. A Comparison of the Quasi-static Mechanical and Nonlinear Viscoelastic Properties of the Human Semitendinosus and Gracilis Tendons. Clinical biomechanics, 2010, 25(4), 325-331.

[3] Alaimo, G., Zingales, M. Laminar flow through fractal porous materials: the fractional-order transport equation. Communications in Nonlinear Science and Numerical Simulation, 2015, 22(1-3), 889-902.

[4] Amabili, M., Balasubramanian, P., & Breslavsky, I. Anisotropic fractional viscoelastic constitutive models for human descending thoracic aortas. Journal of the mechanical behavior of biomedical materials, 2019, 99, 186-197.

[5] Amabili, M., Balasubramanian, P., Bozzo, I., Breslavsky, I. D., & Ferrari, G. Layer-specific hyperelastic and viscoelastic characterization of human descending thoracic aortas. Journal of the mechanical behavior of biomedical materials, 2019, 99, 27-46.

[6] Amabili, M., Balasubramanian, P., Breslavsky, I., Ferrari, G., & Tubaldi, E. Viscoelastic characterization of woven Dacron for aortic grafts by using direction-dependent quasi-linear viscoelasticity. Journal of the mechanical behavior of biomedical materials, 2018, 82, 282-290.

[7] Amabili, M. Nonlinear mechanics of shells and plates in composite, soft and biological materials. Cambridge University Press, 2018.

[8] Atanackovic, M.T., Janev, M., Konjik, S., Pilipovic S, and Zorica, D. Vibrations of an elastic rod on a viscoelastic foundation of complex fractional Kelvin-Voigt type. Meccanica, 2015, 1679-169.

[9] Atanackovic, T. M., Stankovic, B. Generalized wave equation in nonlocal elasticity. Acta Mechanica, 2009, 208(1-2), 1-10.

[10] Atanackovic, M.T, Stankovi, B. On a system of differential equations with fractional derivatives arising in rod theory. Journal of Physics A: Mathematical and General:, 2004, 1241.

[11] Bagley, Ronald L.; Torvik, P. J. A theoretical basis for the application of fractional calculus to viscoelasticity. Journal of Rheology, 1983, 27.3: 201-210.

[12] Bagley, R. L., Torvik, J. Fractional calculus-a different approach to the analysis of viscoelastically damped structures. AIAA journal, 1983, 21(5), 741-748.

[13] Behnke, Ronny, Hüsnü Dal, and Michael Kaliske. An extended tube model for thermo-viscoelasticity of rubberlike materials: Parameter identification and examples. PAMM 11.1 2011, 353-354.

[14] Bernard, M., Yoshioka, H., Rodriguez, E., Van der Rest, M., Kimura, T., Ninomiya, Y., Ramirez, F. Cloning and sequencing of pro-alpha 1 (XI) collagen cDNA demonstrates that type XI belongs to the fibrillar class of collagens and reveals that the expression of the gene is not restricted to cartilagenous tissue. Journal of Biological Chemistry, 1984, 263(32), 17159-17166.

[15] Bernstein, B., Kearsley, E. A., Zapas, L. J. A study of stress relaxation with finite strain. Transactions of the Society of Rheology, 1963, 7(1), 391-410.

[16] Blair, GW Scott; Caffyn, J. E. VI. An application of the theory of quasi-properties to the treatment of anomalous strain-stress relations. The London, Edinburgh, and Dublin Philosophical Magazine and Journal of Science, 1949, 40.300: 80-94.

[17] Bologna E., Graziano F., L. Deseri, Zingales M., Power-Laws hereditariness of biomimetic ceramics for cranioplasty neurosurgery. International Journal of Non-linear Mechanics, 115, 61–67, 2019.

[18] Bologna, E., Lopomo, N., Marchiori, G., Zingales, M. A non-linear stochastic approach of ligaments and tendons fractional-order hereditariness. Probabilistic Engineering Mechanics, 103034, 2020.

[19] Bologna E., Di Paola M., Zingales M. Routh-Hurwitz meth od for the analysis of Beck's Column over fractional-order foundations. In Aimeta 2019.

[20] Bologna, E. Di Paola, M., Dayal K., Deseri L., Zingales M. Fractional Order Non-Linear Hereditariness of Tendons and Ligaments of the Human Knee. peer review Philosophical Transaction:A, 2020.

[21] Bologna, E., Zingales, M. Stability analysis of Beck's column over a fractional-order hereditary foundation. Proceedings of the Royal Society A: Mathematical, Physical and Engineering Sciences, 2018, 474(2218), 20180315.

[22] Castile RM., Skelley NW., Babaei B., Brophy RH., Lake SP. Microstructural properties and mechanics vary between bundles of the human anterior cruciate ligament during stress-relaxation. Journal of biomechanics, 2016 49(1), 87-93.

[23] Ciferri, A. The $\alpha\hat{a} \rightarrow \beta$ transformation in keratin. Transactions of the Faraday Society, 1963,59, 562-569.

[24] Collman, B. D., Noll, W. The thermodynamics of elastic materials with heat conduction. Arch. Ration. Mech. Anal, 13, 1963, 167.

[25] Collman, B. and Noll. W. Foundations of linear viscoelasticity. Reviews of Modern Physics, 33, 239–249 (1961).

[26] Colombatti, A., Poletti, A., Bressan, G. M., Carbone, A., Volpin, D. Widespread codistribution of glycoprotein gp 115 and elastin in chick eye and other tissues. Collagen and related research, 1987, 7(4), 259-275.

[27] Dale, W. C., Baer, E. Fibre-buckling in composite systems: a model for the ultrastructure of uncalcified collagen tissues. Journal of Materials Science, 1974, 9(3), 369-382.

[28] Day, W. A. (1968). Thermodynamics based on a work axiom.

[29] Deak, S. B., Ricotia, J. J., Mariani, T. J., Deak, S. T., Zatina, M. A., Mackenzie, J. W., Boyd, C. D. Abnormalities in the biosynthesis of type III procollagen in cultured skin fibroblasts from two patients with multiple aneurysms. Matrix, 1992 12(2), 92-100.

[30] Deseri, Luca, et al. Power-law hereditariness of hierarchical fractal bones. International journal for numerical methods in biomedical engineering, 2013, 29.12: 1338-1360.

[31] Deseri, L., Pollaci, P., Zingales, M., Dayal, K. Fractional hereditariness of lipid membranes: Instabilities and linearized evolution. journal of the mechanical behavior of biomedical materials, 2016, 58, 11-27.

[32] Deseri, L., M. Di Paola , M. Zingales. Free energy and states of fractional-order hereditariness. International Journal of Solids and Structures 51. 3156–3167, 2014.

[33] Deseri, L., Zingales, M. A mechanical picture of fractional-order Darcy equation. Communications in Nonlinear Science and Numerical Simulation, 2015, 20(3), 940-949.

[34] Deseri, L., Zingales, M., Pollaci, P. The state of fractional hereditary materials (FHM). Discr. Contin. Dyn. Syst. Ser. B, 2014, 19, 2065-2089.

[35] Di Paola M., Pinnola F. P., Zingales M. A discrete mechanical model of fractional hereditary materials. Meccanica, 2013, 48.7: 1573-1586.

[36] Di Paola, M., Pinnola, F. P., Zingales, M. Fractional differential equations and related exact mechanical models. Computers & Mathematics with Applications, 2013, 66(5), 608-620.

[37] Di Paola M., and Zingales M.. Exact mechanical models of fractional hereditary materials. Journal of Rheology 56.5 2012, 983-1004.

[38] Di Paola, M., Zingales, M. Long-range cohesive interactions of non-local continuum faced by fractional calculus. International Journal of Solids and Structures, 2008, 45(21), 5642-5659.

[39] Donahue TLH, Gregersen C, Hull ML, Howell SM. Comparison of viscoelastic structural and material properties of doubled-looped anterior cruciate ligament grafts made from bovine digital tensor and human hamstring tendons. ASME J Biomech Eng 2001, 123:162–169

[40] Drapaca, C. S., Sivaloganathan, S., Tenti, G. Nonlinear constitutive laws in viscoelasticity. Mathematics and mechanics of solids, 2007, 12(5), 475-501.

[41] Drapaca, C. S., Sivaloganathan, S. A fractional model of continuum mechanics. Journal of Elasticity, 2012, 107(2), 105-123.

[42] Erhart-Hledik JC, Chu CR, Asay JL, Andriacchi TP. Gait mechanics 2 years after anterior cruciate ligament reconstruction are associated with longer-term changes in patient-reported outcomes. J Orthop Res 2017, 35:634–640

[43] Failla, G. Stationary response of beams and frames with fractional dampers through exact frequency response functions. Journal of Engineering Mechanics, 2017, 143(5), D4016004.

[44] Feughelman, M. Free-energy difference between the alpha and beta states in keratin. Nature, 1963, 200(4902), 127-129.

[45] Findley W.N., Lai J. S., Onaran K. Creep and Relaxation of Non-linear Viscoelastic Materials. Dover, 1976.

[46] Flugge, W. Viscoelasticity Blaisdell Publishing Company. Waltham, Massachussetts, 1967.

[47] Freeman J, Kwansa A. Recent Advancements in Ligament Tissue Engineering: The Use of Various Techniques and Materials for ACL Repair. Recent Patents Biomed Eng, 2008, 1:18–23

[48] Fung Y. C. Biomechanics: Mechanical Properties of Living Tissues. Springer, 1993.

[49] Gemant A. A Method of Analyzing Experimental Results Obtained from Elasto-Viscous Bodies. Physics,311-317, 1936.

[50] Gordon, M. K., Gerecke, D. R., Olsen, B. R. Type XII collagen: distinct extracellular matrix component discovered by cDNA cloning. Proceedings of the National Academy of Sciences, 1987, 84(17), 6040-6044.

[51] Green, A. E., Rivlin, R. S. The mechanics of non-linear materials with memory. Archive for Rational Mechanics and Analysis, 1957 1(1), 1-21.

[52] Gurtin, M. E., Hrusa, W. J. On energies for nonlinear viscoelastic materials of single-integral type. Quarterly of applied mathematics, 1988, 46(2), 381-392.

[53] Gurtin M. E. and Sternberg E., Arch. Ration. Mech. Analysis11.4, 291 (1962).

[54] Hadjicostas PT, Soucacos PN, Koleganova N, Krohmer G, Berger I. Comparative and morphological analysis of commonly used autografts for anterior cruciate ligament reconstruction with the native ACL: An

electron, microscopic and morphologic study. Knee Surgery, Sport Traumatol Arthrosc, 2008, 16:1099–1107

[55] Hamner DL, Brown CH, Steiner ME, Hecker AT, Hayes WC. Hamstring tendon grafts for reconstruction of the anterior cruciate ligament: biomechanical evaluation of the use of multiple strands and tensioning techniques. J Bone Joint Surg Am, 1999, 81:549–57

[56] Hasegawa, M., Azuma, K., Oashi, T. Proceedings: Dynamic elasticity of the major arterial stem. Nihon seirigaku zasshi. Journal of the Physiological Society of Japan, 1974, 36(8-9), 380.

[57] Hashemi, J., Chandrashekar, N., Slauterbeck, J. The mechanical properties of the human patellar tendon are correlated to its mass density and are independent of sex. Clinical Biomechanics, 2005, 20(6), 645-652.

[58] Haut RC, Powlison AC. The effects of test environment and cyclic stretching on the failure properties of human patellar tendons. J Orthop Res, 1990, 8:532–540

[59] Health and Human Services, FDA. Guidance document for the preparation of investigational device exemptions and premarket approval applications for intra-articular prosthetic ligament devices. FDA Website 1993, 1–43

[60] Hingorani R V., Provenzano PP, Lakes RS, Escarcega A, Vanderby R. Nonlinear viscoelasticity in rabbit medial collateral ligament. Ann Biomed Eng, 2004, 32:306–312

[61] Johnson GA, Tramaglini DM, Levine RE, Ohno K, Choi NY, Woo SLY. Tensile and viscoelastic properties of human patellar tendon. J Orthop Res, 1994, 12:796–803

[62] Kaye, A. (1962). College of Aeronautics, Cranfield (Vol. 134). note.item Kaye, A. (1962). College of Aeronautics, Cranfield (Vol. 134). note.

[63] Lakes, R. S.; Vanderby, R. Interrelation of creep and relaxation: a modeling approach for ligaments. Journal of biomechanical engineering, 1999, 121.6: 612-615.

[64] Lockett, F. J. Nonlinear viscoelastic solids. Academic Press, 1972.

[65] Magin, R. L. Fractional calculus models of complex dynamics in biological tissues. Computers & Mathematics with Applications, 2010, 59(5), 1586-1593.

[66] Mainardi F.. Fractional calculus and waves in linear viscoelasticity: an introduction to mathematical models. World Scientific, 2010.

[67] Mainardi F., Spada G.. Creep, relaxation and viscosity properties for basic fractional models in rheology. The European Physical Journal Special Topics 193.1: 133-160, 2011.

[68] Manley E, Provenzano PP, Heisey D, Lakes R, Vanderby R. Required test duration for group comparisons in ligament viscoelasticity: a statistical approach. Biorheology, 2003, 40:441–50

[69] McGuirt, C. W., Lianis, G. Constitutive equations for viscoelastic solids under finite uniaxial and biaxial deformations. Transactions of the Society of Rheology, 1970, 14(2), 117-134.

[70] McLean SG, Mallett KF, Arruda EM. Deconstructing the Anterior Cruciate Ligament: What We Know and Do Not Know About Function, Material Properties, and Injury Mechanics. J Biomech Eng, 2015, 137:020906 doi:10.1115/1.4029278

[71] Muliana, A., Rajagopal, K. R., Wineman, A. S. A new class of quasi-linear models for describing the nonlinear viscoelastic response of materials. Acta Mechanica, 2013, 224(9), 2169-2183.

[72] Noll, W., Truesdell, C. A. (1992). The non-linear field theories of mechanics. Berlin: Springer-Verlag.

[73] Noll, W. A mathematical theory of the mechanical behavior of continuous media. Archive for rational Mechanics and Analysis, 1958, 2(1), 197-226.

[74] Nutting P.G.Adsorption and pycnometry. Journal of the Washington Academy of Sciences,1-6,1936.

[75] Nutting, P. G. Deformation in relation to time, pressure and temperature. Journal of the Franklin Institute, 1946, 242.6: 449-458.

[76] Palumbo, F. S., Pitarresi, G., Fiorica, C., Rigogliuso, S., Ghersi, G., Giammona, G. Chemical hydrogels based on a hyaluronic acid-graft-α-elastin derivative as potential scaffolds for tissue engineering. Materials Science and Engineering: C, 2013, 33(5), 2541-2549.

[77] Park, S. W., Schapery, R. A. Methods of interconversion between linear viscoelastic material functions. Part I—A numerical method based

on Prony series. International Journal of Solids and Structures, 1999, 36(11), 1653-1675.

[78] Pioletti DP, Rakotomanana, LR. On the independence of time and strain effects in the stress relaxation of ligaments and tendons. Journal of biomechanics, 2000, 33(12), 1729-1732.

[79] Pipkin, A. C., Rogers, T. G. A non-linear integral representation for viscoelastic behaviour. Journal of the Mechanics and Physics of Solids, 1968, 16(1), 59-72.

[80] Provenzano P., Lakes R., Keenan T., Vanderby R., Nonlinear Ligament Viscoelasticity. Annals of Biomedical Engineering, 29, 908–914, 2001.

[81] Rajagopal, K. R. and Wineman, A. S. Response of anisotropic nonlinearly viscoelastic solids. Mathematics and Mechanics of Solids, in press.

[82] Rivlin, R. S., Ericksen, J. L. (1997). Stress-deformation relations for isotropic materials. In Collected Papers of RS Rivlin (pp. 911-1013). Springer, New York, NY

[83] Schmidt, Andre; Gaul, Lothar. FE implementation of viscoelastic constitutive stress-strain relations involving fractional time derivatives. Constitutive models for rubber, 2001, 2: 79-92.

[84] Sobin, S. S., Fung, Y. C., Tremer, H. M. Collagen and elastin fibers in human pulmonary alveolar walls. Journal of Applied Physiology, 1988, 64(4), 1659-1675.

[85] Spencer, A. J. M. (1971). Part III. Theory of invariants. Continuum physics, 1, 239-353.

[86] Suckochi C., A Quasi-Linear Viscoelastic Rehological Model for Thermoplastics and Resins.of Theoretical and Applied Mechanics, 51,117–129, 2013.

[87] Tokimitsu, I., Kato, H., Wachi, H., Tajima, S. Elastin synthesis is inhibited by angiotensin II but not by platelet-derived growth factor in arterial smooth muscle cells. Biochimica et Biophysica Acta (BBA)-Protein Structure and Molecular Enzymology, 1994, 1207(1), 68-73.

[88] Vacek PM, Slauterbeck JR, Tourville TW, Sturnick DR, Holterman L -a., Smith HC, Shultz SJ, Johnson RJ, Tourville KJ, Beynnon BD. Multivariate Analysis of the Risk Factors for First-Time Noncontact ACL

Injury in High School and College Athletes: A Prospective Cohort Study With a Nested, Matched Case-Control Analysis. Am J Sports Med, 2016, 44:1492-1501

[89] Van Dommelen JAW, Jolandan MM, Ivarsson BJ, Millington SA, Raut M, Kerrigan JR, Crandall JR, Diduch DR. Pedestrian injuries: Viscoelastic properties of human knee ligaments at high loading rates. Traffic Inj Prev, 2005, 6:278-287

[90] Vena P., Gastaldi D., Contro R. , A Constituent-Based Model for the Nonlinear Viscoelastic Behavior of Ligaments.Journal of Biomechanical Engineering, 128,449–457, 2005.

[91] Volterra V., Peres J.. Théorie générale des fonctionnelles. Gauthier-Villars, 1936.

[92] Wilkes, N. S. Thermodynamic restrictions on viscoelastic materials. The Quarterly Journal of Mechanics and Applied Mathematics, 1997, 30(2), 209-221

[93] Wineman, A. S. Large axially symmetric stretching of a nonlinear viscoelastic membrane. International Journal of Solids and Structures, 1972, 8(6), 775-790.

[94] Wineman, A. S., Waldron Jr, W. K. Yieldlike response of a compressible nonlinear viscoelastic solid. Journal of Rheology, 1995, 39(2), 401-423.

[95] Woo, S. Y., Lubock, P., Gomez, M. A., Jemmott, G. F., Kuei, S. C., Akeson, W. H. Large deformation nonhomogeneous and directional properties of articular cartilage in uniaxial tension. Journal of biomechanics, 1979, 12(6), 437-446.

[96] Yeh, H., Ornstein-Goldstein, N., Indik, Z., Sheppard, P., Anderson, N., Rosenbloom, J. C., Rosenbloom, J. Sequence variation of bovine elastin mRNA due to alternative splicing. Collagen and related research, 1987, 7(4), 235-247.

[97] Zingales, M. An exact thermodynamical model of power-law temperature time scaling. Annals of Physics, 2016, 365, 24-37.

[98] Zingales, M. Wave propagation in 1D elastic solids in presence of long-range central interactions. Journal of Sound and Vibration, 2011, 330(16), 3973-3989.